7-31-2015

# Spectroscopy and Photophysics of Carotenoids in Solution and in Light-harvesting Pigment-Protein Complexes

Nikki Cecil M. Magdaong
nikkicecil@gmail.com

# Spectroscopy and Photophysics of Carotenoids in Solution and in Light-harvesting Pigment-Protein Complexes

Nikki Cecil M. Magdaong, Ph.D.

University of Connecticut, 2015

This thesis examines the factors affecting the photophysics and energy transfer properties of carotenoids. Steady-state and ultrafast time-resolved spectroscopic experiments were carried out on several carotenoids in various solvents and light-harvesting pigment-protein complexes. The main goal is to probe the excited state properties and kinetics of these molecules and relate the findings to their roles in light-harvesting and photoprotection of the photosynthetic apparatus. The spectroscopic studies on a short conjugated peridinin analogue extend previous studies on synthetic peridinin analogues having different numbers of conjugated carbon-carbon double bonds. The results provide insight into the nature of the intramolecular charge transfer state (ICT) in carbonyl-containing carotenoids. The spectroscopic properties of several light-harvesting pigment-protein complexes isolated from various photosynthetic organisms are also investigated. Some species of purple photosynthetic bacteria produce spectral variants of the well-known B800-850 light harvesting II (LH2) complex depending on the conditions under which they are grown. *Rhodoblastus (Rbl.) acidophilus* strain 7050 produces the B800-820 LH2 spectral variant when grown under low-light conditions. In addition, the carotenoid rhodopinal glucoside is formed in large amounts in this complex whereas rhodopin glucoside is the primary carotenoid in the B800-850 LH2 complex grown under

high-light growth conditions. The conversion of rhodopin glucoside to rhodopinal glucoside increases the efficiency of carotenoid-to-bacteriochlorophyll (BChl) energy transfer to ~100%, as evidenced by results obtained from steady-state absorption, fluorescence, and ultrafast transient absorption spectroscopic measurements on rhodopin and rhodopinal glucoside in different solvents and in the LH2 complexes. *Allochromatium (Alc.) vinosum* is another example of a photosynthetic bacterium that produces various LH2 spectral forms denoted B800-850, B800-840 and B800-820 when grown under different conditions of temperature, illumination, and reduced sulfur nutrient. The analysis of the pigment composition reveals that the LH2 complexes from *Alc. vinosum* contain five carotenoids: lycopene, rhodopin, anhydrorhodovibrin, rhodovibrin and spirilloxanthin. Reconstruction of the absorption and fluorescence excitation spectra demonstrates that there exists significant spectral heterogeneity compared to LH2 complexes obtained from other species of purple bacteria. The combined results from these investigations provide insights into the mechanisms by which photosynthetic organisms adapt and survive under varying environmental conditions. The effect of the protein structure on the spectroscopic properties of carotenoids and (bacterio)chlorophylls (BChls) are also presented in this thesis. In higher plants, aggregation of the light-harvesting complex II (LHCII) has been postulated to be one of the factors affecting the rate and efficiency of the process of dissipation of chlorophyll (Chl) excess excitation energy known as nonphotochemical quenching.

Nikki Cecil M. Magdaong – University of Connecticut, 2015

Spectroscopic measurements were performed on monomeric, trimeric and aggregated monomers and trimers of LHCII, the results of which reveal the differences in the excited state deactivation processes of the Chls and carotenoids bound in these complexes. The last chapter looks at the influence of protein structure on the spectroscopic properties of the protein-bound peridinin and Chl *a* molecules in three native and recombinant peridinin-chlorophyll *a*-protein (PCP) complexes from photosynthetic dinoflagellates. Analysis of the absorption and fluorescence excitation spectra reveal that the individual peridinins in the PCP complexes have distinct spectra depending on their location in the pigment-protein complex and that all of the carotenoids possess the same high (~100%) energy transfer efficiency to Chl.

# Spectroscopy and Photophysics of Carotenoids in Solution and in Light-harvesting Pigment-Protein Complexes

Nikki Cecil M. Magdaong

B.S., University of the Philippines, Diliman, 2003

A Dissertation

Submitted in Partial Fulfillment of the

Requirements for the Degree of

Doctor of Philosophy

at the

University of Connecticut

2015

# APPROVAL PAGE

Doctor of Philosophy Dissertation

Spectroscopy and Photophysics of Carotenoids in Solution and in Light-harvesting Pigment-Protein Complexes

Presented by

Nikki Cecil M. Magdaong, B.S.

Major Advisor _____

Harry A. Frank, Ph.D.

Associate Advisor _____

Robert R. Birge, Ph.D.

Associate Advisor _____

James F. Rusling, Ph.D.

University of Connecticut

2015

# ACKNOWLEDGMENTS

The research covered in this thesis was conducted under the excellent supervision of Prof. Harry A. Frank. To him I express my utmost gratitude for the unwavering support and guidance. His patience, fairness, professional conduct and careful attention to details are something to aspire to. It is truly an honor to have worked in his laboratory and explored the colorful world of carotenoids and photosynthesis. I am also grateful to have an exceptional thesis committee in Profs. Robert R. Birge and James. F. Rusling, my associate advisors, and Prof. Christian Brückner, who have provided helpful discussion and valuable insights on my proposal and dissertation.

The various chapters contained herein would not be possible without the assistance of our much-valued collaborators. I acknowledge Prof. George N. Gibson for his patience and generous assistance in setting up the ultrafast laser system for our pump-probe measurements. Many thanks to Prof. Birge and Jordan Greco, for carrying out the computational work on our molecules. Working with you was always a delightful experience. Thank you to Prof. Rusling and Yun Zhang, from whom I learned much about protein film voltammetry. For those who have provided some of our samples for spectroscopic measurements—Prof. Shigeo Katsumura of Kwansei Gakuin University, Japan and his group for the synthetic analogues of peridinin; Prof. Roger Hiller of Macquarie University, Australia and Prof. Eckhard Hofmann of Ruhr-University Bochum, Germany for the purified PCP complexes; Prof. Richard J. Cogdell from the University of Glasgow, Scotland and his group members for the light harvesting complexes purified from purple photosynthetic bacteria. Special mention to Dr. Dariusz M. Niedzwiedzki for always being available to lend a hand with our experiments. We could always count on him to provide excellent technical support and valuable insights on the many projects we have worked on together.

To former Franklab members Marcel, Jose and Shanti, thank you for your guidance, camaraderie and lively discussion. Although it has been a few years since we have worked together, I have fond memories and feel extremely lucky to have known you all. To Dr. Miriam Enriquez-Sarmiento with whom I shared a good part of this graduate career, with its twists and turns, I cannot think of a better person to have gone this journey with. Thank you for the patience, understanding and sage advice through the years. To Ms. Amy LaFountain, who has been my sounding board for the past two years, I am very privileged to have known and worked with you. You are one of the nicest, kindest people I have ever met. I truly appreciate all the help and ideas as well as morale-boosting especially in these last stages.

To Anwar, Junru, Christian and Bharat, my first labmates from whom I have learned much about biochemistry experimental work, thank you for your support then and now. I am fortunate to have worked with you, albeit briefly. I am very grateful we have remained good friends, my bowling and coffee buddies.

To my merry band of friends—Dr. Reyna Koreen V. Lim, Dr. Major D. Gooyit, Dr. Dennis Kien B. Pacardo, who have gone the way of grad school before me and inspired me to do the same, MARAMING SALAMAT for the much needed advice and constantly providing the humor, comfort and faith needed to navigate the intricacies of graduate school and life. It wasn't long ago when we were just talking about these plans and now we've all done it. I also thank Joshua, Charity, Donna, Tuani, Zarah, Angela, and all other friends who have always believed in my capabilities when I didn't. Thank you all for the laughter, inspiration, and generosity.

My family has always been my compass and guide in whatever undertaking I dared. To Mama and Papa, I am very grateful that in spite of the hardships and difficulties, you made sure I got the best education possible. You never questioned my decisions, always allowed me to explore my options and trusted my judgment. To my siblings—Nikko, Nikka, Nikkita, Nikkito, Nikkitito and Nikkitita, thank you for inspiring me to be the best version of myself. You always keep me grounded and make me aspire to be a good example for you. To the rest of my extended family, far too many to mention, thank you for appreciating all my accomplishments, big and small.

## TABLE OF CONTENTS

# LIST OF TABLES

## Chapter II



## Chapter III



## Chapter IV



## Chapter V

## Chapter VI

# LIST OF FIGURES

## Chapter I



## Chapter II

## Chapter III

## Chapter IV

## Chapter V

## Chapter VI

The work in this thesis is reported in the following publications:

**Chapter II**

Magdaong, N. M.; Niedzwiedzki, D. M.; Greco, J. A.; Liu, H.; Yano, K.; Kajikawa, T.; Sakaguchi, K.; Katsumura, S.; Birge, R. R.; Frank, H. A., Excited state properties of a short π-electron conjugated peridinin analogue. *Chem. Phys. Lett.* **2014,** *593*, 132–139.

**Chapter III**

Magdaong, N. M.; Enriquez, M. M.; LaFountain, A. M.; Rafka, L.; Frank, H. A., Effect of protein aggregation on the spectroscopic properties and excited state kinetics of the LHCII pigment-protein complex from green plants. *Photosynth. Res.* **2013,** *118*, 259–276.

**Chapter IV**

Magdaong, N. M.; LaFountain, A. M.; Greco, J. A.; Gardiner, A. T.; Carey, A-M.; Cogdell, R. J.; Gibson, G. N.; Birge, R. R.; Frank, H. A., High efficiency light harvesting by carotenoids in the LH2 complex from photosynthetic bacteria: unique adaptation to growth under low-light conditions. *J. Phys. Chem. B* **2014,** *118*, 11172–11189.

**Chapter V**

Magdaong, N. M.; LaFountain, A. M.; Hacking, K.; Niedzwiedzki, D. M.; Gibson, G. N.; Cogdell, R. J.; Frank, H. A., Spectral heterogeneity and carotenoid-to-bacteriochlorophyll energy transfer in LH2 light-harvesting complexes from *Allochromatium vinosum*. *Photosynth. Res*. Epub June 06, **2015.**

# *Chapter I*

# *Introduction and Overview*

**Structure, function, electronic states and spectral properties of carotenoids**

Carotenoids are a large class of naturally-occurring pigments whose structures possess a linear polyene chain (Figure 1) that gives rise to their strong visible coloration and photophysical behavior.[1-3] Carotenoids play several roles in photosynthesis including light-harvesting, photoprotection and protein structure stabilization.[4-7] Carotenoids absorb light in the blue-green region of the visible spectrum where chlorophyll (Chl) is a weak absorber and transfer the excitation to Chl via their excited singlet states.[5,7-10] Carotenoids protect the photosynthetic apparatus from photodamage under high light conditions either by quenching Chl triplet states which prevents the formation of the harmful $^1\Delta_g$* excited singlet state of oxygen,[4,11,12] or by scavenging any singlet oxygen that is formed.[7,12-14] Carotenoids also facilitate the assembly of pigment-protein complexes and provide them with structural stability.[15-19]

The electronic states of carotenoids that are responsible for much of this behavior are characterized by their symmetry, the labels for which of are derived from those of all-*trans* polyenes which belong to an idealized $C_{2h}$ point group. Many of the spectroscopic properties of carotenoids resemble those of polyenes.[20] Quantum mechanical selection rules dictate that for spectroscopic transitions to be allowed, the initial and final states must differ in both symmetry ($g \leftrightarrow u$) and pseudoparity ($+ \leftrightarrow -$).[21-26] Thus, one-photon transitions of polyenes and carotenoids involving the ground state, $S_0$ ($1^1A_g^-$), and the lowest-lying excited singlet state, $S_1$ ($2^1A_g^-$), both of which have the same symmetry and pseudoparity, are optically forbidden (Figure 2). As a result, a transition from $S_0$ ($1^1A_g^-$)

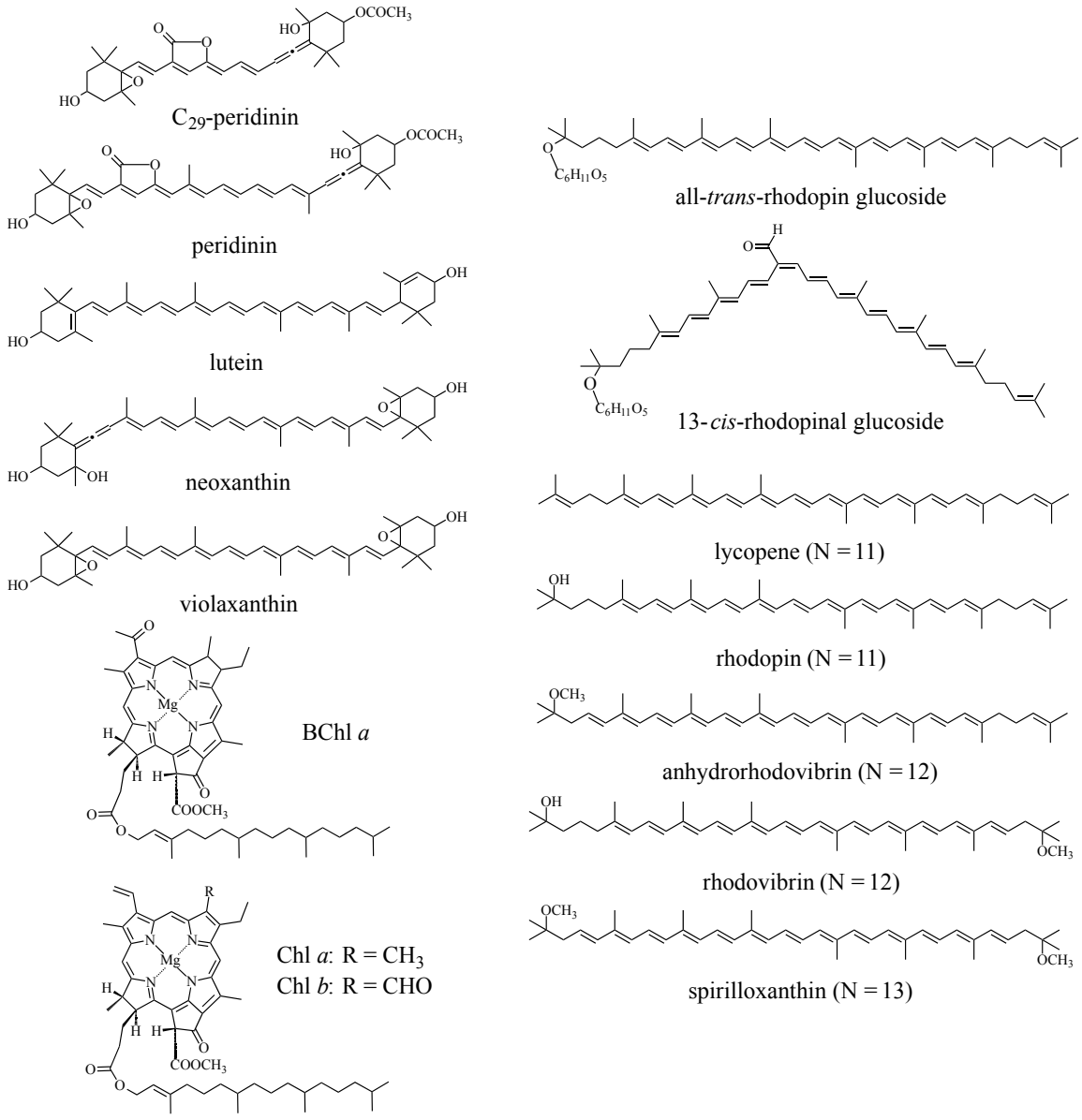


**Figure 1.** Molecular structures of chlorophyll (Chl) *a* and *b*, bacteriochlorophyll (BChl) *a*, and various carotenoids and xanthophylls found in light-harvesting complexes with the exception of $C_{29}$-peridinin which is a synthetic analogue of naturally-occurring peridinin.

to $S_1$ ($2^1A_g^-$) has a very small oscillator strength. Quantum mechanical modeling of the $S_1$ ($2^1A_g^-$) state indicates that it is covalent in nature,[24] and experiments have revealed that its energy and lifetime are essentially independent of the solvent environment.[20,27-30] However, the lifetime of the $S_1$ ($2^1A_g^-$) state can vary depending on the nature of any attached functional groups, and it decreases with increasing π-electron conjugation length, as has been shown by several spectroscopic studies on carotenoids and polyenes having different substituents and numbers of conjugated carbon–carbon double bonds, N.[31-38] This dependence on N has been explained on the basis of the energy gap law for radiationless transitions which states that the narrower the energy gap between two states the faster will be the rate of a nonradiative transition between them.[39-42]

The bright coloration that is characteristic of carotenoids is due to a strongly-allowed transition from the ground state, $S_0$ ($1^1A_g^-$), to the second excited state, $S_2$ ($1^1B_u^+$) (Figure 2). The $S_2$ ($1^1B_u^+$) state has been reported to have significant ionic character.[24,27] Like the $S_1$ ($2^1A_g^-$) state, the excited state properties of $S_2$ ($1^1B_u^+$) are dependent on N as well as attached functional groups, but unlike the $S_1$ ($2^1A_g^-$) state, due to its ionic character, the energy of the $S_2$ ($1^1B_u^+$) state can be modulated by changes in solvent polarity and polarizability.[5,20,25,43-49]

Energy transfer from carotenoids to (B)Chl in light-harvesting pigment-protein complexes involves at least two of the lowest lying excited states of carotenoids (Figure 2),[50-52] and based on theoretical computations[27,41,53-55] and spectroscopic studies,[56-63] additional excited states residing either between or in the vicinity of the $S_1$ ($2^1A_g^-$) and $S_2$ ($1^1B_u^+$) states have also been proposed to play a role. For comprehensive reviews, see Refs. 50,51 and 64–67.

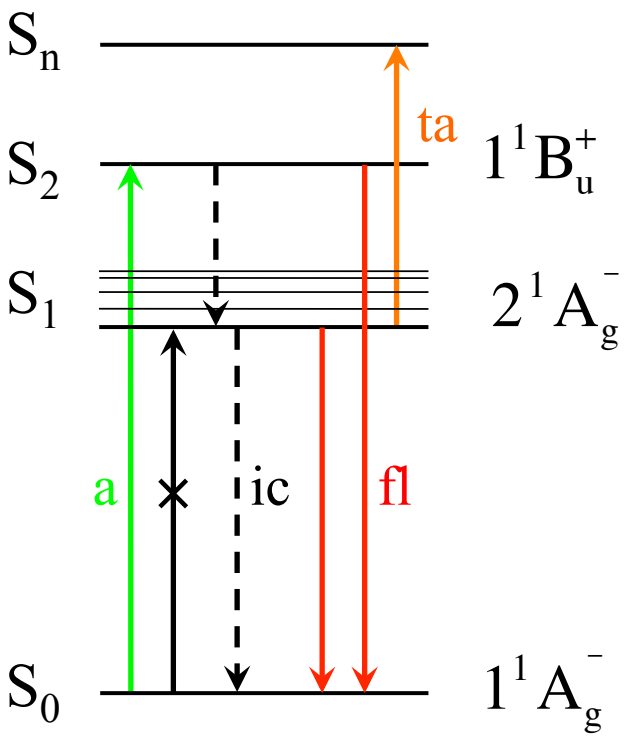


**Figure 2.** Low-lying electronic states of carotenoids and associated transitions. a, absorption; ic, internal conversion; fl, fluorescence; ta, transient absorption. Dashed arrows represent nonradiative processes. Note that the transition from $S_0$ ($1^1A_g^-$) to $S_1$ ($2^1A_g^-$) is forbidden according to both symmetry and pseudoparity selection rules.

As mentioned above, the spectral properties and kinetics of deactivation of the excited states of carotenoids depend on the nature of any attached functional groups. This is exemplified by carbonyl groups in conjugation with the π-electron polyene chain, which can lead to major changes in the absorption spectra and lifetimes of the excited states of carotenoids. In particular, the $S_1$ ($2^1A_g^-$) state dynamics of a carotenoid possessing a conjugated carbonyl group can be modulated by the solvent polarity.[30,68-71] Peridinin (Figure 1) provides a case in point whereby the lifetime of its $S_1$ ($2^1A_g^-$) state is shortened substantially when the molecule is dissolved in polar solvents.[30,69,72,73] This effect has been attributed to the formation of an intramolecular charge transfer (ICT) state,[30] which has been proposed to be either strongly coupled to the $S_1$ ($2^1A_g^-$) state,[68,73] a distinct electronic state from $S_1$ ($2^1A_g^-$),[72,74-77] or the $S_1$ ($2^1A_g^-$) state itself but with a large intrinsic dipole moment.[78] In peridinin, the ICT state has been described as being derived from quantum mechanical mixing of the ionic $S_2$ ($1^1B_u^+$) state and the covalent $S_1$ ($2^1A_g^-$) state[79] which leads to bond-order reversal and solvent reorganization in polar solvents. Despite this detailed characterization of how the ICT state is formed in carbonyl-containing carotenoids, its role in light-harvesting and photoprotection in photosynthetic organisms has yet to be fully elucidated.

**Light-harvesting by photosynthetic organisms**

The initial event in photosynthesis is the absorption of light which is accomplished by a wide variety of pigment-protein complexes that have different structures (Figure 3) depending on the photosynthetic organism in which they are formed.[80] Light-harvesting complexes are comprised of either Chls or BChls and carotenoids that are bound to protein subunits. The pigments absorb light throughout the visible and near-infrared (NIR) regions of the electronic spectrum and transfer the excitation energy to a reaction center (RC) pigment-protein complex where charge separation takes place and a trans-membrane electrical potential is generated.[49,80,81]

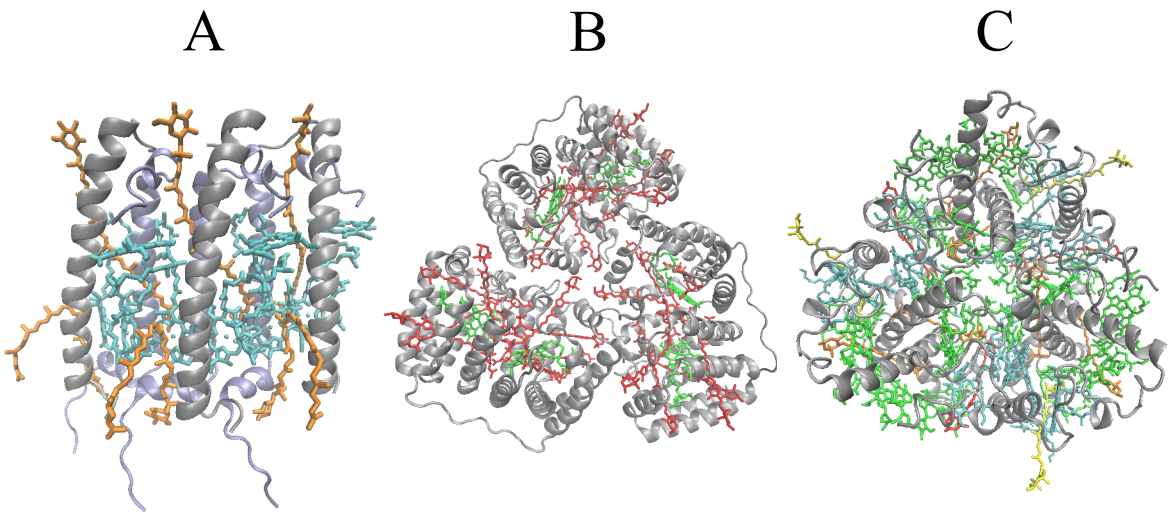


**Figure 3.** Crystal structures of light-harvesting pigment-protein complexes: (A) B800-850 complex from *Rbl. acidophilus* strain 10050[82] (PDB ID 1NKZ); (B) Peridinin-chlorophyll-protein (PCP) complex from *A. carterae*[83] (PDB ID 1PPR); and (C) Light-harvesting complex II (LHCII) from spinach[84] (PDB ID 1RWT). The figures were generated from the indicated PDB coordinates using Visual Molecular Dynamics (VMD) software.[85]

*Purple bacteria*

The antenna complexes of purple bacteria are typically divided into two classes of integral membrane proteins: LH1 and LH2.[86-89] LH1 is closely associated with the reaction center in a 1:1 fixed proportion, whereas LH2 is located on the periphery of the LH1-RC core complex, and its amount relative to LH1 has been reported to vary with light intensity.[80,90-94] LH1 and LH2 are also distinguished by their light-absorption properties. LH1 has a long wavelength absorption band of BChl, denoted $Q_Y$, located at ~875 nm. LH2 typically has two BChl $Q_Y$ absorption bands at ~800 nm and ~850 nm (Figure 4). X-ray crystallographic diffraction studies have revealed the structure of the LH2 (B800-850) complex from *Rhodoblastus (Rbl.) acidophilus* (formerly *Rhodopseudomonas acidophila*)[82,95,96] (Figure 3A) and *Rhodospirillum (Rsp.) molischianum*[97] to be made up of two low molecular weight α-helices denoted α and β that traverse the photosynthetic membrane. The inner α and outer β polypeptides form a homogeneous nonameric (*Rbl. acidophilus*) or octameric (*Rsp. molischianum)* ring structure, and in between these helices, carotenoids and BChls are noncovalently bound.[98] The two BChl $Q_Y$ absorption bands at ~800 nm and ~850 nm in LH2 belong to two separate groups of BChl molecules, the first of which is comprised of a ring of essentially monomeric BChls. The second group contains twice as many BChls in a concentric ring separated from the first by ~17.6 Å across the membrane. The BChls in this second group are in close association and consequently are exciton coupled.[94,96,99,100] Several different carotenoids, examples of which are shown in Figure 1, are bound in the LH2 complexes in a 1:3 stoichiometric ratio with BChl.[82,97]

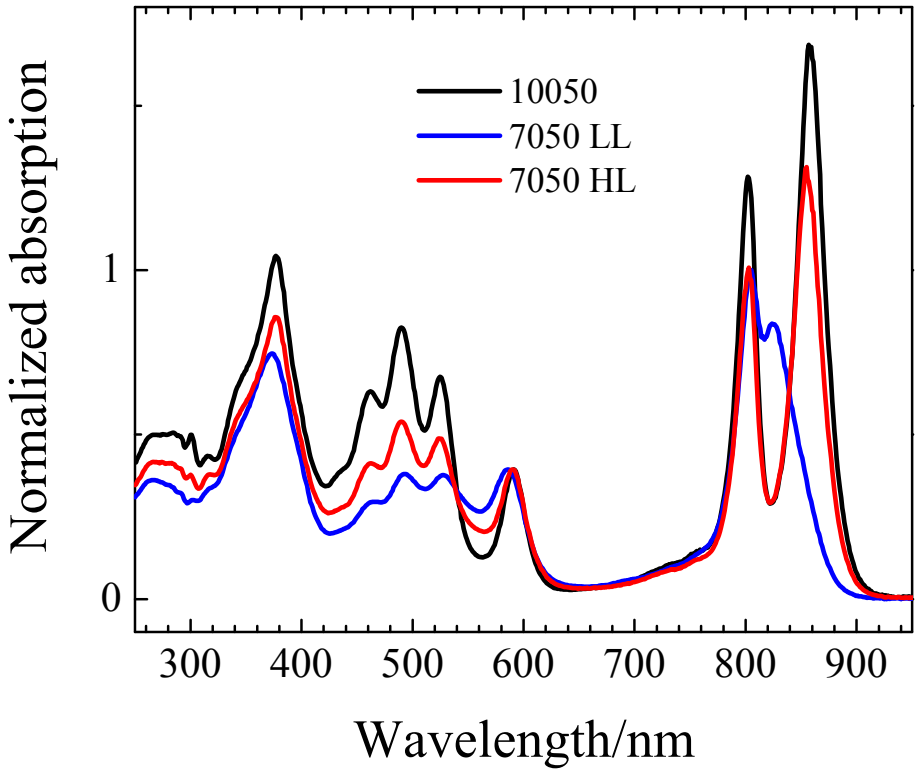


**Figure 4.** Absorption spectra of the LH2 pigment-protein complexes isolated from *Rbl. acidophilus* strains 10050 (black trace) and 7050 grown under low-light (LL, blue trace) and high-light (HL, red trace) conditions.

Under normal growth conditions of temperature and illumination, *Rbl. acidophilus* strain 7050 forms a B800-850 LH2 complex and accumulates primarily the carotenoids, rhodopin and rhodopin glucoside. Under low light conditions, a spectroscopic variant LH2 having absorption maxima near 800 nm and 820 nm, and hence denoted B800-820, is formed, and the carotenoids, rhodopinal and rhodopinal glucoside (Figure 1), are produced.[101-103] The crystal structure of the B800-820 complex determined to 3.0 Å resolution, revealed a similarity to the nonameric quaternary structure of the B800-850 complex from *Rbl. acidophilus* 10050.[102] The blue-shift of the 850 nm absorption band to 820 nm was explained by changes in the hydrogen bonding pattern between BChl *a* and the protein induced by differences in the primary sequence of the apoproteins of the complexes.[102,104] Specifically, the αTyr44 and αPhe45 amino acid residues in the B800-850 complex are substituted by αPhe44 and αLeu45 when the organism is grown under low light conditions. These amino acids do not form hydrogen bonds with the C3-acetyl group of the B850 BChl *a*,[94,98,102,105,106] and the absence of this causes the acetyl group to rotate out-of-plane with respect to the BChl macrocycle ring decreasing the effective π-electron conjugation and leading to a blue-shift of the $Q_Y$ spectral band (Figure 4).[94,98,107] The spectral properties and energy transfer kinetics of the B800-850 and B800-820 LH2 complexes from *Rbl. acidophilus* strain 7050 are described in detail in Chapter IV of this thesis.

*Allochromatium (Alc.) vinosum* (formerly *Chromatium vinosum*) is a purple sulfur bacterium that produces at least three spectral variants of the LH2 complex denoted B800-820, B800-840 and B800-850 (Figure 5) when grown under different conditions of temperature, illumination and type of sulfur nutrient.[108-113] [109,114] The absorption spectrum of some of these LH2 complexes recorded at room temperature has a broad 800 nm band that splits into two distinct peaks when the spectrum is recorded at cryogenic temperatures.[115-119] This splitting has been explained by B800 BChl *a* molecules within the same LH2 ring[118] forming exciton coupled dimers that interact with the B850 BChls.[119] Five carotenoids are present in all of these LH2 complexes: rhodopin, lycopene, rhodovibrin, anhydrorhodovibrin and spirilloxanthin (Figure 1).[113,118] As will be discussed in Chapter V of this thesis, the spectral heterogeneity exhibited in the region of carotenoid absorption in these complexes is significantly more pronounced than in antenna complexes from other purple bacteria.

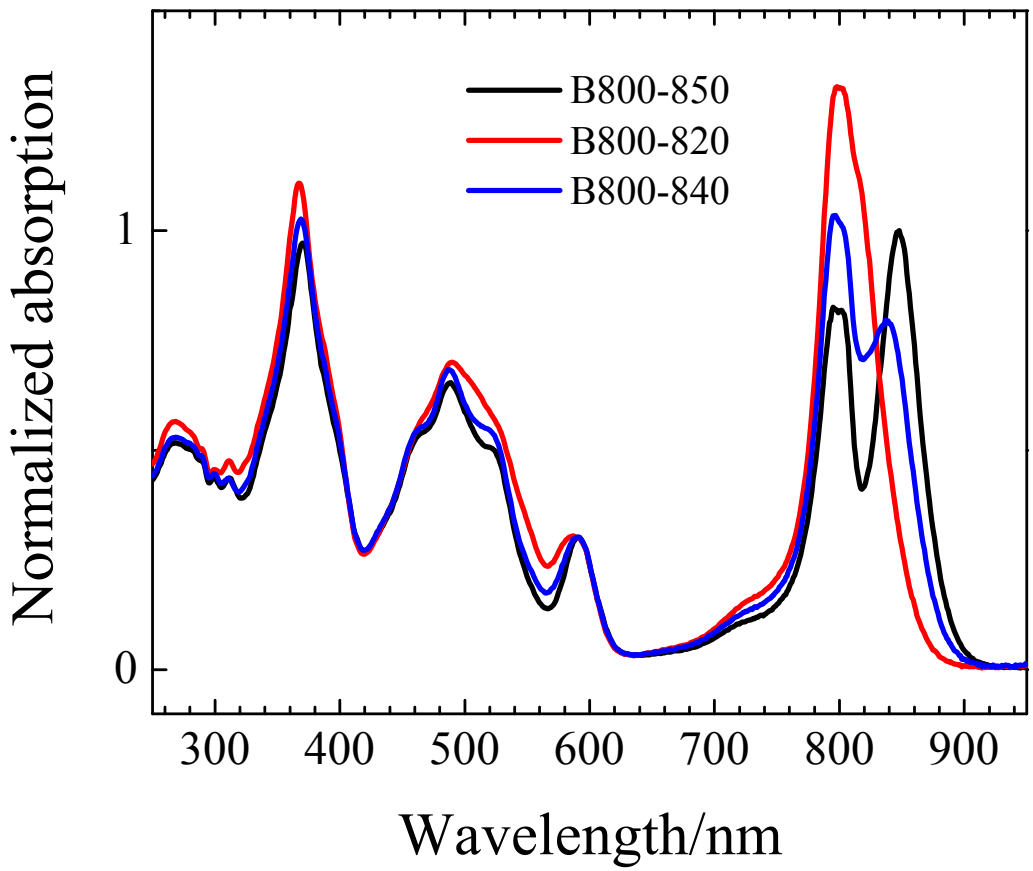


**Figure 5.** Absorption spectra of the LH2 pigment-protein complexes isolated from *Alc. vinosum*.

*Dinoflagellates*

In contrast to the membrane-bound pigment-protein complexes found in the purple bacteria, dinoflagellates contain both integral membrane and water-soluble antenna complexes.[120,121] One such water-soluble complex is the peridinin-chlorophyll-*a*-protein (PCP).[83] A 2.0 Å resolution crystal structure of the PCP complex (Figure 3B) from *Amphidinium (A.) carterae* revealed a trimeric protein structure with each minimal monomeric unit being comprised of two domains, each of which binds noncovalently four peridinins (Figure 1) and one Chl *a*.[83] *A. carterae* contains the main-form PCP (MFPCP).[78,122-137] Recombinant PCP apoprotein refolded with stoichiometric amounts of Chl and peridinin (RFPCP) has also been prepared and used to elucidate the nature of the binding of individual peridinin molecules to the protein and the mechanism of energy transfer between the pigments.[138-148] Another PCP complex isolated from *Heterocapsa (H.) pygmaea*, denoted HPPCP, has been reported to have the same 4:1 peridinin-to-Chl pigment stoichiometric ratio as MFPCP, but it forms a monomeric tertiary structural complex rather than the trimeric structure of MFPCP.[83,149-151] A detailed systematic comparison of the spectroscopic and energy transfer properties of the MFPCP, RFPCP and HPPCP complexes is presented in Chapter VI of this thesis. The aim of the investigation is to provide insight into the relationship between the structure of the PCP complex and the molecular factors that control the light-harvesting function in these photosynthetic organisms.

*Higher plants*

The photosynthetic apparatus of higher plants is embedded in the chloroplast thylakoid membrane.[152,153] There are two pigment-protein complexes known as Photosystems I (PSI)[154,155] and II (PSII)[156,157] that carry out the light reactions.[154-157] PSII is the only protein in nature capable of splitting water and forming molecular oxygen.[158,159] Compared to the photosynthetic bacteria and the dinoflagellates described above, higher plants contain many more (approximately twelve) light-harvesting proteins that transfer the excitation energy to PSI and PSII.[153,156,160 80,152,161,162] The polypeptides that assemble the light-harvesting complexes in green plants are encoded by genes known as Lhca or Lhcb[160,161] depending on whether they are associated with PSI or PSII, respectively.[163] The polypeptides of the peripheral antennas surrounding PSII are gene products denoted Lhcb1–6.[164] By far, the most abundant of these antennas is light-harvesting complex II (LHCII) which can form either homotrimers or heterotrimers of the Lhcb1, Lhcb2 and Lhcb3 polypeptides.[161,164-166] Other minor monomeric pigment-protein complexes associated with PSII are CP24 (Lhcb6),[167] CP26 (Lhcb5)[168] and CP29 (Lhcb4)[156,169] so named due to their apparent (24 kDa, 26 kDa or 29 kDa) molecular weights.[170-173] The crystal structure of LHCII has been determined for preparations from peas[174] and spinach[84] (Figure 3C). The crystallography revealed a trimeric configuration of protein subunits with each monomer binding eight Chl *a* and six Chl *b* molecules in addition to one neoxanthin, two luteins and one violaxanthin.[7,84,175-177] In addition to operating as antenna molecules, these xanthophylls are thought to be involved in dissipating the excess energy that is absorbed but not used by the plant for

photosynthesis.[178-184] Aggregation of LHCII is thought to play a role in energy dissipation and this topic will be addressed in detail in Chapter III of this thesis.

## Objective of the study

The overall goal of this dissertation is to examine the relationship between the structure and function of carotenoids in light-harvesting complexes prepared from various photosynthetic organisms. Data from steady-state and ultrafast transient optical spectroscopic experiments on several carotenoids in solution and in pigment-protein complexes will be presented. The results address how the structures of carotenoids influence their spectroscopic properties and control the efficiency of energy transfer to (B)Chls in light-harvesting pigment-protein complexes. The specific aims and brief descriptions of each chapter are given below.

*Chapter II: Excited state properties of a short conjugated peridinin analogue*

This chapter presents work that builds on results from previous investigations[185,186] which reported the solvent dependence of spectroscopic properties of peridinin and several peridinin analogues having different numbers of carbon-carbon π-electron double bonds, N.[185,186] A very short analogue of peridinin, $C_{29}$-peridinin, was provided for this study by Prof. Shigeo Katsumura. The molecule has five conjugated carbon-carbon double bonds compared to peridinin which contains eight, and it lacks the methyl groups found along the polyene backbone of most carotenoids (Figure 1). The steady-state and transient absorption spectroscopic properties of $C_{29}$-peridinin were investigated and correlated with the results from peridinin and other peridinin analogues.

*Chapter III: Effect of protein aggregation on the spectroscopic properties and excited state kinetics of the LHCII pigment-protein complex from green plants*

This part of the dissertation examines the results from steady-state and time-resolved spectroscopic measurements performed at room and cryogenic temperatures on LHCII complexes prepared from spinach chloroplasts. Monomeric and trimeric forms of LHCII and aggregates formed from them were investigated to elucidate the effect of protein aggregation on the spectroscopic and energy transfer properties of the protein-bound pigments. It has been postulated that protein aggregation is one of the mechanistic factors that affects the rate and efficiency with which excess energy of Chl is dissipated in higher plant systems during the process known as nonphotochemical quenching.[182,187-189] The data obtained from these experiments address this issue of excited state deactivation of the protein-bound Chl and carotenoid pigments.

*Chapter IV: High-efficiency light-harvesting by carotenoids in the LH2 complex from photosynthetic bacteria: Unique adaptation to growth under low-light conditions*

In this chapter, the spectroscopic properties and dynamics of the excited states of rhodopin, rhodopinal and their glucoside derivatives in solution and in LH2 complex are compared and contrasted. Rhodopin, rhodopinal and their glucoside derivatives (Figure 1) are carotenoids that accumulate in different amounts in the photosynthetic bacterium, *Rbl. acidophilus* strain 7050, depending on the intensity of the light under which the organism is grown. In addition, the systematic differences in pigment composition and structure of the chromophores in the LH2 complexes provide an opportunity to explore the effect of these factors on the rate and efficiency of carotenoid-to-BChl energy

transfer. It is found that the enzymatic conversion of rhodopin to rhodopinal by *Rbl. acidophilus* 7050 grown under low-light conditions results in nearly 100% carotenoid-to-BChl energy transfer efficiency in the LH2 complex. This comparative analysis provides insight into how photosynthetic systems are able to adapt and survive under challenging environmental conditions.

*Chapter V: Spectral heterogeneity and carotenoid-to-bacteriochlorophyll energy transfer in LH2 light-harvesting complexes from Allochromatium vinosum*

The work presented in this chapter details the spectroscopic and energy transfer properties of three different spectral forms of the LH2 complex produced by the purple sulfur bacterium *Alc. vinosum* grown under different environmental conditions. Purified B800-820, B800-840 and B800-850 LH2 complexes were provided by Prof. Richard Cogdell at the University of Glasgow, Scotland. All of the complexes were determined by high performance liquid chromatography (HPLC) to contain five carotenoids: lycopene and rhodopin (N = 11), anhydrorhodovibrin and rhodovibrin (N = 12), and spirilloxanthin (N = 13) (Figure 1). Steady-state absorption, fluorescence, and fluorescence excitation, and ultrafast time-resolved absorption spectroscopic experiments were performed on the complexes at room temperature. Spectral reconstructions of the absorption and fluorescence excitation spectra based on the pigment composition revealed significantly more spectral heterogeneity compared to spectra from LH2 complexes isolated from other species of purple bacteria. The data revealed the individual carotenoid-to-BChl energy transfer efficiencies which were correlated with the kinetic data from the ultrafast transient absorption spectroscopic experiments. This systematic

series of LH2 complexes allows exploration of the factors controlling the rate and efficiency of carotenoid-to-BChl energy transfer and, as a complement to the work described in Chapter IV, provides further insight into how photosynthetic systems adapt and survive under varying environmental conditions.

*Chapter VI: Optical spectroscopic investigation of native and recombinant peridinin-chlorophyll a-protein complexes*

The final chapter of this dissertation seeks to understand the relationship between the structure of PCP and the molecular factors controlling its function as a light-harvesting pigment-protein complex. Results from steady-state spectroscopic experiments performed on three PCP complexes, MFPCP, RFPCP and HPPCP, at room and cryogenic temperatures are presented in conjunction with the available crystal structures in an attempt to gain a better understanding of how nature fine tunes the spectroscopic properties of the bound pigments and the molecular mechanisms by which they perform light-harvesting in marine organisms.

## References


(1) Isler, O. *Carotenoids.* Birkhäuser: Basel, 1971.

(2) Young, A.; Britton, G. *Carotenoids in Photosynthesis.* Kluwer Academic: London, 1993.

(3) Frank, H. A.; Cogdell, R. J. Light Capture in Photosynthesis In *Comprehensive Biophysics*; Egelman, E. H., Ed.; Academic Press: Oxford, **2012**; Vol. 8, 94–114.

(4) Cogdell, R. J.; Frank, H. A. *Biochim. Biophys. Acta* **1987**, *895*, 63–79.

(5) Frank, H. A.; Cogdell, R. J. *Photochem. Photobiol.* **1996**, *63*, 257–64.

(6) Britton, G. Functions of Intact Carotenoids In *Carotenoids Volume 4: Natural Functions*; Britton, G., Liaaen-Jensen, S., Pfander, H., Eds.; Birkäuser Verlag: Basel, Switzerland, **2008**; Vol. 4, 189–212.

(7) Telfer, A.; Pascal, A.; Gall, A. Carotenoids in Photosynthesis In *Carotenoids Vol. 4: Natural Functions*; Britton, G., Liaaen-Jensen, S., Pfander, H., Eds.; Birkäuser Verlag: Basel, Switzerland, **2008**; Vol. 4, 265–308.

(8) Cogdell, R. J.; Gillbro, T.; Anderson, P. O.; Liu, R. S. H.; Asato, A. E. *Pure Appl. Chem.* **1994**, *66*, 1041–1046.

(9) Koyama, Y.; Kuki, M.; Andersson, P. O.; Gillbro, T. *Photochem. Photobiol.* **1996**, *63*, 243–256.

(10) Peterman, E. J. G.; Monshouwer, R.; van Stokkum, I. H. M.; van Grondelle, R.; van Amerongen, H. *Chem. Phys. Lett.* **1997**, *264*, 279–284.

(11) Borland, C. F.; Cogdell, R. J.; Land, E. J.; Truscott, T. G. *J. Photochem. Photobiol., B* **1989**, *3*, 237–245.

(12) Cogdell, R. J.; Howard, T. D.; Bittl, R.; Schlodder, E.; Geisenheimer, I.; Lubitz, W. *Philos. Trans. R. Soc. London, Ser. B* **2000**, *355*, 1345–1349.

(13) Foote, C. S. *Acc. Chem. Res.* **1968**, *1*, 104–110.

(14) Foote, C. S.; Denny, R. W. *J. Am. Chem. Soc.* **1968**, *90*, 6233–6235.

(15) Lang, H. P.; Hunter, C. N. *Biochem. J* **1994**, *298*, 197–205.

(16) Jirsakova, V.; Reiss-Husson, F. *FEBS Lett.* **1994**, *353*, 151–154.

(17) Havaux, M. *Trends Plant Sci.* **1998**, *3*, 147–151.

(18) Yamamoto, H.; Bassi, R. Carotenoids: Localization and Function In *Oxygenic Photosynthesis: The Light Reactions*; Ort, D. R., Yocum, C. F., Eds.; Kluwer Academic Publishers: Dordrecht, **1996**, 539–563.

(19) Hobe, S.; Niemeier, H.; Bender, A.; Paulsen, H. *Eur. J. Biochem.* **2000**, *267*, 616–624.

(20) Frank, H. A.; Christensen, R. L. Excited Electronic States, Photochemistry and Photophysics of Carotenoids In *Carotenoids*; Britton, G., Liaaen-Jensen, S., Pfander, H., Eds.; Birkhäuser Basel, **2008**; Vol. 4: Natural Functions, 167–188.

(21) Pariser, R. *J. Chem. Phys.* **1955**, *24*, 250–268.

(22) Hudson, B.; Kohler, B. *Annu. Rev. Phys. Chem.* **1974**, *25*, 437–460.

(23) Callis, P. R.; Scott, T. W.; Albrecht, A. C. *J. Chem. Phys.* **1983**, *78*, 16–22.

(24) Birge, R. R. *Acc. Chem. Res.* **1986**, *19*, 138–146.

(25) Christensen, R. L. The Electronic States of Carotenoids In *The Photochemistry of Carotenoids*; Frank, H. A., Young, A. J., Britton, G., Cogdell, R. J., Eds.; Kluwer Academic Publishers: Dordrecht, **1999**; Vol. 8, 137–159.

(26) Damjanovic, A.; Ritz, T.; Schulten, K. *Phys. Rev. E* **1999**, *59*, 3293–3311.

(27) Hudson, B. S.; Kohler, B. E.; Schulten, K. Linear Polyene Electronic Structure and Potential Surfaces In *Excited States*; Lim, E. D., Ed.; Academic Press: New York, **1982**; Vol. 6, 1–95.

(28) Kohler, B. E. *Journal of Chemical Physics* **1990**, *93*, 5838–5942.

(29) Frank, H. A.; Bautista, J. A.; Gosztola, D.; Wasielewski, M. R. *Photosynth.: Mech. Eff., Proc. Int. Congr. Photosynth., 11th* **1998**, *1*, 473–476.

(30) Frank, H. A.; Bautista, J. A.; Josue, J.; Pendon, Z.; Hiller, R. G.; Sharples, F. P.; Gosztola, D.; Wasielewski, M. R. *J. Phys. Chem. B* **2000**, *104*, 4569–4577.

(31) Andersson, P. O.; Bachilo, S. M.; Chen, R.-L.; Gillbro, T. *J. Phys. Chem.* **1995**, *99*, 16199–16209.

(32) Andersson, P. O.; Gillbro, T. *J. Chem. Phys.* **1995**, *103*, 2509–2519.

(33) Frank, H. A.; Desamero, R. Z. B.; Chynwat, V.; Gebhard, R.; van der Hoef, I.; Jansen, F. J.; Lugtenburg, J.; Gosztola, D.; Wasielewski, M. R. *J. Phys. Chem. A* **1997**, *101*, 149–157.

(34) Andersson, P. A.; Takaichi, S.; Cogdell, R. J.; Gillbro, T. *Photochem. Photobiol.* **2001**, *74*, 549–557.

(35) Yoshizawa, M.; Aoki, H. *Phys. Rev. B: Condens. Matter* **2003**, *67*, 174302

(36) Niedzwiedzki, D.; Koscielecki, J. F.; Cong, H.; Sullivan, J. O.; Gibson, G. N.; Birge, R. R.; Frank, H. A. *J. Phys. Chem. B* **2007**, *111*, 5984–98.

(37) Niedzwiedzki, D. M.; Sandberg, D. J.; Cong, H.; Sandberg, M. N.; Gibson, G. N.; Birge, R. R.; Frank, H. A. *Chem. Phys.* **2009**, *357*, 4–16.

(38) Niedzwiedzki, D. M.; Enriquez, M. M.; LaFountain, A. M.; Frank, H. A. *Chem. Phys.* **2010**, *373*, 80–89.

(39) Bixon, M.; Jortner, J. *J. Chem. Phys.* **1968**, *48*, 715–726.

(40) Englman, R.; Jortner, J. *Mol. Phys.* **1970**, *18*, 145–164.

(41) Tavan, P.; Schulten, K. *Phys. Rev. B: Condens. Matter* **1987**, *36*, 4337–4358.

(42) Chynwat, V.; Frank, H. A. *Chem. Phys.* **1995**, *194*, 237–44.

(43) LeRosen, A. L.; Reid, C. E. *J. Chem. Phys.* **1952**, *20*, 233–236.

(44) Basu, S. *Adv. Quantum Chem.* **1964**, *1*, 145–169.

(45) Andersson, P. O.; Gillbro, T.; Ferguson, L.; Cogdell, R. J. *Photochem. Photobiol.* **1991**, *54*, 353–360.

(46) Nagae, H.; Kuki, M.; Cogdell, R. J.; Koyama, Y. *J. Chem. Phys.* **1994**, *101*, 6750–6765.

(47) Britton, G. Uv/Visible Spectroscopy In *Carotenoids Vol. 1b: Spectroscopy*; Britton, G., Liaaen-Jensen, S., Pfander, H., Eds.; Birkhäuser Verlag: Basel-Boston-Berlin, **1995**, 13–62.

(48) Macpherson, A. N.; Gillbro, T. *J. Phys. Chem. A* **1998**, *102*, 5049–5058.

(49) Frank, H. A.; Young, A. J.; Britton, G.; Cogdell, R. J. The Photochemistry of Carotenoids In *Advances in Photosynthesis*; Govindjee, Ed.; Kluwer Academic Publishers: Dordrecht, **1999**; Vol. 8.

(50) Polívka, T.; Sundström, V. *Chem. Rev.* **2004**, *104*, 2021–2071.

(51) Frank, H. A.; Polivka, T. Energy Transfer from Carotenoids to Bacteriochlorophylls In *The Purple Phototrophic Bacteria*; Hunter, C. N., Daldal, F., Thurnauer, M. C., Beatty, J. T., Eds.; Springer: The Netherlands, **2008**, 213–230.

(52) Polívka, T.; Frank, H. A. *Acc. Chem. Res.* **2010**, *43*, 1125–1134.

(53) Orlandi, G.; Zerbetto, F.; Zgierski, M. Z. *Chem. Rev.* **1991**, *91*, 867–891.

(54) Schmidt, M.; Tavan, P. *J. Chem. Phys.* **2012**, *136*, 124309: 1–13.

(55) Di Donato, M.; Centellas, M. S.; Lapini, A.; Lima, M.; Avila, F.; Santoro, F.; Cappelli, C.; Righini, R. *J. Phys. Chem. B* **2014**, *118*, 9613–9630.

(56) Sashima, T.; Nagae, H.; Kuki, M.; Koyama, Y. *Chem. Phys. Lett.* **1999**, *299*, 187–194.

(57) Gradinaru, C. C.; Kennis, J. T. M.; Papagiannakis, E.; van Stokkum, I. H. M.; Cogdell, R. J.; Fleming, G. R.; Niederman, R. A.; van Grondelle, R. *Proc. Natl. Acad. Sci. USA* **2001**, *98*, 2364–2369.

(58) Papagiannakis, E.; Kennis, J. T. M.; van Stokkum, I. H. M.; Cogdell, R. J.; van Grondelle, R. *Proc. Natl. Acad. Sci. USA* **2002**, *99*, 6017–6022.

(59) Wohlleben, W.; Buckup, T.; Herek, J. L.; Cogdell, R. J.; Motzkus, M. *Biophys. J.* **2003**, *85*, 442–450.

(60) Larsen, D. S.; Papagiannakis, E.; van Stokkum, I. H. M.; Vengris, M.; Kennis, J. T. M.; van Grondelle, R. *Chem. Phys. Lett.* **2003**, *381*, 733–742.

(61) Ostroumov, E. E.; Müller, M. G.; Reus, M.; Holzwarth, A. R. *J. Phys. Chem. A* **2011**, *115*, 3698–3712.

(62) Hauer, J.; Maiuri, M.; Viola, D.; Lukes, V.; Henry, S.; Carey, A.-M.; Cogdell, R. J.; Cerullo, G.; Polli, D. *The Journal of Physical Chemistry A* **2013**, *117*, 6303–6310.

(63) Ostroumov, E. E.; Mulvaney, R. M.; Cogdell, R. J.; Scholes, G. D. *Science* **2013**, *340*, 52–56.

(64) Hashimoto, H.; Yanagi, K.; Yoshizawa, M.; Polli, D.; Cerullo, G.; Lanzani, G.; De Silvestri, S.; Gardiner, A. T.; Cogdell, R. J. *Arch. Biochem. Biophys.* **2004**, *430*, 61–69.

(65) Koyama, Y.; Rondonuwu, F. S.; Fujii, R.; Watanabe, Y. *Biopolymers* **2004**, *74*, 2–18.

(66) Polivka, T.; Sundström, V. *Chem. Phys. Lett.* **2009**, *477*, 1–11.

(67) Beck, W. F.; Bishop, M. M.; Roscioli, J. D.; Ghosh, S.; Frank, H. A. *Archives of Biochemistry and Biophysics* **2015**, *In press*.

(68) Zigmantas, D.; Polivka, T.; Hiller, R. G.; Yartsev, A.; Sundström, V. *J. Phys. Chem. A* **2001**, *105*, 10296–10306.

(69) Zigmantas, D.; Hiller, R. G.; Sharples, F. P.; Frank, H. A.; Sundström, V.; Polivka, T. *Phys. Chem. Chem. Phys.* **2004**, *6*, 3009–3016.

(70) Chábera, P.; Fuciman, M.; Hříbek, P.; Polívka, T. *Phys. Chem. Chem. Phys.* **2009**, *11*, 8795–8803.

(71) Polivka, T.; Kaligotla, S.; Chabera, P.; Frank, H. A. *Phys. Chem. Chem. Phys.* **2011**, *13*, 10787–10796.

(72) Bautista, J. A.; Connors, R. E.; Raju, B. B.; Hiller, R. G.; Sharples, F. P.; Gosztola, D.; Wasielewski, M. R.; Frank, H. A. *J. Phys. Chem. B* **1999**, *103*, 8751–8758.

(73) Zigmantas, D.; Hiller, R. G.; Yartsev, A.; Sundström, V.; Polivka, T. *J. Phys. Chem. B* **2003**, *107*, 5339–5348.

(74) Vaswani, H. M.; Hsu, C. P.; Head-Gordon, M.; Fleming, G. R. *J. Phys. Chem. B* **2003**, *107*, 7940–7946.

(75) Papagiannakis, E.; Vengris, M.; Larsen, D. S.; van Stokkum, I. H. M.; Hiller, R. G.; van Grondelle, R. *J. Phys. Chem. B* **2006**, *110*, 512–521.

(76) Kosumi, D.; Kusumoto, T.; Fujii, R.; Sugisaki, M.; Iinuma, Y.; Oka, N.; Takaesu, Y.; Taira, T.; Iha, M.; Frank, H. A.et al. *Chem. Phys. Lett.* **2009**, *483*, 95–100.

(77) Kosumi, D.; Kusumoto, T.; Fujii, R.; Sugisaki, M.; Iinuma, Y.; Oka, N.; Takaesu, Y.; Taira, T.; Iha, M.; Frank, H. A.et al. *J. Lumin.* **2011**, *131*, 515–518.

(78) Shima, S.; Ilagan, R. P.; Gillespie, N.; Sommer, B. J.; Hiller, R. G.; Sharples, F. P.; Frank, H. A.; Birge, R. R. *J. Phys. Chem. A* **2003**, *107*, 8052–8066.

(79) Wagner, N. L.; Greco, J. A.; Enriquez, M. M.; Frank, H. A.; Birge, R. R. *Biophys. J.* **2013**, *104*, 1314–1325.

(80) Blankenship, R. E. *Molecular Mechanisms of Photosynthesis*. Blackwell Science: Oxford, 2002.

(81) Van Grondelle, R.; Dekker, J. P.; Gillbro, T.; Sundström, V. *Biochim. Biophys. Acta* **1994**, *1187*, 1–65.

(82) Papiz, M. Z.; Prince, S. M.; Howard, T.; Cogdell, R. J.; Isaacs, N. W. *J. Mol. Biol.* **2003**, *326*, 1523–1538.

(83) Hofmann, E.; Wrench, P. M.; Sharples, F. P.; Hiller, R. G.; Welte, W.; Diederichs, K. *Science* **1996**, *272*, 1788–1791.

(84) Liu, Z. F.; Yan, H. C.; Wang, K. B.; Kuang, T. Y.; Zhang, J. P.; Gui, L. L.; An, X. M.; Chang, W. R. *Nature* **2004**, *428*, 287–292.

(85) Humphrey, W.; Dalke, A.; Schulten, K. *J. Mol. Graphics Modell.* **1996**, *14*, 33–38.

(86) Hawthornthwaite, A. M.; Cogdell, R. J. *Chlorophylls* **1991**, 493–528, 1 plate.

(87) Fyfe, P. K.; Cogdell, R. J. *Current Opinion in Structural Biology* **1996**, *6*, 467–472.

(88) Cogdell, R. J.; Isaacs, N. W.; Freer, A. A.; Howard, T. D.; Gardiner, A. T.; Prince, S. M.; Papiz, M. Z. *FEBS Lett.* **2003**, *555*, 35–39.

(89) Gabrielsen, M.; Gardiner, A. T.; Cogdell, R. J. Peripheral Complexes of Purple Bacteria In *The Purple Phototrophic Bacteria*; Hunter, C. N., Daldal, F., Thurnauer, M. C., Beatty, J. T., Eds.; Springer: Dordrecht, The Netherlands, **2009**; Vol. 28, 135–153.

(90) Zuber, H.; Cogdell, R. J. Structure and Organization of Purple Bacterial Antenna Complexes In *Advances in Photosynthesis* Blankenship, R. E., Madigan, M. T., Bauer, C. E., Eds.; Kluwer Academic Publishers: Springer Netherlands, **1995**; Vol. 2, 315–48.

(91) Bauer, C. E.; Bird, T. H. *Cell* **1996**, *85*, 5–8.

(92) Phillips-Jones, M. K. *Symp. Soc. Gen. Microbiol.* **1998**, *56*, 159–184.

(93) Cogdell, R. J.; Isaacs, N. W.; Howard, T. D.; McLuskey, K.; Fraser, N. J.; Prince, S. M. *J. Bacteriol.* **1999**, *181*, 3869–3879.

(94) Cogdell, R. J.; Howard, T. D.; Isaacs, N. W.; McLuskey, K.; Gardiner, A. T. *Photosynth. Res.* **2002**, *74*, 135–141.

(95) McDermott, G.; Prince, S. M.; Freer, A. A.; Hawthornthwaite-Lawless, A. M.; Papiz, M. Z.; Cogdell, R. J.; Isaacs, N. W. *Nature* **1995**, *374*, 517–521.

(96) Prince, S. M.; Papiz, M. Z.; Freer, A. A.; McDermott, G.; Hawthornthwaite-Lawless, A. M.; Cogdell, R. J.; Isaacs, N. W. *J. Mol. Biol.* **1997**, *268*, 412–423.

(97) Koepke, J.; Hu, X.; Schulten, K.; Michel, H. *Structure* **1996**, *4*, 581–597.

(98) Cogdell, R. J.; Gall, A.; Köhler, J. *Q. Rev. Biophys.* **2006**, *39*, 227–324.

(99) Sauer, K.; Cogdell, R. J.; Prince, S. M.; Freer, A.; Isaacs, N. W.; Scheer, H. *Photochem. Photobiol.* **1996**, *64*, 564–576.

(100) Alden, R. G.; Johnson, E.; Nagarajan, V.; Parson, W. W.; Law, C. J.; Cogdell, R. G. *J. Phys. Chem. B* **1997**, *101*, 4667–4680.

(101) Angerhofer, A.; Cogdell, R. J.; Hipkins, M. F. *Biochim. Biophys. Acta* **1986**, *848*, 333–341.

(102) McLuskey, K.; Prince, S. M.; Cogdell, R. J.; Isaacs, N. W. *Biochemistry* **2001**, *40*, 8783–8789.

(103) Gardiner, A. T.; Cogdell, R. J.; Takaichi, S. *Photosynth. Res.* **1993**, *38*, 159–167.

(104) Zuber, H.; Brunisholz, R. A. Structure and Function of Antenna Polypeptides and Chlorophyll-Protein Complexes: Principles and Variability In *Chlorophylls*; Scheer, H., Ed.; CRC Press: Boca Raton, Florida, **1991**, 627–704.

(105) Fowler, G. J.; Sockalingum, G. D.; Robert, B.; Hunter, C. N. *Biochem. J.* **1994**, *299*, 695–700.

(106) Sturgis, J. N.; Jirsakova, V.; Reiss-Husson, F.; Cogdell, R. J.; Robert, B. *Biochemistry* **1995**, *34*, 517–23.

(107) Gudowska-Nowak, E.; Newton, M. D.; Fajer, J. *J. Phys. Chem.* **1990**, *94*, 5795–5801.

(108) Wassink, E. C.; Katz, E.; Dorrestein, R. *Enzymologia* **1939**, *7*, 113–129.

(109) Garcia, A.; Vernon, L. P.; Mollenhauer, H. *Biochemistry* **1966**, *5*, 2399–2407.

(110) Mechler, B.; Oelze, J. *Arch. Microbiol.* **1978**, *118*, 91–97.

(111) Mechler, B.; Oelze, J. *Arch. Microbiol.* **1978**, *118*, 99–108.

(112) Hayashi, H.; Morita, S. *J. Biochem.* **1980**, *88*, 1251–1258.

(113) Carey, A.-M.; Hacking, K.; Picken, N.; Honkanen, S.; Kelly, S.; Niedzwiedzki, D. M.; Blankenship, R. E.; Shimizu, Y.; Wang-Otomo, Z.-Y.; Cogdell, R. J. *BBA-Bioenergetics* **2014**, *1837*, 1849–1860.

(114) Mechler, B.; Oelze, J. *Arch. Microbiol.* **1978**, *118*, 109–114.

(115) Hayashi, H.; Nozawa, T.; Hatano, M.; Morita, S. *J. Biochem.* **1981**, *89*, 1853–1861.

(116) Cogdell, R. J.; Scheer, H. *Photochem. Photobiol.* **1985**, *42*, 669–78.

(117) Kereïche, S.; Bourinet, L.; Keegstra, W.; Arteni, A. A.; Verbavatz, J.-M.; Boekema, E. J.; Robert, B.; Gall, A. *FEBS Lett.* **2008**, *582*, 3650–3656.

(118) Niedzwiedzki, D. M.; Bina, D.; Picken, N.; Honkanen, S.; Blankenship, R. E.; Holten, D.; Cogdell, R. J. *BBA-Bioenergetics* **2012**, *1817*, 1576–1587.

(119) Löhner, A.; Carey, A.-M.; Hacking, K.; Picken, N.; Kelly, S.; Cogdell, R. J.; Köhler, J. *Photosynth. Res.* **2015**, *123*, 23–31.

(120) Hiller, R. G.; Anderson, J. M.; Larkum, A. W. D. The Chlorophyll-Protein Complexes of Algae In *Chlorophylls*; Scheer, H., Ed.; CRC Press: Boca Raton, Florida, **1991**, 529–547.

(121) Macpherson, A. N.; Hiller, R. G. Light-Harvesting Systems in Chlorophyll *c*-Containing Algae In *Light-Harvesting Antennas in Photosynthesis*; Green, B. R., Parson, W. W., Eds.; Kluwer Academic Publishers: Dordrecht, The Netherlands, **2003**; Vol. 13, 323–352.

(122) Sharples, F. P.; Wrench, P. M.; Ou, K.; Hiller, R. G. *Biochim. Biophys. Acta* **1996**, *1276*, 117–123.

(123) Carbonera, D.; Giacometti, G.; Agostini, G. *Spectrochim. Acta* **1995**, *51A*, 115–123.

(124) Bautista, J. A.; Hiller, R. G.; Sharples, F. P.; Gosztola, D.; Wasielewski, M.; Frank, H. A. *J. Phys. Chem. A* **1999**, *103*, 2267–2273.

(125) Carbonera, D.; Giacometti, G.; Segre, U.; Hofmann, E.; Hiller, R. G. *J. Phys. Chem. B* **1999**, *103*, 6349–6356.

(126) Kleima, F. J.; Wendling, M.; Hofmann, E.; Peterman, E. J. G.; van Grondelle, R.; van Amerongen, H. *Biochemistry* **2000**, *39*, 5184–5195.

(127) Krueger, B. P.; Lampoura, S. S.; van Stokkum, I. H. M.; Papagiannakis, E.; Salverda, J. M.; Gradinaru, C. C.; Rutkauskas, D.; Hiller, R. G.; van Grondelle, R. *Biophys. J.* **2001**, *80*, 2843–2855.

(128) Lampoura, S. S.; Krueger, B. P.; van Stokkum, I. H.; Salverda, J. M.; Gradinaru, C. C.; Rutkauskas, D.; Hiller, R. G.; van Grondelle, R. *Int. J. Mod. Phys. B* **2001**, *15*, 3849–3852.

(129) Zimmermann, J.; Linden, P. A.; Vaswani, H. M.; Hiller, R. G.; Fleming, G. R. *J. Phys. Chem. B* **2002**, *106*, 9418–9423.

(130) Zigmantas, D.; Hiller, R. G.; Sundström, V.; Polivka, T. *Proc. Natl. Acad. Sci. USA* **2002**, *99*, 16760–16765.

(131) Linden, P. A.; Zimmermann, J.; Brixner, T.; Holt, N. E.; Vaswani, H. M.; Hiller, R. G.; Fleming, G. R. *J. Phys. Chem. B* **2004**, *108*, 10340–10345.

(132) Ilagan, R. P.; Shima, S.; Melkozernov, A.; Lin, S.; Blankenship, R. E.; Sharples, F. P.; Hiller, R. G.; Birge, R. R.; Frank, H. A. *Biochemistry* **2004**, *43*, 1478–1487.

(133) Krikunova, M.; Lokstein, H.; Leupold, D.; Hiller, R. G.; Voigt, B. *Biophys. J.* **2006**, *90*, 261–271.

(134) Ilagan, R. P.; Koscielecki, J. F.; Hiller, R. G.; Sharples, F. P.; Gibson, G. N.; Birge, R. R.; Frank, H. A. *Biochemistry* **2006**, *45*, 14052–14063.

(135) Polívka, T.; Hiller, R. G.; Frank, H. A. *Archives of Biochemistry and Biophysics* **2007**, *458*, 111–120.

(136) Wormke, S.; Mackowski, S.; Brotosudarmo, T. H. P.; Jung, C.; Zurnbusch, A.; Ehrl, M.; Scheer, H.; HofMann, E.; Hiller, R. G.; Brauchle, C. *Biochim. Biophys. Acta-Bioenerg.* **2007**, *1767*, 956–964.

(137) Van Stokkum, I. H. M.; Papagiannakis, E.; Vengris, M.; Salverda, J. M.; Polivka, T.; Zigmantas, D.; Larsen, D. S.; Lampoura, S. S.; Hiller, R. G.; van Grondelle, R. *Chem. Phys.* **2009**, *357*, 70–78.

(138) Miller, D. J.; Catmull, J.; Puskeiler, R.; Tweedale, H.; Sharples, F. P.; Hiller, R. G. *Photosynth. Res.* **2005**, *86*, 229–240.

(139) Polívka, T.; Pascher, T.; Sundström, V.; Hiller, R. G. *Photosynth. Res.* **2005**, *86*, 217–227.

(140) Brotosudarmo, T. H. P.; Hofmann, E.; Hiller, R. G.; Wormke, S.; Mackowski, S.; Zumbusch, A.; Brauchle, C.; Scheer, H. *FEBS Lett.* **2006**, *580*, 5257–5262.

(141) Ilagan, R. P.; Chapp, T. W.; Hiller, R. G.; Sharples, F. P.; Polivka, T.; Frank, H. A. *Photosynth. Res.* **2006**, *90*, 5–15.

(142) Mackowski, S.; Wormke, S.; Brotosudarmo, T. H. P.; Jung, C.; Hiller, R. G.; Scheer, H.; Brauchle, C. *Biophys. J.* **2007**, *93*, 3249–3258.

(143) Polivka, T.; Pascher, T.; Hiller, R. G. *Biophys. J.* **2008**, *94*, 3198–3207.

(144) Mackowski, S.; Woermke, S.; Brotosudarmo, T. H. P.; Scheer, H.; Brauchle, C. *Photosynth. Res.* **2008**, *95*, 253–260.

(145) Wormke, S.; Mackowski, S.; Schaller, A.; Brotosudarmo, T. H. P.; Johanning, S.; Scheer, H.; Brauchle, C. *J. Fluor.* **2008**, *18*, 611–617.

(146) Di Valentin, M.; Agostini, G.; Salvadori, E.; Ceola, S.; Giacometti, G. M.; Hiller, R. G.; Carbonera, D. *Biochim. Biophys. Acta-Bioenerg.* **2009**, *1787*, 168–175.

(147) Schulte, T.; Niedzwiedzki, D. M.; Birge, R. R.; Hiller, R. G.; Polívka, T.; Hofmann, E.; Frank, H. A. *Proc. Natl. Acad. Sci. USA* **2009**, *106*, 20764–20769.

(148) Schulte, T.; Johanning, S.; Hofmann, E. *European Journal of Cell Biology* **2010**, *89*, 990–997.

(149) Song, P. S.; Koka, P.; Prézelin, B. B.; Haxo, F. T. *Biochemistry* **1976**, *15*, 4422–4427.

(150) Hofmann, E., 1999.

(151) Hiller, R. G.; Crossley, L. G.; Wrench, P. M.; Santucci, N.; Hofmann, E. *Molecular Genetics and Genomics* **2001**, *266*, 254–259.

(152) Green, B. R.; Durnford, D. G. *Annu. Rev. Plant Physiol. Plant Mol. Biol* **1996**, *47*, 685–714.

(153) Green, B. R.; Parson, W. W. *Light-Harvesting Antennas in Photosynthesis.* Kluwer Academic Publishers: Dordrecht, 2003.

(154) Witt, H. T.; Witt, I.; Krauss, N.; Hinrichs, W.; Fromme, P.; Saenger, W. *Biophys. J.* **1994**, *66*, A2–A2.

(155) Fromme, P.; Mathis, P. *Photosynth. Res.* **2004**, *80*, 109–124.

(156) Peter, G. F.; Thornber, J. P. *J. Biol. Chem.* **1991**, *266*, 16745–16754.

(157) Nelson, N.; Yocum, C. F. *Annual Reviews of Plant Biology* **2006**, *57*, 521–565.

(158) Hankamer, B.; Barber, J.; Boekema, E. J. *Annual Review of Plant Physiology and Plant Molecular Biology* **1997**, *48*, 641-671.

(159) Williamson, A.; Conlan, B.; Hillier, W.; Wydrzynski, T. J. *Photosynth. Res.* **2011**, *107*, 71–86.

(160) Bassi, R.; Sandona, D.; Croce, R. *Physiol. Plant.* **1997**, *100*, 769–779.

(161) Jansson, S. *Biochim. Biophys. Acta* **1994**, *1184*, 1–19.

(162) Paulsen, H. *Photochem. Photobiol.* **1995**, *62*, 367–382.

(163) Jansson, S.; Pichersky, E.; Bassi, R.; Green, B. R.; Ikeuchi, M.; Melis, A.; Simpson, D. J.; Spangfort, M.; Staehelin, L. A.; Thornber, J. P. *Plant Molecular Biology Reporter* **1992**, *10*, 242–253.

(164) Jansson, S. *Trends Plant Sci.* **1999**, *4*, 236–240.

(165) Jackowski, G.; Kacprzak, K.; Jansson, S. *BBA-Bioenergetics* **2001**, *1504*, 340–345.

(166) Standfuss, J.; Kühlbrandt, W. *The Journal of Biological Chemistry* **2004**, *279*, 36884–36891.

(167) Dunahay, T. G.; Staehelin, L. A. *Plant Physiol.* **1986**, *80*, 429–434.

(168) Bassi, R.; Rigoni, F.; Barbato, R.; Giacometti, G. M. *J. Biol. Chem.* **1987**, *262*, 13333–13341.

(169) Machold, O.; Meister, A. *BBA-Bioenergetics* **1979**, *546*, 472–480.

(170) Murata, N. *Biochim. Biophys. Acta* **1969**, *172*, 242–251.

(171) Bonaventura, C.; Myers, J. *BBA-Bioenergetics* **1969**, *189*, 366–383.

(172) Murata, N. *Photosynth. Res.* **2009**, *99*, 155–160.

(173) Wientjes, E.; Amerongen, H. v.; Croce, R. *BBA-Bioenergetics* **2013**, *1827*, 420–426.

(174) Standfuss, J.; van Scheltinga, A. C. T.; Lamborghini, M.; Külbrandt, W. *EMBO J.* **2005**, *24*, 919–928.

(175) Kühlbrandt, W.; Wang, D. N.; Fujiyoshi, Y. *Nature* **1994**, *367*, 614–621.

(176) Ruban, A. V.; Lee, P. J.; Wentworth, M.; Young, A. J.; Horton, P. *J. Biol. Chem.* **1999**, *274*, 10458–10465.

(177) Croce, R.; Weiss, S.; Bassi, R. *J. Biol. Chem.* **1999**, *274*, 29613–29623.

(178) Demmig-Adams, B.; Adams, W. W. I. *Annual Review of Plant Physiology and Plant Molecular Biology* **1992**, *43*, 599–626.

(179) Havaux, M.; Niyogi, K. K. *Proc. Natl. Acad. Sci. USA* **1999**, *96*, 8762–8767.

(180) Müller, P.; Li, X.-P.; Niyogi, K. K. *Plant Physiol.* **2001**, *125*, 1588–1566.

(181) Havaux, M.; Dall'Osto, L.; Cuine, S.; Giuliano, G.; Bassi, R. *J. Biol. Chem.* **2004**, *279*, 13878–13888.

(182) Pascal, A. A.; Liu, Z.; Broess, K.; van Oort, B.; van Amerongen, H.; Wang, C.; Horton, P.; Robert, B.; Chang, W.; Ruban, A. V. *Nature* **2005**, *436*, 134–137.

(183) Demmig-Adams, B. *Photosynth. Res.* **2006**, *76*, 73–80.

(184) Dall'Osto, L.; Cazzaniga, S.; Havaux, M.; Bassi, R. *Molecular Plant* **2010**, *3*, 576–593.

(185) Niedzwiedzki, D. M.; Chatterjee, N.; Enriquez, M. M.; Kajikawa, T.; Hasegawa, S.; Katsumura, S.; Frank, H. A. *J. Phys. Chem. B* **2009**, *113*, 13604–13612.

(186) Niedzwiedzki, D. M.; Kajikawa, T.; Aoki, K.; Katsumura, S.; Frank, H. A. *J. Phys. Chem. B* **2013**, *117*, 6874–6887.

(187) Ruban, A. V.; Berera, R.; Ilioaia, C.; van Stokkum, I. H. M.; Kennis, J. T. M.; Pascal, A. A.; van Amerongen, H.; Robert, B.; Horton, P.; van Grondelle, R. *Nature* **2007**, *450*, 575–579.

(188) Miloslavina, Y.; Wehner, A.; Lambrev, P. H.; Wientjes, E.; Reus, M.; Garab, G.; Croce, R.; Holzwarth, A. R. *FEBS Lett.* **2008**, *582*, 3625–3631.

(189) Holzwarth, A. R.; Miloslavina, Y.; Nilkens, M.; Jahns, P. *Chem. Phys. Lett.* **2009**, *483*, 262–267.

# *Chapter II*

# *Excited state properties of a short π-electron conjugated peridinin analogue*

## Introduction

Ocean-dwelling algal organisms are well-known for the proliferation of carbonyl-containing carotenoids in light-harvesting pigment-protein complexes that facilitate capturing sunlight for photosynthetic growth.[1-3] These functionally derivatized keto-carotenoids exhibit spectroscopic and kinetic behavior that can be strikingly different from carotenoids that lack a carbonyl group in conjugation with the π-electron system of conjugated carbon-carbon double bonds. One of the characteristic differences is that the lifetime of the lowest-lying excited state, $S_1$, of carotenoids possessing a carbonyl group in conjugation with the polyene backbone is strongly dependent on the polarity of the solvent.[4-8] This is unusual because the $S_1$ state of carotenoids is a state into which absorption from the ground state, $S_0$, is quantum mechanically forbidden, and therefore the spectra and dynamics associated with $S_1$ are typically not affected by the solvent environment.[9-13] The forbiddeness of the $S_0 \rightarrow S_1$ transition is due to the fact that both $S_0$ and $S_1$ have $A_g^-$ symmetry in the idealized $C_{2h}$ point group. According to the selection rules for one-photon optical transitions, a change in symmetry and pseudoparity is required for the transition to be allowed. The strongly allowed transition that gives carotenoids their vibrant visible coloration occurs between the $S_0$ ($1^1A_g^-$) and $S_2$ ($1^1B_u^+$) states, which differ in both symmetry and pseudoparity.[14]

The dependence of the $S_1$ lifetime of carbonyl-containing carotenoids has been explained by the formation of an intramolecular charge transfer (ICT) state whose energy and electronic coupling is modulated by the solvent polarity.[5] Recent ultrafast time-resolved spectroscopic and computational investigations of the carbonyl-containing carotenoid, peridinin, have suggested that after photoexcitation into the $S_2$ ($1^1B_u^+$) state, a shift of electron density from the allenic side of peridinin toward the lactone ring occurs resulting in a bond-order reversal along the polyene chain.[15] These effects are accompanied by solvent reorganization, which together generate the ICT state through quantum mechanical mixing of the $S_2$ ($1^1B_u^+$) ionic state with the lowest-lying $S_1$ ($2^1A_g^-$) covalent state. The charge transfer character evolves in less than 100 fs and results in a very large (~35 D) dipole moment.

In order to explore the nature of the ICT state, several analogues of peridinin having various extents of π-electron conjugation (Figure 1) have been synthesized and characterized spectroscopically and computationally.[16-20] Naturally-occurring peridinin has a $C_{37}$ carbon skeleton rather than the typical $C_{40}$ system present in most carotenoids.[21] In this chapter, new results are presented on the shortest member of this series of synthetic peridinins, an analogue that has a $C_{29}$ carbon skeleton, hereafter denoted $C_{29}$-peridinin. This molecule is not only a shortened version of peridinin: $C_{29}$-peridinin has five conjugated carbon-carbon double bonds compared to eight possessed by peridinin (Figure 1), but it also lacks the methyl functionalities typically present along the polyene chain of carotenoids. These structural modifications lead to unique excited state spectral and kinetic properties and provide important insights regarding the factors that control the

photophysics of peridinin and other carbonyl-containing carotenoids that are critical components in the light-harvesting systems of an abundance of photosynthetic organisms.

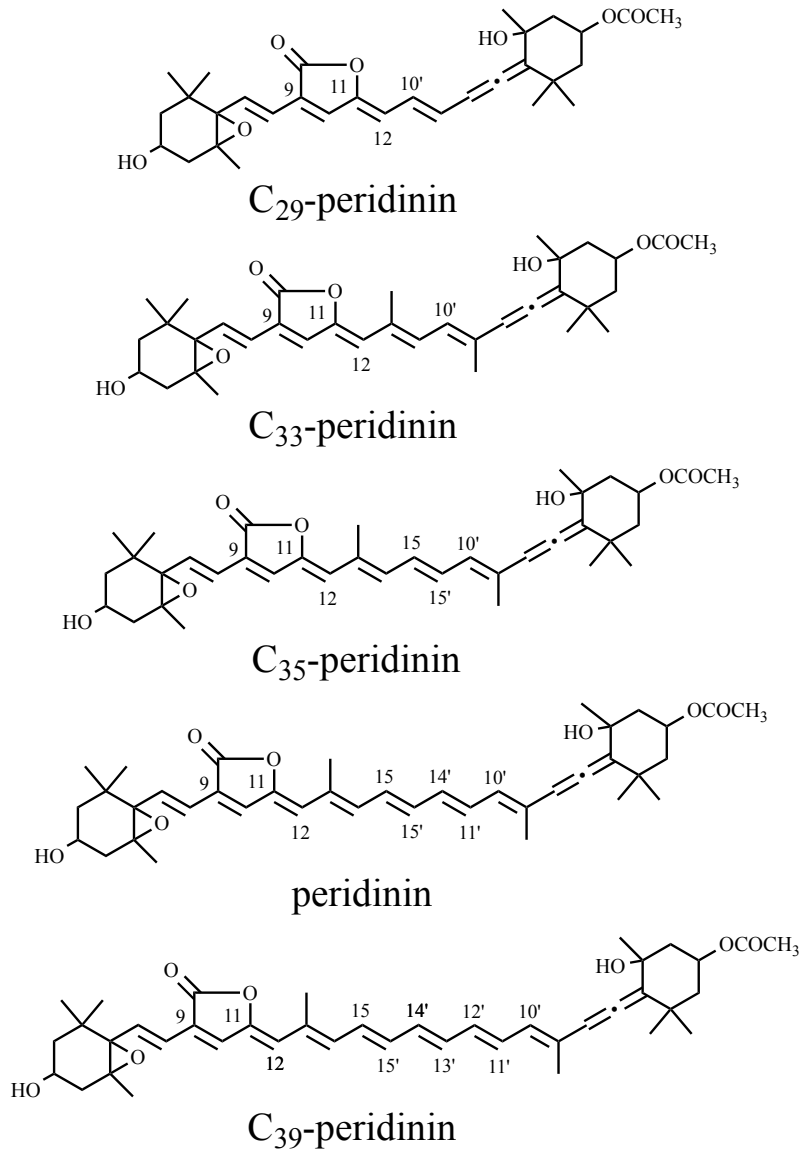


**Figure 1.** Structure of $C_{29}$-peridinin and other peridinins.

# Materials and Methods

***Sample preparation***

The details of the synthesis of $C_{29}$-peridinin will be reported elsewhere. Prior to the optical experiments, the molecule was dissolved in acetonitrile and injected into a Millipore Waters 600E high-performance liquid chromatograph (HPLC) employing a $C_{30}$ YMC column and an isocratic mobile phase protocol consisting of 87:10:3, acetonitrile:methanol:water (v/v/v) at a flow rate of either 0.8 or 1 mL/min. The sample volume was 200 μL for each injection. Pure $C_{29}$-peridinin eluting from the column was identified using a Waters 996 single diode-array detector, collected, dried using a gentle stream of gaseous nitrogen, and stored at −80°C until ready for use.

***Spectroscopic Methods***

*Steady state absorption and fluorescence*

All of the spectroscopic experiments were carried out at room temperature. $C_{29}$-peridinin was dissolved in spectroscopic grade *n*-hexane (Sigma Aldrich), tetrahydrofuran (Alfa Aesar), acetonitrile (Sigma Aldrich), and methanol (Sigma Aldrich). Absorption spectra were recorded using a Cary 50 UV-visible spectrometer. Fluorescence spectroscopy was carried out using a Jobin-Yvon Horiba Fluorolog-3 model FL3-22 equipped with double monochromators having 1200 grooves/mm gratings, a Hamamatsu R928P photomultiplier tube detector, and a 450 W ozone-free Osram XBO xenon arc lamp. The emission spectra were collected using 376 nm (*n*-hexane) and 400 nm (tetrahydrofuran, methanol, acetonitrile) excitation at a right angle relative to the emission beam and corrected using a file generated using a 200 W quartz tungsten-

halogen filament lamp. Both the emission and excitation slit widths were set to a bandpass value of 3 nm (*n*-hexane, tetrahyrofuran, methanol) or 5 nm (acetonitrile).

*Time-resolved fluorescence*

Time-resolved fluorescence data were obtained at room temperature using the setup previously described.[20] The samples had an OD of ~0.3 at the maximum in their absorption recorded in a 1 cm cuvette. Depending on the solvent, the excitation beam had a wavelength between 380 and 430 nm and was positioned at a right angle relative to the detector. The beam power was 40–130 mW (at 80 MHz frequency) which corresponds to 0.5–1.5 nJ of energy and, with a spot size ~0.5 mm in diameter, yielded a photon intensity of 5–10 x $10^{11}$ photons/cm$^2$.

*Transient absorption spectroscopy*

Time-resolved pump-probe absorption experiments were performed at room temperature using Helios, a femtosecond transient absorption spectrometer (Ultrafast Systems LLC, Sarasota, FL, USA) coupled to a femtosecond laser system described previously.[22] The samples were excited with pump beam energy of 500 nJ in a spot size of 1 mm diameter corresponding to an intensity of ~2 × $10^{14}$ photons/cm$^2$. The pump wavelength was 400 nm. Steady-state absorption spectra were recorded before and after all transient experiments to confirm the stability of the $C_{29}$-peridinin sample during laser excitation. The procedure for processing the ultrafast transient absorption data is given in Appendix A.

## Results and Discussion

To better understand the nature of the steady-state absorption and fluorescence spectral features of $C_{29}$-peridinin, it is useful to view them in the same context as the spectra recorded from peridinin and the $C_{33}$-, $C_{35}$- and $C_{39}$-peridinin analogues in the same solvents. The steady-state absorption and fluorescence spectra recorded at room temperature in *n*-hexane and methanol from all of these molecules are shown in Figure 2.

The absorption spectrum of $C_{29}$-peridinin, which corresponds to an $S_0 \rightarrow S_2$ transition, is significantly blue-shifted relative to the spectra from the other molecules. In *n*-hexane, the spectral origin (0–0) vibronic band of $C_{29}$-peridinin is sufficiently resolved that it can be located at ~400 nm; i.e., the $S_0 \rightarrow S_2$ transition corresponds to an energy of ~25,000 $cm^{-1}$. As the solvent polarity increases, the absorption band broadens substantially, but retains a small amount of vibronic structure compared to the other peridinins, as can be seen in the absorption spectrum of $C_{29}$-peridinin in methanol (bottom left panel of Figure 2).

Room temperature fluorescence spectra of $C_{29}$-peridinin in *n*-hexane and methanol are also shown in Figure 2 along with the spectra from peridinin and the other peridinin analogues. The spectra are broad and red-shifted compared to their respective absorption spectra in both solvents, but clearly resemble fluorescence emission lineshapes associated with the $S_1 \rightarrow S_0$ transition. An exception is $C_{39}$-peridinin, which displays emission from both the $S_1$ state, whose (0–0) band is at ~650 nm, and the $S_2$ state, which is characterized by an emission band at ~540 nm in both solvents.

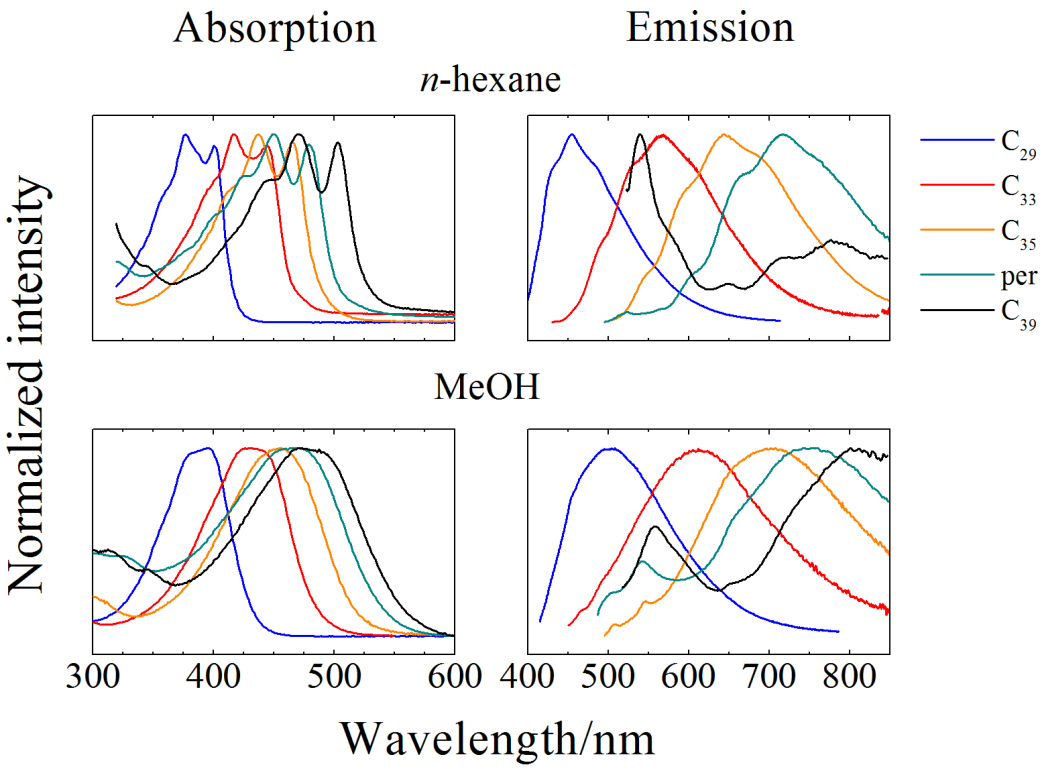


**Figure 2.** Steady-state absorption and emission spectra. Data for peridinin, $C_{33}$-, $C_{35}$-, and $C_{39}$- peridinin in *n*-hexane and methanol were taken from reference 17.

As the π-electron conjugated chain length decreases, the energy difference between the $S_2$ and $S_1$ states also decreases. For the longest molecule in the series, $C_{39}$-peridinin, the energy difference between the $S_2$ and $S_1$ states is ~3100 $cm^{-1}$ based on the position of their (0–0) absorption and fluorescence bands. For $C_{29}$-peridinin, the (0–0) band of the $S_1$ fluorescence occurs at ~410 nm which is very close to the (0–0) band of the absorption spectrum at ~400 nm, resulting in a substantially smaller $S_2$–$S_1$ energy difference of ~600 $cm^{-1}$. Also, the intensity of emission decreases substantially as the solvent polarity increases. The relative fluorescence quantum yield of $C_{29}$-peridinin is smaller by approximately an order of magnitude in methanol compared to in the nonpolar solvent, *n*-hexane.

The transient absorption spectra of $C_{29}$-peridinin recorded in *n*-hexane, tetrahydrofuran, methanol, and acetonitrile in the visible spectral region at various delay times after excitation into the $S_2$ state are shown in the first column of Figure 3A. As indicated above for the steady-state spectra, in order to understand the nature of the transient absorption spectral bands, it is useful to view them in context with the transient absorption spectra from peridinin and the other peridinin analogues recorded in the same solvents. These spectra are shown in Figure 3A. Note that excitation of the longest molecule in the series, $C_{39}$-peridinin dissolved in the non-polar solvent, *n*-hexane (top panel in the last column of Figure 3A), results in a rapid bleaching of the $S_0 \rightarrow S_2$ absorption bands followed in a few hundred femtoseconds by the build-up of a narrow excited state absorption (ESA) band at ~540 nm. As the polarity of the solvent is increased, an additional broader ESA band appears between 550 and 700 nm concomitant with the narrow band. However, unlike the narrow ESA band whose position remains

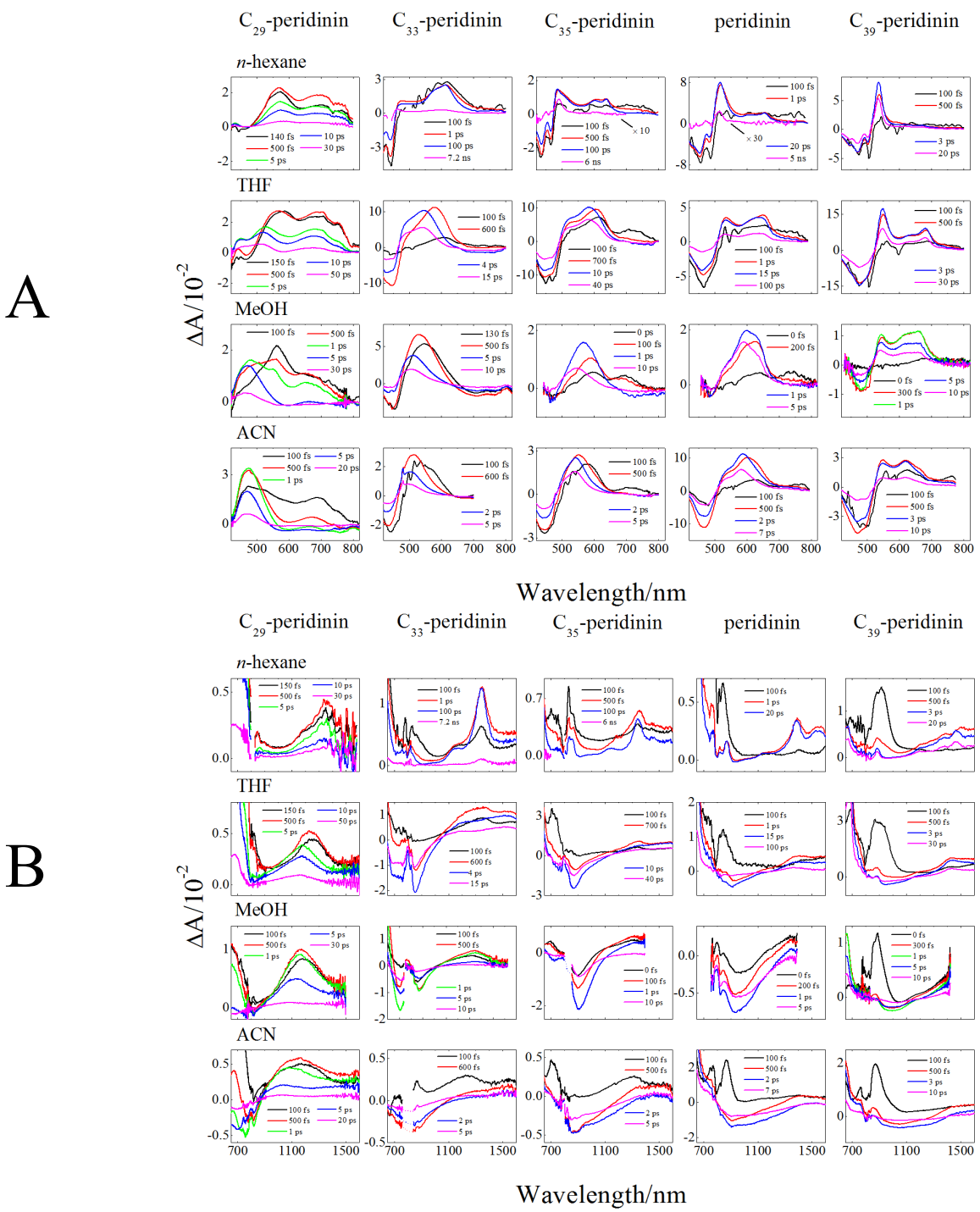


**Figure 3.** Transient absorption spectra recorded in the **(A)** visible and **(B)** NIR spectral regions. Data for peridinin, $C_{33}$-, $C_{35}$-, and $C_{39}$- peridinin in *n*-hexane, tetrahydrofuran (THF), and acetonitrile (ACN) were taken from reference 20, while data for $C_{35}$-, peridinin and $C_{39}$- peridinin in methanol were taken from reference 17.

relatively unaffected by solvent polarity, the broader feature in the spectra from $C_{39}$-peridinin increases in intensity and shifts from longer to shorter wavelength with increasing solvent polarity. This suggests that the narrow and broad bands belong to two different electronic transitions.

As the π-electron conjugation is shortened by going down the series from $C_{39}$-peridinin to peridinin, $C_{35}$-peridinin, $C_{33}$-peridinin and $C_{29}$-peridinin, both the broad and narrow ESA spectral bands shift to shorter wavelength owing to a decrease in the extent of π-electron conjugation (top row of spectra in Figure 3A). In *n*-hexane, the narrow ESA band shifts ~40 nm to the blue for each one fewer double bond. Also, in this solvent, as the π-electron conjugation length of the molecule is decreased, the intensity of the narrow ESA band becomes less pronounced relative to that of the broad band, which for $C_{29}$-peridinin in *n*-hexane, appears at ~560 nm (top left hand traces in Figure 3A).

The narrow ESA band in the transient absorption spectra of $C_{29}$-peridinin recorded in *n*-hexane has shifted to such a short wavelength (<440 nm) that it is out of the spectral response window of the spectrometer. Also for $C_{29}$-peridinin, another broad band not observed in the transient absorption spectra of any of the other peridinins appears at ~700 nm, and its wavelength remains relatively invariant to solvent polarity as seen in the ESA spectra shown in the first column of Figure 3A. Like the broad band at ~560 nm, this additional band is prominently observed in the ESA traces taken at the shortest (<150 fs) delay times. This indicates that the state from which these two broad ESA transitions originate is populated from the $S_2$ state. At subsequent times, both broad bands (the one at ~560 nm in *n*-hexane that is shifted to the blue with solvent polarity and the one at

~700 nm that does not shift) decay at the same rate. This suggests that the states from which these two spectral features originate are in fast dynamic equilibrium.

The transient absorption spectra of the peridinins in the different solvents recorded in the near infrared (NIR) spectral region at various delay times after excitation into its $S_2$ state are shown in Figure 3B. Focusing initially on $C_{39}$-peridinin (last column in Figure 3B), there is a strong band at ~900 nm that rises and decays within the time course of the laser excitation pulse indicating it is an ESA transition originating from the $S_2$ state. This band is not affected by solvent polarity, but shifts to shorter wavelength upon decreasing the π-electron conjugation length of the molecule. This is seen most clearly in the ESA spectra for the series of peridinins recorded in *n*-hexane (top row of spectra in Figure 3B). As the fast feature decays, a lower-energy band appears at ~1450 nm for $C_{39}$-peridinin in *n*-hexane, which suggests that it is directly populated from the $S_2$ state subsequent to photoexcitation. This band decays in several picoseconds depending on the solvent, and shifts slightly to shorter wavelength and becomes stronger as the π-electron conjugation of the molecule is decreased; e.g., see top row of spectra in Figure 3B. The band appears at ~1350 nm for $C_{29}$-peridinin. This longer-lived band also becomes broader and shifts to the blue with increasing solvent polarity; e.g., see the first column of spectra in Figure 3B. The fact that this band is long-lived suggests that it originates from the lowest excited state of the molecules. For peridinin and $C_{39}$-peridinin, this band is very likely a higher vibronic feature associated with the $S_1 \rightarrow S_2$ transition as suggested by Zigmantas, et al.[7]. However, this feature cannot be an $S_1 \rightarrow S_2$ transition for the shortest in the series, $C_{29}$-peridinin, because the (0–0) vibronic bands of the $S_0 \rightarrow S_2$ absorption and $S_2 \rightarrow S_0$ fluorescence spectra differ by only ~10 nm. This indicates an

energy separation between the $S_1$ and $S_2$ states of only ~600 $cm^{-1}$ (see above), which would put the $S_1 \rightarrow S_2$ transition at a very long wavelength. Therefore, the band must be associated with a transition to a higher-lying state than $S_2$.

In addition to the ESA features in the transient spectra, stimulated emission is evident as broad negative amplitude, particularly in the spectra of the molecules dissolved in polar solvents (see for example the transient NIR spectra from $C_{35}$-peridinin in tetrahydrofuran, methanol, and acetonitrile, center column in Figure 3B). This emission has been assigned as originating from the ICT state.[6,7,20,23-25]

In order to probe more deeply into the origin and dynamics of the electronic states giving rise to the transient spectra, global fitting according to a sequential decay model was done on the spectral and temporal datasets from $C_{29}$-peridinin. The resulting amplitude traces are termed evolution associated decay spectra (EADS)[26] and are shown in Figure 4 for the datasets taken in the visible region (left hand column). In all solvents, four kinetic components were required to achieve a satisfactory fit based on a chi square ($\chi^2$) test and minimization of the residuals.[26,27]

The EADS traces for $C_{29}$-peridinin in all of the solvents in the visible region (Figure 4, left hand column) show a very fast 150–170 fs decay component that is very likely associated with the lifetime of the photoexcited $S_2$ state. The bleaching of the $S_0 \rightarrow S_2$ absorption profile is not evident because that band occurs below 425 nm which is outside the spectral response window of the spectrometer. The initial fast component decays into a second EADS component that has the two broad bands at ~560 nm and ~700 nm described above. This EADS component has a lifetime of 6.3 ps in *n*-hexane, but decreases as the polarity of the solvent increases. The values are 1.3 ps in

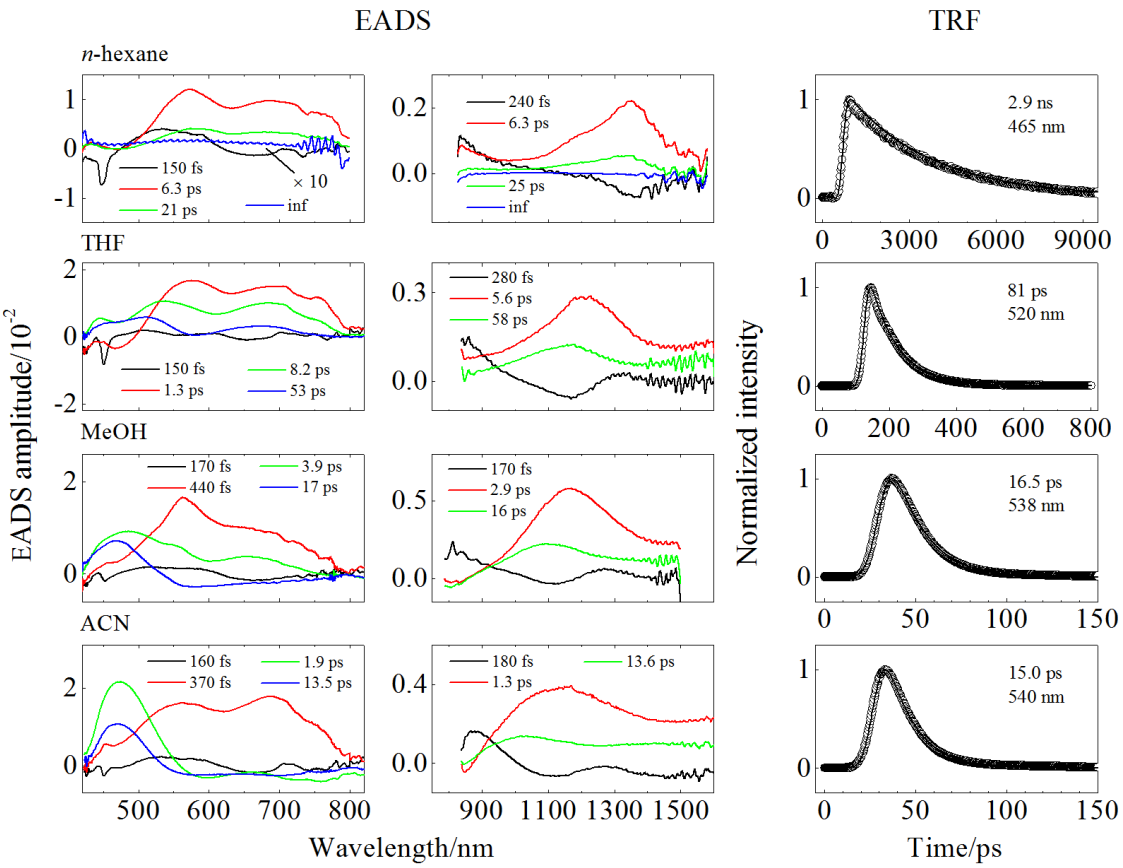


**Figure 4.** Evolution associated difference spectra (EADS, left and middle columns) obtained from the global fitting of the transient absorption in the visible and near infrared region and time-resolved fluorescence kinetic profiles (TRF, right column) of $C_{29}$-peridinin in different solvents.

tetrahydrofuran, 440 fs in methanol and 370 fs in acetonitrile. Consistent with previous analyses of the other peridinin analogues,[20] this decay component is associated with a vibronically hot $S_1$ state or in polar solvents, possibly a mixture of non-equilibrated $S_1$ and ICT states. The third EADS component also decays faster as the solvent polarity is increased. In *n*-hexane this component decays in 21 ps and has a similar band shape to the second EADS component, albeit less intense. As the polarity of the solvent is increased, the spectral lineshape narrows and shifts to shorter wavelength consistent with an assignment of the bands to a transition originating from a relaxed $S_1$/ICT state.[27,28] The lifetimes of this third EADS component are 8.2 ps in tetrahydrofuran, 3.9 ps in methanol, and 1.9 ps in acetonitrile. The fourth and final EADS component is most likely associated with the lifetime of the $S_1$ state which appears very small because the $S_1 \rightarrow S_N$ transition is out of the spectral window of the spectrometer. Because of its small amplitude and apparently lengthy lifetime, the global fitting assigns this component as infinitely long. In actuality, the lifetime of the $S_1$ state of $C_{29}$-peridinin in *n*-hexane is 2.9 ns as measured more precisely using time-resolved fluorescence (right hand column in Figure 4). As the solvent polarity is increased, the lifetime of the fourth EADS becomes shorter at 53 ps in tetrahyrofuran, 17 ps in methanol, and 13.5 ps in acetonitrile. These values are wholly consistent with those measured by time-resolved fluorescence which reveal 81 ps in tetrahydrofuran, 16.5 ps in methanol, and 15 ps in acetonitrile (Figure 4). Table 1 summarizes the kinetics data from the transient absorption and time-resolved fluorescence experiments.

**Table 1.** Dynamics of the excited states of $C_{29}$-peridinin obtained in various solvents using transient absorption (TA) and time-resolved fluorescence (TRF) spectroscopy.[a]

| | Probe | TA | | | | TRF | |
|---|---|---|---|---|---|---|---|
| solvent | region | $\tau_1$ | $\tau_2$ | $\tau_3$ | $\tau_4$ | $\tau_{F1}$ | $\tau_{F2}$ |
| *n*-hexane | Vis | 0.15 ± 0.01 | 6.3 ± 0.2 | 21 ± 1 | inf | < FWHM | 2900 ± 100 |
| | NIR | 0.24 ± 0.01 | 6.3 ± 0.1 | 25 ± 2 | inf | (300) | |
| THF | Vis | 0.15 ± 0.01 | 1.3 ± 0.1 | 8.2 ± 0.2 | 53 ± 3 | n.e. | 81 ± 2 |
| | NIR | 0.28 ± 0.2 | 5.6 ± 0.5 | 58 ± 3 | | (28) | |
| MeOH | Vis | 0.17 ± 0.01 | 0.44 ± 0.02 | 3.9 ± 0.2 | 17 ± 1 | < FWHM | 16.5 ± 0.5 |
| | NIR | 0.17 ± 0.01 | 2.9 ± 0.3 | 16 ± 1 | | (12) | |
| ACN | Vis | 0.16 ± 0.01 | 0.37 ± 0.01 | 1.9 ± 0.1 | 13.5 ± 0.4 | < FWHM | 15.0 ± 0.5 |
| | NIR | 0.18 ± 0.01 | 1.3 ± 0.1 | 13.6 ± 0.6 | | (12) | |

[a]The lifetimes are all given in picosecond units and were obtained from the global fitting of the transient absorption (TA) and time-resolved fluorescence (TRF) datasets. The uncertainties were determined by exploring the region of solution for each fitted parameter based on the goodness of fit and values of the residuals. FWHM—full width at half maximum of the instrument response function (in parenthesis in picoseconds); n.e., not evident, THF, tetrahydrofuran; MeOH, methanol; ACN, acetonitrile.

The global fits to the datasets taken in the NIR region are also given in Figure 4 (middle column) and depending on the solvent, required three or four components for a good fit. The kinetic parameters derived from both the visible and NIR datasets are summarized in Table 1 and show good agreement among the values. However, for the experiments in the more polar solvents, the component assigned to the vibronically hot ICT state from the EADS analysis of the visible datasets is not resolved, presumably because of low amplitude of this component in the NIR spectral region.

From the trends in the positions and amplitudes of the transient spectral features seen for the entire series of peridinins shown in Figures 3A and 3B, it is clear there are four different spectral bands of $C_{29}$-peridinin that need explanation: Two of these bands, one in the NIR and one in the visible region, broaden and shift to higher energy with increasing solvent polarity, and two of the bands (at ~700 nm and < 440 nm) remain relatively unaffected by changing the solvent. These observations suggest that the bands that are affected by the solvent originate from the ICT state, which has significant $B_u^+$ character.[15,17,20,28] Because this state has a large dipole moment, it is expected to decrease in energy with increasing solvent polarity, thereby leading to a shift to higher energy of the transitions originating from it. The bands that are unaffected by the solvent most likely originate from the $S_1$ state, which has a significant $A_g^-$ symmetry known to be less prone to changing its position upon alteration of the solvent polarity.

As the above discussion suggests, $C_{29}$-peridinin is somewhat of an outlier in terms of its spectroscopic and photophysical properties compared to the other peridinin derivatives. The two lowest excited states of $C_{29}$-peridinin are observed to be much closer

in energy than for the other peridinins, and the transient absorption spectra provide evidence for new transitions that were not observed in the longer chain molecules.

Molecular orbital calculations were carried out by Mr. Jordan A. Greco and Prof. Robert R. Birge[29] of the University of Connecticut to explore these issues in more detail. The details of the calculations will be presented in the Ph.D. dissertation of Mr. Greco. A truncated chromophore having a $C_s$ symmetry was used for the computational work, consistent with a previous study of peridinin.[15] The results from equation-of-motion coupled-cluster with singles and doubles (EOM-CCSD) calculations suggest that the two lowest excited singlet states of $C_{29}$- peridinin are closer in energy to peridinin and strongly mixed, as well as having a level ordering similar to those of protonated Schiff base retinal polyenes.[30-33] This prediction is in good agreement with the spectroscopic results. Likewise, a simulation of the transient absorption spectra was performed on $C_{29}$-peridinin and peridinin in *n*-hexane and acetonitrile based on full single configuration interaction (CIS) methods and PCM solvent effect theory. Results from the calculations provide some insights into the multiple bands observed in the experimental transient absorption spectra and useful perspective on the significant differences between $C_{29}$-peridinin and peridinin. First, the intensities of the bands are less for all transitions in $C_{29}$-peridinin compared to analogous bands in peridinin. Second, there is one additional band predicted for both the set originating from the $1^1A_g^-$ state and the relaxed $^1B_u^+$/ICT-like state), which is consistent with the experimental observation of a long-lived band at 700 nm whose position does not depend on the solvent. The computations show that this additional band corresponds to the transition, $S_1$ (relaxed) $\rightarrow S_8$, and that it is more apparent in polar solvent due to separation from nearby bands that partially mask it.

Moreover, the wavelength of the band is predicted to be insensitive to the solvent environment. Thus, the calculations are in good agreement with the general features of the observed spectra (Figure 3) and provide an explanation for the appearance of an additional band at 700 nm for $C_{29}$-peridinin. This band is also predicted to be present in peridinin in polar solvent, but it is significantly weaker and therefore not observed experimentally.

In view of these findings, it is important to reflect on the nature of the ICT state in $C_{29}$-peridinin and address the question of whether this molecule actually generates an ICT state or simply possesses a lowest-lying relaxed $^1B_u^+$ state having the properties of an ICT state. The best perspective on this question is provided by the symmetry-adapted-cluster configuration-interaction (SAC-CI) calculations where the electrostatic properties of $C_{29}$-peridinin and peridinin in methanol are shown for the relaxed excited singlet state. Examining the relaxed excited singlet state is critical to an analysis of the ICT state because both experiment and theory provide strong evidence that the ICT state is an evolved state that is created through relaxation in the singlet manifold.[15] In comparing the properties of the lowest-lying relaxed excited singlet state of $C_{29}$-peridinin with those of peridinin, significant differences observed when the molecules are dissolved in methanol suggest that $C_{29}$-peridinin has an ICT-like state rather than a full ICT state for the following reasons: First, the dipole moment change for $C_{29}$-peridinin upon excitation into this state is significant ($\delta\mu$ = 8.4 D), but it is a fraction of that calculated for peridinin ($\delta\mu$ = 21 D). This value is considerable, but it is more similar to the $^1B_u^+$ states of polar retinyl polyenes and carotenoids than to the ICT state of peridinin.[15,28,30-35] Nevertheless, the dipole moment direction and charge shift contours are indicative of a charge transfer

from the allenic region into the lactone region; i.e. ICT-like behavior. Furthermore, one of the unique characteristics of the ICT state in peridinin is its significant doubly excited character (41.6%),[15] which is considerably larger than predicted for $C_{29}$-peridinin (19.8%). The smaller dipole moment and doubly excited character of the $C_{29}$-peridinin $S_1$ state is not due to a fundamental difference in the charge transfer process, rather it occurs as a consequence of the length of the polyene. A shorter polyene system cannot support as large a charge transfer configuration. Hence, it can be concluded that $C_{29}$-peridinin does indeed have an ICT state, but that this state is better viewed as an ICT-like or partial ICT state rather than a full ICT state as was found in the parent molecule, peridinin.

# Conclusions

These findings reveal an apparent contradiction between the computations which indicate that $C_{29}$-peridinin does not support the formation of a full ICT state in polar solvents, and the experimental observations which reveal a large effect of solvent polarity on the lifetime of the lowest excited singlet state. The present investigation shows that it is an over-simplification to assume that the extent of ICT character is the sole factor controlling the dynamics of the lowest excited state of $C_{29}$-peridinin, peridinin, and other analogues when they are dissolved in polar solvents. This is because a short lifetime can also be associated with a level ordering reversal of the lowest $2^1A_g^-$ and $1^1B_u^+$ states in polar solvents as is clearly the case for $C_{29}$-peridinin and peridinin in acetonitrile. Moreover, the excited state lifetimes of these molecules will scale inversely with the oscillator strengths of their relaxed singlet states.[36] Therefore, the impact of the ICT state on the lifetime of the lowest excited singlet state of peridinin and analogues is not due solely to its large dipole moment, but also to an increase in the oscillator strength of the ICT transition in polar solvents.[15]

# References


(1) Hiller, R. G. Carotenoids as Components of the Light-Harvesting Proteins of Eukaryotic Algae In *The Photochemistry of Carotenoids*; Frank, H. A., Young, A. J., Britton, G., Cogdell, R. J., Eds.; Kluwer Academic: Dordrecht, **1999**; Vol. 8, 81–98.

(2) Macpherson, A. N.; Hiller, R. G. Light-Harvesting Systems in Chlorophyll *C*-Containing Algae In *Light-Harvesting Antennas in Photosynthesis*; Green, B. R., Parson, W. W., Eds.; Kluwer Academic Publishers, **2002**; Vol. 13, 323–352.

(3) Mimuro, M.; Akimoto, S. Carotenoids of Light Harvesting Systems: Energy Transfer Processes from Fucoxanthin and Peridinin to Chlorophyll In *Photosynthesis in Algae*; Larkum, A., Douglas, S., Raven, J., Eds.; Kluwer Academic Publishers, **2003**, 335–349.

(4) Bautista, J. A.; Connors, R. E.; Raju, B. B.; Hiller, R. G.; Sharples, F. P.; Gosztola, D.; Wasielewski, M. R.; Frank, H. A. *J. Phys. Chem. B* **1999**, *103*, 8751–8758.

(5) Frank, H. A.; Bautista, J. A.; Josue, J.; Pendon, Z.; Hiller, R. G.; Sharples, F. P.; Gosztola, D.; Wasielewski, M. R. *J. Phys. Chem. B* **2000**, *104*, 4569–4577.

(6) Zigmantas, D.; Hiller, R. G.; Yartsev, A.; Sundström, V.; Polivka, T. *J. Phys. Chem. B* **2003**, *107*, 5339–5348.

(7) Zigmantas, D.; Hiller, R. G.; Sharples, F. P.; Frank, H. A.; Sundström, V.; Polivka, T. *Phys. Chem. Chem. Phys.* **2004**, *6*, 3009–3016.

(8) Chábera, P.; Fuciman, M.; Hříbek, P.; Polívka, T. *Phys. Chem. Chem. Phys.* **2009**, *11*, 8795–8803.

(9) Pariser, R. *J. Chem. Phys.* **1955**, *24*, 250–268.

(10) Hudson, B.; Kohler, B. *Annu. Rev. Phys. Chem.* **1974**, *25*, 437–460.

(11) Callis, P. R.; Scott, T. W.; Albrecht, A. C. *J. Chem. Phys.* **1983**, *78*, 16–22.

(12) Birge, R. R. *Acc. Chem. Res.* **1986**, *19*, 138–146.

(13) Christensen, R. L.; Barney, E. A.; Broene, R. D.; Galinato, M. G. I.; Frank, H. A. *Arch. Biochem. Biophys.* **2004**, *430*, 30–36.

(14) Christensen, R. L. The Electronic States of Carotenoids In *The Photochemistry of Carotenoids*; Frank, H. A., Young, A. J., Britton, G., Cogdell, R. J., Eds.; Kluwer Academic Publishers: Dordrecht, **1999**; Vol. 8, 137–159.

(15) Wagner, N. L.; Greco, J. A.; Enriquez, M. M.; Frank, H. A.; Birge, R. R. *Biophys. J.* **2013**, *104*, 1314–1325.

(16) Kajikawa, T.; Hasegawa, S.; Iwashita, T.; Kusumoto, T.; Hashimoto, H.; Niedzwiedzki, D. M.; Frank, H. A.; Katsumura, S. *Org. Lett.* **2009**, *11*, 5006–5009.

(17) Niedzwiedzki, D. M.; Chatterjee, N.; Enriquez, M. M.; Kajikawa, T.; Hasegawa, S.; Katsumura, S.; Frank, H. A. *J. Phys. Chem. B* **2009**, *113*, 13604–13612.

(18) Chatterjee, N.; Niedzwiedzki, D. M.; Aoki, K.; Kajikawa, T.; Katsumura, S.; Hashimoto, H.; Frank, H. A. *Arch. Biochem. Biophys.* **2009**, *483*, 146–155.

(19) Kaligotla, S.; Doyle, S.; Niedzwiedzki, D. M.; Hasegawa, S.; Kajikawa, T.; Katsumura, S.; Frank, H. A. *Photosynth. Res.* **2010**, *103*, 167–174.

(20) Niedzwiedzki, D. M.; Kajikawa, T.; Aoki, K.; Katsumura, S.; Frank, H. A. *J. Phys. Chem. B* **2013**, *117*, 6874–6887.

(21) Britton, G.; Liaaen-Jensen, S.; Pfander, H. *Carotenoids Handbook.* Birkhäuser Verlag: Basel-Boston-Berlin, 2004.

(22) Niedzwiedzki, D. M.; Fuciman, M.; Frank, H. A.; Blankenship, R. E. *Biochim. Biophys. Acta-Bioenerg.* **2011**, *1807*, 518–528.

(23) Zigmantas, D.; Polivka, T.; Hiller, R. G.; Yartsev, A.; Sundström, V. *J. Phys. Chem. A* **2001**, *105*, 10296–10306.

(24) Ehlers, F.; Wild, D. A.; Lenzer, T.; Oum, K. *J. Phys. Chem. A* **2007**, *111*, 2257–2265.

(25) Kopczynski, M.; Ehlers, F.; Lenzer, T.; Oum, K. *J. Phys. Chem. A* **2007**, *111*, 5370–5381.

(26) van Stokkum, I. H. M.; Larsen, D. S.; van Grondelle, R. *Biochim. Biophys. Acta* **2004**, *1657*, 82–104.

(27) Niedzwiedzki, D.; Koscielecki, J. F.; Cong, H.; Sullivan, J. O.; Gibson, G. N.; Birge, R. R.; Frank, H. A. *J. Phys. Chem. B* **2007**, *111*, 5984–5998.

(28) Enriquez, M. M.; Fuciman, M.; LaFountain, A. M.; Wagner, N. L.; Birge, R. R.; Frank, H. A. *J. Phys. Chem. B* **2010**, *114*, 12416–12426.

(29) Magdaong, N. M.; Niedzwiedzki, D. M.; Greco, J. A.; Liu, H.; Yano, K.; Kajikawa, T.; Sakaguchi, K.; Katsumura, S.; Birge, R. R.; Frank, H. A. *Chem. Phys. Lett.* **2014**, *593*, 132–139.

(30) Mathies, R.; Stryer, L. *Proc. Natl. Acad. Sci. USA* **1976**, *73*, 2169–2173.

(31) Birge, R. R.; Hubbard, L. M. *Journal of American Chemical Society* **1980**, *102*, 2195–2204.

(32) Birge, R. R.; Zhang, C. F. *J. Chem. Phys.* **1990**, *92*, 7178–7195.

(33) Ponder, M.; Mathies, R. *J. Phys. Chem.* **1983**, *87*, 5090–5098.

(34) Zigmantas, D.; Hiller, R. G.; Sundström, V.; Polivka, T. *Proc. Natl. Acad. Sci. USA* **2002**, *99*, 16760–16765.

(35) Premvardhan, L.; Papagiannakis, E.; Hiller, R. G.; van Grondelle, R. *J. Phys. Chem. B* **2005**, *109*, 15589–15597.

(36) Strickler, S. J.; Berg, R. A. *J. Chem. Phys.* **1962**, *37*, 814–822.

# *Chapter III*

# *Effect of protein aggregation on the spectroscopic properties and excited state kinetics of the LHCII pigment-protein complex from green plants*

## Introduction

All photosynthetic organisms contain pigment-protein complexes that carry out energy transfer and electron transfer in implementing the process of photosynthesis.[1-5] Energy transfer is accomplished by light-harvesting (or antenna) complexes that absorb light in the visible region of the electromagnetic spectrum and transfer the energy to the reaction center protein which undergoes a series of oxidation-reduction reactions to convert the absorbed energy into electrical potential.[2]

Green plants contain two different reaction center proteins, Photosystem I (PSI)[6,7] and Photosystem II (PSII),[8] and many different light-harvesting proteins.[9-11] The most abundant light-harvesting protein in green plants is the so-called LHCII complex (Figure 1) which binds fourteen chlorophyll (Chl) molecules non-covalently to the protein: eight Chl *a* and six Chl *b*.[2,4,12,13] Carotenoids are also found in the structure.[2,14,15] These include two luteins that are arranged crosswise in the complex, one neoxanthin and one violaxanthin per monomeric unit.[4,12]

A

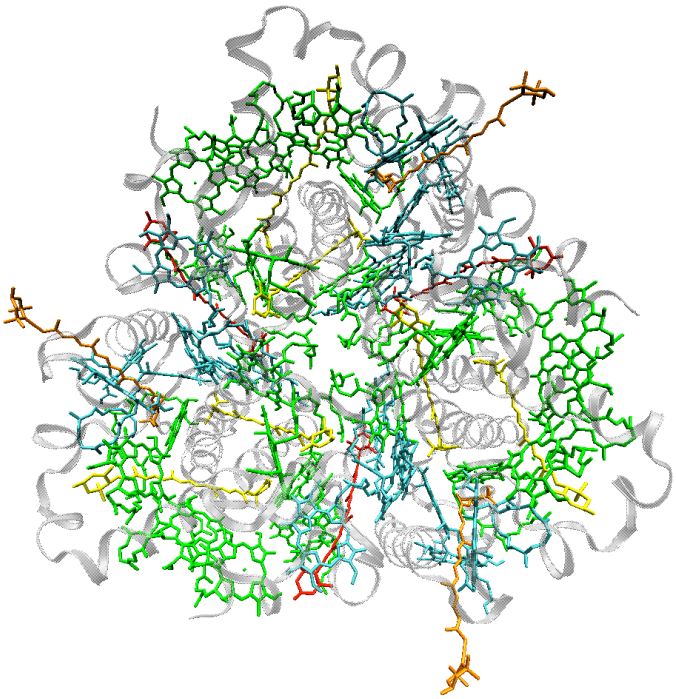

B

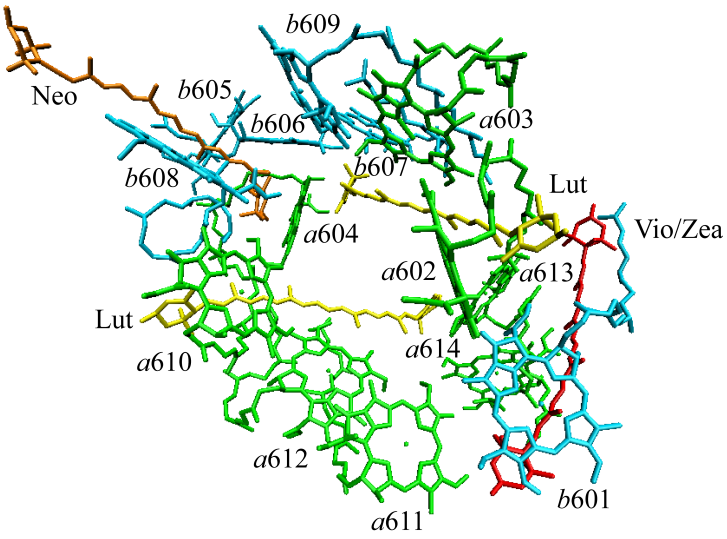


**Figure 1. (A)** Structure and arrangement of pigments in the LHCII trimer. **(B)** Each LHCII monomer subunit consists of 8 Chl *a* (green), 6 Chl *b* (cyan), 2 lutein (yellow), 1 neoxanthin (orange) and 1 violaxanthin or zeaxanthin (red). The notation for the Chl pigments is taken from Ref 4.

As photosynthetic organisms capture and convert light energy, the amount of energy absorbed but not channeled to the reaction center must be deactivated so that it does not lead to the photodestruction of the photosynthetic apparatus. This excess excitation energy may result in the formation of Chl triplet states which can sensitize the formation of singlet oxygen, a powerful oxidizing agent of Chl.[16-18] Carotenoid pigments protect photosynthetic organisms by quenching Chl triplet states.[19-21] Plants also dissipate excess energy prior to Chl triplet state formation and regulate the flow of energy to the reaction center,[22-26] but the mechanisms by which these processes occur are the subject of intense debate.[10,25,27-30] The dissipation of excess light energy is typically monitored by the extent to which Chl fluorescence originating from the light-harvesting pigment-protein complexes associated with PSII is quenched under different sample conditions.[23,31,32] The overall process is called nonphotochemical quenching (NPQ).[24,33-35] NPQ has many different components,[24] but the largest and most rapid component in green plants is the pH-dependent component known as qE.

At least four hypotheses have been advanced to explain the molecular basis of the qE component of NPQ. In one model, it is proposed to result from aggregation of the major trimeric LHCII complex which produces a conformational change that opens an energy transfer pathway to the lowest excited, $S_1$, state of a carotenoid for the deactivation of excess Chl excited states.[28,30] In a second model, energy from bulk Chls finds its way to a Chl/carotenoid heterodimer which undergoes charge transfer to form a carotenoid radical cation/Chl radical anion pair followed by subsequent charge recombination as the means of deactivating excess Chl *a* excited states.[36,37] Fleming and Niyogi et al.[26,37-39] have reported that this process occurs solely in the minor Chl-protein

complexes (Lhcb) and not in LHCII, whereas Kühlbrandt et al.[40,41] have proposed that carotenoid radical cation formation is facilitated by the binding of a separate protein, the PsbS complex,[42] with either LHCII or an Lhcb subunit. A third model proposes that carotenoid/Chl exciton coupling provides a pathway for deactivation of excess excited Chl via the rapidly-decaying $S_1$ state of a carotenoid.[43-45] A fourth model requires oligomerization or aggregation of LHCII trimers to form Chl/Chl exciton pairs that undergo charge transfer as the pathway for Chl excited state deactivation.[46-48]

In this chapter, the effect of aggregation of the LHCII pigment-protein complex on the spectroscopic properties and dynamics of the bound pigments is examined. Many reports of fluorescence quenching induced by aggregation of the LHCII complex have appeared,[28,49-56] but the issue of whether aggregation plays a role in facilitating quenching of Chl excited states *in vivo* has yet to be fully addressed. It should be emphasized that although aggregation of pigment-protein complexes has been implicated in at least one of the mechanisms seeking to explain NPQ, aggregating randomly-dispersed LHCII *in vitro* may lead to the pigment-protein complex being arranged in orientations different from those achieved when the complex is constrained by the two-dimensional structure of the photosynthetic membrane in which it is naturally bound. Nevertheless, the studies presented here and elsewhere[57-61] on aggregated monomeric and trimeric LHCII are assessing how much quenching occurs when the protein forms aggregates and what molecular factors control the process of Chl fluorescence quenching. In addition, the changes in the energy transfer rates and efficiencies that result from protein aggregation will help understand the behavior of closely-associated LHCII pigment-protein complexes *in vivo*.

# Materials and Methods

### *Preparation of LHCII complexes*

LHCII trimers were prepared from spinach leaves using previously described procedures.[62] Thylakoid membranes were isolated from spinach leaves and further resuspended and solubilized to obtain BBY particles.[63] Sucrose density gradient ultracentrifugation was employed to separate the components of BBY. The second band from the top contained the monomeric LHCII and CP complexes while the third band contained the trimeric LHCII complex. LHCII trimers were further purified by a second sucrose density gradient ultracentrifugation step, dialyzed against buffer containing 10 mM HEPES, 0.06% *n*-dodecyl-β-D-maltoside (β-DM), pH 7.6 and stored at −80 °C.

Monomeric LHCII was separated from the CP complexes using the isoelectric focusing (IEF) protocol described previously[62] but with slight modifications. One hundred mL of slurry was prepared and contained 5% (w/v) Sephadex G-100, 2% (w/v) Pharmalyte carrier ampholytes (pH 2.5–5.0), 1% (w/v) glycine, 0.06% (w/v) β-DM and distilled water. Six IEF electrode strips were cut into 10.5 cm lengths and soaked in 2% (w/v) Pharmalyte solution. The strips were then placed on both ends of the Pharmacia Multiphor II Electrophoresis system gel tray (26.0 cm × 11.0 cm). The slurry was slowly poured onto the tray and allowed to form a homogenous layer. Air bubbles were removed carefully and the tray with the slurry was placed on a balance below approximately 50 cm of a small fan. ~17–18 g of water was allowed to evaporate over a period of 2 h. Anode and cathode strips were placed on top of the electrode strips prepared by soaking strips in either 1 M phosphoric acid (anode solution) or 1 M sodium hydroxide (cathode solution). To ensure thermal conductivity between the cooling plate and the gel tray, a 0.1% (v/v)

solution of Triton X-100 was applied to the cooling plate. The gel was pre-focused for 1 h at 8.0 watts with the temperature maintained at 4 °C. 1 mL of band 2 containing the PS II antenna complexes from the previous sucrose density gradient ultracentrifugation step was mixed with 1 mL of deionized water and 0.5 mL of 3% β-DM. The mixture was then kept on ice and stirred occasionally for 30 min before centrifugation at 12,000 × g for 5 min at 4 °C using a Sorvall SS-34 rotor. ~2.0 mL of the supernatant was mixed with the gel scraped out using a 10 × 2 cm sample applicator applied at about 2 cm from the cathode. The sample slurry was then poured back into the sample applicator and the applicator removed after which time the sample was allowed to equilibrate hydrostatically for ~3 min. The focusing was continued for 15 h at a constant power of 8.0 W, 4 °C. The green bands observed after the completion of the focusing were separated using a fractionating grid frame, collected using a spatula, and eluted in PEGG elution columns using a minimum amount of buffer which contained 100 mM HEPES and 0.06% β-DM at pH 7.6. Prior to elution, a small amount of each band was dissolved in deionized water and the isoelectric point (pI) was measured using a microelectrode. Carrier ampholytes and sucrose were removed from the sample by dialysis against buffer containing 10 mM HEPES, 0.02% β-DM at pH 7.6. LHCII monomers were then frozen at −80 °C until used in the spectroscopic experiments.

Aggregated LHCII complexes were prepared using Bio-Beads (Bio-Rad 152-8920), which upon addition to the solution, reduce the β-DM concentration.[30] This was accomplished by adding 200 mg of beads/mL to the LHCII sample and stirring in the dark at room temperature for approximately 15 min.

***Pigment analysis***

The pigment composition of the LHCII complexes was confirmed by extraction using 50/50 (v/v) acetone/methanol and by HPLC analysis as follows: Approximately 1 mL of the LHCII complex was dialyzed against 1 L of 10 mM HEPES buffer, pH 7.6 (without β-DM detergent) for 24 h at 4 ºC. The dialyzed sample was then placed in a 1.5 mL Eppendorf tube having small holes at the top and lyophilized for 48 h. After lyophilization, the sample was redissolved in 50/50 (v/v) HPLC grade acetone/methanol and dried under a stream of nitrogen. The dried sample was then taken up in acetonitrile, which was the HPLC injection solvent, and filtered through a Millex microsyringe (0.2 μm). The HPLC solvents were: solvent A consisting of 87% acetonitrile, 10% methanol, and 3% water; and solvent B consisting of 100% ethyl acetate. All solvents were HPLC grade and purchased from Fisher Scientific. The HPLC protocol was programmed for a flow rate of 1 mL/min and was isocratic for the first 15 min using 99% solvent A and 1% solvent B. Then, a linear gradient was applied over 25 min until the solvent composition was 60% solvent A and 40% solvent B. This solvent composition was maintained for the remaining 20 min of the protocol. Figure 2 shows a representative HPLC trace.

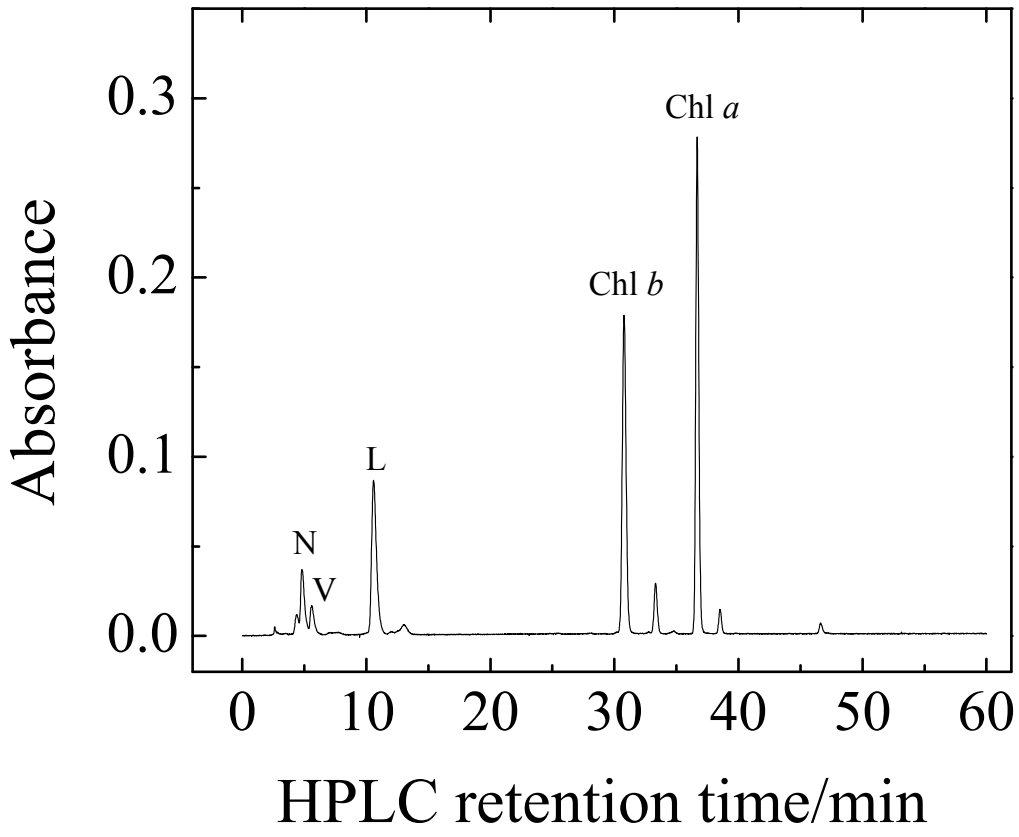


**Figure 2.** HPLC chromatogram of LHCII trimers monitored at 440 nm. N, neoxanthin; V, violaxanthin; L, lutein.

***Steady-state spectroscopic methods***

A Varian Cary 50 UV/Vis spectrophotometer was used to obtain steady-state absorption spectra. For the steady-state fluorescence measurements, a Jobin-Yvon Horiba Fluorolog-3 Model FL3-22 fluorimeter having double emission and excitation monochromators, 1200 grooves/mm gratings, a Hamamatsu R928P PMT detector, and a 450 W Osram XBO xenon arc lamp were used. The emission spectra of LHCII samples were obtained with a sample OD of 0.05 at the 640 nm excitation wavelength. The bandpass settings were 2 nm and 1 nm, for the excitation and emission monochromators, respectively. The fluorescence excitation spectra of the samples were recorded with the emission wavelength set to 700 nm and the bandpass settings were 2 nm and 4 nm, for the excitation and emission monochromators, respectively. For spectroscopic experiments on LHCII samples at cryogenic temperatures, a mixture of glycerol and 10 mM HEPES buffer, pH 7.6 was added to the samples to a final concentration of 70% (v/v) glycerol in plastic cuvettes (Plastibrand model no. 759150).

For absorption and fluorescence experiments at 77 K, a custom made optical immersion dewar cryostat was used to hold the samples. The cuvette containing the sample was secured into a sample holder and lowered slowly into the cryostat containing liquid nitrogen. For the experiments below 77 K, the sample was placed in a cryostat (Janis Model STVP-100-1) and liquid helium was introduced via a transfer arm (Janis ST-LINE).

***Time-resolved fluorescence spectroscopy***

Time-resolved fluorescence spectra of the LHCII samples were obtained using Jobin-Yvon Horiba Fluorolog-3 Model FL3-22 fluorimeter with a time-correlated single-photon counting (TCSPC) module and a pulsed NanoLED-670L diode generating 665 nm light with a <200 ps pulse duration as excitation light source. Lifetimes and amplitudes were extracted by fitting the time response data detected at 680 nm using a sum of exponentials function.

*Femtosecond time-resolved transient absorption spectroscopy*

Room temperature transient absorption spectroscopy experiments were performed using the femtosecond transient absorption spectrometer setup previously described.[64,65] The optical densities (OD) of the LHCII samples were adjusted to 0.4–0.6 at the excitation wavelength in a cuvette with 2 mm path length. Excitation of the samples was achieved by tuning the pump beam to either 490 nm which excited the $S_2$ state of the carotenoids and the Soret band of Chl *b* or to 677 nm which excited the $Q_Y$ band of Chl *a*. The measurements were averaged over 5 s. The pump beam had 1.2 μJ/pulse energy in a 1 mm diameter spot size, which corresponded to $3.8 \times 10^{14}$ and $5.2 \times 10^{14}$ photons/cm$^2$ pulse intensity at 490 and 677 nm excitation, respectively. In order to prevent photodegradation, the samples were continuously mixed using a magnetic microstirrer and the absorption spectra before and after transient absorption experiments were taken to assess sample integrity. The procedure for processing the ultrafast transient absorption data is given in Appendix A.

## Results and Discussion

***Steady-state absorption and fluorescence spectroscopy***

The absorption spectra of the LHCII monomers, trimers and aggregates taken at room temperature and 10 K are presented in Figure 3. As can be seen in the figure, and especially in the insets which emphasize the $Q_Y$ region of Chl *a* and *b* absorption between 600 and 700 nm, aggregation leads to only very small changes in the absorption spectral features of the complexes. Lowering the temperature to 10 K results in more structured and resolved spectra compared to those seen at room temperature. Also, at any given temperature, the absorption spectra in the $Q_Y$ region of the aggregated LHCII proteins were slightly broader, and in the case of aggregated trimers, the maximum absorption in this region was also slightly red-shifted by 1 nm, compared to those of the unaggregated proteins.

In contrast to the minimal effect of protein aggregation on the absorption spectra, the effect on the emission spectral intensities and lineshapes is striking.[66-69] Figure 4 shows that ~15 min after addition of the Bio-Beads to the samples which promotes protein aggregation, the fluorescence intensity is reduced substantially. Aggregation of the monomers and trimers reduced the fluorescence emission intensity by 93% and 91%, respectively (Figure 4). By comparison, the exact same samples exhibited only a 17% and 5% change, respectively, in the intensity of their absorption spectra (Figure 4). This indicates that the large reduction in fluorescence intensity cannot be attributed to protein precipitation or degradation. Thirty minutes after the addition of the Bio-Beads, the emission intensity reached a constant level that was approximately an order of magnitude less than that of its initial value.

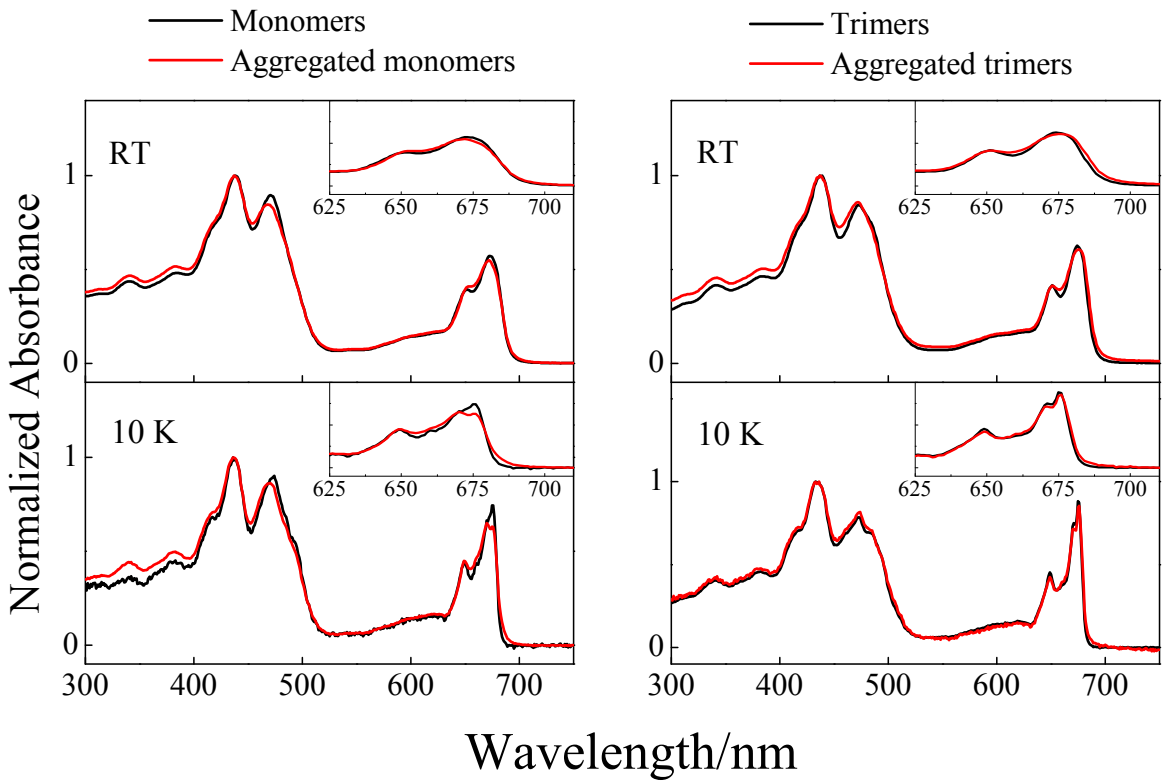


**Figure 3.** Overlay of the steady-state absorption spectra of LHCII complexes (black line) and aggregates (red line) at room and cryogenic temperatures. Insets show an expanded view of the $Q_Y$ absorption region between 625 nm and 700 nm.

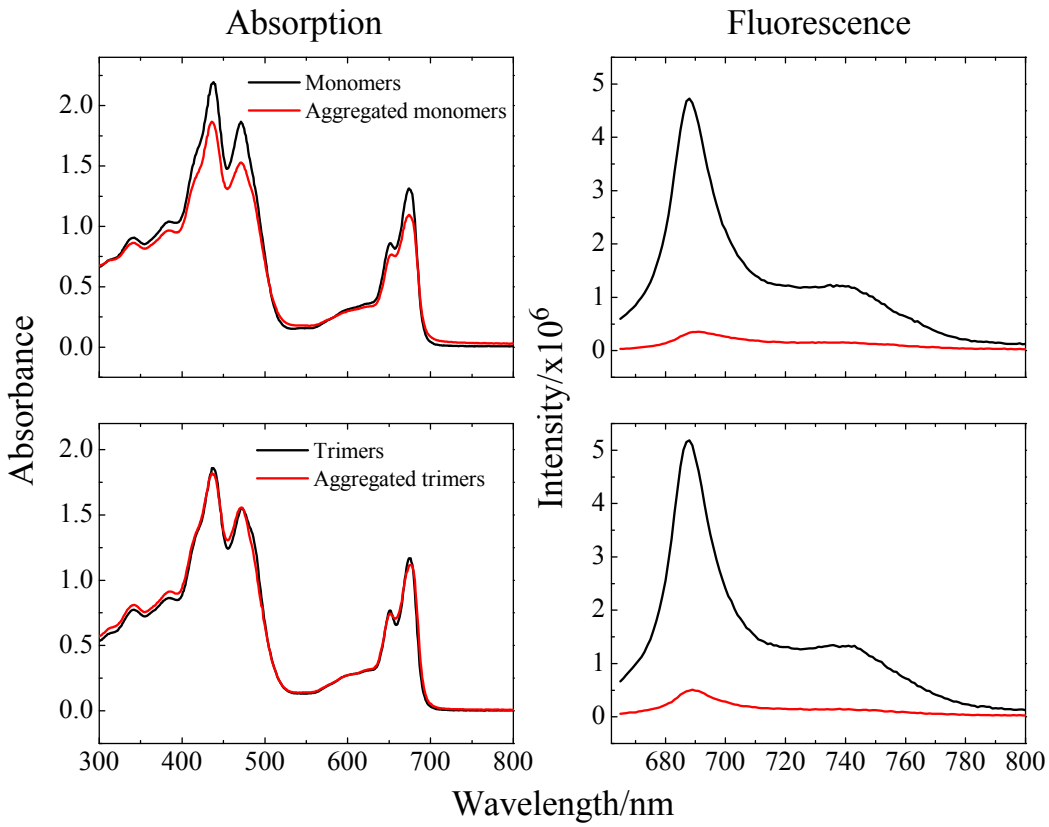


**Figure 4.** Effect of aggregation on the absorption and fluorescence spectra of LHCII monomers and trimers. The spectra of the aggregated monomers was taken ~20 min following the addition of the Biobeads, and that of the aggregated trimers was taken after ~10 min.

As has been reported previously,[60,67,70] there is also a substantial difference in the emission spectral lineshapes of the aggregated versus unaggregated LHCII samples taken at various temperatures (Figure 5). For the unaggregated monomers, at room temperature, the maximum intensity appeared at 682 nm. As the temperature was lowered to 80 K, the maximum blue-shifted to 679 nm, where it remained as the temperature was further lowered to 10 K. Also, as the temperature was lowered, the spectra became more intense and narrower. The 10 K spectrum had a full-width at half-maximum (FWHM) of 7 nm and was noticeably sharper than the room temperature spectrum which had a FWHM of 18 nm (Figure 5).

For the aggregated monomers at room temperature, the emission band maximum appeared at 681 nm (Figure 5). As the temperature was lowered to 80 K, the spectrum increased in intensity, broadened noticeably to a FWHM of 23 nm, and a shoulder appeared on the long wavelength side of the major band. When the temperature was lowered to 10 K, the spectrum gained even more in intensity and, unlike the spectrum of the unaggregated monomers which narrowed as the temperature was lowered, remained very broad with a FWHM of 18 nm. Also, its maximum at this temperature was red-shifted relative to that of the unaggregated monomers and appeared at 685 nm.

For the unaggregated trimer sample at room temperature, the maximum intensity appeared at 682 nm just like the unaggregated monomer sample. As the temperature was lowered to 80 K, the maximum blue-shifted slightly to 680 nm. At 10 K, the maximum shifted back to 682 nm. Also like the monomeric sample, as the temperature was lowered, the spectrum became more intense and narrower. The FWHM for the

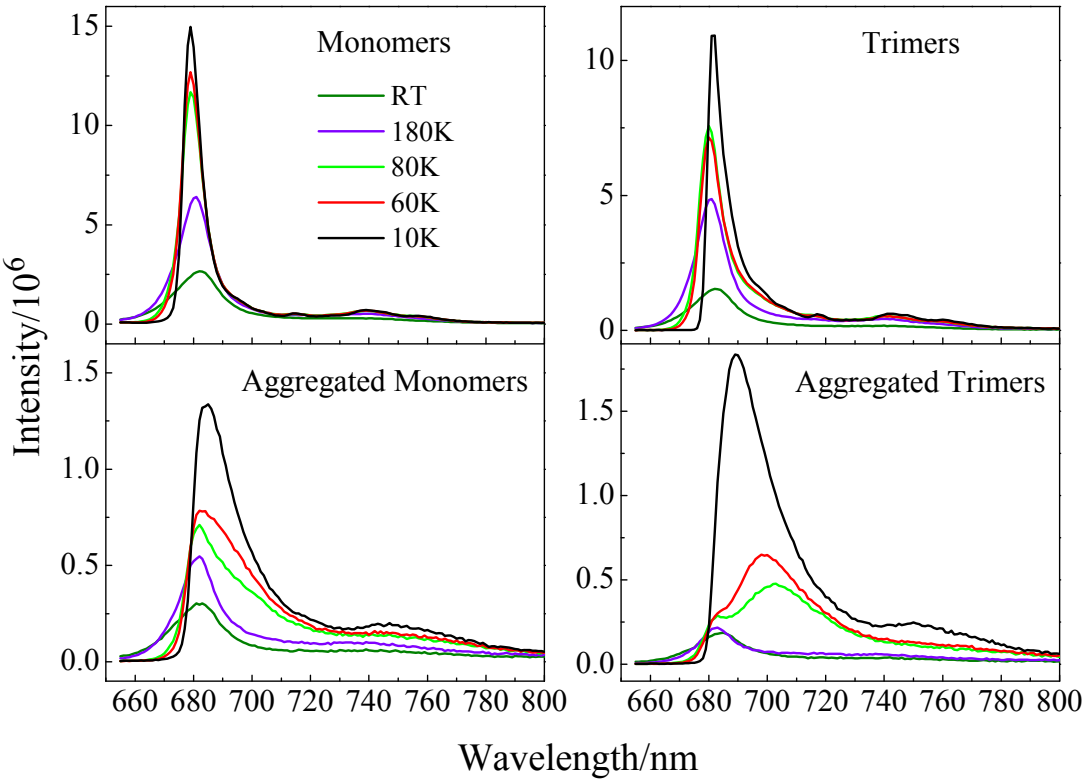


**Figure 5.** Temperature dependence of the steady-state emission spectra of LHCII complexes after excitation at 640 nm. Samples were adjusted to have the same absorption at the excitation wavelength.

unaggregated trimer spectrum at 10 K was 7 nm, whereas at room temperature it was 17 nm.

For the aggregated trimers at room temperature, the emission band maximum was red-shifted to 685 nm compared to 682 nm for the unaggregated trimers at the same temperature. As the temperature was lowered to 80 K, the spectrum increased in intensity and split into two noticeable bands having maxima at 683 nm and 703 nm. When the temperature was lowered further to 10 K, the spectrum continued to increase in intensity, but it coalesced into a single major broad band having a maximum at 689 nm and a FWHM of 21 nm. It is important to note that for both the monomer and trimer LHCII samples, the 10 K emission spectra of the aggregated proteins were substantially broader than those of the unaggregated samples. Also, in all cases a minor low energy vibronic emission band appeared between 740 and 750 nm.

As control samples and for use in interpreting the effect of protein binding and aggregation on the Chl emission profiles, the fluorescence spectra of purified Chls *a* and *b* in 2-MTHF were recorded as a function of temperature (Figure 6). From room temperature to 10 K the FWHM of the $Q_Y$ band of the emission spectrum of Chl *a* was found to be only very slightly narrower by ~1 nm than that of Chl *b*. Also, as the temperature was lowered from room temperature to 10 K, the maximum in the emission spectrum of Chl *a* shifted from 668 to 670 nm. For Chl *b*, there was also a noticeable shift in the band maximum from 651 nm at room temperature to 657 nm at 10 K.

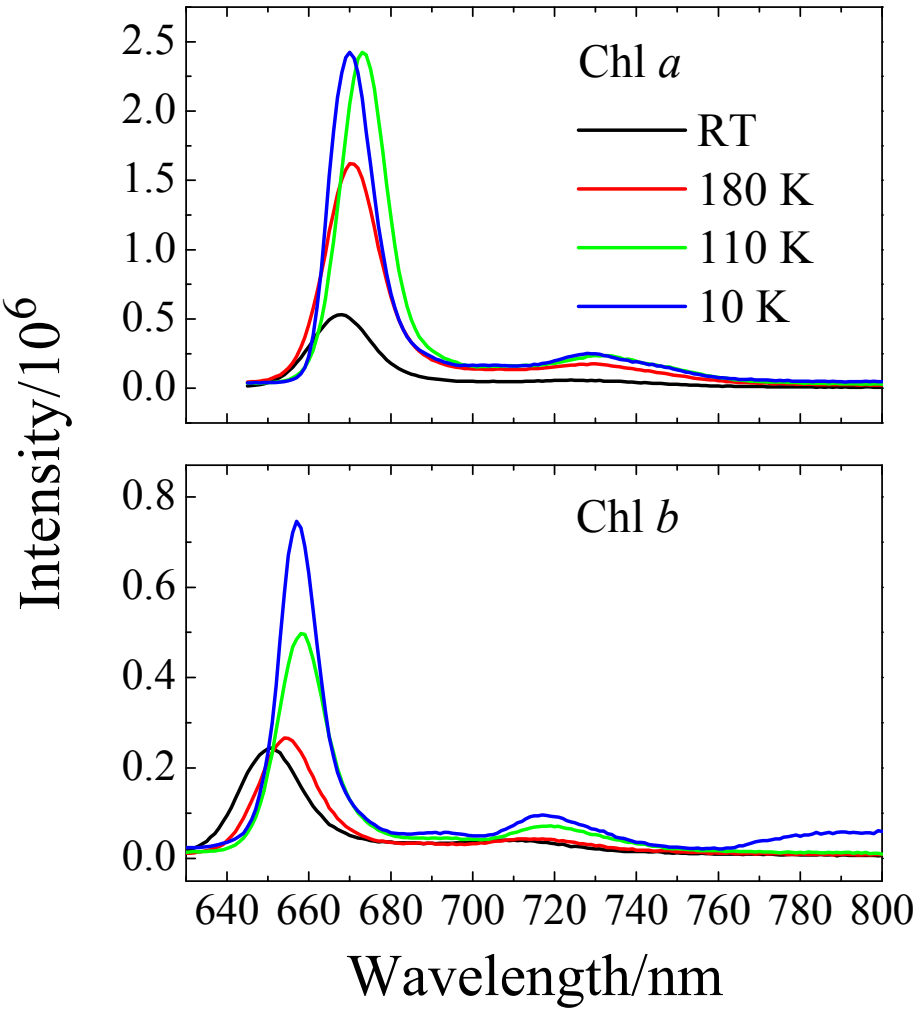


**Figure 6.** The effect of temperature on the fluorescence spectra of purified Chl *a* (top) and Chl *b* (bottom).

***Fluorescence excitation spectroscopy***

Figure 7 shows the excitation spectra of the LHCII unaggregated and aggregated monomeric and trimeric proteins monitored at 700 nm overlaid with their respective 1−T spectra, where T is transmittance. The spectra show a difference in intensity between the 1−T and excitation spectra primarily in the carotenoid absorption region between approximately 400 and 520 nm indicating that energy transfer from the carotenoids to Chl *a* is not 100% efficient. This is consistent with previous reports.[62,71-73] However, for the monomeric LHCII complexes (left four panels in Figure 7), the excitation spectra in this region match the 1−T spectra better at low temperatures than at room temperature regardless of whether the complexes are aggregated or not. This indicates that as the temperature is lowered, the efficiency of energy transfer from the carotenoids to Chl *a* is enhanced. This is not the case for the trimeric complexes (right four panels in Figure 7) where the efficiency of carotenoid-to-Chl *a* energy transfer remains constant at ~70%. For all the samples, whether monomeric or trimeric, aggregated or unaggregated, the agreement between the excitation and 1−T spectra in the region of the Chl *b* $Q_Y$ band near 640 nm is excellent indicating a high efficiency of energy transfer from Chl *b* to Chl *a*.

***Fluorescence kinetics***

The effect that aggregation of the LHCII complexes had on the kinetics of decay of Chl *a* fluorescence was investigated using time-correlated single-photon counting spectroscopy. Figure 8 shows the results of monitoring the time course of Chl *a* fluorescence decay probed at 681 nm following excitation into the Chl *b* $Q_Y$ band at 665 nm. It is seen in Figure 8 that the Chl *a* fluorescence decay time of unaggreggated

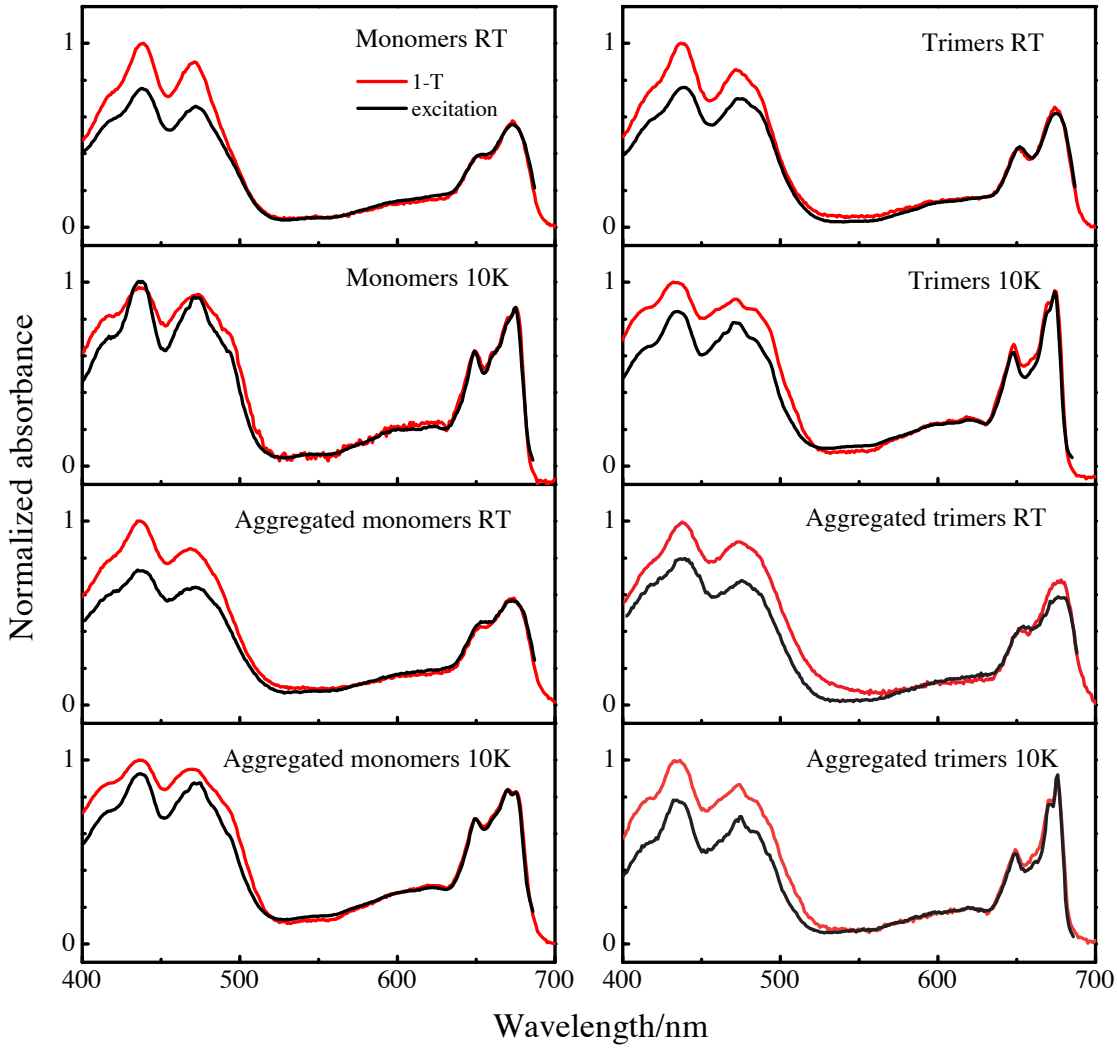


**Figure 7.** Excitation spectra (black lines) overlaid with 1−T spectra (red lines) of LHCII complexes at room and cryogenic temperatures. Excitation spectra were monitored at 700 nm. The intensities were normalized at the Chl *a* $Q_Y$ band maximum.

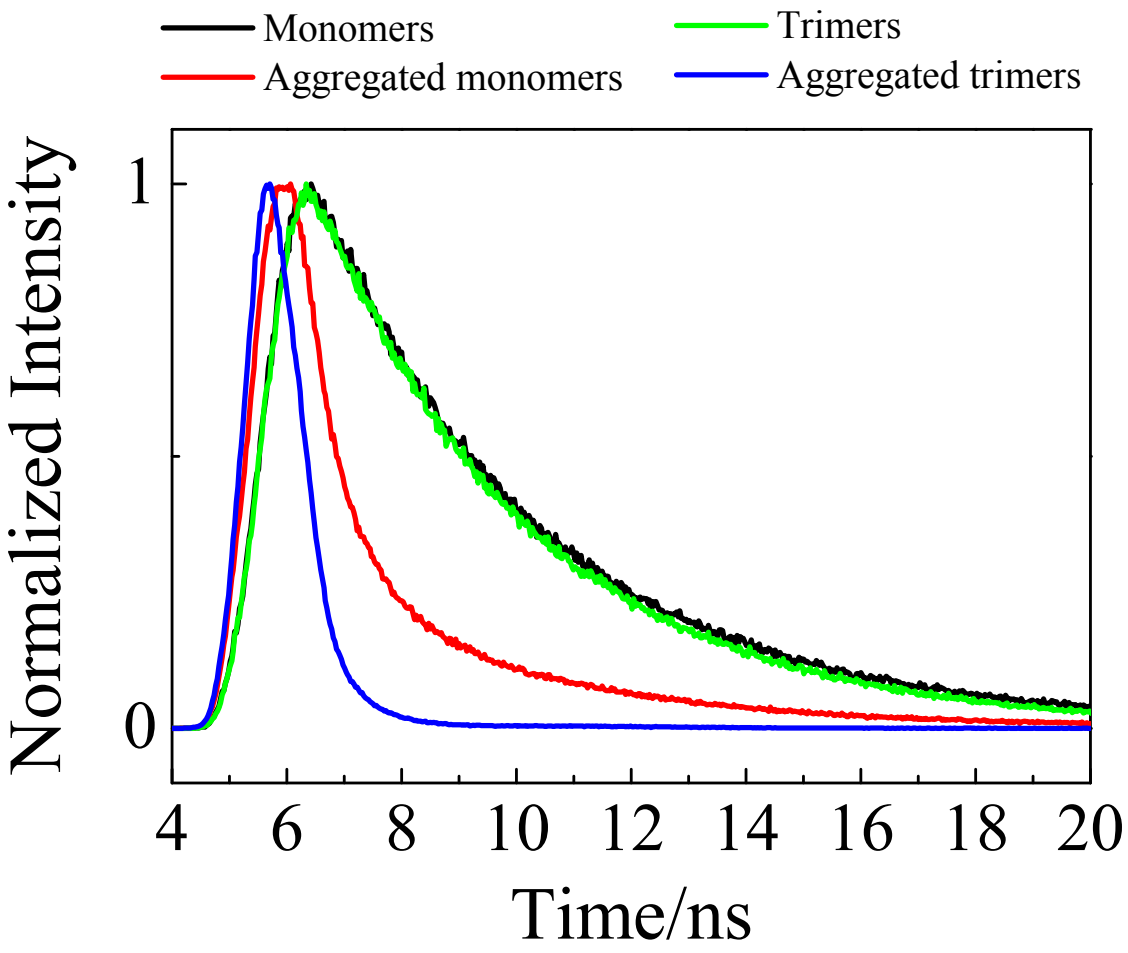


**Figure 8.** Time-resolved fluorescence decay profiles of LHCII complexes excited at 665 nm and probed at 681 nm at room temperature.

monomeric and trimeric LHCII are essentially the same. However, aggregation of the monomeric and trimeric LHCII complexes leads to significantly faster deactivation of Chl *a* excited states with the aggregated trimers decaying approximately 50% faster than the aggregated monomers (compare blue and red traces in Figure 8). The results also show that aggregating monomeric LHCII complexes does not lead solely to trimeric LHCII or to aggregated LHCII trimers, but instead has its own Chl fluorescence quenching characteristics.

In order to gain a better understanding of the kinetic components responsible for the Chl *a* fluorescence decay, the time-resolved data were globally fit to a sum of exponentials function which produced decay-associated spectra (DAS). These are shown in Figure 9. The fluorescence kinetics from all of the samples can be accounted for by three decay components which for the unaggregated LHCII monomers and trimers (top two panels in Figure 9) fall within the ranges of 0.21 ± 0.4 ns, 3.3 ns ± 0.1 ns, and 4.9 ± 0.5 ns which are very similar to what was reported previously using picosecond time-resolved fluorescence on Chl-*a*/*b* protein complex at room temperature.[58] The DAS from these two samples all have very similar lineshapes with only minor wavelength shifts. The first and fastest component has a maximum in the range 677 ± 2 nm and very likely corresponds to unequilibrated Chl *a* excitation. The second and third components have maxima that are slightly red-shifted to 682 ± 1 nm and 679 ± 2 nm, respectively and based on previous work[58,73,74] can be assigned to the decay of the vibrationally-equilibrated lowest excited singlet state of Chl *a* in different protein environments.

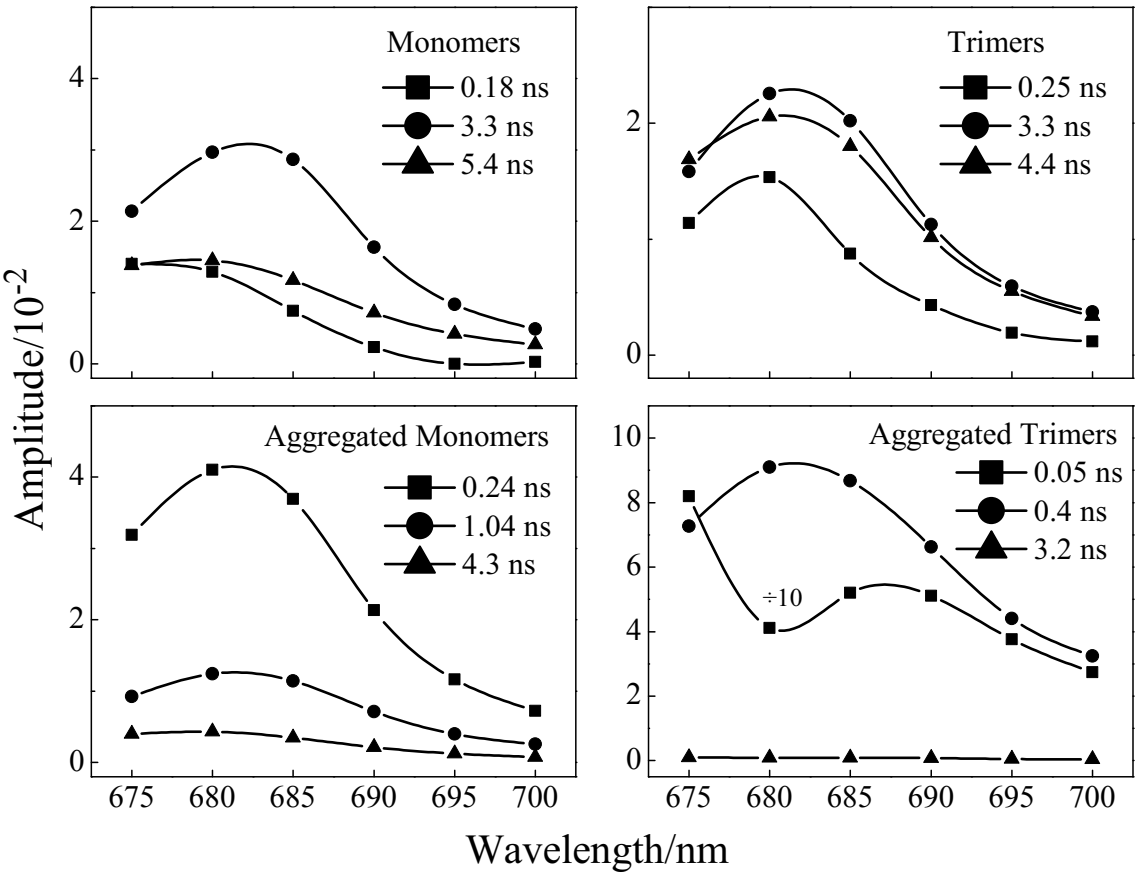


**Figure 9.** Decay associated fluorescence spectra of the LHCII complexes taken using 665 nm excitation at room temperature as described in the text. All of the samples were measured at the same total Chl concentration.

Aggregation of the monomeric LHCII complex slightly increases the lifetime of the fastest component (square symbols in the two left hand panels of Figure 9) and decreases the lifetimes of the two long-lived components by a moderate amount (circle and triangle symbols in the two left hand panels of Figure 9). The more important observation is that upon aggregation, the fastest component (square symbols in the two left hand panels of Figure 9) increases in amplitude by nearly a factor of 4 and red-shifts by ~7 nm, whereas the amplitudes of the two longer-lived components decrease by a factor of ~3 and their wavelength maxima remain relatively unchanged. Aggregation of the trimeric LHCII complex leads to even more dramatic changes in the DAS profiles and lifetimes of the components. The fastest component observed in the aggregated trimers has a unique band at ~687 nm which may represent the deactivation of a rapidly-populated low-energy excitation trap. Also remarkable is the observation that the amplitude of the slowest component has been diminished by an order of magnitude relative to that observed in the unaggregated trimer sample. These kinetic results are entirely consistent with the steady-state fluorescence experiments (Figure 4) which revealed that the aggregated monomer and trimer samples were both ~90% quenched with respect to the unaggregated samples. However, the more interesting aspect in comparing the lifetimes of the kinetic components of the aggregated monomers and trimers is the qualitative differences observed between these two forms of the LHCII protein.

***Transient absorption***

Transient absorption spectra of the monomeric and trimeric, aggregated and unaggregated LHCII complexes taken at various delay times after laser excitation are presented in Figure 10. Spectra in the visible region recorded upon excitation at 490 nm (left hand column in Figure 10) show that essentially within the time profile of the excitation laser pulse, there occurs an onset of bleaching of the carotenoid bands in the region 450 to 525 nm, a bleaching of the Chl *a* and *b* $Q_Y$ absorption bands at ~685 nm and ~650 nm, respectively, and a buildup of carotenoid $S_1 \rightarrow S_N$ transient absorption between 500 and 600 nm. In all of the samples, the carotenoid transient absorption signal decreases by about 30% and the Chl *b* $Q_Y$ band bleaching decreases by approximately 90% in 5 ps (see green traces in the left hand panels of Figure 10). However, the kinetics of the recovery of the Chl *a* $Q_Y$ band bleaching depend on the aggregation state of the LHCII complex. The recovery is much faster for the aggregated monomers and trimers compared to the unaggregated complexes. This is evidenced by the fact that at 500 ps, the bleaching of the Chl *a* $Q_Y$ band in the aggregated complexes is completely gone (see the blue traces in the second and fourth panels on the left hand side of Figure 10), indicating that all the Chl *a* molecules have returned to the ground state within this time frame. However, for the unaggregated monomers and trimers, a significant amount of bleaching of the Chl *a* $Q_Y$ band persists in the transient spectra taken at 500 ps (see the blue traces in the first and third panels on the left hand side of Figure 10). This indicates that many Chl *a* molecules are remaining in the excited state well beyond 500 ps.

Transient NIR spectra recorded upon 490 nm excitation show a fast-decaying carotenoid signal between 900 and 1200 nm presumably associated with the $S_2 \rightarrow S_N$

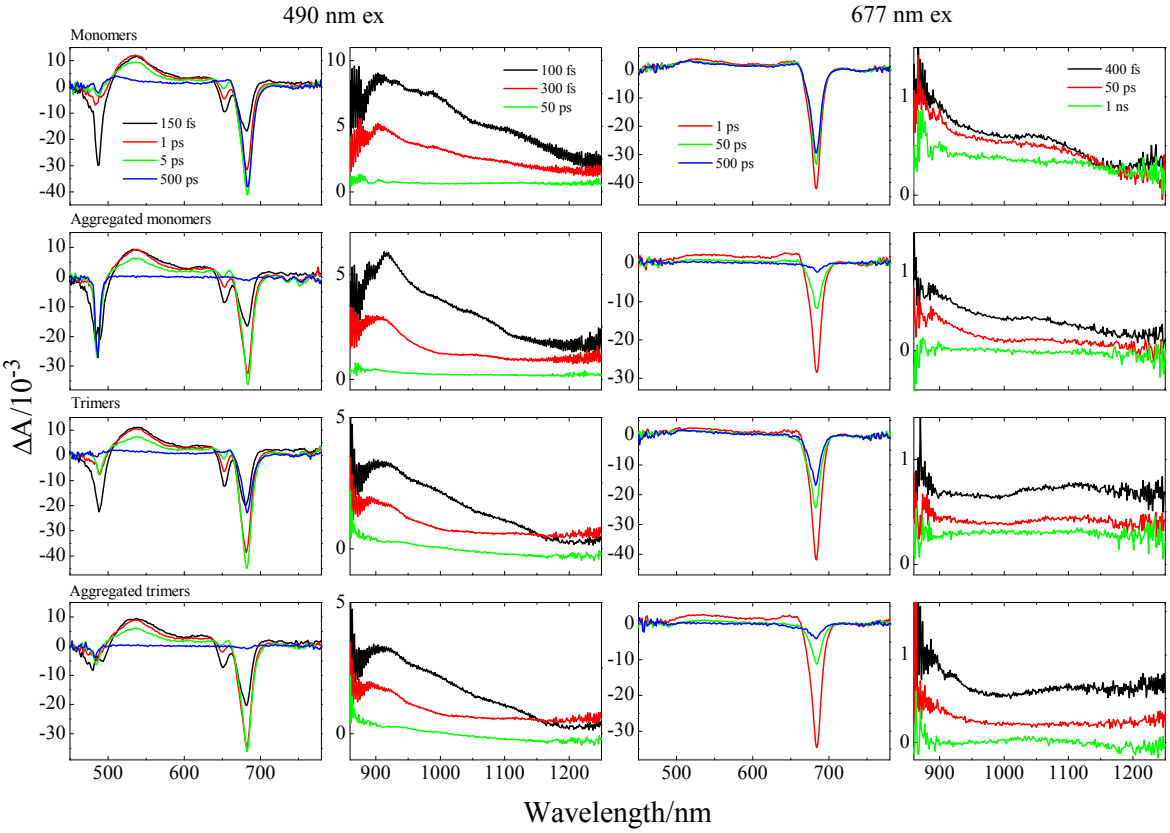


**Figure 10.** Transient absorption spectra of LHCII complexes in the visible and NIR regions. The spectra were recorded at the indicated delay times after excitation at 490 nm and 677 nm.

transition (see the black traces in the second column of panels in Figure 10). The transient absorption feature at ~910 nm appears slightly sharper in the monomeric complexes, but otherwise the spectra taken at this delay time and at 300 fs and 50 ps are very similar for all the complexes. Transient NIR spectra recorded after exciting the samples directly into the $Q_Y$ band of Chl *a* with 677 nm light (see the fourth column of panels in Figure 10) display features that are not sufficiently distinct from each other to draw any significant conclusions regarding the differences between the monomers and trimers, or aggregated and unaggregated LHCII complexes.

Spectra taken at 1 ps in the visible region after 677 nm excitation directly into the Chl *a* $Q_Y$ band (third column in Figure 10) show a pronounced bleaching of this band, but also display a weak positive signal in the spectral region between 480 and 600 nm which is much more noticeable for the aggregated complexes compared to the unaggregated complexes (see the red traces in the third column of panels in Figure 10). The maxima in the weak positive signals for the aggregated monomers and trimers correspond precisely to the position of the $S_1 \rightarrow S_N$ transitions seen upon 490 nm excitation (first column of panels in Figure 10). This suggests that upon excitation into the $Q_Y$ band of Chl *a* at 677 nm, there is some energy transfer from Chl *a* to the $S_1$ state of a carotenoid which then rapidly deactivates to the ground state as a mechanism for quenching. The weak intensity of the carotenoid transient absorption signal supports the kinetic model for quenching proposed by[30] whereby a relatively slow rate of energy transfer from Chl *a* to a carotenoid is followed by fast deactivation of the excited state energy to the ground state by the carotenoid. At 50 ps, the weak positive signal has disappeared, but the Chl *a* $Q_Y$ band bleaching persists albeit to a lesser extent than seen at 1 ps. By 500 ps the Chl *a* $Q_Y$

band bleaching is greatly diminished in the aggregated LHCII samples (see the blue traces in the second and fourth panels in the third column of Figure 10), indicating that almost all the Chl *a* molecules have returned to the ground state. This is not the case for the unaggregated LHCII samples (see the blue traces in the first and third panels in the third column of Figure 10) where the Chl *a* band bleaching is still substantial. This indicates once again that for the aggregated complexes there is a rapid pathway for deactivation of excited Chl *a*, but for the unaggregated complexes, many Chl *a* molecules are remaining in the excited state well beyond 500 ps.

The profound differences in the kinetics of Chl *a* excited state relaxation among the complexes is further illustrated by the time traces shown in Figure 11. Upon excitation at 490 nm and monitoring the recovery of the Chl *a* $Q_Y$ band bleaching, monomeric LHCII decays relatively slowly (in ~3 ns) back to the ground state. Trimeric LHCII undergoes a multiphasic recovery where part of the population decays rapidly in ~25 ps, presumably due to exciton annihilation owing to close proximity between pigments in the trimeric system, and the remaining excited states population decays in ~1 ns. Both aggregated monomers and trimers deactivate much faster (~120 ps) than the unaggregated systems consistent with the observation of extensive Chl *a* excited state quenching seen in the fluorescence experiments (Figures 4, 8 and 9).

In order to obtain a more detailed understanding of the dynamics of energy transfer and excited state deactivation, the spectral and temporal datasets from the transient absorption experiments recorded in the visible and NIR regions using either 490 nm or 677 nm excitation were globally fit according to a sequential excited state decay model. The analysis yielded evolution associated differential spectra (EADS)[75] that

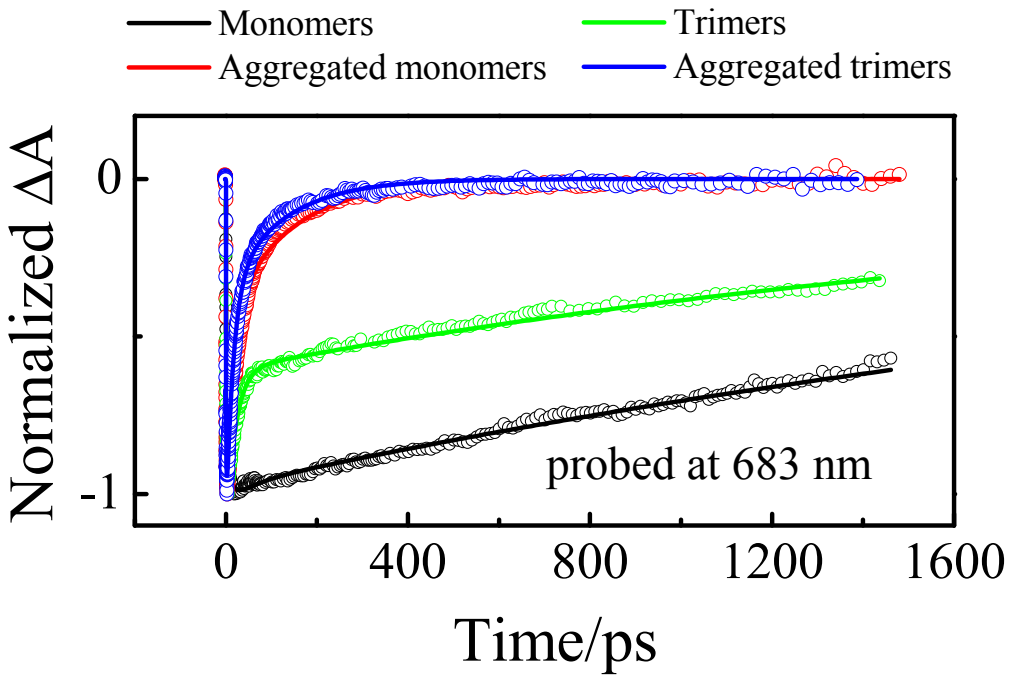


**Figure 11.** Transient absorption decay profiles monitored at 683 nm in the $Q_Y$ region of Chl *a* absorption upon 490 nm excitation at room temperature.

characterize the excited state energy transfer pathways and decay components of the carotenoids and Chls bound in the LHCII complexes. The results of the analysis are presented in Figure 12, and the lifetimes of the components obtained from the fits to the data are given in Table 1. For the experiments using 490 nm excitation, five kinetic components were required to obtain a satisfactory fit to the data. In going from the first to the second EADS component, in all cases, there is a decrease in the bleaching of the $S_0 \rightarrow S_2$ transition of the carotenoids and a substantial increase in the bleaching of the Chl *a* $Q_Y$ absorption band (see the red traces in the left hand column of Figure 12). Also, the bleaching of the Chl *b* $Q_Y$ absorption band at ~650 nm either remains the same (aggregated monomers) or decreases (all other complexes). This indicates that no further energy transfer from the carotenoids to Chl *b* is taking place, but that energy transfer to Chl *a* is occurring from either the carotenoids or Chl *b* or both. This second EADS component also shows a large, broad, positive feature between 500 and 600 nm that can be attributed to the buildup of excited state population in the $S_1$ state of the carotenoids via deactivation of the $S_2$ state in ≤155 fs. From previous work[65] this broad feature can be assigned to a vibronically hot $S_1 \rightarrow S_N$ transition of the carotenoids.

As the second EADS component decays to form the third EADS component the amplitude of the broad positive feature between 500 and 600 nm remains relatively constant, but the width of the band narrows (see the green traces in the left hand column panels in Figure 12). This change is accompanied by a further reduction in the magnitude of the bleaching of the Chl *b* $Q_Y$ band, but a continued rise in the extent of bleaching of the Chl *a* $Q_Y$ band. The narrowing of the $S_1 \rightarrow S_N$ transition of the carotenoid is very likely due to relaxation of the vibrationally hot $S_1$ state of the carotenoids.[76] Because the

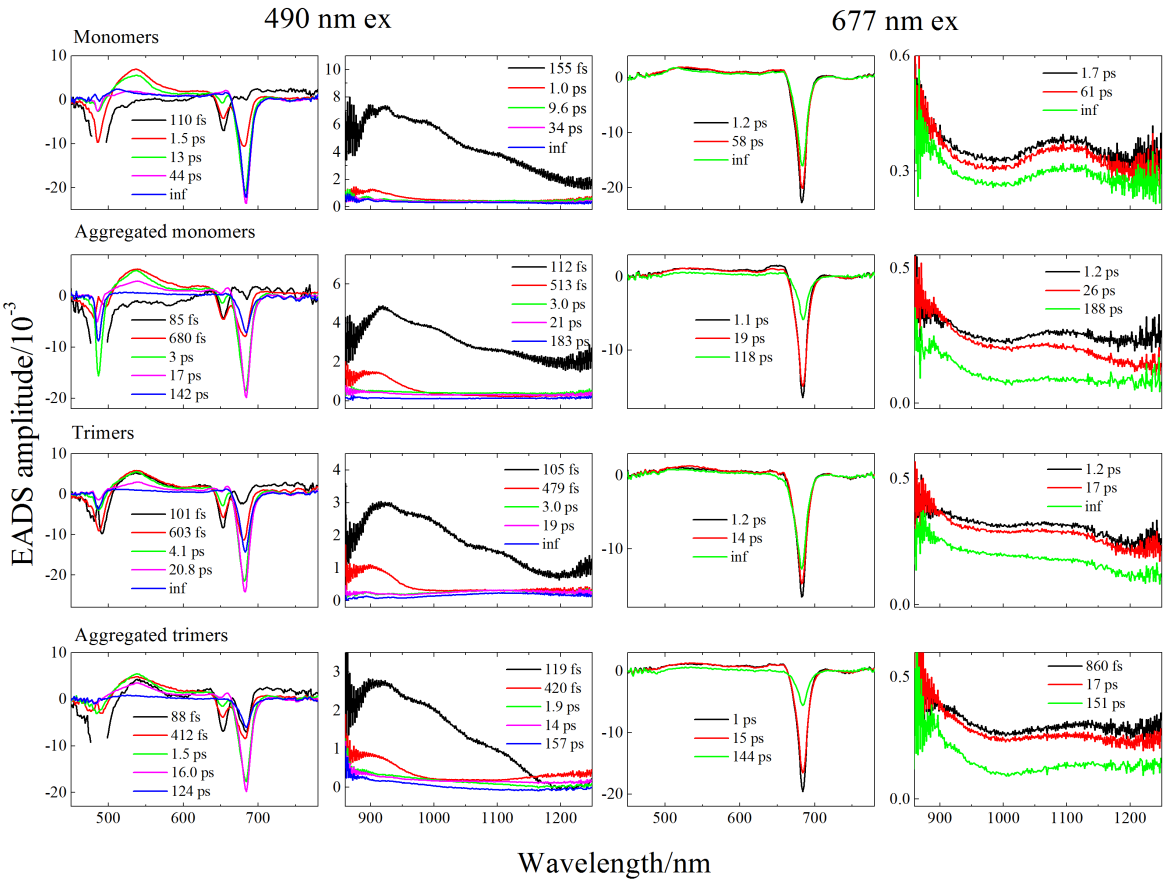


**Figure 12.** Evolution associated difference spectra (EADS) of unaggregated and aggregated LHCII complexes obtained from global fitting the transient absorption datasets recorded in the visible and NIR regions using 490 and 677 nm excitation.

**Table 1**. Dynamics of the excited states of LHCII monomers, trimers and aggregates. Uncertainties in the values based on the goodness of fit amount to no more than 10% in all cases.

| LHCII sample | Excitation λ/nm | Probe region | lifetime/ps | | | | |
|---|---|---|---|---|---|---|---|
| | | | $\tau_1$ | $\tau_2$ | $\tau_3$ | $\tau_4$ | $\tau_5$ |
| Monomers | 490 | vis | 0.110 | 1.5 | 13 | 44 | inf |
| | | NIR | 0.155 | 1.0 | 9.6 | 34 | inf |
| | 677 | vis | 1.2 | 58 | inf | – | – |
| | | NIR | 1.7 | 61 | inf | – | – |
| Aggregated monomers | 490 | vis | 0.085 | 0.68 | 3.0 | 17 | 142 |
| | | NIR | 0.112 | 0.513 | 3.0 | 21 | 183 |
| | 677 | vis | 1.1 | 19 | 118 | – | – |
| | | NIR | 1.2 | 26 | 188 | – | – |
| Trimers | 490 | vis | 0.101 | 0.603 | 4.1 | 20.8 | inf |
| | | NIR | 0.105 | 0.479 | 3.0 | 19 | inf |
| | 677 | vis | 1.2 | 14 | inf | – | – |
| | | NIR | 1.2 | 17 | inf | – | – |
| Aggregated trimers | 490 | vis | 0.088 | 0.412 | 1.5 | 16 | 124 |
| | | NIR | 0.119 | 0.420 | 1.9 | 14 | 157 |
| | 677 | vis | 1 | 15 | 144 | – | – |
| | | NIR | 0.860 | 17 | 151 | – | – |

magnitude of this band is not changing very much, the additional bleaching of the Chl *a* $Q_Y$ band that occurs can be accounted for by energy transfer from Chl *b* to Chl *a*.

In going from the third to the fourth EADS component (purple traces in the left hand column panels of Figure 12), there is a significant reduction in the positive amplitude attributable to the $S_1 \rightarrow S_N$ excited state absorption of the carotenoids. Yet, only a very small increase in the amplitude associated with the bleaching of the $Q_Y$ band of Chl *a* is seen, and this can be correlated with the disappearance of the bleaching of the $Q_Y$ band of Chl *b*. This argues that no further energy transfer from the carotenoids to Chl *a* is taking place, but Chl *b* is transferring all of its remaining excited state energy to Chl *a* in this time domain. Moreover, this observation strongly suggests that the $S_1$ state of the carotenoids is not involved in transferring energy to Chl *a*.[77] This is because the lifetime of the third EADS components is very similar to the $S_1$ lifetime reported for the carotenoids in LHCII complexes.[65,72]

The fourth EADS component has a lifetime between 16 and 44 ps, and it decays into the final EADS component (blue traces in the left hand column panels of Figure 12). The most notable spectral change accompanying this decay is that in all of the samples except the unaggregated monomeric LHCII complex, there is a profound decrease in the bleaching of the $Q_Y$ band of Chl *a*. In the unaggregated monomeric LHCII complex there is no change in the magnitude of the bleaching of this band in going from the fourth to the final EADS trace (see the purple and blue lines in the top left hand panel in Figure 12). Also, the lifetime of the final EADS component is very long (infinite) for the unaggregated samples, but much faster at 142 ps and 124 ps for the aggregated monomers and aggregated trimers, respectively.

The EADS lineshapes resulting from a fit of the transient data taken using 677 nm are shown in the right hand column panels of Figure 12. In all cases, three kinetic components were required to fit the data. Whereas the first two kinetic components have reasonably similar lifetimes for all the samples, there is a major difference in the lifetime of the third and final component. The lifetime of this component for the unaggregated monomers and trimers is essentially infinite (non-decaying). However, as was evident in the fits to the data taken using 490 nm excitation (left hand column panels of Figure 12), the lifetime of this final component decreases significantly upon aggregation of the LHCII complexes and becomes 118 ps for the monomers and 144 ps for the trimers. These results together with those obtained from the global fitting analysis of the data recorded using 490 nm excitation described above, clearly demonstrate that aggregation of either monomeric or trimeric LHCII complexes accelerates the decay of Chl *a* excited states.

The striking reduction in fluorescence intensity upon aggregation of the monomeric and trimeric LHCII complexes (Figure 4) is highly suggestive of the formation of a quenching center (or centers) that facilitates deactivation of Chl *a* excited states. This idea is reinforced by the emission spectra of the aggregated LHCII samples taken at cryogenic temperatures (bottom two panels in Figure 5) which show red-shifted (low-energy) fluorescence bands not seen in the spectra of purified Chl *a* and *b* (Figure 6) nor in those from unaggregated LHCII complexes (top two panels in Figure 5). The structure of the LHCII trimer[4] and previous work based on spectroscopy and mutagenesis[59,78-83] suggest which Chls may be involved in the formation of these low energy quenching centers.

It is very challenging to try to gain some insight into which specific protein-bound Chl molecules may be giving rise to the spectral differences that occur upon aggregation. Nevertheless, Gaussian deconvolution in the $Q_Y$ region was carried out on the 10 K absorption spectra from aggregated and unaggregated monomeric and trimeric LHCII complexes (Figure 13). The figure reveals that a large number of individual Chl *a* and *b* spectra having various amplitudes and widths are required to simulate the experimental absorption spectral lineshapes. However, it is clear that only some of the peaks have shifted or changed intensity upon aggregation. Difference spectra generated by subtracting the spectra of the unaggregated complexes from those of the aggregated complexes reveal that the major change in the lineshapes upon aggregation occurs on the low energy side of the $Q_Y$ band of Chl *a*. Gaussian components 1 and 2 from the trimers undergo a red-shift of 2 nm. The spectral shifts of all the other Gaussian components induced by aggregation of either the monomers or trimers is only 1 nm. Aggregation of the monomeric LHCII complex leads to an increase in the amplitude of the Chl *a* spectral component (Gaussian peak 2) having a maximum at 682 nm (14,660 $cm^{-1}$) and a decrease in the amplitude of the Chl *a* spectral component (Gaussian peak 3) having a maximumat 676 nm (14,790 $cm^{-1}$), while aggregation of the trimeric LHCII complex leads to a decrease in the amplitude of the Chl *a* spectral component (Gaussian peak 2) having a maximum at 679 nm (14,720 $cm^{-1}$) and an increase in the amplitude of the Chl *a* spectral component (Gaussian peak 3) having a maximum at 676 nm (14,800 $cm^{-1}$). (See Table 2 for a summary of all the Gaussian fitting parameters.) For the aggregated monomers the decrease in peak 3 leads to a pronounced dip in a broad positive band formed from small increases in the amplitudes of several other Chl absorption bands

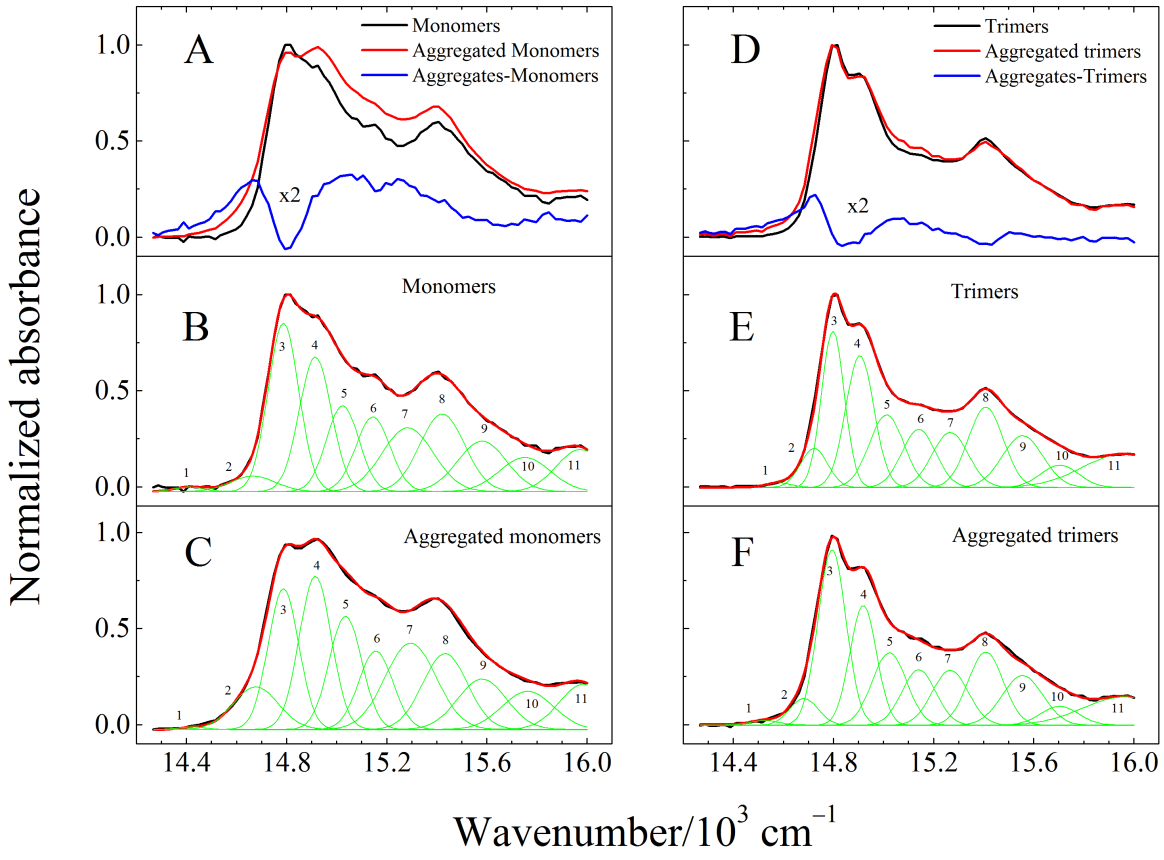


**Figure 13.** Gaussian fits of the 10 K steady-state absorption spectra of unaggregated and aggregated LHCII monomers and trimers. The parameters used in the fits are summarized in Table 2.

**Table 2.** Parameters from the Gaussian fits to the absorption spectra of LHCII monomers, trimers and aggregates shown in Figure 13.

| | Monomers | | | | | Aggregated monomers | | | | |
|---|---|---|---|---|---|---|---|---|---|---|
| Peak | Center of gravity, $cm^{-1}$ | Wavelength, nm | Max height | Peak area | FWHM, $cm^{-1}$ | Center of gravity, $cm^{-1}$ | Wavelength, nm | Max height | Peak area | FWHM, $cm^{-1}$ |
| 1 | 14410 | 694 | 0.0241 | 3.512 | 138 | 14420 | 693 | 0.0143 | 2.106 | 139 |
| 2 | 14660 | 682 | 0.0810 | 18.30 | 212 | 14680 | 681 | 0.2218 | 50.12 | 212 |
| 3 | 14790 | 676 | 0.8763 | 134.6 | 144 | 14790 | 676 | 0.7316 | 112.4 | 144 |
| 4 | 14920 | 670 | 0.7013 | 112.4 | 151 | 14920 | 670 | 0.7981 | 128.0 | 151 |
| 5 | 15020 | 666 | 0.4473 | 72.82 | 153 | 15040 | 665 | 0.5901 | 96.067 | 153 |
| 6 | 15140 | 660 | 0.3886 | 66.65 | 161 | 15160 | 660 | 0.4085 | 70.06 | 161 |
| 7 | 15280 | 654 | 0.3323 | 85.26 | 241 | 15300 | 654 | 0.4491 | 115.2 | 241 |
| 8 | 15420 | 648 | 0.4041 | 90.68 | 211 | 15430 | 648 | 0.3951 | 88.66 | 211 |
| 9 | 15580 | 642 | 0.2630 | 64.41 | 230 | 15580 | 642 | 0.2625 | 64.29 | 230 |
| 10 | 15750 | 635 | 0.1780 | 45.04 | 239 | 15760 | 634 | 0.1993 | 50.29 | 239 |
| 11 | 15970 | 626 | 0.2193 | 32.21 | 223 | 15980 | 626 | 0.2348 | 31.88 | 223 |

| | Trimers | | | | | Aggregated trimers | | | | |
|---|---|---|---|---|---|---|---|---|---|---|
| Peak | Center of gravity, $cm^{-1}$ | Wavelength, nm | Max height | Peak area | FWHM, $cm^{-1}$ | Center of gravity, $cm^{-1}$ | Wavelength, nm | Max height | Peak area | FWHM, $cm^{-1}$ |
| 1 | 14580 | 686 | 0.0239 | 3.241 | 127 | 14530 | 688 | 0.0232 | 3.305 | 134 |
| 2 | 14720 | 679 | 0.2037 | 27.64 | 127 | 14680 | 681 | 0.1399 | 19.90 | 134 |
| 3 | 14800 | 676 | 0.8154 | 92.91 | 107 | 14790 | 676 | 0.9153 | 128.2 | 132 |
| 4 | 14900 | 671 | 0.6878 | 96.66 | 132 | 14920 | 670 | 0.6241 | 83.22 | 125 |
| 5 | 15010 | 666 | 0.3777 | 65.18 | 162 | 15020 | 666 | 0.3780 | 65.18 | 162 |
| 6 | 15140 | 660 | 0.3033 | 51.31 | 159 | 15140 | 660 | 0.2897 | 49.00 | 159 |
| 7 | 15270 | 655 | 0.2872 | 51.77 | 169 | 15270 | 655 | 0.2872 | 51.77 | 169 |
| 8 | 15410 | 649 | 0.4192 | 73.48 | 165 | 15410 | 649 | 0.3818 | 66.93 | 165 |
| 9 | 15560 | 643 | 0.2700 | 55.11 | 192 | 15560 | 643 | 0.2592 | 52.91 | 192 |
| 10 | 15700 | 637 | 0.1163 | 22.15 | 179 | 15710 | 637 | 0.0989 | 18.83 | 179 |
| 11 | 15960 | 626 | 0.1752 | 43.31 | 388 | 15960 | 627 | 0.1472 | 36.38 | 388 |

(Figure 13A). This broad positive band in the difference spectrum is much less evident upon aggregation of the trimers (Figure 13D). These results suggest that the Chl *a* molecules associated with the red-most absorption bands in the unaggregated complexes are the ones most affected by aggregation. It remains to be demonstrated that these are the Chls involved in fluorescence quenching. If this were the case, one would expect to see agreement between the spectra of one or more of the fast-decaying fluorescence kinetic components shown in Figure 9 and the red-shifted fluorescence peaks appearing in the spectra of the aggregated LHCII complexes (Figure 5). For both monomeric and trimeric samples, aggregation leads to a very noticeable increase in intensity and red-shift in the spectrum of the fastest fluorescence decay component recorded at room temperature (see the square symbols in Figure 9), but the relatively low-resolution steady-state fluorescence spectra taken at room temperature precludes a precise assignment of the maximum in the red-shifted peak.

## Conclusions

Remelli et al.[81] proposed on the basis of site-directed mutagenesis of pigment-binding residues in recombinant, pigment-reconstituted, refolded monomeric LHCII that Chl A2 (denoted *a*612 in Figure 1B) accounted for 75% of the absorption at 681 nm, that it was the chromophore with the lowest energy in LHCII, and consequently represented an important avenue for energy transfer to neighboring antenna proteins. These authors also suggested that three other Chl molecules, A1, A6 and B1, denoted Chl *a*610, *a*604 and *b*608 in the notation of Liu et al.[4] (Figure 1), and Chls 1, 6 and 11 in the notation of Standfuss et al.,[27] contribute to the low energy absorption band at 681 nm for the monomers.[81] Subsequently, Rogl et al.[82] argued from similar studies on trimeric complexes that Chl *a*612, denoted Chl a2 by these authors, but absorbing at 676 nm in the trimers rather than at 681 nm for the monomeric LHCII, represented the terminal state in the energy transfer pathway of LHCII as suggested by Remelli et al.[81] However, definitive assignment of the individual Chl molecules in the LHCII structure to specific spectral features on the basis of mutagenesis and/or pigment reconstitution is complicated by the fact that changing the environment of one Chl may affect the spectrum of another. Nevertheless, subsequent experimental work and modeling revealed the details of the interactions between the pigments, and that Chls *a*610, *a*611 and *a*612 (Figure 1B) represented the lowest energy emitters in LHCII.[84,85] These Chls are in close contact with lutein 1 (Figure 1B) which has been reported to undergo a distortion during the transition of LHCII into the quenched state.[86,87] Ilioaia et al. also showed that isolated LHCII complexes immobilized in a gel matrix display the same spectral characteristics as seen for LHCII aggregates.[87] In addition, this work supported the proposal that spectral

changes in the bands associated with Chls *a*610, *a*611 and *a*612 are indicative of an altered protein environment that enhances energy transfer to the $S_1$ excited state of lutein 1 as the quenching site.[28,30,88] Van Oort et al. showed that different crystal forms of LHCII display different extents of fluorescence quenching.[89] Therefore, not only aggregation but any perturbation that results in a protein structural change could alter the spectral and kinetic behavior of the bound pigments. In any case, it is apparent that aggregation of the LHCII complex causes alterations in the absorption and fluorescence spectral profiles, the energy transfer and fluorescence kinetics, and dissipation of a large portion of the absorbed light energy by the protein-bound pigments.

# References


(1) Hofmann, E.; Wrench, P. M.; Sharples, F. P.; Hiller, R. G.; Welte, W.; Diederichs, K. *Science* **1996**, *272*, 1788–1791.

(2) Blankenship, R. E. *Molecular Mechanisms of Photosynthesis.* Blackwell Science: Oxford, 2002.

(3) Roszak, A. W.; Howard, T. D.; Southall, J.; Gardiner, A. T.; Law, C. J.; Isaacs, N. W.; Cogdell, R. J. *Science* **2003**, *302*, 1969–1972.

(4) Liu, Z. F.; Yan, H. C.; Wang, K. B.; Kuang, T. Y.; Zhang, J. P.; Gui, L. L.; An, X. M.; Chang, W. R. *Nature* **2004**, *428*, 287–292.

(5) Frank, H. A.; Cogdell, R. J. Light Capture in Photosynthesis In *Comprehensive Biophysics*; Egelman, E. H., Ed.; Academic Press: Oxford, **2012**; Vol. 8, 94–114.

(6) Witt, H. T.; Witt, I.; Krauss, N.; Hinrichs, W.; Fromme, P.; Saenger, W. *Biophys. J.* **1994**, *66*, A2–A2.

(7) Fromme, P.; Mathis, P. *Photosynth. Res.* **2004**, *80*, 109–124.

(8) Nelson, N.; Yocum, C. F. *Annual Reviews of Plant Biology* **2006**, *57*, 521–565.

(9) Peter, G. F.; Thornber, J. P. *J. Biol. Chem.* **1991**, *266*, 16745–16754.

(10) Horton, P.; Ruban, A. V.; Young, A. J. Regulation of the Structure and Function of the Light Harvesting Complexes of Photosystem II by the Xanthophyll Cycle In *The Photochemistry of Carotenoids*; Frank, H. A., Young, A. J., Britton, G., Cogdell, R. J., Eds.; Kluwer Academic Publishers: Dordrecht, **1999**; Vol. 8, 271–291.

(11) Green, B. R.; Parson, W. W. *Light-Harvesting Antennas in Photosynthesis.* Kluwer Academic Publishers: Dordrecht, 2003.

(12) Kühlbrandt, W.; Wang, D. N.; Fujiyoshi, Y. *Nature* **1994**, *367*, 614–621.

(13) Telfer, A.; Pascal, A.; Gall, A. Carotenoids in Photosynthesis In *Carotenoids Vol. 4: Natural Functions*; Britton, G., Liaaen-Jensen, S., Pfander, H., Eds.; Birkäuser Verlag: Basel-Boston_Berlin, **2008**; Vol. 4.

(14) Ruban, A. V.; Lee, P. J.; Wentworth, M.; Young, A. J.; Horton, P. *J. Biol. Chem.* **1999**, *274*, 10458–10465.

(15) Croce, R.; Weiss, S.; Bassi, R. *J. Biol. Chem.* **1999**, *274*, 29613–29623.

(16) Foote, C. S. *Science* **1968**, *162*, 963–970.

(17) Foote, C. S.; Chang, Y. C.; Denny, R. W. *J. Am. Chem. Soc.* **1970**, *92*, 5216–5218.

(18) Krieger-Liszkay, A. *J. Exp. Bot.* **2004**, *56*, 337–346.

(19) Frank, H. A.; Cogdell, R. J. *Photochem. Photobiol.* **1996**, *63*, 257–264.

(20) Foyer, C.; Harbinson, J. Relationships between Antioxidant Metabolism and Carotenoids in the Regulation of Photosynthesis. In *The Photochemistry of Carotenoids*; Frank, H. A., Young, A. J., Britton, G., Cogdell, R. J., Eds.; Kluwer Academic Publishers: Dordrecht, The Netherlands, **1999**; Vol. 8, 305–325.

(21) Mozzo, M.; Dall'Osto, L.; Hienerwadel, R.; Bassi, R.; Croce, R. *J. Biol. Chem.* **2008**, *283*, 6184–6192.

(22) Demmig-Adams, B.; Adams, W. W. I. *Annual Review of Plant Physiology and Plant Molecular Biology* **1992**, *43*, 599–626.

(23) Horton, P.; Ruban, A. V.; Walters, R. G. *Annual Review of Plant Physiology and Plant Molecular Biology* **1996**, *47*, 655–684.

(24) Müller, P.; Li, X.-P.; Niyogi, K. K. *Plant Physiol.* **2001**, *125*, 1588–1566.

(25) Holt, N. E.; Fleming, G. R.; Niyogi, K. K. *Biochem.* **2004**, *43*, 8281–8289.

(26) Avenson, T. J.; Ahn, T. K.; Zigmantas, D.; Niyogi, K.; Li, Z.; Ballottari, M.; Bassi, R.; Fleming, G. R. *J. Biol. Chem.* **2008**, *283*, 3550–3558.

(27) Standfuss, J.; van Scheltinga, A. C. T.; Lamborghini, M.; Külbrandt, W. *EMBO J.* **2005**, *24*, 919–928.

(28) Pascal, A. A.; Liu, Z.; Broess, K.; van Oort, B.; van Amerongen, H.; Wang, C.; Horton, P.; Robert, B.; Chang, W.; Ruban, A. V. *Nature* **2005**, *436*, 134–137.

(29) Amarie, S.; Standfuss, J.; Barros, T.; Külbrandt, W.; Dreuw, A.; Wachtveitl, J. *J. Phys. Chem. B* **2007**, *111*, 3481–3487.

(30) Ruban, A. V.; Berera, R.; Ilioaia, C.; van Stokkum, I. H. M.; Kennis, J. T. M.; Pascal, A. A.; van Amerongen, H.; Robert, B.; Horton, P.; van Grondelle, R. *Nature* **2007**, *450*, 575–579.

(31) Phillip, D.; Ruban, A. V.; Horton, P.; Asato, A.; Young, A. J. *Proc. Natl. Acad. Sci. USA* **1996**, *93*, 1492–1497.

(32) Ruban, A. V.; Young, A. J.; Horton, P. *Biochem.* **1996**, *35*, 674–678.

(33) Demmig-Adams, B.; Adams, W. W. *Science* **2002**, *298*, 2149–2153.

(34) Kulheim, C.; Agren, J.; Jansson, S. *Science* **2002**, *297*, 91–93.

(35) Horton, P.; Ruban, A. *J. Exp. Bot.* **2005**, *56*, 365–373.

(36) Holt, N. E.; Zigmantas, D.; Valkunas, L.; Li, X. P.; Niyogi, K. K.; Fleming, G. R. *Science* **2005**, *307*, 433–436.

(37) Ahn, T. K.; Avenson, T. J.; Ballottari, M.; Cheng, Y. C.; Niyogi, K. K.; Bassi, R.; Fleming, G. R. *Science* **2008**, *320*, 794–797.

(38) Cheng, Y.-C.; Ahn, T.-K.; Avenson, T. J.; Zigmantas, D.; Niyogi, K. K.; Ballottari, M.; Bassi, R.; Fleming, G. R. *J. Phys. Chem. B* **2008**, *112*, 13418–13423.

(39) Avenson, T. J.; Ahn, T. K.; Niyogi, K. K.; Ballottari, M.; Bassi, R.; Fleming, G. R. *J. Biol. Chem.* **2009**, *284*, 2830–2835.

(40) Barros, T.; Kuhlbrandt, W. *Biochim. Biophys. Acta* **2009**, *1787*, 753–772.

(41) Barros, T.; Royant, A.; Standfuss, J.; Dreuw, A.; Kuhlbrandt, W. *EMBO J.* **2009**, *28*, 298–306.

(42) Niyogi, K.; Li, X.-P.; Rosenberg, V.; Jung, H.-S. *J. Exp. Bot.* **2005**, *56*, 375–382.

(43) Bode, S.; Quentmeier, C. C.; Liao, P.-N.; Barros, T.; Walla, P. J. *Chem. Phys. Lett.* **2008**, *450*, 379–385.

(44) Bode, S.; Quentmeier, C. C.; Liao, P.-N.; Hafi, N.; Barros, T.; Wilk, L.; Bittner, F.; Walla, P. J. *Proc. Natl. Acad. Sci. USA* **2009**, *106*, 12311–12316.

(45) Liao, P. N.; Bode, S.; Wilk, L.; Hafi, N.; Walla, P. J. *Chem. Phys.* **2010**, *373*, 50–55.

(46) Miloslavina, Y.; Wehner, A.; Lambrev, P. H.; Wientjes, E.; Reus, M.; Garab, G.; Croce, R.; Holzwarth, A. R. *FEBS Lett.* **2008**, *582*, 3625–3631.

(47) Holzwarth, A. R.; Miloslavina, Y.; Nilkens, M.; Jahns, P. *Chem. Phys. Lett.* **2009**, *483*, 262–267.

(48) Muller, M. G.; Lambrev, P.; Reus, M.; Wientjes, E.; Croce, R.; Holzwarth, A. R. *Chemical Physics and Physical Chemistry* **2010**, *11*, 1289–1296.

(49) Bassi, R.; Silvestri, M.; Dainese, P.; Moya, I.; Giacometti, G. *J. Photochem. Photobiol., B* **1991**, *9*, 335–354.

(50) Mullineaux, C. W.; Pascal, A. A.; Horton, P.; Holzwarth, A. R. *Biochim. Biophys. Acta* **1993**, *1141*, 23–28.

(51) Gilmore, A. M.; Hazlett, T. L.; Govindjee *Proc. Natl. Acad. Sci. USA* **1995**, *92*.

(52) Vasil'ev, S.; Irrgang, K.-D.; Schrötter, T.; Bergmann, A.; Eichler, H.-J.; Renger, G. *Biochem.* **1997**, *36*, 7503–7512.

(53) Moya, I.; Silvestri, M.; Vallon, O.; Cinque, G.; Bassi, R. *Biochem.* **2001**, *40*, 12552–12561.

(54) Palacios, M. A.; de Weerd, F. L.; Ihalainen , J. A.; van Grondelle, R. v.; Amerongen, H. v. *J. Phys. Chem. B* **2002**, *106*, 5782–5787.

(55) Huyer, J.; Eckert, H.-J.; Irrgang, K.-D.; Miao, J.; Eichler, H.-J.; Renger, G. *J. Phys. Chem. B* **2004**, *108*, 3326–3334.

(56) van Oort, B.; van Hoek, A.; Ruban, A. V.; van Amerongen, H. *J. Phys. Chem. B* **2007**, *111*, 7631–7637.

(57) Nordlund, T. M. *Biophys. J.* **1981**, *36*, 193–201.

(58) Ide, J. P.; Klug, D. R.; Kühlbrandt, W.; Giorgi, L. B.; Porter, G. *Biochim. Biophys. Acta* **1987**, *893*, 349–364.

(59) Pieper, J.; Irrgang, K.-D.; Rätsep, M.; Jankowiak, R.; Schrötter, T.; Voigt, J.; Small, G. J.; Renger, G. *J. Phys. Chem. A* **1999**, *103*, 2422–2428.

(60) Andreeva, A.; Abarova, S.; Stoitchkova, K.; Busheva, M. *Eur. Biophys. J.* **2009**, *38*, 199–208.

(61) Gruszecki, W. I.; Luchowski, R.; Grudzinski, W.; Gryczynski, I. Photosynthetic Antenna Complex Lhcii Studied with Novel Fluorescence Techniques In

*Spectroscopic Methods of Analysis: Methods and Protocols*; Bujalowski, W. M., Ed.; Springer Science: New York, **2012**; Vol. 875, 263–269.

(62) Das, S. K.; Frank, H. A. *Biochem.* **2002**, *41*, 13087–13095.

(63) Berthold, D. A.; Babcock, G. T.; Yocum, C. F. *FEBS Lett.* **1981**, *134*, 231–234.

(64) Ilagan, R. P.; Christensen, R. L.; Chapp, T. W.; Gibson, G. N.; Pascher, T.; Polivka, T.; Frank, H. A. *J. Phys. Chem. A* **2005**, *109*, 3120–3127.

(65) Fuciman, M.; Enriquez, M. M.; Polivka, T.; Dall'Osto, L.; Bassi, R.; Frank, H. A. *J. Phys. Chem. B* **2012**, *116*, 3834–3849.

(66) Naqvi, K. R.; Melo, T. B.; Raju, B. B.; Javorfi, T.; Simidjiev, I.; Garab, G. *Spectrochimica Acta Part A: Molecular and Biomolecular Spectroscopy* **1997**, *53*, 2659–2667.

(67) Ruban, A. V.; Calkoen, F.; Kwa, S. L. S.; van Grondelle, R.; Horton, P.; Dekker, J. P. *Biochim. Biophys. Acta* **1997**, *1321*, 61–70.

(68) Barzda, V.; Gulbinas, V.; Kananavicius, R.; Cervinskas, V.; Van Amerongen, H.; Van Grondelle, R.; Valkunas, L. *Biophys. J.* **2001**, *80*, 2409–2421.

(69) Gruszecki, W. I.; W., G.; M., G.; M., P.; W., M. *Biochim. Biophys. Acta* **2006**, *1757*, 1504–1511.

(70) Ruban, A. V.; Dekker, J. P.; Horton, P.; van Grondelle, R. *Photochem. Photobiol.* **1995**, *61*, 216–221.

(71) Gradinaru, C. C.; van Stokkum, I. H. M.; Pascal, A. A.; van Grondelle, R.; van Amerongen, H. *J. Phys. Chem. B* **2000**, *104*, 9330–9342.

(72) Croce, R.; Muller, M. G.; Bassi, R.; Holzwarth, A. R. *Biophys. J.* **2001**, *80*, 901–915.

(73) Frank, H. A.; Das, S. K.; Bautista, J. A.; Bruce, D.; Vasilev, S.; Crimi, M.; Croce, R.; Bassi, R. *Biochem.* **2001**, *40*, 1220–1225.

(74) Andersson, J.; Walters, R. G.; Horton, P.; Jansson, S. *Plant Cell* **2001**, *13*, 1193–1204.

(75) van Stokkum, I. H. M.; Larsen, D. S.; van Grondelle, R. *Biochim. Biophys. Acta* **2004**, *1657*, 82–104.

(76) Billsten, H. H.; Zigmantas, D.; Sundström, V.; Polívka, T. *Chem. Phys. Lett.* **2002**, *355*, 465–470.

(77) Connelly, J. P.; Mueller, M. G.; Bassi, R.; Croce, R.; Holzwarth, A. R. *Biochem.* **1997**, *36*, 281–287.

(78) Zucchelli, G.; Jennings, R. C.; Garlaschi, F. M. *J. Photochem. Photobiol., B* **1990**, *6*, 381–394.

(79) Trinkunas, G.; Connelly, J. P.; Müller, M. G.; Valkunas, L.; Holzwarth, A. R. *J. Phys. Chem. B* **1997**, *101*, 7313–7320.

(80) Pieper, J.; Rätsep, M.; Jankowiak, R.; Irrgang, K.-D.; Voigt, J.; Renger, G.; Small, G. J. *J. Phys. Chem. A* **1999**, *103*, 2412–2421.

(81) Remelli, R.; Varotto, C.; Sandona, D.; Croce, R.; Bassi, R. *J. Biol. Chem.* **1999**, *274*, 33510–33521.

(82) Rogl, H.; Schödel, R.; Lokstein, H.; Kühlbrandt, W.; Schubert, A. *Biochem.* **2002**, *41*, 2281–2287.

(83) Croce, R.; Muller, M. G.; Caffari, S.; Bassi, R.; Holzwarth, A. R. *Biophys. J.* **2003**, *84*, 2517–2532.

(84) van Grondelle, R.; Novoderezhkin, V. I. *Phys. Chem. Chem. Phys.* **2006**, *8*, 793–807.

(85) Georgakopoulou, S.; van der Zwan, G.; Bassi, R.; van Grondelle, R.; van Amerongen, H.; Croce, R. *Biochem.* **2007**, *46*, 4745–4754.

(86) Johnson, M. P.; Ruban, A. V. *J. Biol. Chem.* **2009**, *284*, 23592–23601.

(87) Ilioaia, C.; Johnson, M. P.; Liao, P.-N.; Pascal, A. A.; van Grondelle, R.; Walla, P. J.; Ruban, A. V.; Robert, B. *J. Biol. Chem.* **2011**, *286*, 27247–27254.

(88) Wahadoszamen, M.; Berera, R.; Ara, A. M.; Romero, E.; van Grondelle, R. *Phys. Chem. Chem. Phys.* **2012**, *14*, 759–766.

(89) van Oort, B.; Maréchal, A.; Ruban, A. V.; Robert, B.; Pascal, A. A.; de Ruijter, N. C. A.; van Grondelle, R.; van Amerongen, H. *Phys. Chem. Chem. Phys.* **2011**, *13*, 12614–12622.

# *Chapter IV*

# *High Efficiency light-harvesting by carotenoids in the LH2 complex from photosynthetic bacteria: Unique adaptation to growth under low-light conditions*

## Introduction

The competition for solar photons among aquatic photosynthetic organisms striving to maintain viability at various depths in the water column is fierce, often requiring adaptation of the species for survival. A prime example of the development of adaptive traits is found in the purple photosynthetic bacterium, *Rhodoblastus* (*Rbl.*) *acidophilus* (formerly *Rhodopseudomonas acidophila*) strain 7050.[1-3] This bacterium is able to alter its number and size of photosynthetic units as well as its pigment composition and light absorption properties of the major light harvesting II (LH2) antenna pigment-protein complex in response to changes in illumination conditions.[2,4-6] If the bacterium is grown under high light, the well-characterized B800-850 LH2 complex is formed having bacteriochlorophyll (BChl) absorption bands near 800 and 850 nm, and rhodopin and rhodopin glucoside are the primary carotenoid pigments.[1,3,7,8] Under low-light conditions, genes that code for a variant LH2 denoted B800-820 (also sometimes referred to as LH3 in the literature) are activated,[1-3] the BChl $Q_Y$ absorption band near 850 nm shifts to ~820 nm, and the organism accumulates rhodopinal and rhodopinal glucoside in the LH2 complex as primary carotenoid pigments (Figures 1A and B).[1,3,7,9,10] This response to changes in ambient light is controlled by a combination of a classical two component regulatory system and bacteriophytochromes that regulate the synthesis

**A**

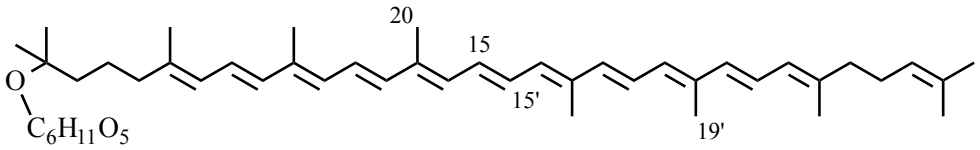


all-*trans*-rhodopin glucoside

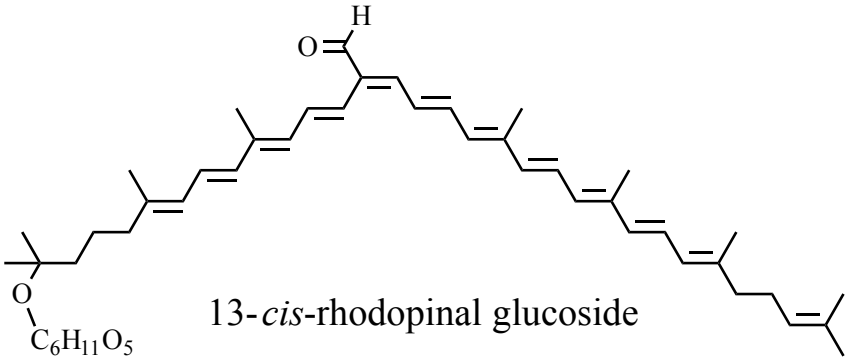


13-*cis*-rhodopinal glucoside

**B**

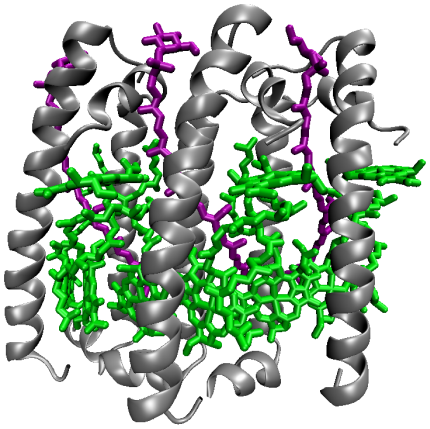

**Figure 1.** Structures of **(A)** all-*trans*-rhodopin glucoside and 13-*cis*-rhodopinal glucoside; **(B)** One-third portion of the LH2 B800-820 ring complex from *Rbl. acidophilus* strain 7050 (PDB 1IJD) showing the protein-bound BChls (green) and carotenoids (purple).

of the photosynthetic apparatus.[11-13]

The shift of the BChl $Q_Y$ band from ~850 nm to ~820 nm that occurs at low light is due to alterations in the amino acid sequence of the apoproteins that are assembled in the variant LH2 pigment-protein complex.[14-18] Results from X-ray crystallography (Figure 1B),[18] site-directed mutagenesis,[15] and resonance Raman spectroscopy[16] indicate that H-bonding residues α44 (Tyr) and α45 (Trp) in the B800-850 LH2 prevent rotation of the C3-acetyl group of the B850 BChl and fix the functional group so that its C=O π-electron bond resides in a planar orientation relative to the porphyrin macrocycle. This configuration allows extension of the π-electron conjugation into the acetyl group. The conversion of these H-bonding residues to non-H-bonding α44 (Phe) and α45 (Leu) in the B800-820 LH2 leads to a rotation of the C3-acetyl group out of the plane of the porphyrin ring, thereby inhibiting delocalization of the π-electron conjugation to the acetyl carbonyl, resulting in more restricted π-electron delocalization and consequently a blue-shift of the $Q_Y$ band from ~850 nm to ~820 nm.

Accompanying the shift of the BChl $Q_Y$ absorption band in the LH2 complex is a change in the absorption spectrum of the carotenoid. Under low-light growth conditions, rhodopin and rhodopin glucoside are enzymatically converted to rhodopinal and rhodopinal glucoside as an aldehyde group replaces the methyl group at carbon C20 in the carotenoid structures (Figure 1A).[19-21] The spectral origin (0–0) vibronic band of rhodopin glucoside in methanol appears at ~500 nm, whereas for rhodopinal glucoside, the band is less resolved spectrally, and it is located at ~540 nm in the same solvent (Figure 2). Previous workers compared the carotenoid-to-BChl energy transfer properties of LH2 complexes isolated from cells of *Rbl. acidophilus* strain 7050 grown under

different illumination conditions and found that there was an increase in the energy transfer efficiency from between 50–55% for the B800-850 complex to between 70–75% for the B800-820 complex.[2] However, the previous investigation did not address the specific reasons for the increase; *i.e.* whether changes in the BChl absorption spectra, or the conversion of rhodopin to rhodopinal in the protein complex, or both factors, were responsible for the enhanced ability of the LH2 complex to effectively harvest photons in the region of carotenoid absorption. Moreover, the previous work and subsequent ultrafast spectroscopic experiments carried out on the B800-820 LH2 complex from *Rbl. acidophilus* strain 7050[22] did not assign specific values to the energy transfer efficiencies of the individual carotenoids bound in the complexes, nor has there been any direct comparison of the spectra and dynamics of the excited states of rhodopin and rhodopinal either in solution or in the LH2 complexes. These data are important for addressing the specific mechanism of how these alterations in BChl and carotenoid structures and spectra increase the carotenoid-to-BChl energy transfer efficiency and as a consequence, enhance the viability of the photosynthetic bacterial organism.

Energy transfer from carotenoids involves at least two excited singlet states that can act as donors of absorbed light energy to BChl. These are the $S_1$ ($2^1A_g^-$) and $S_2$ ($1^1B_u^+$) states whose properties are strikingly distinct. A one-photon transition from the ground $S_0$ ($1^1A_g^-$) state to the $S_1$ ($2^1A_g^-$) state is forbidden by symmetry, whereas a transition to the $S_2$ ($1^1B_u^+$) state is strongly allowed.[23-29] The $S_0$ ($1^1A_g^-$) $\rightarrow$ $S_2$ ($1^1B_u^+$) transition is responsible for the vibrant coloration of carotenoids in nature.[30] Motivated by the landmark report of the X-ray crystal structure of the LH2 complex from *Rbl. acidophilus* strain 10050,[31] several investigators sought to understand the role of the $S_1$

($2^1A_g^-$) and $S_2$ ($1^1B_u^+$) excited singlet states in the mechanism of energy transfer to BChl in this pigment-protein complex.[32-35] For example, Macpherson, et al.[33] used ultrafast time-resolved optical spectroscopy applied to the LH2 complex prepared from *Rbl. acidophilus* strain 10050 and reported that the $S_2$ ($1^1B_u^+$) state of rhodopin glucoside dominated the pathway for energy transfer to BChl despite its extremely short intrinsic lifetime of ~120 fs in solution. The $S_1$ ($2^1A_g^-$) state of rhodopin glucoside, which has a much longer lifetime of ~4 ps in solution, was reported to make only a minor contribution to the overall energy transfer efficiency. In another study using steady-state and ultrafast time-resolved spectroscopy to elucidate the carotenoid-to-BChl energy transfer mechanism in the LH2 complex from *Rbl. acidophilus* 10050, Cong et al[34] reported the partitioning of energy transfer to be 23 ± 7% from the $S_1$ ($2^1A_g^-$) state and 63 ± 10% from the $S_2$ ($1^1B_u^+$) state. A recent broadband 2D electronic spectroscopic investigation of LH2 complexes from *Rbl. acidophilus* 10050 and *Rhodobacter sphaeroides* strain 2.4.1 provided convincing evidence for the additional involvement of a dark intermediate state in the carotenoid-to-BChl energy transfer pathway.[35]

This chapter provides a detailed experimental and computational comparison of the excited state energy levels, spectra, and dynamics of rhodopin, rhodopinal and their associated glucosides in various solvents and in their respective LH2 complexes isolated from *Rbl. acidophilus* 10050 and 7050 grown under different illumination conditions. The use of steady-state absorption, fluorescence and fluorescence excitation spectroscopy, and ultrafast time-resolved transient absorption spectroscopy in the visible spectral region have revealed the rates and efficiencies of carotenoid-to-BChl energy transfer for the individual carotenoids. The data address the questions of how and why

photosynthetic organisms alter their pigment composition and light-harvesting characteristics to ensure survival under the challenging, light-deprived environmental conditions in which they are sometimes found.

# Materials and Methods

### *Sample preparation and characterization*

*Bacterial growth conditions*

*Rbl. acidophilus* 10050 and 7050 cultures were grown anaerobically in the light using Pfennig's medium.[36] Normal growth conditions (hereafter referred to as high-light (HL) conditions) used continuous illumination at an intensity of 30 μmol $s^{-1}$ $m^{-2}$. The *Rbl. acidophilus* 7050 culture was also grown at a lower light intensity (hereafter denoted low-light (LL)) ranging from 3.7 to 5 μmol $s^{-1}$ $m^{-2}$. Cells were harvested by centrifugation at 4,000 × g in a Beckman Model J-6B centrifuge. The resulting pellets were resuspended in 1 L of 20 mM MES pH 6.8 buffer, containing 100 mM KCl, and centrifuged again to remove any residual media.

*Carotenoid isolation*

Extraction of the carotenoids from whole cells of the bacteria was accomplished by mixing 2–4 g of thawed cells with 30 mL methanol at room temperature and stirring in the dark for 15 min. The mixture was then centrifuged at 3,000 × g using an SS-34 rotor at 4 °C in a Sorvall RC-5B centrifuge. The supernatant contained primarily BChl and was not used further. The pellet was then mixed with 30 mL of fresh methanol and centrifuged repeatedly until the cells appeared gray, signifying that all the pigments had been extracted. The supernatant from the second and subsequent extractions contained primarily carotenoids as evidenced by absorption spectra recorded using a Varian Cary

50 UV/visible spectrometer. These fractions were pooled and evaporated to dryness using nitrogen gas.

The dried extracts were dissolved in acetonitrile/methanol (6:4, v/v) and analyzed using a Waters 600E/600S HPLC system equipped with a Waters Atlantis T3 OBD preparative column having dimensions of 19 × 100 mm. The mobile phase consisted of acetonitrile/methanol (6:4, v/v) delivered isocratically at a flow rate of 7.0 mL/min. Individual peaks were collected and identified by mass spectrometry using a Fisons Quattro II instrument employing atmospheric pressure chemical ionization (APCI) in negative mode with the following conditions: corona voltage, 2.5 V; cone voltage, 25 V; source temperature, 120 °C; probe temperature, 300 °C, mobile phase, acetonitrile. All solvents were HPLC-grade and were purchased from Sigma-Aldrich Corp. (St. Louis, MO).

*Preparation of light-harvesting complexes*

The cells were disrupted according to the methods described by Cogdell et al.[1] Briefly, ~5 g of pelleted whole cells of the bacteria were suspended in ~30 mL of 20 mM Tris buffer adjusted to pH 8.0 using 6 M HCl (hereafter referred to as Tris buffer), and ~20–50 mg of DNase and a few grains of $MgCl_2$ were added to degrade the released DNA during cellular disruption. The sample was briefly homogenized using a glass tissue homogenizer to ensure smooth passage through the French press operating at 15,000 psi. Cells were passed through the press three times to ensure complete disruption and the resulting suspension was centrifuged for 2 h at 4 °C in a Type 70 Ti rotor spinning at 180,000 × g in a Beckman L8-55M ultracentrifuge.

The resultant pellet containing membrane fragments was diluted using Tris buffer to an OD of 50 measured in a 1 cm cuvette at the BChl $Q_Y$ absorption band maximum (800 nm for LL grown *Rbl. acidophilus* 7050 complexes, 850 nm for the HL grown complexes). The membranes were then solubilized by adding 30% lauryldimethylamine oxide (LDAO) dropwise to a final concentration of 1.0% and allowing the sample to incubate for 60 min while stirring at room temperature in the dark. The sample was then centrifuged for 30 min at 27,000 × g in the Sorvall RC-5B centrifuge to remove denatured protein and any non-solubilized material. The supernatant containing the solubilized proteins was then collected for further treatment using sucrose density gradient ultracentrifugation.

Sucrose density gradients were prepared in 30 mL polycarbonate Beckman centrifuge tubes. Solutions of 0.2, 0.4, 0.6 and 0.8 M sucrose were prepared using Tris buffer containing 0.1% LDAO and were carefully layered to form discontinuous gradients in the tubes by using the following amounts: 0.8 M, 5.0 mL; 0.6 M, 6.5 mL; 0.4 M, 6.5 mL; and 0.2 M, 5.0 mL. Each tube was then topped off with 2.5 mL of the solubilized sample. The tubes were then placed in a Ti70 rotor and spun at 160,000 × g for 12 h at 4 ºC in the Beckman L8-55M ultracentrifuge. The procedure effectively separates any free pigments present in the 0.2 M sucrose layer, from the LH2 complex appearing in the 0.4 M sucrose layer, from the LH1-RC 'core' complexes that appear at the interface of the 0.6 M and 0.8 M sucrose solutions.

The 0.4 M sucrose solution layer containing the LH2 complex was carefully removed from each tube and pooled. The complex was then purified further by column chromatography using DE52 anion exchange resin (15 g, Whatman Scientific) packed

into a 5 cm diameter × 30 cm long solid phase, sintered glass column pre-equilibrated with several bed volumes of Tris buffer. After loading the sample onto the column, several bed volumes of TL buffer (0.1% LDAO, 20 mM Tris pH 8.0) were applied to remove the sucrose. The LH2 complex was then eluted using TL buffer containing increasing concentrations of NaCl in 30 mM increments starting with 10 mM. The HL LH2 complexes from *Rbl. acidophilus* 10050 and 7050 cells eluted between 10 and 20 mM NaCl, whereas that isolated from LL *Rbl. acidophilus* 7050 cells eluted at ~180 mM NaCl. The purity of the eluting fractions was monitored by absorption spectroscopy using a Shimadzu UV-1700 PharmaSpec spectrometer. Fractions from HL samples exhibiting spectra with an 850 nm to 280 nm ratio of > 3.0 were pooled for further purification. For the LL sample, the 800 nm to 280 nm absorbance ratio of > 2.5 were pooled for further purification.

The pooled sample was reduced to a volume of < 1 mL by centrifugation using Vivaspin 4 50 K M.W. cutoff concentrators (Sartorius Stedim Biotech) placed in an 11390 rotor and spun at 3,250 × g Sigma 3K30 centrifuge. The concentrated LH2 was further purified using an Akta Primeplus (GE Healthcare) automated chromatography system equipped with a XK-16 long gel filtration column filled with Superdex-200. 0.5 ml fractions were collected of the LH2 band and subsequently assayed using the ratio of the absorbance maximum of the BChl $Q_Y$ band to the protein absorbance at 280 nm. Fractions having an 800 nm to 280 nm (from the LL-grown *Rbl. acidophilus* 7050) ratio of > 2.7 or an 850 nm to 280 nm ratio (from the HL-grown *Rbl. acidophilus* cells) ≥ 3.3 were pooled and concentrated using the Vivaspin 4 50 K M.W. cutoff concentrators to an OD of 100 measured at the absorbance maximum of the BChl $Q_Y$ band in a 1 cm cuvette.

The sample was then divided into 30 μL aliquots, placed in PCR tubes, flash frozen in liquid nitrogen and stored in a −80 °C freezer.

*Quantitative analysis of pigment composition of the LH2 complexes*

A 10 μL aliquot of the frozen *Rbl. acidophilus* 7050 LH2 complex was thawed on ice and the liquid was evaporated to dryness using nitrogen gas. The remaining residue was then redissolved in 2 mL of methanol to release the pigments. This extract was then centrifuged at 13,600 × g for 2 min at room temperature in a Fisher Scientific 235C bench top microcentrifuge.

The supernatant was then analyzed using a Waters 600E/600S HPLC system equipped with a Waters Atlantis T3 5 μm analytical column having dimensions of 4.6 × 250 mm. The mobile phase consisted of an isocratic delivery of acetonitrile/methanol (6:4, v/v) at a rate of 2.0 mL/min. Similarly, a 30 μL aliquot of the *Rbl. acidophilus* 10050 LH2 complex was dried under nitrogen gas and denatured with 2 mL of acetone. Following centrifugation, the supernatant was removed and 2 mL of fresh acetone was added to the remaining pellet, and the mixture was centrifuged again, this time resulting in a colorless pellet. The supernatants from the two centrifugations were combined and dried using nitrogen gas. The sample was taken up in 1 mL of acetonitrile/methanol (6:4, v/v) and analyzed on the same HPLC system with a Waters Atlantis T3 OBD 5 μm preparative column. The mobile phase was the same as described above, but with the flow rate increased to 7.0 mL/min.

The molar percentages of the carotenoids were calculated using the area of each HPLC peak detected at the wavelength of maximum absorption divided by the extinction coefficient of the carotenoid,[3] and then determining the percentage of each pigment relative to the total carotenoid content. Peaks that could not be conclusively identified by mass spectrometry remain unidentified, but are presumed to be isomers formed during the extraction procedure.

***Spectroscopic methods***

All steady-state absorption and fluorescence emission and excitation spectroscopic measurements were carried out in 1 cm square cuvettes at room temperature unless otherwise stated. Rhodopin glucoside and rhodopinal glucoside were dissolved in spectroscopic grade carbon disulfide (Acros Organics), benzyl alcohol (Sigma Aldrich), methanol (Sigma Aldrich) or acetonitrile (Sigma Aldrich). LH2 complexes were suspended in Tris buffer containing 1% LDAO at pH 8. Steady-state absorption spectra of the carotenoids in various solvents and in the LH2 complexes were obtained using either a Varian Cary 50 or a Cary 5000 UV-visible spectrophotometer. Fluorescence emission and excitation spectra were recorded using a Jobin-Yvon Horiba FL3-22 fluorimeter equipped with double excitation and emission monochromators having 1200 grooves/mm gratings, a 450 W Osram XBO xenon arc lamp and a Hamamatsu R928P photomultiplier tube detector.

Emission spectra of the LH2 complexes were recorded using samples having an OD between 0.025 and 0.1 in a 1 cm path cuvette at the BChl $Q_X$ band at 591 nm, which was also the excitation wavelength. The excitation and emission slit widths corresponded to bandpasses of 6 nm and 3 nm respectively for experiments on the LH2 complex from *Rbl. acidophilus* 10050. Emission spectra from the *Rbl. acidophilus* 7050 (HL and LL) LH2 complexes were obtained using excitation and emission slit widths corresponding to bandpasses of 12 nm and 6 nm, respectively. All emission spectra were corrected using an emission correction factor file generated by taking the ratio of the spectral response of a calibrated 200 W quartz tungsten-halogen filament lamp and the instrument detection system.

Fluorescence excitation spectra were recorded by monitoring the BChl emission at its maximum wavelength (870 nm for the B800-850 complexes and 860 nm for the B800-820 complex) using samples with an OD of 0.025 in a 1 cm path cuvette at the BChl $Q_X$ band. Emission was detected at a right angle relative to the excitation with bandpasses corresponding to 6 nm (10050 LH2), 7 nm (7050 HL) and 4 nm (7050 LL) for the excitation monochromator, and 12 nm (10050 LH2) and 14 nm (7050 HL and LL) for the emission monochromator. An excitation correction factor file was used to correct for the wavelength variability of the source lamp and excitation monochromator. This file was generated using a photodiode calibration kit consisting of a photodiode assembly and a DM303-P module that was rented from Horiba.

Pump-probe ultrafast transient absorption spectroscopy was carried out using a Helios femtosecond transient absorption spectrometer (Ultrafast Systems LLC, Sarasota, FL, USA) coupled to a laser setup that has been previously described.[37,38] Surface Xplorer Pro 1.2.2.26 (Ultrafast Systems LLC, Sarasota, FL, USA) was used to correct for the dispersion in the transient absorption spectra. Samples having an OD between 0.2 and 0.5 in a 2 mm path cuvette at the carotenoid spectral origin (0–0) band were mixed continuously using a magnetic microstirrer to avoid photodegradation. The pump laser had an energy of 1 μJ/pulse focused on a 1 mm diameter spot which corresponds to a laser intensity between 3.2–3.9 $\times$ $10^{14}$ photons/$cm^2$. The integrity of the samples was assayed by taking steady-state absorption spectra before and after laser excitation.

Global fitting of the transient absorption datasets was performed in ASUFit 3.0 provided by Dr. Evaldas Katilius at Arizona State University and carried out according to a sequential excited state decay model which yielded evolution associated difference spectra (EADS).[39] The procedure for processing the ultrafast transient absorption data is given in Appendix A. Reconstruction of the 1−T and fluorescence excitation spectra was done using Origin software version 9.

# Results

***Steady-state absorption and fluorescence spectroscopy***

The steady-state absorption spectra of rhodopin glucoside and rhodopinal glucoside recorded in carbon disulfide, benzyl alcohol, methanol and acetonitrile are shown in Figure 2. The primary bands in these spectra represent an electronic transition from the ground $S_0$ ($1^1A_g^-$) state to the $S_2$ ($1^1B_u^+$) state. In any particular solvent, the spectrum of rhodopinal glucoside is shifted to longer wavelength by 30–40 nm compared to that of rhodopin glucoside. The spectrum of rhodopin glucoside displays well-resolved vibronic bands in all of the solvents, whereas the spectrum of rhodopinal glucoside is much less structured, except in carbon disulfide where a shoulder on the long-wavelength side of the primary absorption band is observed. Also, the high polarizability of carbon disulfide ($P(\varepsilon)$ = 0.354) results in a 30–40 nm red-shift of the spectra of rhodopin glucoside and rhodopinal glucoside compared to their spectra recorded in the less polarizable solvents, acetonitrile ($P(\varepsilon)$ = 0.210) and methanol ($P(\varepsilon)$ = 0.202). Benzyl alcohol, which has a polarizability value ($P(\varepsilon)$ = 0.314) in between carbon disulfide and methanol or acetonitrile, red-shifts the spectrum of rhodopinal glucoside more than for rhodopin glucoside (Figure 2). This is undoubtedly due to the presence of the aldehyde group on rhodopinal glucoside, which interacts more strongly with this solvent than the methyl group in the same position on rhodopin glucoside. Except for a small change in relative intensities of the vibronic bands of rhodopin glucoside, the spectra are not significantly affected by changing the solvent from a protic (methanol) to a non-protic (acetonitrile) polar solvent. It should be mentioned that the glucoside moiety has no effect on the positions and intensities of the absorption bands. The spectra of rhodopin

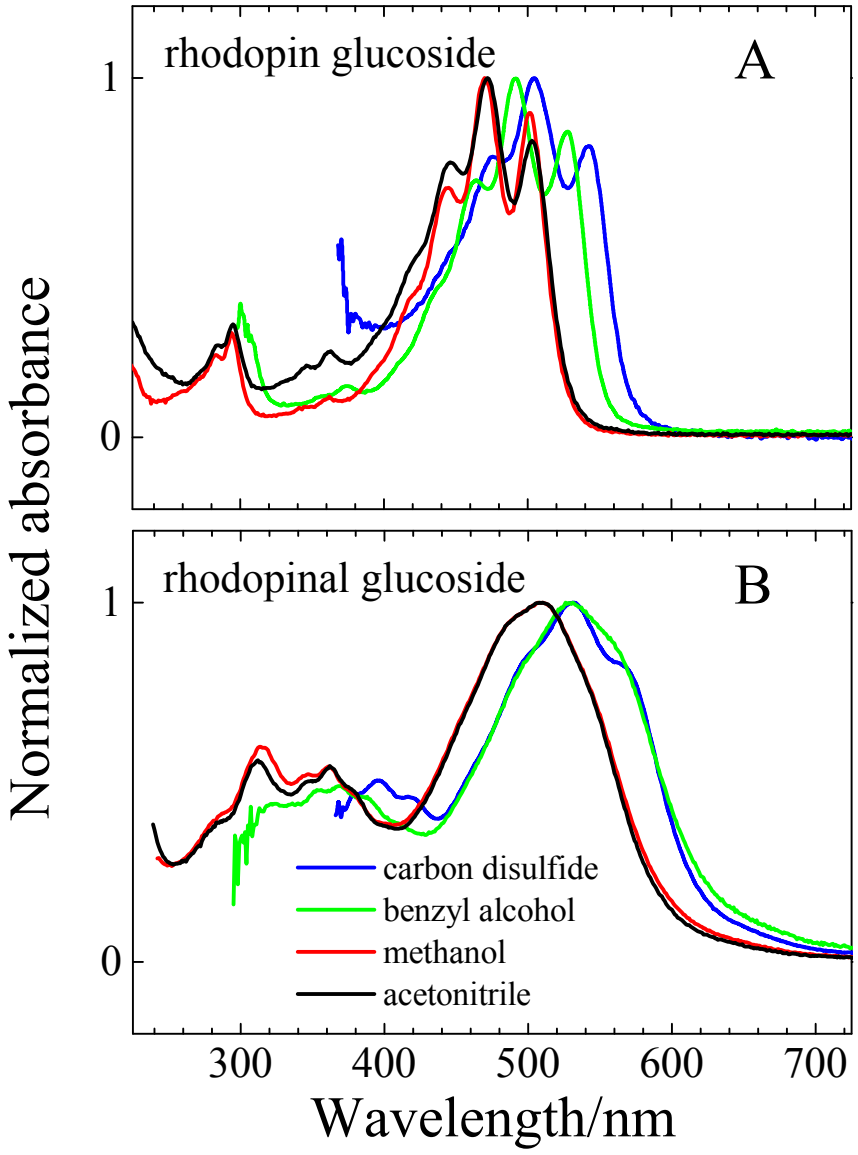


**Figure 2.** Normalized steady-state absorption spectra of **(A)** rhodopin glucoside and **(B)** rhodopinal glucoside in carbon disulfide, benzyl alcohol, methanol and acetonitrile recorded in 2 mm path length cuvettes at room temperature.

glucoside and rhodopinal glucoside are indistinguishable from the corresponding spectra of rhodopin and rhodopinal.[3]

The absorption spectra of the LH2 complexes from *Rbl. acidophilus* 10050, 7050 HL and 7050 LL recorded at room temperature are shown in Figure 3. All spectra show the strong $S_0$ ($1^1A_g^-$) $\rightarrow$ $S_2$ ($1^1B_u^+$) transition characteristic of carotenoids in the 400–550 nm region. Also, the positions of the BChl Soret band at ~375 nm and the BChl $Q_X$ band at ~590 nm are nearly identical for all of the complexes. However, one BChl $Q_Y$ band of the LH2 complex is located at 800 nm, and the other is at 859 nm for strain 10050, at 855 nm for 7050 HL, and at 823 nm for 7050 LL. In addition, compared to the spectrum of the LH2 complex from strain 10050, the spectra of the LH2 complexes from 7050 HL and 7050 LL show more absorption in the region between 550–600 nm where the spectrum of the carotenoid partially overlaps with the BChl $Q_X$ band at ~590 nm. This is due to the presence of rhodopinal and rhodopinal glucoside in the LH2 complexes from strain 7050. These carotenoids are not present in the LH2 complex of *Rbl. acidophilus* 10050. It should be mentioned that the growth conditions for the cells of *Rbl. acidophilus* 7050 will always result in a very small amount of the B800-820 LH2 complex in HL cells due to the effect of light shading in the culture media. Likewise, a small amount of B800-850 LH2 complex will be present in the LL cells due to the fact that there is a limit to how low the light intensity can be adjusted to ensure a realistic amount of bacterial growth. A spectral analysis of the BChl absorption bands in the $Q_Y$ region (Figure 4) shows that this amount is less than 20%. The determination was carried out by subtracting the spectrum of B800-850 LH2 preparation obtained from *Rbl. acidophilus* 7050 grown under high-light (HL, red trace) conditions which contains almost

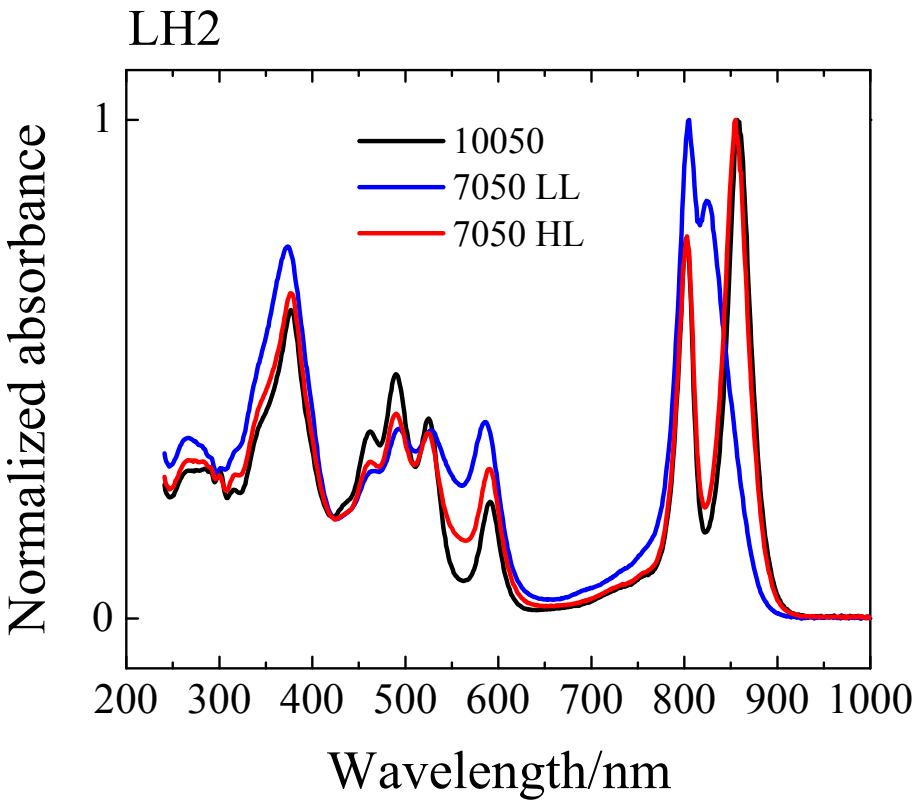


**Figure 3.** Normalized steady-state absorption spectra of the LH2 complexes from *Rbl. acidophilus* 10050, 7050 LL and 7050 HL recorded in 2 mm path length cuvettes at room temperature.

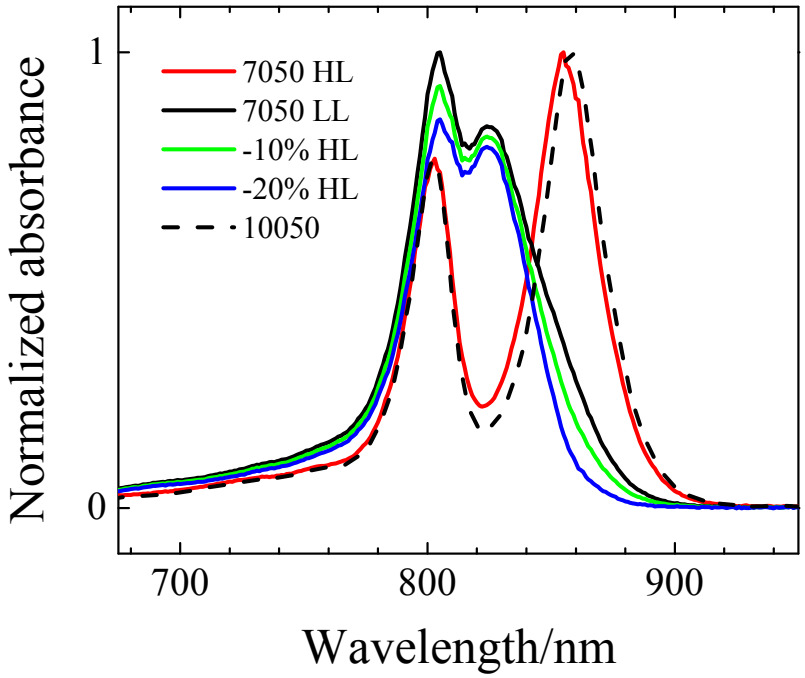


**Figure 4.** Determination of the amount of B800-850 protein in the sample of the LH2 pigment-protein complex obtained from cells of *Rbl. acidophilus* 7050 LL. The spectra of the B800-850 LH2 complex from *Rbl. acidophilus* 10050 is also shown as a dashed trace.

exclusively B800-850 complex, from the spectrum of the LH2 complex obtained from *Rbl. acidophilus* 7050 grown under low-light (LL, black trace) conditions until a ratio of the absorption at 800 nm to that at 820 nm reached 0.93. This is generally considered to be sufficiently pure B800-820 complex to be used for protein crystallography.[40] Moreover, it should be noted that the regulatory pathways for the switch from rhodopin glucoside to rhodopinal glucoside and from B800-850 to B800-820 are independent of each other. During growth at progressively decreasing light intensity, the carotenoid pathway switch is activated before; *i.e.* at a higher light intensity than the switch that controls the type of complex present.[3] Therefore, it is possible to obtain a B800-850 complex that contains a significant amount of rhodopinal glucoside as is the case for LH2 complex isolated from 7050 HL cells (Table 1). The pronounced similarity in the structures of the B800-850 and B800-820 protein complexes precludes complete separation by chromatographic techniques. However, by a judicious choice of excitation and detection wavelengths in the steady-state and transient absorption spectroscopic experiments, the properties of the individual pigment-protein complexes can be studied.

The carotenoid composition of the different LH2 complexes was determined by HPLC analyses carried out as illustrated in Figure 5. The molar percentages of the carotenoids in the different LH2 complexes are given in Table 1. These data are in agreement with previous reports that LL grown *Rbl. acidophilus* 7050 cells display a significant increase in total rhodopinal (defined in this context as rhodopinal plus rhodopinal glucoside) concurrent with a decrease in total rhodopin (defined here as rhodopin plus rhodopin glucoside) compared to that found in the bacterium grown under HL conditions.[3,4] Total rhodopinal in the LH2 complexes increased from 32% in the 7050

HL sample to 65% (58% + 7%) in the 7050 LL sample (Table 1). Concurrently, total rhodopin in the LH2 complexes decreased from 56% (28% + 28%) to 15% (5% + 10%) when cells were grown using LL (Table 1). As previously reported[3,33] and confirmed by the present work, the LH2 complex from *Rbl. acidophilus* strain 10050 did not contain any rhodopinal or rhodopinal glucoside.

**Table 1.** Molar percentages of the carotenoid pigments in the LH2 complexes isolated from *Rbl. acidophilus* 10050*,* 7050 HL and 7050 LL.[1]

| | Molar percentage | | |
|---|---|---|---|
| | 10050 | 7050 HL | 7050 LL |
| rhodopin glucoside | 52 | 28 | 5 |
| rhodopin | 40 | 28 | 10 |
| rhodopinal glucoside | n.d.[2] | 32 | 58 |
| rhodopinal | n.d. | n.d. | 7 |
| lycopene | 8 | 8 | 13 |
| unknown | n.d. | 4 | 8 |

[1]Percentages are based on the average of multiple extractions and HPLC analyses. Uncertainties in the values, based on standard deviations from the mean, were equal to or less than two percentage points. [2]n.d.= not detected

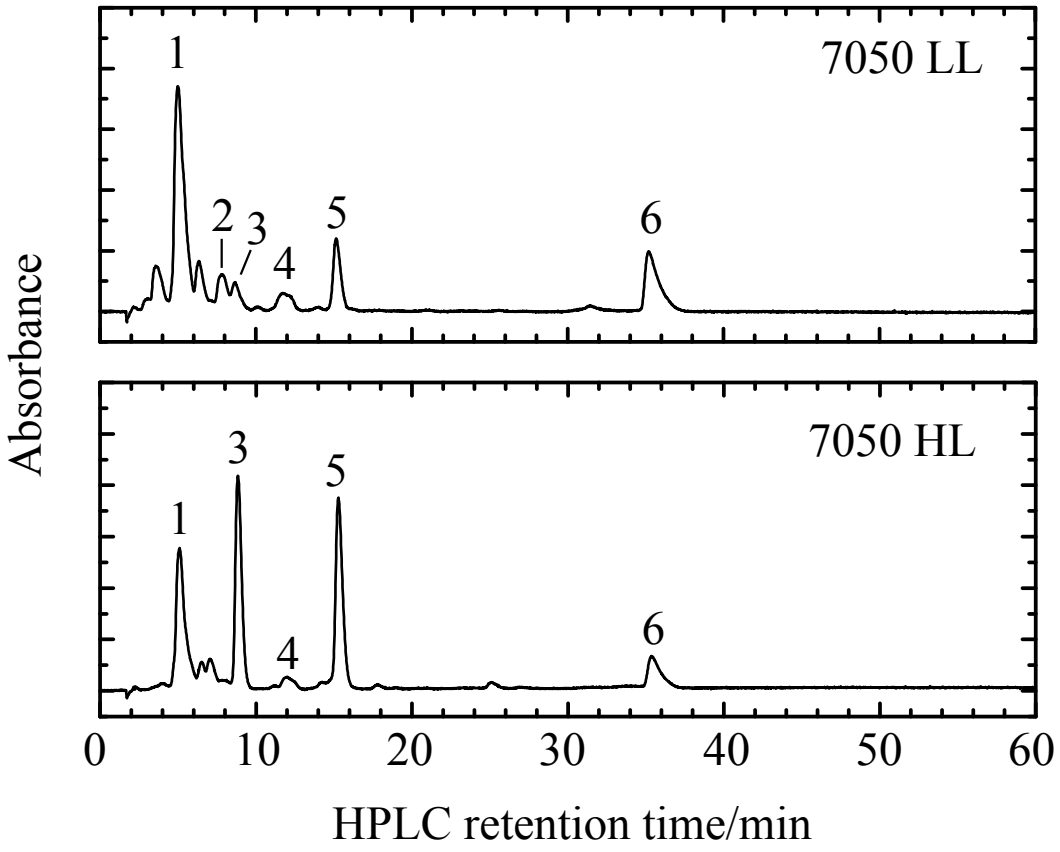


**Figure 5.** HPLC chromatograms of the pigment extract from *Rbl. acidophilus* 7050 LH2 complexes prepared from cells grown under LL (top trace) and HL (bottom trace) conditions. Both chromatograms were detected at 502 nm. The major pigments were identified as follows: 1, rhodopinal glucoside; 2, rhodopinal; 3, rhodopin glucoside; 4, BChl *a*; 5, rhodopin; and 6, lycopene. The minor unlabeled peaks are primarily *cis* isomers of the major carotenoids.

The fluorescence spectra of the LH2 complexes recorded using 591 nm excitation, which excites the BChl $Q_X$ band, are shown in Figure 6 (blue traces). The maximum wavelength of emission occurs at 870 nm for the LH2 complexes from 10050 and 7050 HL, and at 860 nm for the LH2 complex from 7050 LL. Fluorescence spectra were also recorded using excitation wavelengths of 560, 570, 580 and 590 nm, but no changes in the position or shape of the resulting emission spectra were observed. Fluorescence excitation spectra of the LH2 complexes are also shown in Figure 6 (red traces). These spectra were recorded by detecting the fluorescence from the samples at the maximum wavelength of BChl emission, but identical lineshapes were observed using any detection wavelength between 820 and 880 nm (Figure 7).

It is somewhat surprising that the fluorescence maximum of the B800-820 complex occurs at 860 nm rather than closer to the 820 nm $Q_Y$ band. However, as mentioned above, previous work detailing the effect of light intensity and temperature on cell growth and the formation of the B800-820 complex indicated that the conversion of rhodopin to rhodopinal occurs prior to the conversion of B800-850 to B800-820.[3] Therefore, it is likely that the fraction of B800-850 complex in our LL sample (see Figure 4) contains rhodopinal and represents the main emission component. This interpretation rationalizes the appearance of the fluorescence maximum at 860 nm and the fluorescence excitation spectra not being affected by changing the detection wavelength.

The absorption spectra, expressed as 1−T, where T is transmittance (black traces), and the excitation spectra (red traces) were normalized at the BChl $Q_X$ and $Q_Y$ bands, and the ratio of the excitation and 1−T spectral amplitudes were determined in the region from 300 nm to 650 nm (green traces). These traces represent the efficiency of

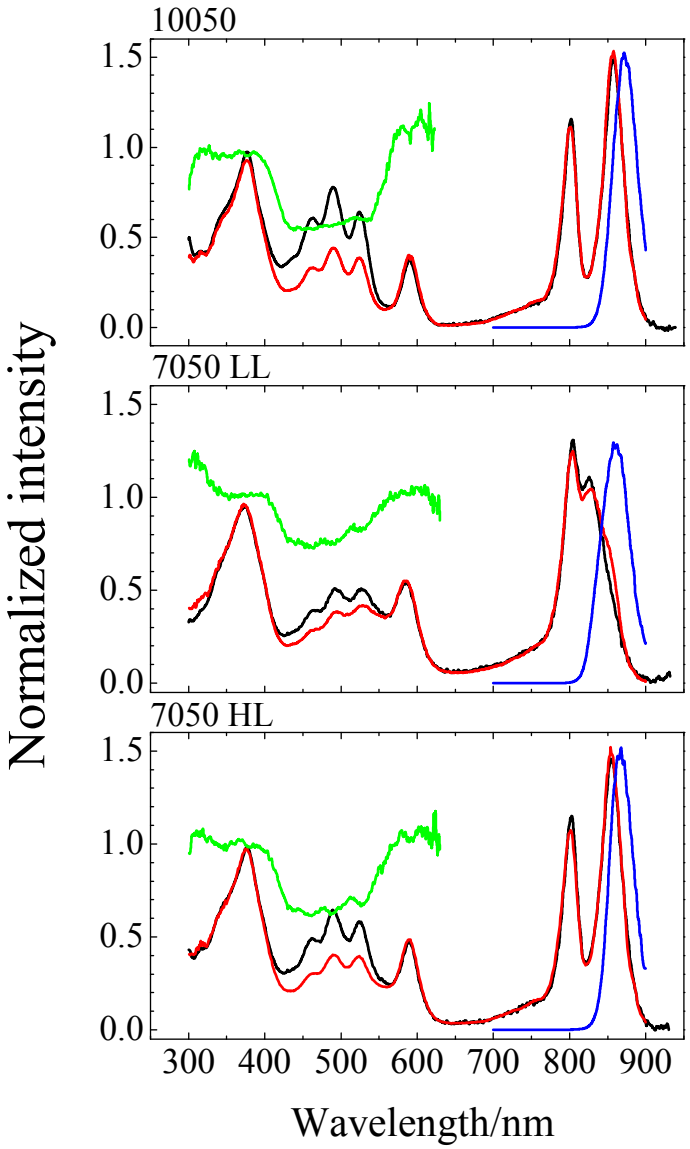


**Figure 6.** Emission (blue), excitation (red) and 1−T (black) spectra of LH2 complexes obtained from *Rbl. acidophilus* 10050, 7050 LL and 7050 HL. The green line shows the ratio of the normalized excitation and 1−T spectra and in the region of carotenoid absorption gives a quantitative measurement of the carotenoid-to-BChl energy transfer efficiency.

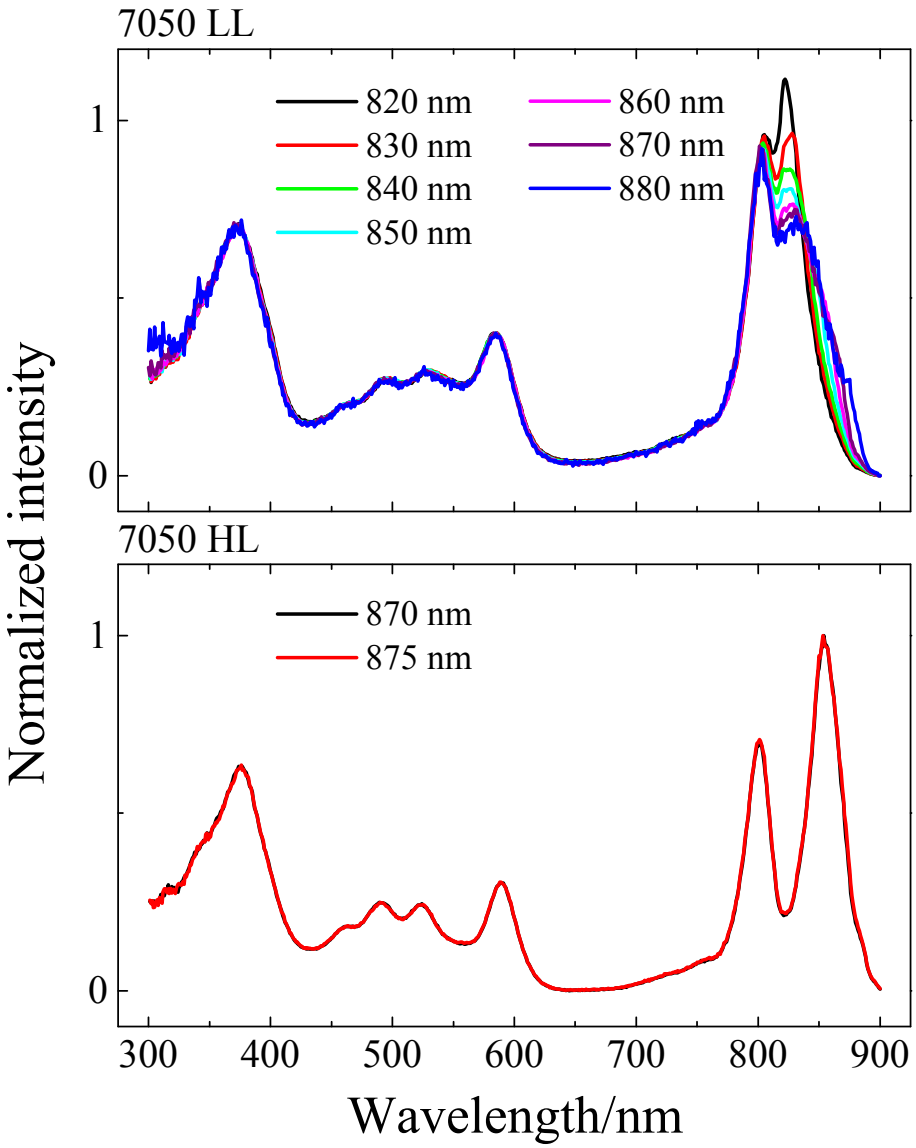


**Figure 7.** Fluorescence excitation spectra of the 7050 LL and HL LH2 complexes demonstrating that identical lineshapes were observed in the region of the carotenoid absorption between 400 and 575 nm regardless of the detection wavelength of BChl emission between 820 and 880 nm.

excitation energy transfer (EET) to BChl, which was found in the carotenoid absorption region between 425 nm and 550 nm to be in the range of 55% to 61% for the 10050 LH2 complex consistent with previously published results.[33,34] The LH2 complexes from 7050 HL and 7050 LL displayed higher carotenoid-to-BChl EET efficiencies and were in the range of 63% to 71% and 76% to 86%, respectively.

HPLC analysis (Table 1) revealed that the LH2 samples from the 7050 samples contain both rhodopin and rhodopinal (and their associated glucosides) in different amounts. Therefore, in order to examine the contributions of these individual chromophores to the spectra of the pigment-protein complexes, reconstructions of the 1−T (left panel, Figure 8) and fluorescence excitation (right panel, Figure 8) spectra were carried out based on the absorption spectra of the HPLC-purified carotenoids recorded in benzyl alcohol. The spectra of the carotenoids in the LH2 protein (Figure 3) are well-reproduced by their spectra in benzyl alcohol (Figure 2) due to the fact that this solvent has a polarity and polarizability similar to the average of those of the protein in the binding environment of the carotenoid.[33] The BChl Soret and $Q_X$ bands were modeled by sums of Gaussian functions. The spectral reconstructions yielded the specific carotenoid-to-BChl EET efficiencies for rhodopin and rhodopinal from the ratios of the individual fluorescence excitation and 1−T bands in the profiles. (Because rhodopin and rhodopinal have identical absorption (and 1−T) spectra as their corresponding glucoside derivatives,[3] in this context and unless explicitly noted otherwise, any statements about the spectra of rhodopin or rhodopinal should be taken to mean the combined contribution from the chromophores associated with both the glucoside and non-glucoside molecules.) The

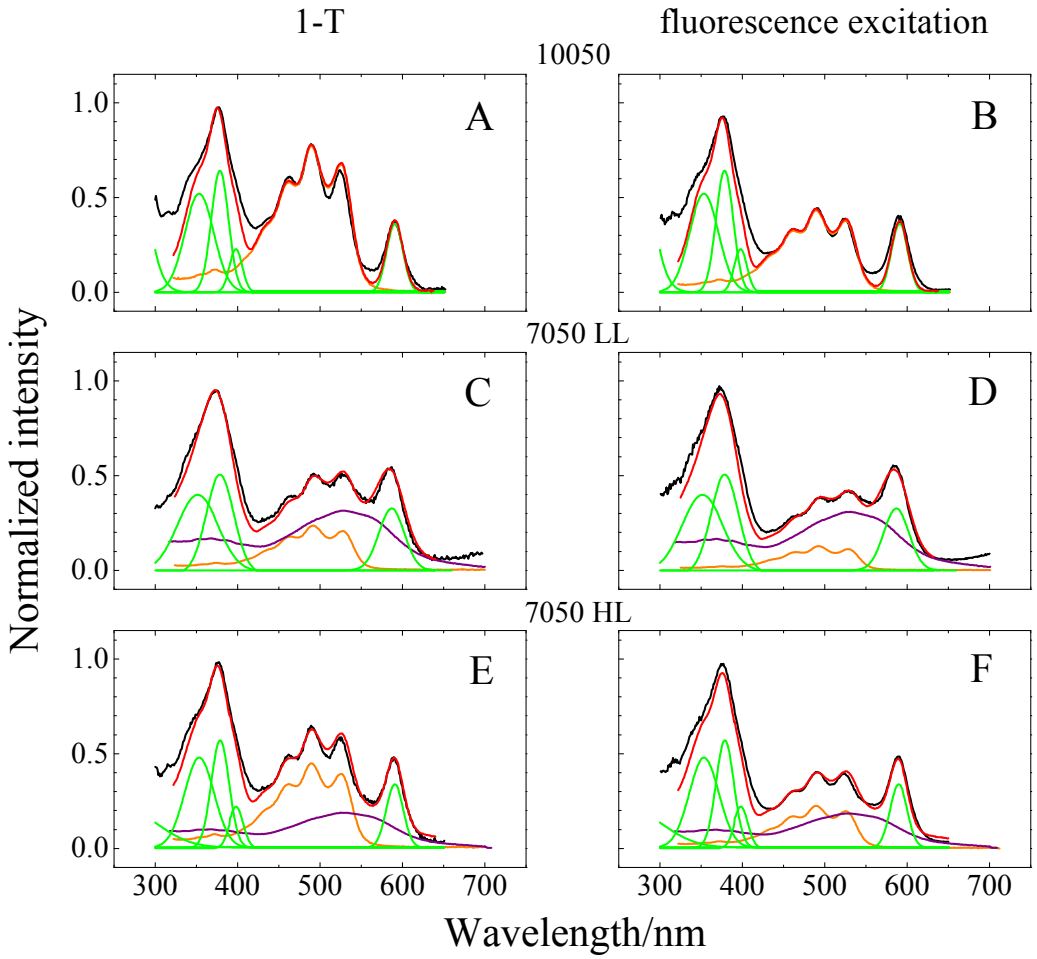


**Figure 8.** Reconstruction of the (A, C and E) 1−T and (B, D and F) fluorescence excitation spectra (black traces) of the LH2 complexes from *Rbl. acidophilus* 10050, 7050 LL and 7050 HL. The 1−T spectra of purified rhodopin glucoside (orange traces) and rhodopinal glucoside (purple traces) were recorded in benzyl alcohol and summed to generate the reconstructed spectra (red traces). The BChl bands in the Soret region between 300 and 400 nm and in the $Q_X$ region near 600 nm were modeled using Gaussian functions (green lines) for simplicity.

EET efficiency for rhodopin in the LH2 complex from the 10050 sample becomes evident from a side-by-side, horizontal comparison of the amplitudes of the 1−T and fluorescence excitation spectra (Figures 8A and B) in the region of carotenoid absorption, and was found to be 56 ± 1% consistent with previous reports.[33,34]

A similar analysis was carried out to obtain the values for the individual carotenoid-to-BChl EET efficiencies in the LH2 complex from the 7050 LL sample (Figures 8C and D) which were found from the spectral reconstruction to be 54 ± 5% for rhodopin (orange traces) and 97 ± 2% for rhodopinal (purple traces). The computed individual carotenoid-to-BChl EET efficiencies for the LH2 complex prepared from 7050 HL cells (Figure 8E and F) were 50 ± 3% for rhodopin (orange traces) and 98 ± 2% for rhodopinal (purple traces), consistent with the values determined for the LH2 complex from 7050 LL. These results are summarized in Table 2 and reveal the remarkable finding that rhodopinal in the LH2 complex from *Rbl. acidophilus* 7050 transfers essentially all of its excited state energy to BChl with minimal loss through internal conversion to the ground state. This stands in striking contrast to rhodopin in the LH2 complexes from all *Rbl. acidophilus* strains, which transfers energy to BChl with only ~50% efficiency.

**Table 2.** Efficiency of Car-to-BChl excitation energy transfer from the spectral reconstruction of fluorescence excitation and 1−T spectra.

| | Amplitude | | EET Efficiency |
|---|---|---|---|
| | Fluorescence excitation | 1−T | |
| 10050 | | | |
| rhodopin | 0.44 ± 0.01 | 0.78 ± 0.01 | 56 ± 1% |
| 7050 LL | | | |
| rhodopin | 0.13 ± 0.01 | 0.24 ± 0.01 | 54 ± 5% |
| rhodopinal | 0.309 ± 0.005 | 0.320 ± 0.005 | 97 ± 2% |
| 7050 HL | | | |
| rhodopin | 0.22 ± 0.01 | 0.44 ± 0.01 | 50 ± 3% |
| rhodopinal | 0.185 ± 0.003 | 0.189 ± 0.003 | 98 ± 2% |

***Transient absorption spectroscopy***

*Transient absorption and dynamics of carotenoids in solution*

Figure 9 shows ultrafast time-resolved transient absorption spectra of rhodopin glucoside (left panels) and rhodopinal glucoside (right panels) recorded in carbon disulfide, benzyl alcohol, methanol or acetonitrile at various delay times after laser excitation. Upon excitation, an immediate onset of bleaching of the strongly allowed $S_0$ ($1^1A_g^-$) $\rightarrow$ $S_2$ ($1^1B_u^+$) transition occurs resulting in a negative signal in the 450–550 nm region. In addition, a strong positive signal in the 520–700 nm region appears that can be attributed to excited state absorption (ESA) associated with the $S_1$ ($2^1A_g^-$) $\rightarrow$ $S_N$ transition. This suggests that the decay of the $S_2$ state via internal conversion to populate the $S_1$ state is occurring on the same time scale as the instrument response time of ~100 fs. Similar to the steady-state absorption spectra of the carotenoids, the excited state absorption bands shift to longer wavelength and are broader as the polarizability of the solvent increases. The spectra are broadest and most red-shifted in the highly polarizable solvent, carbon disulfide, compared to the spectra recorded in the other solvents. A similar effect is evident in the spectrum of rhodopinal glucoside in carbon disulfide and benzyl alcohol (Figure 9, right panels), where it is also clear that the spectral bands are broader overall than the spectra of rhodopin glucoside in the same solvents (Figure 9, left panels). Also, an additional peak at ~740 nm, which is not found in the spectra of rhodopin glucoside, is seen in the transient absorption spectra from rhodopinal glucoside. Unlike the main $S_1$ ($2^1A_g^-$) $\rightarrow$ $S_N$ transient absorption band, this feature is insensitive to the polarizability of the solvent, and therefore appears more separated from the main ESA feature in methanol and acetonitrile compared to in carbon disulfide.

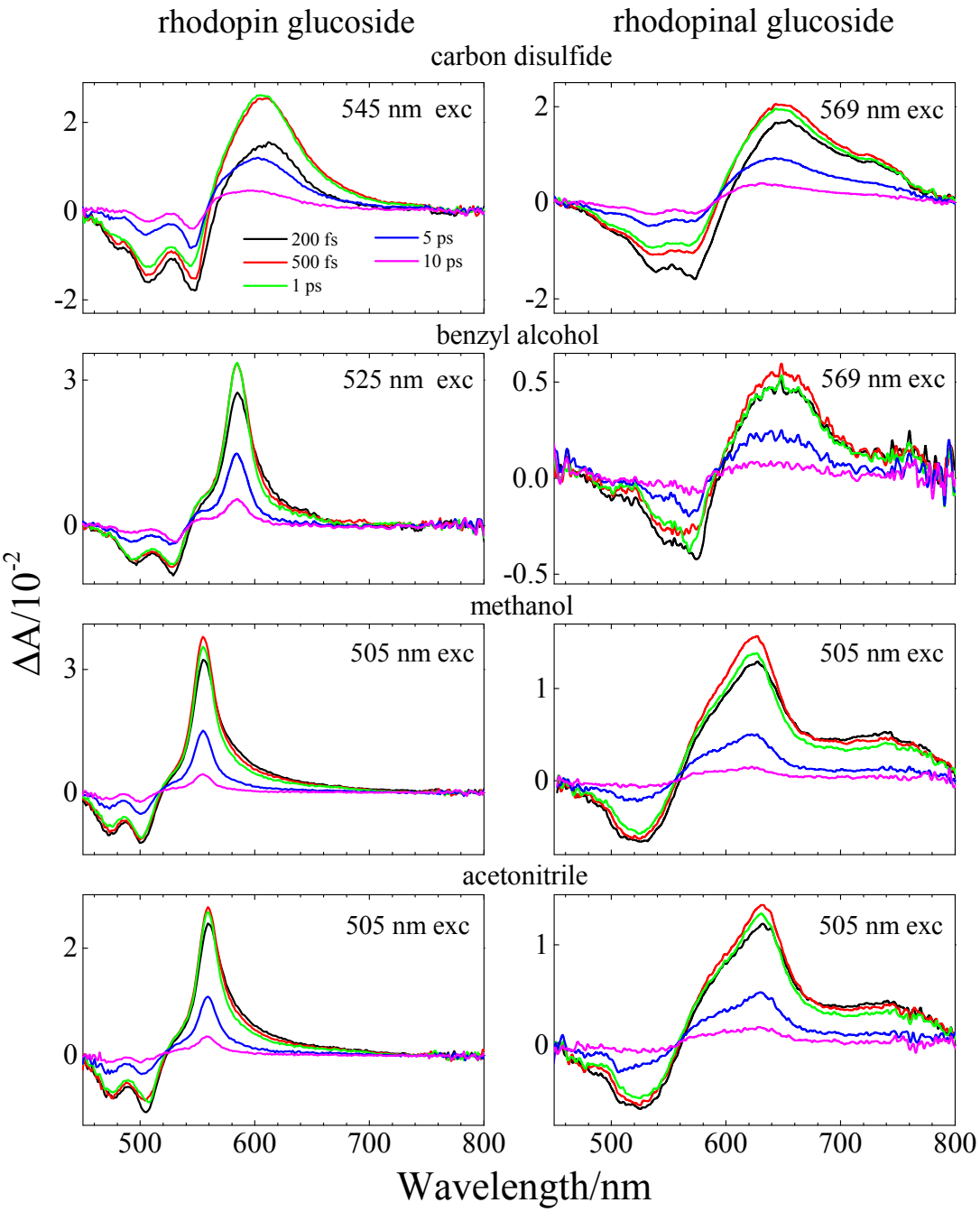


**Figure 9.** Transient absorption spectra of rhodopin glucoside and rhodopinal glucoside in carbon disulfide, benzyl alcohol, methanol and acetonitrile recorded at room temperature using the indicated excitation wavelengths.

In order to obtain detailed information regarding the dynamics of the excited states of the carotenoids, global fitting according to a sequential decay model, resulting in evolution associated difference spectra (EADS), was carried out on the transient absorption datasets. EADS components obtained from this fitting are shown in Figure 10 and summarized in Table 3. For both rhodopin glucoside and rhodopinal glucoside in all four solvents, the first EADS has a very short lifetime ranging from <100–120 fs, and the profile of this component shows bleaching of the ground state $S_0$ ($1^1A_g^-$) → $S_2$ ($1^1B_u^+$) absorption and stimulated emission from the $S_2$ ($1^1B_u^+$) state. It is important to point out here that although the best global fitting results are achieved in some cases using time constants smaller than 100 fs, these very small values cannot be taken factually because the instrument response time of the laser spectrometer is on the order of ~100 fs. Hence, these values are specified as <100 fs. More precise values in this time domain were reported by Macpherson et al.[33] who used fluorescence upconversion spectroscopy and found the $S_2$ ($1^1B_u^+$) lifetime of rhodopin glucoside in benzyl alcohol to be 124 ± 8 fs. The second EADS component for both molecules has a time constant that ranges from 330 to 530 fs in the different solvents. This component can be assigned to a transition from a vibronically-hot $S_1$ ($2^1A_g^-$) → $S_N$ excited singlet state due to the fact that its broad ESA peak narrows and shifts to shorter wavelength upon decaying to form the third EADS component.[41-45] The second and third EADS for rhodopinal glucoside in all solvents also show the additional peak at ~740 nm alluded to above, which is not found in the spectra of rhodopin glucoside. The fact that this feature does not depend on solvent polarity indicates that it is not associated with the formation of an intramolecular charge transfer (ICT) state in rhodopinal glucoside.[46,47]

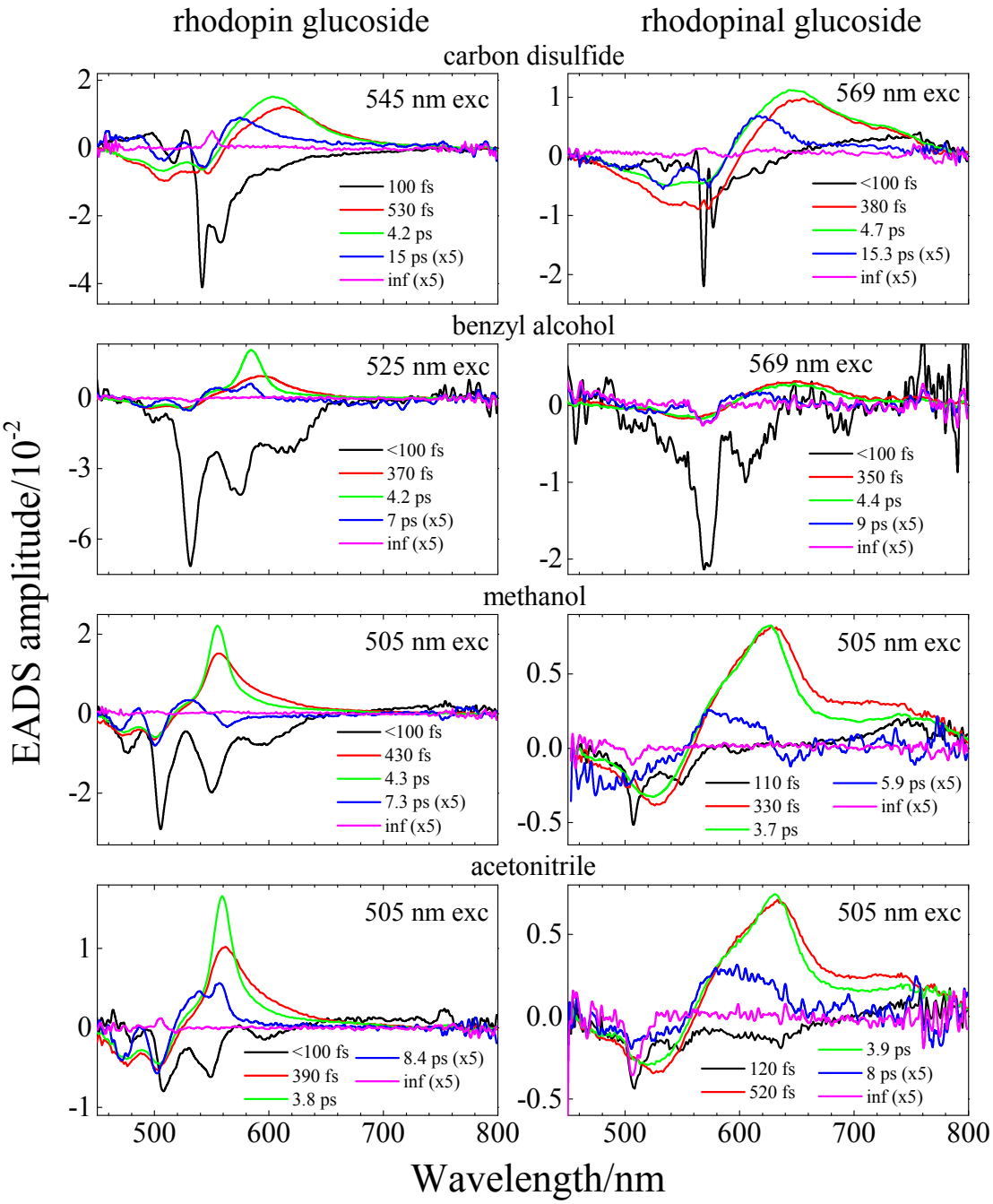


**Figure 10.** Evolution associated difference spectra (EADS) obtained from globally fitting the transient absorption datasets from rhodopin glucoside and rhodopinal glucoside in carbon disulfide, benzyl alcohol, methanol and acetonitrile given in Figure 9.

**Table 3.** Lifetimes of the EADS components obtained by global fitting the transient absorption datasets recorded for rhodopin glucoside and rhodopinal glucoside in various solvents.[1]

| | | Lifetime/ps | | | |
|---|---|---|---|---|---|
| Carotenoid | Solvent | $\tau_1$ | $\tau_2$ | $\tau_3$ | $\tau_4$ |
| rhodopin | $CS_2$ | 0.10 ± 0.01 | 0.53 ± 0.05 | 4.2 ± 0.3 | 15 ± 1 |
| glucoside | benzyl alcohol | <0.10 | 0.37 ± 0.02 | 4.2 ± 0.2 | 7 ± 1 |
| | MeOH | <0.10 | 0.43 ± 0.04 | 4.3 ± 0.2 | 7.3 ± 0.2 |
| | ACN | <0.10 | 0.39 ± 0.01 | 3.8 ± 0.1 | 8.4 ± 0.9 |
| rhodopinal | $CS_2$ | <0.10 | 0.38 ± 0.03 | 4.7 ± 0.3 | 15.3 ± 0.3 |
| glucoside | benzyl alcohol | <0.10 | 0.35 ± 0.01 | 4.4 ± 0.2 | 9 ± 1 |
| | MeOH | 0.11 ± 0.01 | 0.33 ± 0.02 | 3.7 ± 0.1 | 5.9 ± 0.6 |
| | ACN | 0.12 ± 0.01 | 0.52 ± 0.03 | 3.9 ± 0.2 | 8 ± 1 |

[1]The uncertainties in the values were obtained by exploring the region of solution for each parameter according to the goodness of fit and minimization of the residuals. An infinitely long (on the time scale of the experiment) component was required for a good fit in all cases. $CS_2$, carbon disulfide; MeOH, methanol; ACN, acetonitrile.

The band profile of the third EADS component for both molecules is very strong and well-known to be associated with ESA from the relaxed $S_1$ ($2^1A_g^-$) state making a transition to a higher excited singlet state. The lifetime of this component for rhodopin glucoside in all solvents was found to be in the narrow range of 3.8 to 4.3 ps with no obvious effect of solvent polarity on the value. However, the $S_1$ ($2^1A_g^-$) lifetime for rhodopinal glucoside in the polar solvents methanol and acetonitrile was 3.7 ps and 3.9 ps respectively, which are slightly shorter than the 4.4 ps and 4.7 ps values found for the molecule in the less polar solvents, benzyl alcohol and carbon disulfide, respectively. The fact that the lifetime of this component is reasonably similar for both rhodopin glucoside and rhodopinal glucoside indicates that neither the configuration, which is 13-*cis* for rhodopinal glucoside in solution compared to all-*trans* for rhodopin glucoside (Figure 1A), nor the presence of the aldehyde group at carbon C20 on rhodopinal glucoside compared to the methyl group at the same position on rhodopin glucoside, results in any significant change in the dynamics of the $S_1$ state that would impact its role in light-harvesting.

The fourth EADS component of both molecules in all solvents has a lifetime that ranges from 5.9 to 15.3 ps. This component is rather weak, but displays negative features associated with ground state bleaching as well as a positive feature on the short wavelength side of the main $S_1 \rightarrow S_N$ absorption profile. The negative features indicate that some fraction of the carotenoid population is still in an excited state. The short wavelength band is reminiscent of the S* state initially proposed to be an intermediate state between the $S_1$ ($2^1A_g^-$) and $S_2$ ($1^1B_u^+$) excited singlet states that is involved in both $S_2$ ($1^1B_u^+$) depopulation and carotenoid triplet state formation in light harvesting

complexes.[48-50] Subsequent work[43] on several open-chain carotenoids has shown that the S* yield is larger for molecules with longer π-electron conjugation suggestive of it being associated with a twisted molecular conformation of the carotenoid in the $S_1$ ($2^1A_g^-$) state.[43,51] Finally, a very weak, infinitely long-lived component was necessary to obtain a completely satisfactory fit to the datasets.

*Transient absorption of LH2 complexes*

The LH2 complexes were excited in the region of carotenoid absorption at either 525 or 570 nm and then transient absorption spectra were recorded at various delay times after the pump laser pulse (Figure 11). The LH2 complex from *Rbl. acidophilus* 10050 displayed transient absorption profiles (top panel of Figure 11) that were similar to previously reported spectra and include the instantaneous onset of bleaching of the carotenoid ground state spectrum, broad positive ESA at intermediate times, followed by the appearance of a strong narrow $S_1 \rightarrow S_N$ transition at ~580 nm at later times.[34] The HPLC pigment analysis of the LH2 complex from strain 10050 (Table 1) revealed that the carotenoid composition consists of roughly equal amounts of rhodopin and rhodopin glucoside with a small amount of lycopene, all of which have identical absorption spectra. Using this information regarding the spectra of the carotenoids in the LH2 complex from *Rbl. acidophilus* 10050 as a control, the features attributable to rhodopin and rhodopinal can be distinguished in the transient spectra of the LH2 complexes prepared from 7050 LL and 7050 HL cells which contain a mixture of these carotenoids (Table 1). (Recall that any reference to rhodopin or rhodopinal in this context should be taken to mean the combined spectral properties of the molecules and their respective glucosides, which are indistinguishable.) Laser excitation at 525 nm of the 7050 LL or

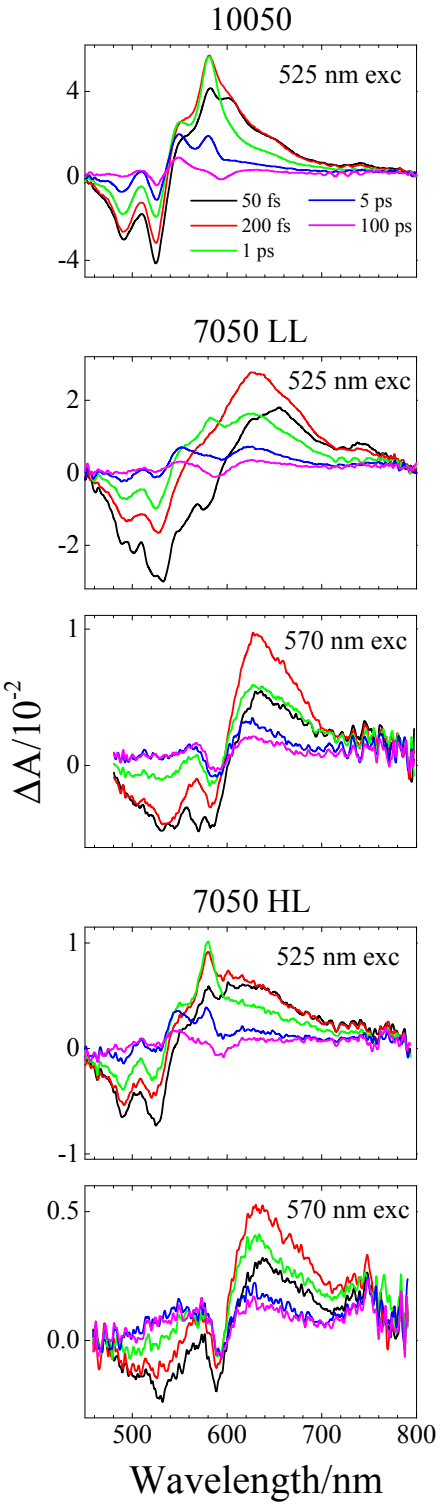


**Figure 11.** Transient absorption spectra of LH2 complexes from *Rbl. acidophilus* 10050, 7050 LL and 7050 HL recorded at room temperature using the indicated excitation wavelengths.

7050 HL LH2 complexes results in a combination of transient absorption signals from rhodopin and rhodopinal because both molecules absorb at this wavelength. Selective excitation of rhodopinal can be achieved by tuning the pump laser to 570 nm, which is a wavelength where rhodopin does not absorb. (See Figure 8.)

Transient absorption spectra from the 7050 LL and HL LH2 complexes excited at 525 nm (combined rhodopin plus rhodopinal excitation) or at 570 nm (selective rhodopinal excitation) are shown in Figure 11. Similar to the transient absorption spectra from strain 10050, the transient spectra recorded for these LH2 complexes at a 50 fs delay time (black traces in Figure 11) have negative features corresponding to the bleaching of the carotenoid $S_0$ ($1^1A_g^-$) $\rightarrow$ $S_2$ ($1^1B_u^+$) ground state absorption bands. In addition, there is a positive signal in the 540–700 nm region which represents an $S_1$ ($2^1A_g^-$) $\rightarrow$ $S_N$ transition indicating very fast decay of the $S_2$ ($1^1B_u^+$) state to populate the $S_1$ ($2^1A_g^-$) state of the carotenoid. In the 200 fs delay time spectra (red traces), the ground state bleaching has partially recovered, indicative of energy transfer to BChl, but the strong positive $S_1$ ($2^1A_g^-$) $\rightarrow$ $S_N$ absorption band has gained amplitude and is broader compared to the subsequent 1 ps delay time spectrum (green traces). The gain in amplitude of the feature associated with the $S_1$ ($2^1A_g^-$) $\rightarrow$ $S_N$ transition indicates that internal conversion from $S_2$ to populate the $S_1$ state is competing effectively with EET from $S_2$ to BChl.

A close examination of the 1 ps time delay (green trace) spectrum recorded for the 7050 LL LH2 excited at 525 nm (second panel in Figure 11) shows a narrow positive feature at ~580 nm and a broader one at ~630 nm. Comparison of this spectrum with those taken at the same time delay from the 10050 LH2 excited at 525 nm (selective

rhodopin excitation, upper panel of Figure 11) and the 7050 LL LH2 sample excited at 570 nm (selective rhodopinal excitation, third panel of Figure 11) reveals that the narrow peak at ~580 nm in the spectrum from the 7050 LL LH2 excited at 525 nm is due to the $S_1 \rightarrow S_N$ transition of rhodopin whereas the ~630 nm peak is from rhodopinal. This is expected because excitation of the 7050 LL sample using 525 nm light excites both carotenoids which are present in this LH2 sample (Table 1). This interpretation is supported by the transient absorption spectra resulting from 525 nm excitation of the 7050 HL LH2 complex (fourth panel of Figure 11). Note that the narrow positive feature at ~580 nm in the 1 ps time delay spectrum (green trace) attributable to the $S_1 \rightarrow S_N$ transition of rhodopin is much more pronounced relative to the broader band at ~630 nm associated with rhodopinal. This is because the LH2 complex from 7050 HL contains 56% total rhodopin compared to the 7050 LL LH2 sample which has only 15% rhodopin (Table 1). As expected, selective excitation of rhodopinal at 570 nm in the 7050 HL LH2 sample (bottom panel of Figure 11) shows no sign of the narrow $S_1 \rightarrow S_N$ feature belonging to rhodopin. The major positive band in the 1 ps time delay spectrum (green trace) is that of the $S_1 \rightarrow S_N$ ESA of rhodopinal.

The 5 ps delay time spectra of the 10050 and 7050 LL LH2 samples (blue traces in Figure 11) show significantly diminished carotenoid ground state bleaching and reduced $S_1 \rightarrow S_N$ ESA indicating that a substantial amount of the carotenoid $S_1$ state excited state population has either been transferred to BChl or has decayed via internal conversion back to the ground state. Also in this time frame, an additional peak appears at ~560 nm on the short wavelength side of the main ESA peak and persists longer than 100 ps (magenta trace). This is very likely attributable to a carotenoid triplet state.[52]

*Global analysis of transient absorption data*

The EADS components of the LH2 complexes obtained from a global fitting of the transient absorption datasets are shown in Figure 12 and summarized in Table 4. The fitting of the transient absorption spectra required five components, the first of which has a lifetime <100 fs for all the LH2 complexes and has features associated with the bleaching of the ground state absorption as well as stimulated emission from $S_2$ ($1^1B_u^+$). This is consistent with the value of 57 fs reported by Macpherson et al[33] for the $S_2$ lifetime of rhodopin in the LH2 complex from *Rbl. acidophilus* 10050. The second EADS component (red traces in Figure 12) has a lifetime ranging from 250 to 490 fs and has broad features in the carotenoid absorption region characteristic of vibronically-hot $S_1$ ($2^1A_g^-$) $\rightarrow$ $S_N$ excited singlet state transition. This second EADS has weaker negative bands in the carotenoid ground state absorption region than the first EADS indicating that some of the carotenoid molecules have returned to the ground state via EET from the $S_2$ state to BChl. Also evident in the second EADS is a small negative dip at ~590 nm appearing on the broad positive ESA spectrum. This is due to the bleaching of the BChl $Q_X$ band brought about by EET to BChl from the carotenoids. As the second EADS component decays into a third (green lines in Figure 12) the lineshape narrows considerably for the 10050 LH2 excited at 525 nm and a strong band associated with the $S_1$ ($2^1A_g^-$) $\rightarrow$ $S_N$ transition is evident at 580 nm. This line narrowing is accompanied by a decrease in the extent of ground state bleaching indicating that more of the carotenoid molecules have returned to the ground state, perhaps by EET from the vibronically-hot $S_1$ state. This third component decays in 3.0 ps for the 10050 LH2 and represents the $S_1$ lifetime of rhodopin in the LH2 pigment-protein complex. The peak at 580 nm has much

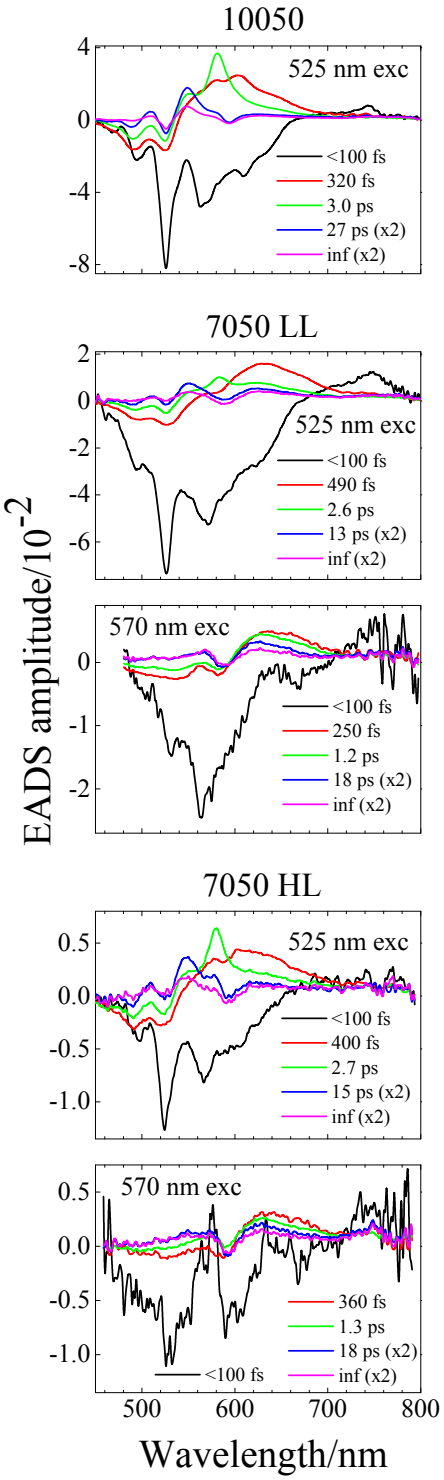


**Figure 12.** Evolution associated difference spectra (EADS) obtained from globally fitting the transient absorption datasets of LH2 complexes from *Rbl. acidophilus* 10050, 7050 LL and 7050 HL given in Figure 11.

**Table 4.** Lifetimes of the EADS components obtained by global fitting the transient absorption datasets recorded for the LH2 complexes from *Rbl. acidophilus* 10050, 7050 HL and 7050 LL.[a]

| LH2 | Excitation λ/nm | Lifetime/ps $\tau_1$ | $\tau_2$ | $\tau_3$ | $\tau_4$ |
|---|---|---|---|---|---|
| 10050 | 525 | <0.10 | 0.32 ± 0.02 | 3.0 ± 0.1 | 27 ± 3 |
| 7050 LL | 525 | <0.10 | 0.49 ± 0.05 | 2.6 ± 0.2 | 13 ± 1 |
| | 570 | <0.10 | 0.25 ± 0.02 | 1.2 ± 0.1 | 18 ± 2 |
| 7050 HL | 525 | <0.10 | 0.4 ± 0.1 | 2.7 ± 0.2 | 15 ± 2 |
| | 570 | <0.10 | 0.36 ± 0.01 | 1.3 ± 0.1 | 18 ± 2 |

[a]The uncertainties were obtained by exploring the region of solution for each parameter according to the goodness of fit and minimization of the residuals. An infinitely long (on the time scale of the experiment) component was required for a good fit in all cases.

less amplitude in the third EADS component from the 7050 LL LH2 sample obtained from data also using 525 nm excitation (green trace in the second panel of Figure 12). This is due to the fact that this sample has much less total rhodopin (rhodopin plus rhodopin glucoside) than the 10050 LH2. In fact, the peak at 580 nm is completely absent in the third EADS obtained from data using 570 nm excitation (green trace in the third panel of Figure 12). Instead, a broad lineshape peaking at ~620 nm and belonging to rhodopinal is observed. This is because excitation at 570 nm selectively excites rhodopinal. Note that the lifetime of this component is 1.2 ps in the 7050 LL LH2 and 1.3 ps in the 7050 HL LH2 which is significantly shorter than the average value of 4.1 ps found for rhodopinal in the different solvents and also shorter than the value of 3.0 ps found for rhodopin in the LH2 complex from strain 10050. (See Tables 3 and 4.) This is suggestive of significantly faster EET to BChl from the $S_1$ state of rhodopinal compared to rhodopin.

The fourth EADS component has a lifetime in the range 13 ps to 27 ps for all the datasets and a significantly diminished overall amplitude relative to the preceding EADS profiles. The lifetime of this component, along with the clearly evident positive band on the short wavelength side of the feature attributable to the main $S_1 \rightarrow S_N$ absorption band, and the wavy features in the region of the carotenoid ground state absorption are all characteristics of the S* state in accord with previous reports.[34,43,48-50,53,54] The fifth and final EADS component has an infinitely long lifetime on the time scale of the experiment and was necessary to obtain a satisfactory fit in all cases. The primary spectral feature in this last EADS component is the negative amplitude at 590 nm, which corresponds to the bleaching of the BChl $Q_X$ band that is expected to persist on the order of nanoseconds

until the $S_1$ state of BChl relaxes back to the ground state.

***Quantum computational analysis***

Quantum computations were carried out by Mr. Jordan A. Greco and Prof. Robert R. Birge[55] of the University of Connecticut to augment the experimental results. The details of the calculations will be presented in the Ph.D. dissertation of Mr. Greco. In order to make the computations tractable, the majority were carried out on the model chromophores which include the entire central polyene portion of rhodopin and rhodopinal, but replace the glucoside and aliphatic end groups with methyl groups. The resulting model polyenes have $C_s$ or $C_{2h}$ symmetry, and this symmetry, in combination with the smaller size, allows higher quality calculations to be carried out than would otherwise be possible. Test calculations on the full and model chromophores indicate that the end groups do not have a significant impact on the atomic charges other than small changes in the charges on the carbon atoms at the ends of the polyene chains. Single configuration interaction (CI) calculations on the full and model systems demonstrate that the end groups create less than 0.02 eV shift in the transition energies. This conclusion is consistent with the observation that the absorption spectra of rhodopin and rhodopin glucoside are indistinguishable.[3]

# Discussion

### *Carotenoid structure, energy levels and electronic transitions*

*Configuration of rhodopinal in solution*

Although a primary goal of this work is to understand the photophysical properties of rhodopinal in LH2 complexes, the process is started by identifying the geometry of rhodopinal in solution. Previous studies have proposed that rhodopinal acquires a *cis* configuration in solution.[19,56-58] Computational results by Greco and Birge based on density functional theory and an analysis of the absorption spectra demonstrated that rhodopinal takes on a *cis* configuration in both nonpolar and polar solvent. Experimental support for the 13-*cis* configuration of rhodopinal in solution is provided by comparing the excited state manifolds calculated for both the *cis* and the *trans* configurations with the experimental spectra. The MNDO-PSDCI calculations indicate that the band at 28,000 $cm^{-1}$ observed in the experimental spectra band is associated with a $^1A_g^+$ excited state, resulting in transition from the ground state that is often called the "*cis*-band".[59] The high relative intensity of the "*cis*-band" band provides spectroscopic evidence for a *cis* linkage near the center of the polyene chain.[60] Very similar results are obtained for rhodopinal in acetonitrile. The combination of theory and experiment provide strong support for rhodopinal having a *cis* configuration in both polar and nonpolar solvent.

The computations suggest, however, that 13-*cis*-rhodopinal may form a corkscrew conformation to help stabilize the molecule in solution. A corkscrew conformation involves clockwise or counterclockwise dihedral distortion involving both single and double bonds, with a majority of the distortion in the single bonds.[43] The change in

geometry costs very little in terms of torsional distortion energy but provides intramolecular electrostatic stabilization in nonpolar solvent and solute-solvent stabilization in polar solvent.

*Photophysical properties of rhodopinal in the LH2 complex*

The crystal structure of the B800-820 LH2 complex[18] did not fully resolve the rhodopinal structure, but provided ample evidence that the structure is in an all-*trans* configuration. Given the above results that demonstrate that 13-*cis*-rhodopinal is more stable than *trans*-rhodopinal in solution, the question arises as to why an all-*trans* configuration for rhodopinal exists in the LH2 complex. There are a number of trivial reasons for this. First, the binding site for rhodopinal glucoside, which as mentioned previously, is formed independently of, and prior to the conversion of B800-850 to B800-820, must also serve as the binding site for rhodopin glucoside, whose most stable configuration is undisputedly all-*trans*. Second, the formation of rhodopinal requires enzymatic activity to attach the aldehyde group. The enzyme would likely release *trans*-rhodopinal glucoside into solution for assembly into the pigment-protein complex, and formation of the 13-*cis*-rhodopinal glucoside would either require an isomerase or >30 min for thermal isomerization to generate the equilibrium structure.

*Theoretical simulation of the transient absorption spectra*

As shown in Figure 9, there are significant differences in the transient absorption spectra of rhodopinal compared to rhodopin. In particular, the transient absorption maximum is red-shifted and an additional feature at ~740 nm is observed for rhodopinal. To explore these differences theoretically, MNDO-PSDCI theory was used to calculate the energies and oscillator strengths for excitations from the ground state and the relaxed

first excited state. The computations also simulated the transient absorption spectra based on the assumption that the origin states are the fully relaxed lowest-excited $2^1A_g^-$ states generated using full single CI and acetonitrile as the solvent. However, the MNDO-PSDCI calculations are for vacuum conditions, and the effect of solvent is limited to the geometry of the relaxed origin state. The simulated spectra reproduce the key features shown in Figure 9 by predicting both the red-shift of the transient maximum as well as the farther red-shifted weaker band observed only for rhodopinal. This more red-shifted band is associated with a transition from the $2^1A_g^-$ excited state to the 8$^{th}$ excited ($5^1A_g^+$) singlet state. Durchan et al.[61] reported similar red-shifted transient absorption bands from 8'-apo-β-carotenal and also interpreted the results in terms of a transition from the $S_1$ ($2^1A_g^-$) state to a higher $A_g^+$ state. Moreover, they proposed that the allowedness for the transition arises due to the carbonyl group introducing asymmetry into the conjugated polyene system. The presence of asymmetry in the molecule would have the effect of relaxing the selection rules that prohibit the transition from appearing in a more symmetric, linear carotenoid; e.g. rhodopin.

The above-mentioned red-shifted band calculated to be at ~680 nm appears to be present in both *cis*- and *trans*-rhodopinal. This observation can be traced to the fact that, whereas a transition from the ground $S_0$ ($1^1A_g^-$) state to the $5^1A_g^+$ state only has intensity in molecules with *cis* configurations, hence its designation as the "*cis*-band", a transition from the $S_1$ ($2^1A_g^-$) excited state is strong for both *trans*- and *cis*-rhodopinal. Therefore, the additional red-shifted band seen only in the transient absorption spectrum of rhodopinal in solution is due to the presence of the aldehyde group on the molecule, and not to the configuration of the carotenoid.

***Energy transfer in the LH2 complexes***

Reconstruction and comparison of the 1−T and fluorescence excitation spectra from the LH2 complexes (Figures 6 and 8) show clearly that rhodopinal is much more efficient than rhodopin at transferring excited state energy to BChl. The precise factors responsible for this effect can be obtained from a consideration of the rate constants for de-excitation of the carotenoid excited states derived from the global fitting analysis.

The $S_1$ and $S_2$ states of carotenoids represent important donor excited states for EET to BChl. These routes are represented in Figure 13 by the rate constants $k_{ET1}$ and $k_{ET2}$, respectively. Deactivation of these two excited states may also occur via internal conversion, and these processes are indicated in the figure by the rate constants, $k_{10}$ and $k_{21}$. It is important to mention here that broadband 2D electronic spectroscopic results provide compelling evidence for the participation in EET of a dark intermediate state of the carotenoid having an energy in the vicinity of the state associated with the $Q_X$ transition of BChl.[35] This dark state was reported to be populated in 21 fs and depopulated in 62 fs. Both of these times are shorter than the ~100 fs time resolution of the laser spectrometer used in the present work. Hence, the rate constant $k_{ET2}$ illustrated in Figure 13 should be interpreted as including the kinetics of this dark state in addition to those of $S_2$.

The total EET efficiency, $\phi_{ET}$ resulting from both the $S_1$ and $S_2$ pathways is given by the expression

$$\phi_{ET} = \phi_{ET2} + k\phi_{ET1} = \left[ \frac{k_{ET2}}{k_{ET2} + k_{21}} + \left( \frac{k_{21}}{k_{ET2} + k_{21}} \right) \left( \frac{k_{ET1}}{k_{ET1} + k_{10}} \right) \right] \times 100 \qquad (1)$$

where the rate constants correspond to the processes illustrated in Figure 13. The rate constants can be computed from the lifetimes of the $S_1$ and $S_2$ excited states measured in

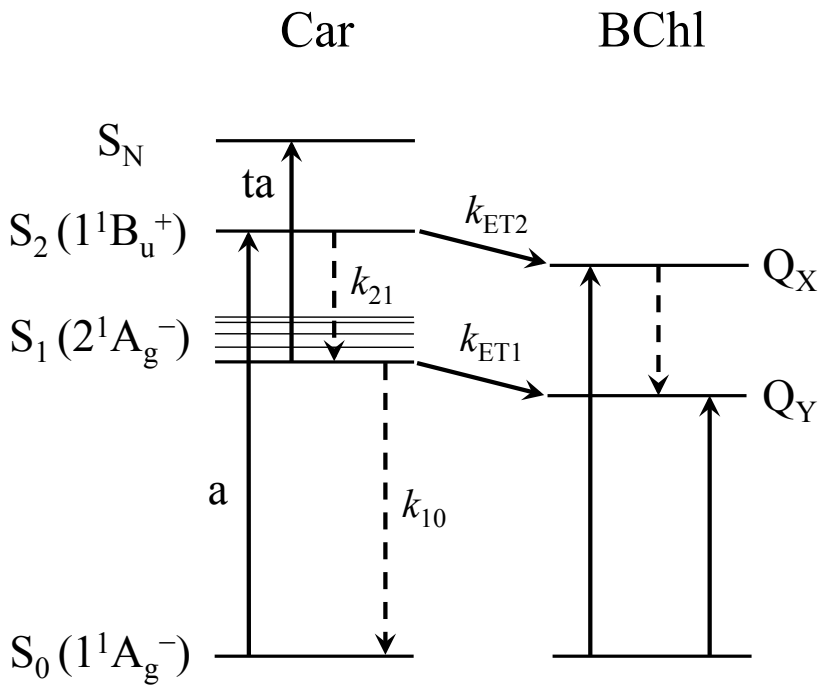


**Figure 13.** Pathways of energy transfer in the LH2 complex. a, absorption; ta, transient absorption. Dashed arrows indicate radiationless processes.

solution, $\tau_{S_i}^{SOLN}$, and in the LH2 complexes, $\tau_{S_i}^{LH2}$. The relevant expressions are[34]

$$k_{ETi} = \frac{1}{\tau_{S_i}^{LH2}} - \frac{1}{\tau_{S_i}^{SOLN}} \qquad i = 1, 2 \qquad (2)$$

and

$$k_{21} = \frac{1}{\tau_{S_2}^{SOLN}}, \; k_{10} = \frac{1}{\tau_{S_1}^{SOLN}} \qquad (3)$$

Tables 3, 4 and 5 summarize the lifetimes obtained from the global fits and the rate constants and efficiencies obtained either from the data presented here and using Equations 1–3 or from previous work.[33,34]

The key result for rhodopin (and rhodopin glucoside) in the LH2 complex from *Rbl. acidophilus* 10050 is the extent of partitioning between the $S_1$ and $S_2$ donor states of the efficiency of energy transfer to BChl. The data in Table 5 show that $\phi_{ET1}$ = 27% and $\phi_{ET2}$ = 40% which according to Equation 1 leads to an overall energy transfer efficiency of 56%. However, it is important to point out that in the current analysis, the lifetime of the $S_2$ state of rhodopin in solution was treated as an adjustable parameter and set to 95 fs to achieve agreement between the energy transfer efficiency of 56% computed from the dynamics data, and that measured by fluorescence excitation spectroscopy (Figures 6 and 8). The value of 95 fs is in very good agreement with the $S_2$ lifetime of ~105 fs reported by Macpherson et al.[33] for rhodopin glucoside in ethanol, and is consistent with the present findings that the value is <100 fs. Previous workers concur that the $S_2$ pathway is most important in the carotenoid-to-BChl energy transfer mechanism in this LH2 complex (Table 5).[33,34]

When rhodopinal (and rhodopinal glucoside) is present in the LH2 complex, as is the case for *Rbl. acidophilus* 7050 LL and HL, the overall carotenoid-to-BChl energy

**Table 5.** Rate constants, $k_{ET1}$, $k_{ET2}$, $k_{10}$, and $k_{21}$ and energy transfer efficiencies, $\phi_{ET1}$, $\phi_{ET2}$, $\phi_{ET(dyn)}$, and $\phi_{ET(fl)}$ for rhodopin and rhodopinal in LH2 complexes isolated from *Rbl. acidophilus*.[a] The values were obtained using Equations 1–3 given in the text.

| LH2 complex (carotenoid) | $k_{ET1}$ ($ps^{-1}$) | $k_{10}$ ($ps^{-1}$) | $\phi_{ET1}$ (%) | $k_{ET2}$ ($ps^{-1}$) | $k_{21}$ ($ps^{-1}$) | $\phi_{ET2}$ (%) | $\phi_{ET}$(dyn)[b] (%) | $\phi_{ET}$(fl)[c] (%) | Reference |
|---|---|---|---|---|---|---|---|---|---|
| 10050 (rhodopin) | 0.089[d] | 0.24 | 27 | 7.0[e] | 10.5 | 40 | 56 | 56 | This work and 33 |
| 7050 LL (rhodopinal) | 0.59[f] | 0.24 | 71 | 90[g] | 10 | 90 | 97 | 97 | This work |

[a]Rate constants for the LH2 complexes were obtained using laser excitation at 525 nm (rhodopin excitation) for the sample prepared from *Rbl. acidophilus* strain 10050 (which contains only the rhodopin chromophore) and at 570 nm (selective rhodopinal excitation) for the sample prepared from *Rbl. acidophilus* strain 7050 LL.

[b]Determined from the dynamics (dyn) of the excited states according to Equation 1.

[c]Determined from steady-state fluorescence excitation spectroscopy (fl) as shown in Figures 6 and 8.

[d]Computed from Equation 2 using the values of 3.0 ps ($\tau_3$ in Table 4) and 4.1 ps measured here for the lifetime of the $S_1$ state of rhodopin in the LH2 complex and as an average value in solution ($\tau_3$ in Table 3), respectively.

[e]Computed from Equation 2 using the values of 57 fs and 95 fs for the lifetime of the $S_2$ state in the LH2 complex and in solution, respectively. The 57 fs value was obtained from fluorescence up-conversion spectroscopic experiments reported in Reference 33. The lifetime of the $S_2$ state in solution was treated as an adjustable parameter to achieve agreement between the energy transfer efficiency of 56% computed from the dynamics data and that measured by fluorescence excitation spectroscopy.

[f]Computed from Equation 2 using the values of 1.2 ps ($\tau_3$ in Table 4) and 4.1 ps measured here for the lifetime of the $S_1$ state of rhodopinal in the LH2 complex and as an average value in solution ($\tau_3$ in Table 3), respectively.

[g]Computed from Equation 2 using the values of 10 fs and 100 fs for the lifetime of the $S_2$ state in the LH2 complex and in solution, respectively. In fact, the $S_2$ lifetime obtained for rhodopinal glucoside in solution was found here to be <100 fs which means that the $k_{21}$ value of 10 $ps^{-1}$ based on this lifetime is a lower limit to what the value could be. The lifetime of the $S_2$ state in the complex was treated as an adjustable parameter to achieve agreement between the energy transfer efficiency of 97% computed from the dynamics data and that measured by fluorescence excitation spectroscopy.

transfer efficiency becomes much greater. As shown clearly from the analysis of the fluorescence excitation spectra given in Figure 8, this can be traced directly to the fact that rhodopinal is much more efficient at transferring energy to BChl than rhodopin. The data presented in Table 5 reveal that this enhancement is due to a significant increase in both $k_{ET1}$ and $k_{ET2}$ for rhodopinal compared to those obtained for rhodopin. Note from the data in Table 5 that $k_{ET1}$ increases from 0.089 $ps^{-1}$ to 0.59 $ps^{-1}$ and $k_{ET2}$ increases from 7.0 $ps^{-1}$ to 90 $ps^{-1}$ in going from rhodopin to rhodopinal as the energy donor to BChl in the LH2 complex from 7050 LL. These combined increases result in a substantial enhancement in the carotenoid-to-BChl EET efficiency from 56% for rhodopin to 97% for rhodopinal. However, as was the case for the $S_2$ lifetime of rhodopin discussed above, owing to the fact that lifetime of the $S_2$ state of rhodopinal in solution and in the LH2 complex are faster than the time resolution of the laser spectrometer, these values were treated as adjustable parameters to achieve agreement between the energy transfer efficiency computed from the dynamics data, and that measured by fluorescence excitation spectroscopy.

A consideration of the fundamental quantum mechanical expression for the rate constant for EET[62,63]

$$k_{ET} = \frac{1}{c\hbar}|T|^2 J \tag{4}$$

where $T$ is the electronic coupling term and $J$ is the normalized spectral overlap

$$J = \int_{-\infty}^{\infty} F_d(\nu)\varepsilon_a(\nu)d\nu \tag{5}$$

and $F_d(\nu)$ is the emission spectrum of the donor carotenoid and $\varepsilon_a(\nu)$ is the absorption spectrum of the BChl acceptor, leads to the conclusion that the increase in the values of

the rate constants in going from rhodopin to rhodopinal (Table 5) cannot be attributed solely to the different positions of the energy levels of the carotenoids, and consequently neither to differences in spectral overlap. This is particularly evident for the route involving the $S_2$ ($1^1B_u^+$) state of the carotenoid and the state corresponding to the $Q_X$ band of BChl. Taking the $S_0$ ($1^1A_g^-$) $\rightarrow$ $S_2$ ($1^1B_u^+$) absorption spectrum of rhodopin and rhodopinal reflected about their spectral origins as approximations to their (very weak) emission profiles, and overlaying these lineshapes with the $Q_X$ absorption band of BChl in the LH2 complex (Figure 14), one obtains a rhodopinal-to-rhodopin spectral overlap ratio of 1.2. This value is significantly different from the rhodopinal-to-rhodopin ratio of $k_{ET2}$ rate constants given in Table 5 which indicate a value of (90/7.0) = 13. Although it is impossible to compute the spectral overlap integrals associated with the $S_1$ ($2^1A_g^-$) state of the carotenoid due to the lack of either detectable $S_0$ ($1^1A_g^-$) $\rightarrow$ $S_1$ ($2^1A_g^-$) absorption or fluorescence from the $S_1$ ($2^1A_g^-$) state, the small difference in the $S_1$ lifetimes of rhodopin and rhodopinal in solution (Table 3) suggests very similar $S_1$ excited state energies for the two molecules. Therefore, a minimal effect of the position of the energy levels, and consequently of spectral overlap, is expected for the $k_{ET1}$ rate constant in the LH2 complexes. However, a significant change in $k_{ET1}$ is evidenced by comparing the $S_1$ lifetime of rhodopin in the LH2 complex from *Rbl. acidophilus* 10050 (3.0 ps) with that of rhodopinal (selectively excited at 570 nm) in the LH2 complex from *Rbl. acidophilus* 7050 LL (1.2 ps). Using Equation 2 and an average lifetime of 4.1 ps for the carotenoids in the four different solvents, the value of $k_{ET1}$ is shown in Table 5 to increase by a factor of (0.59/0.089) = 6.6 in going from rhodopin to rhodopinal. Because only small differences in excited state energies and spectral overlap with the BChl $Q_X$ and $Q_Y$

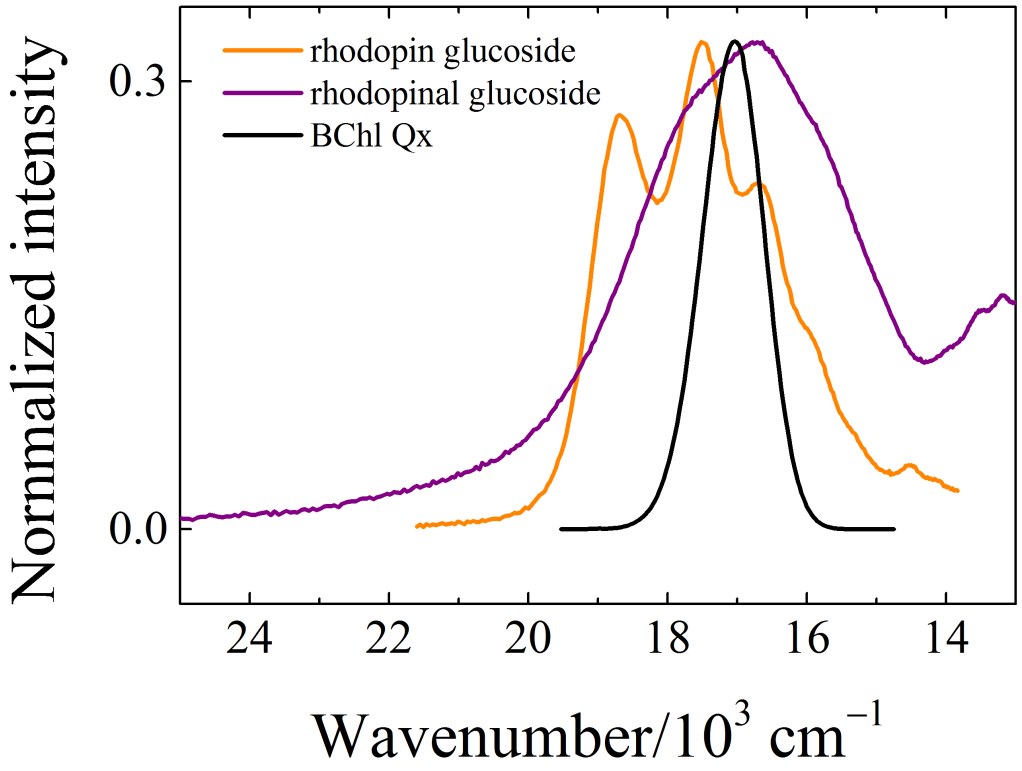


**Figure 14.** Spectral overlap of the hypothetical fluorescence of the carotenoid donor (orange and purple traces) and absorption of the BChl acceptor (black trace). The absorption spectra of the carotenoids were reflected about their spectral origins to obtain approximations to the $S_2 \rightarrow S_0$ fluorescence spectra.

absorption bands are evident for both the $S_1$ and $S_2$ states of these carotenoids, stronger electronic coupling between the donor and acceptor electronic states induced by the presence of the aldehyde group on the π-electron polyene chain in rhodopinal must be a major factor determining why rhodopinal is much more efficient at carotenoid-to-BChl EET than rhodopin in the LH2 pigment-protein complex.

Although a rigorous analysis of the Coulomb coupling terms describing EET from $S_1$ and $S_2$ is beyond the scope of this chapter, this issue is addressed for $S_1$ by the level ordering analysis from the computational results. The lowest excited singlet state of both *cis*- and *trans*- configurations is calculated to be a "forbidden" $2^1A_g^-$ state that gains oscillator strength due to dipole-induced coupling with the higher energy, strongly allowed $1^1B_u^+$ state. The above kinetics analysis has revealed that energy is transferred from the $S_1$ ($2^1A_g^-$) state to the BChl acceptor 6.6 times faster than the corresponding state in rhodopin. The computations predict that the enhanced energy transfer rate is associated in part with a significant increase in the oscillator strength of the $S_1$ state in rhodopinal relative to rhodopin. Moreover, the increase in oscillator strength in *trans*-rhodopinal is ~35% larger than observed in 13-*cis*-rhodopinal. Because the Förster coupling efficiency is proportional to the allowedness of the donor excited state, the all-*trans* configuration of rhodopinal provides added value to its light-harvesting function.

As mentioned in the Introduction, when *Rbl. acidophilus* 7050 is grown under LL conditions, two major changes in the spectrum of the LH2 complex occur: A blue-shift of the BChl $Q_Y$ band from ~850 nm to ~820 nm which is caused by a change in the orientation of the C3-acetyl group of the B850 BChl; and a red-shift and broadening of the spectrum of the carotenoid, which is a consequence of the enzymatic substitution of

an aldehyde group for a methyl group on rhodopin resulting in its conversion to rhodopinal. An important question is then, which of these factors is most important for enhancing the rate and efficiency of carotenoid-to-BChl EET? The answer is that the conversion of rhodopin to rhodopinal is more important than the shift of the BChl $Q_Y$ band. Data suggestive of this conclusion was provided previously by Deinum et al.[4] who investigated the B800-820 LH2 complex from *Rbl. acidophilus* 7750. Cells of this strain grown either at low temperatures or at LL do not contain rhodopinal (or rhodopinal glucoside),[3,64] and the carotenoid-to-BChl EET efficiency of its associated LH2 complex, which contains primarily rhodopin and rhodopin glucoside was found to be 45 ± 5%.[4] If the change in the position of the BChl $Q_Y$ band from ~850 nm to ~820 nm was important for enhancing the efficiency of EET from the carotenoid to BChl, one would expect that the efficiency for *Rbl. acidophilus* strain 7750 would have a value above 45% or even higher than 56%, which is the value found for rhodopin in the B800-850 LH2 complex from strain 10050 (Table 2). The fact that it is not larger than 56%, and in fact is smaller than this value; i.e. 45 ± 5%, indicates that the change in the position of the $Q_Y$ band of BChl is not a factor in determining the efficiency of carotenoid-to-BChl EET. Instead, the conversion of rhodopin to rhodopinal, which incidentally occurs prior to the conversion of B800-850 to B800-820, is the primary controlling factor leading to more efficient EET in the LH2 complex of *Rbl. acidophilus* 7050 LL compared to the LH2 of *Rbl. acidophilus* strain 10050.

## Conclusions

The enzymatic conversion of rhodopin to rhodopinal in cells of *Rbl. acidophilus* 7050 grown under LL conditions results in a significant enhancement in the ability of the organism to transfer absorbed light energy to the reaction center. This is due almost entirely to the fact that rhodopinal, and its corresponding glucoside, are nearly 100% efficient at transferring excited state energy to BChl in the LH2 complex. Also, the spectrum of rhodopinal occurs at a longer wavelength compared to that of rhodopin, which allows the bacterium containing this carotenoid to capture light energy in a spectral region where its photosynthetic bacterial competitors do not absorb light. This provides an important advantage for this organism as it competes for life-sustaining photons in the water column. Moreover, based on the $k_{ET1}$ and $k_{ET2}$ rate constants given in Table 5, the energy absorbed by rhodopinal is transferred to BChl in the LH2 complex 6.6 times faster from the $S_1$ state and >10 times faster from the $S_2$ state than energy absorbed by rhodopin. More effective electronic coupling between the electronic states of the carbonyl-containing rhodopinal and BChl are the primary reason for the increase in these rates.

Even though the blue-shift of the BChl $Q_Y$ band from ~850 nm to ~820 nm induced by growing *Rbl. acidophilus* 7050 under LL conditions does not have an effect on the rate and efficiency of carotenoid-to-BChl EET, this spectral change has another consequence. It has been shown on the basis of singlet-singlet annihilation measurements that, compared to the B800-850 complex, the B800-820 complex provides a more effective energy barrier for preventing back transfer of excitation energy out of the reaction center core complex and into the photosynthetic unit.[4] Thus, the combined

effects of alterations in carotenoid and BChl structures and spectral properties resulting from the adaptation of the bacterial photosynthetic organism to the challenging environmental condition of limited light availability, contribute in a very tangible way to ensure survival of this species.

# References


(1) Cogdell, R. J.; Durant, I.; Valentine, J.; Lindsay, J. G.; Schmidt, K. *Biochim. Biophys. Acta* **1983**, *722*, 427–435.

(2) Angerhofer, A.; Cogdell, R. J.; Hipkins, M. F. *Biochim. Biophys. Acta* **1986**, *848*, 333–341.

(3) Gardiner, A. T.; Cogdell, R. J.; Takaichi, S. *Photosynth. Res.* **1993**, *38*, 159–167.

(4) Deinum, G.; Otte, S. C. M.; Gardiner, A. T.; Aartsma, T. J.; Cogdell, R. J.; Amesz, J. *Biochim. Biophys. Acta* **1991**, *1060*, 125–131.

(5) Cogdell, R. J.; Howard, T. D.; Isaacs, N. W.; McLuskey, K.; Gardiner, A. T. *Photosynth. Res.* **2002**, *74*, 135–141.

(6) Gabrielsen, M.; Gardiner, A. T.; Cogdell, R. J. Peripheral Complexes of Purple Bacteria In *The Purple Phototrophic Bacteria*; Hunter, C. N., Daldal, F., Thurnauer, M. C., Beatty, J. T., Eds.; Springer: Dordrecht, The Netherlands, **2009**; Vol. 28, 135–153.

(7) Gardiner, A. T.; Takaichi, S.; Cogdell, R. J. *Biochem. Soc. Trans.* **1992**, *21*, 6S.

(8) Prince, S. M.; Papiz, M. Z.; Freer, A. A.; McDermott, G.; Hawthornthwaite-Lawless, A. M.; Cogdell, R. J.; Isaacs, N. W. *J. Mol. Biol.* **1997**, *268*, 412–423.

(9) Heinemeyer, E.-A.; Schmidt, K. *Arch. Microbiol.* **1983**, *134*, 217–221.

(10) Takaichi, S.; Gardiner, A. T.; Cogdell, R. J. *Res. Photosynth., Proc. Int. Congr. Photosynth., 9th* **1992**, *1*, 149–152.

(11) Bauer, C. E.; Bird, T. H. *Cell* **1996**, *85*, 5–8.

(12) Giraud, E.; Fardoux, J.; Fourrier, N.; Hannibal, L.; Genty, B.; Bouyer, P.; Dreyfus, B.; Vermeglio, A. *Nature* **2002**, *417*, 202–205.

(13) Evans, K.; Georgiou, T.; Hillon, T.; Fordham-Skelton, A.; Papiz, M. Bacteriophytochromes Control Photosynthesis in *Rhodopseudomonas palustris* In *The Purple Phototrophic Bacteria*; Hunter, C. N., Daldal, F., Thurnauer, M. C., Beatty, J. T., Eds.; Springer: Dordrecht, The Netherlands, **2009**; Vol. 28, 799–809.

(14) Brunisholz, R. A.; Zuber, H. In *Photosynthetic Light-Harvesting Systems*; Scheer, H., Schneider, S., Eds.; Walter de Gruyter & Co.: New York, **1988**, 103–114.

(15) Fowler, G. J. S.; Visschers, R. W.; Grief, G. G.; van Grondelle, R.; Hunter, C. N. *Nature* **1992**, *355*, 848–850.

(16) Fowler, G. J.; Sockalingum, G. D.; Robert, B.; Hunter, C. N. *Biochem. J.* **1994**, *299*, 695–700.

(17) Cogdell, R. J.; Gall, A.; Köhler, J. *Quarterly Reviews of Biophysics* **2006**, *39*, 227–324.

(18) McLuskey, K.; Prince, S. M.; Cogdell, R. J.; Isaacs, N. W. *Biochem.* **2001**, *40*, 8783–8789.

(19) Aasen, A. J.; Jensen, S. L. *Acta Chem. Scand.* **1967**, *21*, 2185-2204.

(20) Takaichi, S. Carotenoids and Carotenogenesis in Anoxygenic Photosynthetic Bacteria In *The Photochemistry of Carotenoids*; Frank, H. A., Young, A. J., Britton, G., Cogdell, R. J., Eds.; Kluwer Academic Publishing: Dordrecht, **1999**; Vol. 8, 39–69.

(21) Takaichi, S. Distribution and Biosynthesis of Carotenoids In *The Purple Phototrophic Bacteria*; Hunter, C. N., Daldal, F., Thurnauer, M. C., Beatty, J. T., Eds.; Springer Science: Dordrecht, The Netherlands, **2009**; Vol. 28, 97–117.

(22) Krueger, B. P.; Scholes, G. D.; Jimenez, R.; Fleming, G. R. *J. Phys. Chem. B* **1998**, *102*, 2284–2292.

(23) Pariser, R. *J. Chem. Phys.* **1955**, *24*, 250–268.

(24) Hudson, B.; Kohler, B. *Annu. Rev. Phys. Chem.* **1974**, *25*, 437–460.

(25) Callis, P. R.; Scott, T. W.; Albrecht, A. C. *J. Chem. Phys.* **1983**, *78*, 16–22.

(26) Birge, R. R. *Acc. Chem. Res.* **1986**, *19*, 138–146.

(27) Kohler, B. E. Electronic Structure of Carotenoids In *Carotenoids*; Britton, G., Liaaen-Jensen, S., Pfander, H., Eds.; Birkhäuser Verlag AG: Basel, **1995**; Vol. 1B: Spectroscopy, 3–12.

(28) Christensen, R. L. The Electronic States of Carotenoids In *The Photochemistry of Carotenoids*; Frank, H. A., Young, A. J., Britton, G., Cogdell, R. J., Eds.; Kluwer Academic Publishers: Dordrecht, **1999**; Vol. 8, 137–159.

(29) Christensen, R. L.; Barney, E. A.; Broene, R. D.; Galinato, M. G. I.; Frank, H. A. *Arch. Biochem. Biophys.* **2004**, *430*, 30–36.

(30) Frank, H. A.; Young, A. J.; Britton, G.; Cogdell, R. J. The Photochemistry of Carotenoids In *Advances in Photosynthesis*; Govindjee, Ed.; Kluwer Academic Publishers: Dordrecht, **1999**; Vol. 8.

(31) McDermott, G.; Prince, S. M.; Freer, A. A.; Hawthornthwaite-Lawless, A. M.; Papiz, M. Z.; Cogdell, R. J.; Isaacs, N. W. *Nature (London)* **1995**, *374*, 517–521.

(32) Scholes, G. D.; Fleming, G. R. *J. Phys. Chem. B* **2000**, *104*, 1854–1868.

(33) Macpherson, A. N.; Arellano, J. B.; Fraser, N. J.; Cogdell, R. J.; Gillbro, T. *Biophys. J.* **2001**, *80*, 923–930.

(34) Cong, H.; Niedzwiedzki, D.; Gibson, G. N.; LaFountain, A. M.; Kelsh, R. M.; Gardiner, A. T.; Cogdell, R. J.; Frank, H. A. *J. Phys. Chem. B* **2008**, *112*, 10689–10703.

(35) Ostroumov, E. E.; Mulvaney, R. M.; Cogdell, R. J.; Scholes, G. D. *Science* **2013**, *340*, 52–56.

(36) Pfennig, N. *J. Bacteriol.* **1969**, *99*, 597–602.

(37) Ilagan, R. P.; Christensen, R. L.; Chapp, T. W.; Gibson, G. N.; Pascher, T.; Polivka, T.; Frank, H. A. *J. Phys. Chem. A* **2005**, *109*, 3120–3127.

(38) Fuciman, M.; Enriquez, M. M.; Polivka, T.; Dall'Osto, L.; Bassi, R.; Frank, H. A. *J. Phys. Chem. B* **2012**, *116*, 3834–3849.

(39) van Stokkum, I. H. M.; Larsen, D. S.; van Grondelle, R. *Biochim. Biophys. Acta* **2004**, *1657*, 82–104.

(40) McLuskey, K.; Prince, S. M.; Cogdell, R. J.; Isaacs, N. W. *Acta crystallographica section D-biological crystallography* **1999**, *55*, 885–887.

(41) Pendon, Z. D.; Gibson, G. N.; van der Hoef, I.; Lugtenburg, J.; Frank, H. A. *J. Phys. Chem. B* **2005**, *109*, 21172–21179.

(42) Niedzwiedzki, D. M.; Sullivan, J. O.; Polivka, T.; Birge, R. R.; Frank, H. A. *J. Phys. Chem. B* **2006**, *110*, 22872–22885.

(43) Niedzwiedzki, D.; Koscielecki, J. F.; Cong, H.; Sullivan, J. O.; Gibson, G. N.; Birge, R. R.; Frank, H. A. *J. Phys. Chem. B* **2007**, *111*, 5984–5998.

(44) Enriquez, M. M.; Fuciman, M.; LaFountain, A. M.; Wagner, N. L.; Birge, R. R.; Frank, H. A. *J. Phys. Chem. B* **2010**, *114*, 12416–12426.

(45) Magdaong, N. M.; Niedzwiedzki, D. M.; Greco, J. A.; Liu, H.; Yano, K.; Kajikawa, T.; Sakaguchi, K.; Katsumura, S.; Birge, R. R.; Frank, H. A. *Chem. Phys. Lett.* **2014**, *593*, 132–139.

(46) Bautista, J. A.; Connors, R. E.; Raju, B. B.; Hiller, R. G.; Sharples, F. P.; Gosztola, D.; Wasielewski, M. R.; Frank, H. A. *J. Phys. Chem. B* **1999**, *103*, 8751–8758.

(47) Frank, H. A.; Bautista, J. A.; Josue, J.; Pendon, Z.; Hiller, R. G.; Sharples, F. P.; Gosztola, D.; Wasielewski, M. R. *J. Phys. Chem. B* **2000**, *104*, 4569–4577.

(48) Gradinaru, C. C.; Kennis, J. T. M.; Papagiannakis, E.; van Stokkum, I. H. M.; Cogdell, R. J.; Fleming, G. R.; Niederman, R. A.; van Grondelle, R. *Proc. Natl. Acad. Sci. USA* **2001**, *98*, 2364–2369.

(49) Papagiannakis, E.; Kennis, J. T. M.; van Stokkum, I. H. M.; Cogdell, R. J.; van Grondelle, R. *Proc. Natl. Acad. Sci. USA* **2002**, *99*, 6017–6022.

(50) Papagiannakis, E.; van Stokkum, I. H.; Vengris, M.; Cogdell, R. J.; van Grondelle, R.; Larsen, D. S. *J. Phys. Chem. B* **2006**, *110*, 5727–5736.

(51) Cong, H.; Niedzwiedzki, D. M.; Gibson, G. N.; Frank, H. A. *J. Phys. Chem. B* **2008**, *112*, 3558–3567.

(52) Niedzwiedzki, D. M.; Kobayashi, M.; Blankenship, R. E. *Photosynth. Res.* **2011**, *107*, 177–186.

(53) Papagiannakis, E.; Das, S. K.; Gall, A.; Stokkum, I. H. M.; Robert, B.; van Grondelle, R.; Frank, H. A.; Kennis, J. T. M. *J. Phys. Chem. B* **2003**, *107*, 5642–5649.

(54) Wohlleben, W.; Buckup, T.; Hashimoto, H.; Cogdell, R. J.; Herek, J. L.; Motzkus, M. *J. Phys. Chem. B* **2004**, *108*, 3320–3325.

(55) Magdaong, N. M.; Lafountain, A. M.; Greco, J. A.; Gardiner, A. T.; Carey, A.-M.; Cogdell, R. J.; Gibson, G. N.; Birge, R. R.; Frank, H. A. *J. Phys. Chem. B* **2014**, *118*, 11172–11189.

(56) Liaaen-Jensen, S. *Pure Appl. Chem.* **1969**, *20*, 421–448.

(57) Ke, B.; Imsgard, F.; Kjøsen, H.; Liaaen-Jensen, S. *Biochimica et Biophysica Acta-Lipids and Lipid Metabolism* **1969**, *210*, 139–152.

(58) Chin, C.-A.; Song, P.-S. *J. Mol. Spectrosc.* **1974**, *52*, 216–223.

(59) Zechmeister, L. *Cis-Trans Isomeric Carotenoids, Vitamin a, and Arylpolyenes.* Academic Press: New York, 1962.

(60) Pendon, Z. D.; Sullivan, J. O.; van der Hoef, I.; Lugtenburg, J.; Cua, A.; Bocian, D. F.; Birge, R. R.; Frank, H. A. *Photosynth. Res.* **2005**, *86*, 5–24.

(61) Durchan, M.; Fuciman, M.; Šlouf, V.; Keşan, G.; Polívka, T. *J. Phys. Chem. A* **2012**, *116*, 12330–12338.

(62) Scholes, G. D.; Harcourt, R. D.; Fleming, G. R. *J. Phys. Chem. B* **1997**, *101*, 7302–7312.

(63) Desamero, R. Z. B.; Chynwat, V.; van der Hoef, I.; Jansen, F. J.; Lugtenburg, J.; Gosztola, D.; Wasielewski, M. R.; Cua, A.; Bocian, D. F.; Frank, H. A. *J. Phys. Chem.* **1998**, *102*, 8151–8162.

(64) Schmidt, K. *Arch. Microbiol.* **1971**, *77*, 231–238.

# *Chapter V*

# *Spectral heterogeneity and carotenoid-to-bacteriochlorophyll energy transfer in LH2 light-harvesting complexes from Allochromatium vinosum*

## Introduction

The major light-harvesting pigment-protein complex found in many photosynthetic purple sulfur and non-sulfur bacterial species is known as LH2.[1-5] It is characterized by two strong $Q_Y$ absorption bands of bacteriochlorophyll *a* (BChl *a*) in the near-infrared (NIR) region at approximately 800 nm and 850 nm.[6-8] The structure of this so-called B800-850 pigment-protein complex has been determined from high-resolution X-ray diffraction studies of *Rhodoblastus (Rbl.) acidophilus* (formerly *Rhodopseudomonas acidophila*)[5,9-11] and *Rhodospirillum (Rsp.) molischianum*[12] to be comprised of several copies of two hydrophobic proteins, denoted α and β, in which two collections of BChl *a* molecules are arranged in distinct, concentric rings, separated from each other along an axis that is directed perpendicular to the plane of the photosynthetic membrane. One carotenoid molecule per α/β pair of apoproteins is also noncovalently bound in the LH2 complex.[13] The ring associated with the 800 nm-absorbing BChls (B800) consists of either eight (*Rsp. molischianum*) or nine (*Rbl. acidophilus*) monomeric BChl *a* molecules, whereas the ring associated with the 850 nm-absorbing BChls (B850) is made up of twice that number of closely associated and interacting BChl *a* molecules.

It is the difference in site energies and strength of the interaction between BChl *a* molecules that gives rise to the two different NIR absorption bands in the LH2 complex.[14]

*Allochromatium (Alc.) vinosum* (formerly *Chromatium (Ch.) vinosum* strain D) is a photosynthetic purple sulfur bacterium that possesses the remarkable ability to alter the absorption spectral characteristics of its LH2 complex depending on the environmental conditions under which the organism is grown.[15-18] With variations in light intensity, temperature or type of reduced sulfur nutrient in the growth media, the position of the 850 nm absorption band can be blue-shifted to either 840 nm or 820 nm. In addition, in some cases, the BChl *a* $Q_Y$ absorption band at 800 nm can be observed to split into two distinct spectral components.[19-23] A circular dichroism (CD) and polarization-resolved single-molecule spectroscopic investigation of the split-peaked spectrum of the B800-850 LH2 complex from *Alc. vinosum* has proposed a structural model for the antenna complex in which the BChl *a* molecules form concentric rings made up of 12 B800 and B850 repeat units.[23] The model further proposes that the B800 molecules form exciton coupled dimers that interact with the B850 BChls which then gives rise to the split 800 nm $Q_Y$ band. An earlier investigation using electron microscopy carried out by Kereïche et al.[21] on LH2 complexes from *Alc. vinosum* argued that the organism was able to form antenna rings having various diameters, one of which was composed of potentially 12 or 13 α/β subunit pairs. In light of the work by Cleary et al.,[24] who proposed that only structures of 8, 9, 10 or 12 α/β subunit pairs were energetically stable, the determination of an LH2 complex consisting of 12 α/β subunit pairs is supported.

Several investigations of the spectroscopic properties of LH2 complexes from purple photosynthetic bacteria have shown that, despite major shifts in the position of the B850 BChl *a* $Q_Y$ and carotenoid absorption bands induced by alterations in bacterial growth conditions, the symmetry of the pigment-protein complex, and hence the exciton structure that produced the NIR BChl *a* absorption bands in the first place, remained unaltered.[14,18] This is particularly evident in studies on *Rbl. acidophilus* strain 7050 grown under low light conditions where a large portion of the bound carotenoid, rhodopin glucoside, is converted to rhodopinal glucoside, which shifts the carotenoid absorption band to longer wavelength, and the $Q_Y$ absorption band of the B850 BChl *a* in the LH2 complex shifts from 850 nm to 820 nm.[25-29] An important conclusion from these investigations was that although the structures of the pigments and the site energy and spectral form of the long wavelength $Q_Y$ band of BChl *a* were changed in going from the B800-850 to the B800-820 LH2 complex, the apoprotein composition, though changed, remained homogeneous.[14]

*Allochromatium vinosum* is quite different in this respect in that it has been reported to have multiple *puc* BA genes[30] that are capable of producing many different types of α and β apoproteins that may assemble within a single LH2 ring and lead to both structural and spectral heterogeneity.[18,31,32] This chapter seeks to examine the effect of this heterogeneity on the spectral and energy transfer properties of the carotenoids and BChl *a* pigments bound in three LH2 complexes, B800-820, B800-840 and B800-850 produced when *Alc. vinosum* is grown under different conditions. These three forms of LH2 were isolated, purified and examined using high-performance liquid chromatography (HPLC), steady-state absorption and fluorescence spectroscopy, and

ultrafast time-resolved absorption spectroscopy. This systematic series of LH2 complexes provides the means of exploring the factors that control the spectral properties and determine the rate and efficiency of carotenoid-to-BChl energy transfer. It is hoped that the results will provide insight into how photosynthetic systems are able to adapt and survive under varying environmental conditions.

## Materials and Methods

### *Sample Preparation and Characterization*

*Preparation of light-harvesting complexes*

*Alc. vinosum* cells were grown anaerobically using thiosulfate (T) as an electron donor, under high light (HL, 70–80 μmol $s^{-1}$ $m^{-2}$) or low light (LL, 2 μmol $s^{-1}$ $m^{-2}$) illumination, and at a temperature of 30 or 40 °C, as previously described.[18] B800-850, B800-840 and B800-820 LH2 complexes were then isolated from cultures denoted THL40, THL30 and TLL30, respectively, which indicate the electron donor (T), light intensity (HL or LL), and temperature (30 or 40 ºC) used for bacterial growth. Twenty microliters of each LH2 complex suspended in 20 mM Tris buffer containing 0.02% sodium dodecyl maltoside (DDM) detergent were stored in Eppendorf tubes at −80 ºC until needed for the pigment analysis or spectroscopic experiments. These stock samples had an optical density (OD) of ~100 in a 1 cm cuvette measured at the $\lambda_{max}$ of the BChl *a* $Q_Y$ band, which is 848 nm for the B800-850 complex and 798 nm for the B800-840 and B800-820 complexes.

*Carotenoid Analysis*

For the analysis of the carotenoid composition of the LH2 proteins, one eppendorf tube containing a stock solution of one of the complexes was thawed at room temperature and the pigments were then extracted using a mixture of acetone and methanol followed by partitioning with petroleum ether as described previously.[18] The solvent containing the extract was evaporated to dryness using nitrogen gas, and the residue was taken up in 0.5 mL of 9:1 (v/v) hexane:tetrahydrofuran for injection into a Waters 600E/600S HPLC system. The HPLC was equipped with a 2996 photodiode array detector (PDA) and

employed a normal-phase Waters Sunfire 5 μm silica column having dimensions of 4.6 × 250 mm. The column was maintained at 30 °C throughout the duration of the chromatographic run using a Phenomenex TS-130 heater. The mobile phase consisted of an isocratic delivery of 9:1 (v/v) hexane:tetrahydrofuran as previously described.[22,33] The flow rate was 1.5 mL/min. The carotenoids were identified based on their PDA absorption spectra and retention times by comparison with data obtained from previous investigations.[33]

To determine the relative molar concentration of the carotenoids present in the LH2 complexes, the Waters Empower II software was used to integrate the area under each HPLC peak at the detection wavelength of maximum absorbance for that pigment. The values of the area were then divided by the extinction coefficient of each carotenoid which yielded the molar concentrations. The published extinction coefficients for lycopene, anhydrorhodovibrin, and rhodopin in petroleum ether, and spirilloxanthin in benzene[34] were used in these calculations. Because the extinction coefficient of rhodovibrin was not available, the molar concentration of that molecule was determined by first calculating the specific absorption coefficient from anhydrorhodovibrin[34] which is a carotenoid with the same chromophore length, and then calculating the molar absorption coefficient using the method described previously.[35] Relative molar percentages were then determined by dividing the molar concentration of each carotenoid by the sum total of all the molar concentrations and multiplying by 100.

***Spectroscopic Methods***

All steady-state spectroscopic experiments were conducted at room temperature in a 1 cm path length quartz cuvette. Absorption spectra were recorded using a Varian Cary 50 UV-visible spectrophotometer. When necessary, the absorption spectra were converted to 1−T (where T is transmittance) spectra.

Fluorescence emission and excitation spectra were obtained using a Fluorolog-3 FL3-22 fluorimeter (Horiba Jobin Yvon) equipped with an Osram XBO 450 W xenon arc lamp, a Hamamatsu R928P PMT detector, and double excitation and emission monochromators having 1200 grooves/mm gratings. The fluorescence spectra were recorded using samples having an OD of 0.03 measured in a 1 cm cuvette at the maximum of the BChl *a* $Q_Y$ band. The spectra were recorded using excitation into the BChl *a* $Q_X$ band at 591 nm for the B800-850 and B800-840 complexes and 588 nm for the B800-820 complex. The slit widths of the emission and excitation monochromators were set to correspond to bandpasses of 6 and 12 nm, respectively. Fluorescence excitation spectra were recorded by monitoring the emission intensity at the wavelengths corresponding to the emission maxima which were 867 nm for the B800-850 complex, 858 nm for the B800-840 complex, and 830 nm for the B800-820 complex. For this experiment the slit widths of the emission and excitation monochromators corresponded to bandpasses of 12 and 6 nm, respectively for the B800-850 and B800-820 complexes, and 14 and 7 nm, respectively for the B800-840 complex.

Transient absorption (TA) spectra of the LH2 complexes in the visible region were recorded using the Helios (Ultrafast Systems LLC) TA spectrometer coupled to a femtosecond laser setup described previously.[36,37] The laser setup for recording the TA in

the near infrared (NIR) region is detailed in Niedzwiedzki et al.[22] LH2 samples with OD ~0.2–0.5 in a 2 mm path cuvette measured at the $\lambda_{max}$ in the carotenoid absorption region, were continuously stirred with a magnetic microstirrer to avoid photodegradation. For TA measurements in the visible region, the pump laser had 0.5 μJ/pulse energy focused on a 1 mm diameter spot which corresponds to a laser intensity of $1.6 \times 10^{14}$ and $1.7 \times 10^{14}$ photons/cm$^2$ for 490 and 540 nm excitation, respectively. The pump laser for recording the TA in the NIR region had 0.2 μJ/pulse energy which corresponds to $6 \times 10^{13}$ and $7 \times 10^{13}$ photons/cm$^2$ for 490 and 540 nm excitation, respectively. Steady-state absorption spectra of the samples were obtained before and after TA measurements to ensure sample integrity.

Dispersion correction of the TA spectra was carried out using Surface Xplorer Pro 1.2.2.26 (Ultrafast Systems LLC). Global analysis of the spectral and temporal datasets obtained from TA experiments was performed using ASUFit 3.0 software, provided by Dr. Evaldas Katilius of Arizona State University. The procedure for processing the ultrafast transient absorption data is given in Appendix A.

# Results

### *Pigment Composition*

The pigment extracts of the LH2 complexes of *Alc. vinosum* were found to contain five carotenoids, which eluted from the HPLC column in the order: lycopene, anhydrorhodovibrin, spirilloxanthin, rhodopin, and rhodovibrin (Figures 1 and 2). The relative molar percentages of the carotenoids in the three LH2 complexes are given in Table 1. Rhodopin and lycopene have 11 π-electron conjugated carbon-carbon double bonds, N (Figure 2). Therefore, they possess the same chromophore and have the same absorption spectrum (Figure 1). This is also the case for the carotenoids anhydrorhodovibrin and rhodovibrin (Figure 1), both of which have N=12 (Figure 2). Spirilloxanthin has N=13 (Figure 2). A direct comparison of the carotenoid composition (Table 1) of the THL30 and TLL30 LH2 complexes, which is based on the light intensity at which the cells were grown, reveals that under low-light growth conditions, the percentage of carotenoids with N=11 chromophores becomes smaller while the percentage of molecules having N=12 and 13 becomes larger. This observation was also reported in a previous investigation.[22]

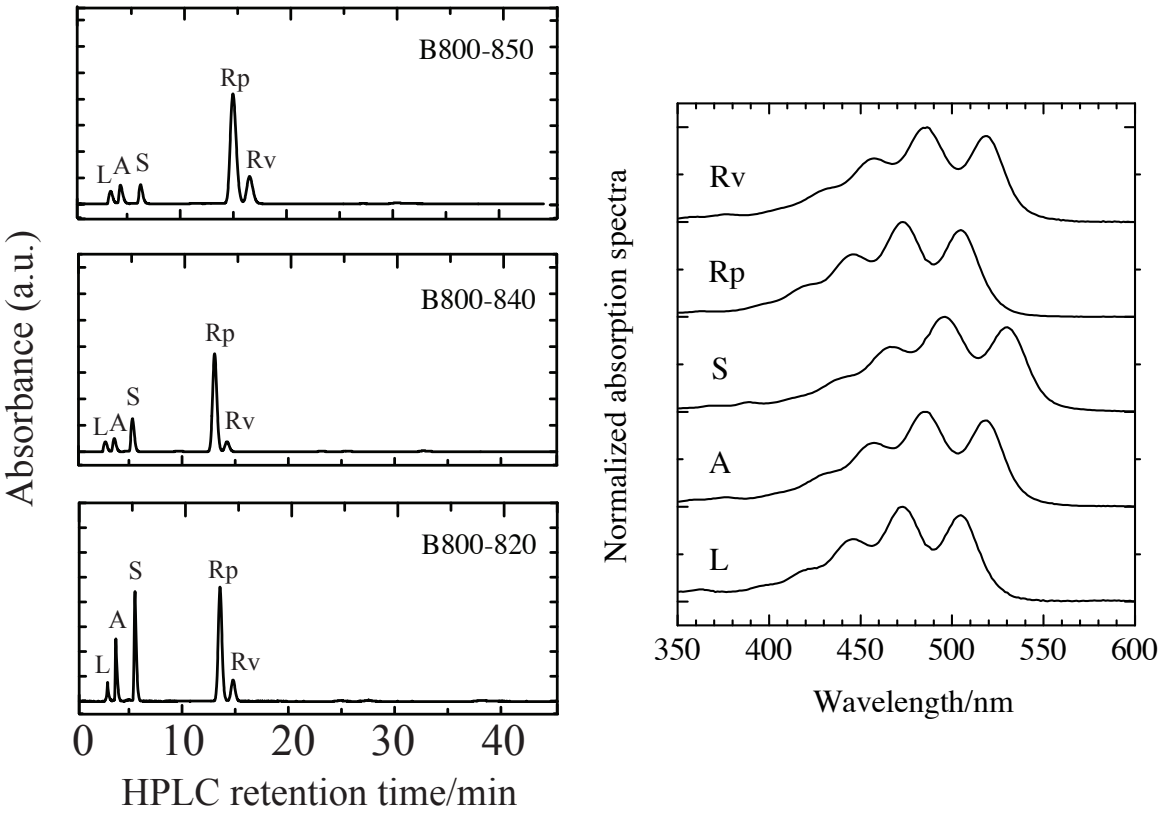


**Figure 1.** (Left) Normal phase (NP)-HPLC chromatograms of the carotenoid extracts from *Alc. vinosum* B800-850, B800-840 and B800-820 complexes. The detection wavelength was 500 nm. (Right) Absorption spectra of pigments measured by the HPLC-PDA detector. L= lycopene; A= anhydrorhodovibrin; S= spirilloxanthin; Rp= rhodopin; Rv= rhodovibrin.

**Table 1.** Relative molar percentages of the carotenoids determined by HPLC. The number of π-electron conjugated carbon-carbon double bonds, N, for each of the molecules is noted in parentheses. Also, the culture conditions as described in the text are given in parentheses below the type of LH2 complex.

| LH2 | lycopene (N=11) | rhodopin (N=11) | anhydro-rhodovibrin (N=12) | rhodovibrin (N=12) | spirillo-xanthin (N=13) |
|---|---|---|---|---|---|
| B800-850 (THL40) | 3.8 ± 0.4 | 59 ± 7 | 9 ± 1 | 22 ± 3 | 6.0 ± 0.7 |
| B800-840 (THL30) | 4.1 ± 0.5 | 62 ± 7 | 9 ± 1 | 11 ± 1 | 15 ± 2 |
| B800-820 (TLL30) | 2.3 ± 0.3 | 44 ± 5 | 17 ± 2 | 14 ± 2 | 23 ± 3 |

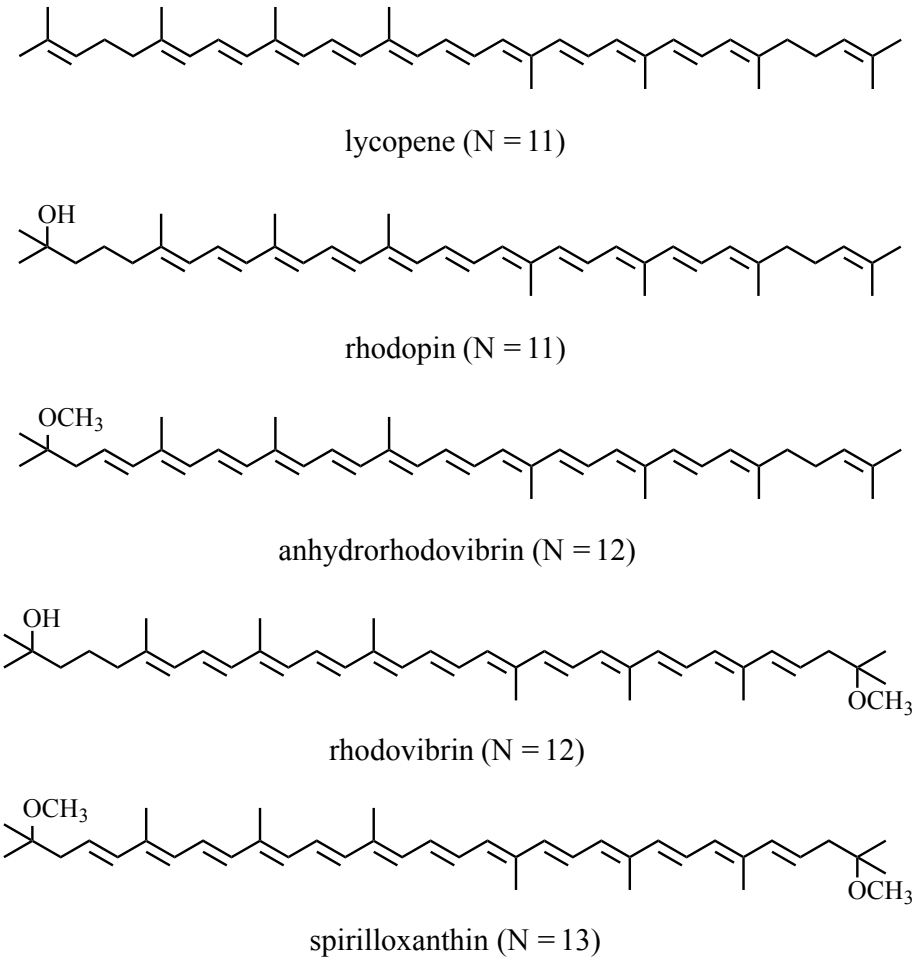


**Figure 2.** Structures of the carotenoids from the LH2 complexes of *Alc. vinosum*. The N values in parentheses indicate the number of conjugated C=C bonds.

***Steady-State Absorption and Fluorescence Spectroscopy***

Figure 3 shows emission spectra of the LH2 complexes along with a determination of the overall carotenoid-to-BChl energy transfer efficiencies which were obtained by overlaying the fluorescence excitation and 1−T spectra and adjusting the intensities of the spectra so that there was reasonable agreement in the BChl *a* Soret, $Q_X$ and $Q_Y$ band regions. Subsequently, the maximum intensity of the excitation spectrum in the carotenoid absorption region around 490 nm was divided by that of the 1−T spectrum and the resulting value was multiplied by 100 to obtain the overall carotenoid-to-BChl energy transfer efficiency. The values are given in the panels of Figure 3 and are 33% for the B800-840 LH2 and 38% for the B800-820 and B800-850 complexes.

Figure 4A shows the absorption spectra of the carotenoids isolated from the LH2 complexes of *Alc. vinosum* recorded after dissolving the molecules in benzyl alcohol. As expected, the spectra shift to longer wavelength as the length (N value) of the chromophore increases. Figure 4B overlays all of these spectral traces after shifting their $\lambda_{max}$ values to the same wavelength. The remarkable result is that the spectra exhibit virtually identical lineshapes despite the molecules having different N values. Figure 4C shows the spectrum of rhodopin recorded in the solvents, methanol, *n*-hexane, acetone, dimethyl sulfoxide (DMSO), benzyl alcohol and carbon disulfide ($CS_2$), which have different polarities and polarizabilities. Figure 4D shows that these spectral lineshapes are also very similar, with those recorded in the more polarizable solvents, DMSO, benzyl alcohol and $CS_2$ being only slightly broader.

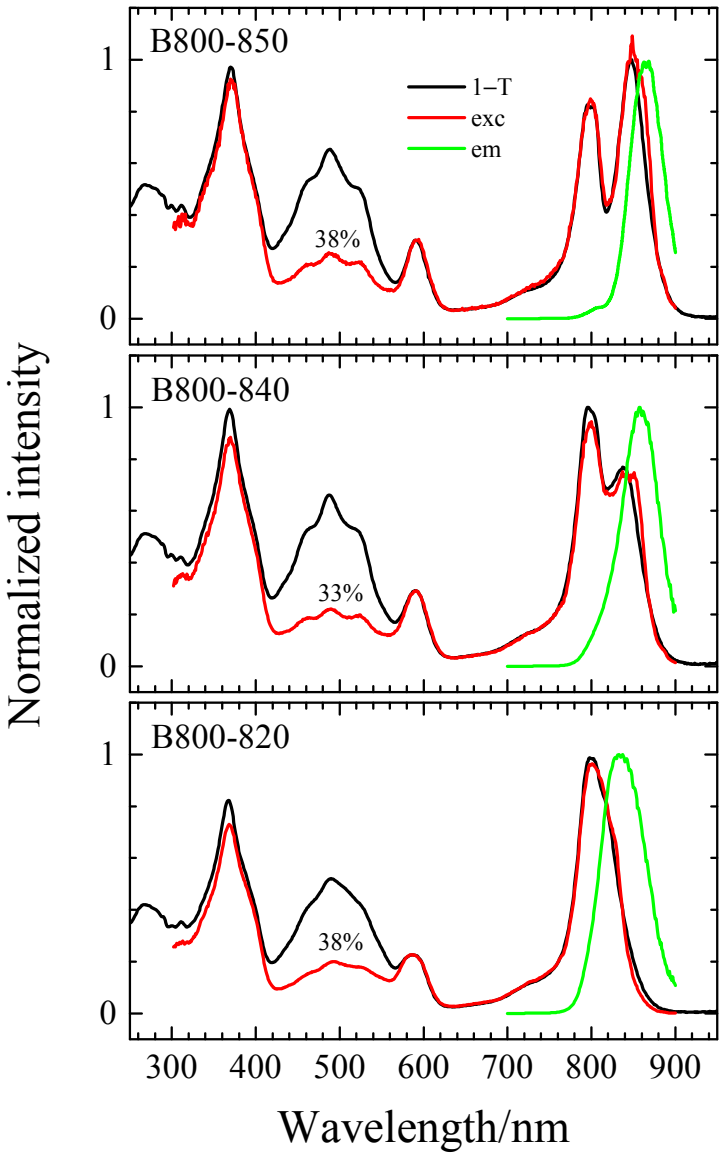


**Figure 3.** 1−T (black trace), fluorescence excitation (red trace) and emission (green trace) spectra of the B800-850 (top), B800-840 (middle) and B800-820 (bottom) LH2 complexes from *Alc. vinosum*. The percentages represent the carotenoid-to-BChl energy transfer efficiency obtained by normalizing the fluorescence excitation and 1−T spectra at the various BChl *a* bands as well as could be done, and then dividing the maximum intensity of the fluorescence excitation spectrum by that of the 1−T spectrum in the carotenoid absorption region, and multiplying by 100.

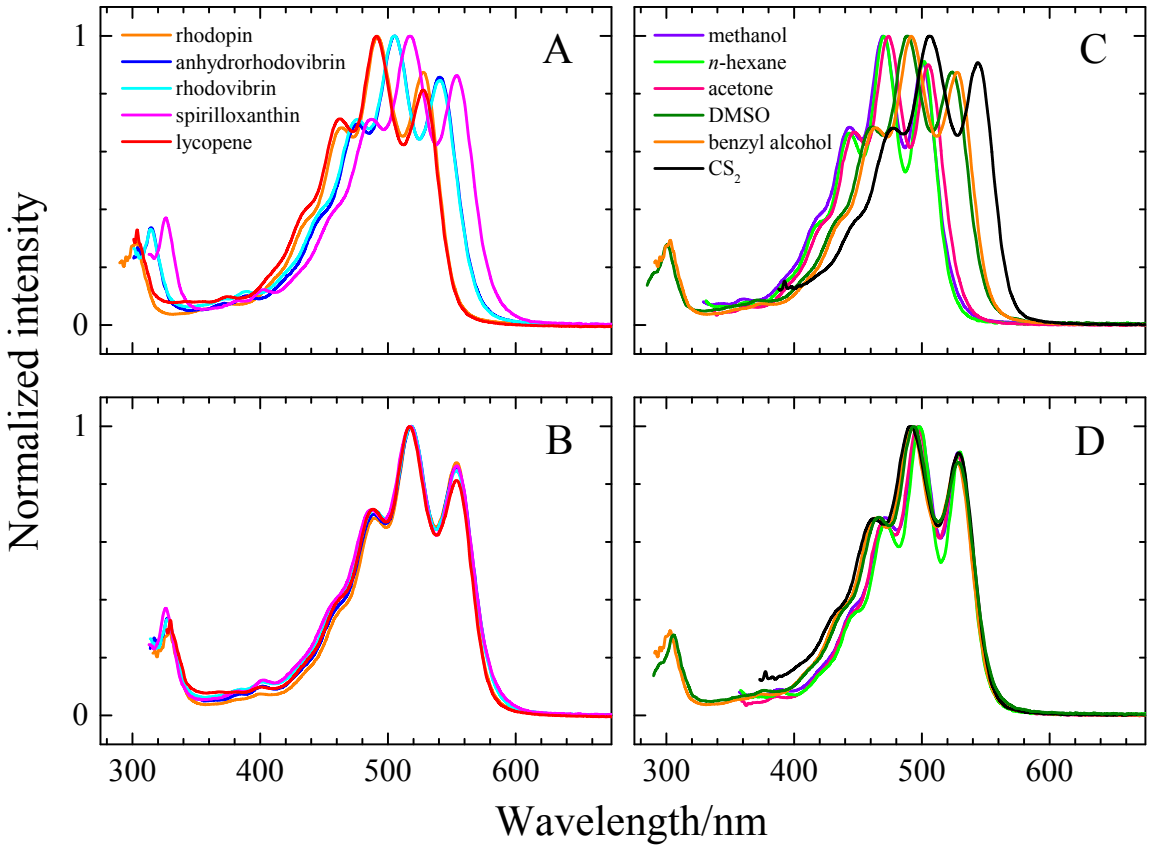


**Figure 4.** Room temperature absorption spectra of: (A) the carotenoids from *Alc. vinosum* recorded in benzyl alcohol. The spectra were normalized to the intensity at their $\lambda_{max}$ values; (B) The spectra from (A) shifted in wavelength to the same $\lambda_{max}$ value and overlaid; (C) Absorption spectra of rhodopin recorded in solvents having different polarities and polarizabilities; and (D) rhodopin spectra from (C) shifted and overlaid as was done in (B). The spectra in (B) and (D) demonstrate that similar lineshapes are obtained from the carotenoids regardless of differences in the value of N or in the solvent in which they are dissolved.

Given that the shapes of the carotenoid absorption spectra are not very sensitive to either the π-electron conjugation length or the solvent in which they are dissolved, it is possible then to use either the lineshapes of each of the individual carotenoids, or that of only one of them, to reconstruct the overall absorption (or 1−T) and fluorescence excitation spectra of the LH2 complexes. Figure 5 shows the reconstructed 1−T (left column) and fluorescence excitation (right column) spectra of the three LH2 complexes obtained by summing multiple traces of the absorption spectrum of rhodopin recorded in benzyl alcohol, which is a solvent in which the absorption spectra of carotenoids bound to the LH2 complex are well-reproduced.[38] In order to generate the overall spectral lineshapes of the LH2 complexes, the component spectra were adjusted in wavelength and intensity, while keeping the intensities of the components consistent with the carotenoid composition determined by HPLC. At least four individual carotenoid 1−T spectral traces were needed to be summed to achieve reasonable agreement between the computed spectral lineshapes and the features of the experimental LH2 spectra in the carotenoid absorption region. For simplicity, the BChl *a* absorption bands were treated as Gaussian functions. After acceptable reconstructions of the 1−T spectra were obtained, the wavelength positions of the individual carotenoid component spectra were kept constant, and only the intensities of the spectra were varied until reasonable reconstructed fluorescence excitation spectra were obtained. These were then compared with the 1−T spectra to generate the carotenoid-to-BChl energy transfer efficiencies for each of the carotenoid chromophores. The wavelength and intensity parameters, as well as the individual carotenoid-to-BChl energy transfer efficiencies revealed by this analysis are given in Table 2.

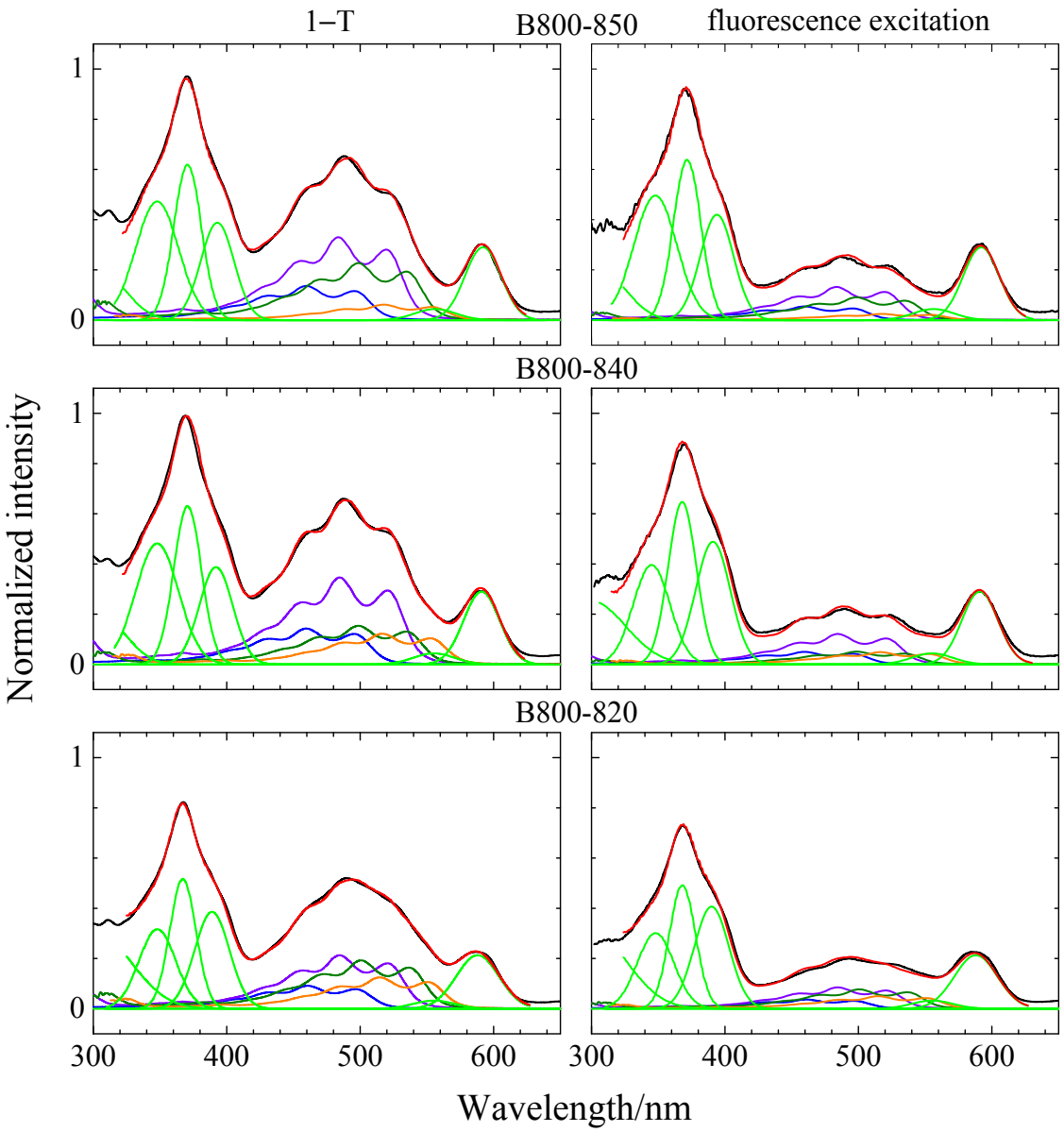


**Figure 5.** Reconstruction of the experimental 1−T (left panels) and fluorescence excitation (right panels) spectra (black traces) of the B800-850 (top), B800-840 (middle) and B800-820 (bottom) LH2 complexes from *Alc. vinosum*. Four individual traces of the 1−T spectrum of rhodopin recorded in benzyl alcohol were summed to obtain the reconstructed spectra (red traces). The Soret region between 300–400 nm and the (0–0) and (0–1) vibronic bands of the $Q_X$ transition were modeled using simple Gaussian functions (green traces).

**Table 2.** Parameters used in the reconstruction of the 1−T and fluorescence excitation spectra shown in Figure 5. Uncertainties in the excitation energy transfer (EET) efficiencies are on the order of 10% based on the range of intensities of 1−T spectral components that generated lineshapes in reasonable agreement with the experimental spectra.

| LH2 | Carotenoid component | 1−T Spectral origin (nm) | Relative 1−T intensity (%) | EET efficiency (%) |
|---|---|---|---|---|
| B800-850 | 1 | 495 | 18 | 40 |
| | 2 | 519 | 44 | 40 |
| | 3 | 534 | 30 | 40 |
| | 4 | 553 | 8 | 40 |
| B800-840 | 1 | 495 | 19 | 35 |
| | 2 | 520 | 45 | 35 |
| | 3 | 534 | 20 | 33 |
| | 4 | 552 | 16 | 40 |
| B800-820 | 1 | 496 | 15 | 40 |
| | 2 | 520 | 34 | 40 |
| | 3 | 536 | 31 | 40 |
| | 4 | 550 | 20 | 40 |

***Transient Absorption (TA) Spectroscopy***

The three different LH2 complexes were excited in the region of carotenoid absorption at either 490 nm or 540 nm and TA spectra were recorded in the visible and NIR regions at different delay times after the pump laser pulse (Figure 6). All of the TA profiles recorded in the visible region revealed an instantaneous onset of bleaching of the carotenoid ground state spectrum accompanied by the buildup of a small broad positive excited state absorption (ESA) at ~600 nm (black dashed traces in Figure 6). Also instantaneously appearing was a strong negative (bleaching) signal in the NIR region which is the result of ultrafast energy transfer from carotenoids to the B850, B840 or B820 BChl *a* depending on the LH2 complex. The position of this negative band shifted to longer wavelength at later times suggestive of equilibration of excitonic energy among the spectrally heterogeneous BChls.[32] The B850 LH2 complex also displayed a prominent positive band at ~825 nm (top NIR panels in Figure 6) which represents an $S_1 \rightarrow S_n$ ESA transition of BChl *a*, where n indexes the position of a high excited singlet state.

At 500 fs, the carotenoid ground state bleaching signal decreased in intensity due to energy transfer to BChl *a*, evidenced by additional bleaching of the B850, B840 or B820 NIR BChl *a* absorption bands and the negative peak at 800 nm indicating some energy transfer to the B800 BChl *a*. The broad ESA signal in the visible region tails out beyond 650 nm and contains two noticeable peaks at 581 nm and 605 nm (solid black traces in Figure 6). These two peaks are very likely $S_1 \rightarrow S_n$ ESA transitions belonging to carotenoid molecules having different extents of π-electron conjugation; *i.e.* N values, because the relative intensity of these bands depends on the excitation wavelength

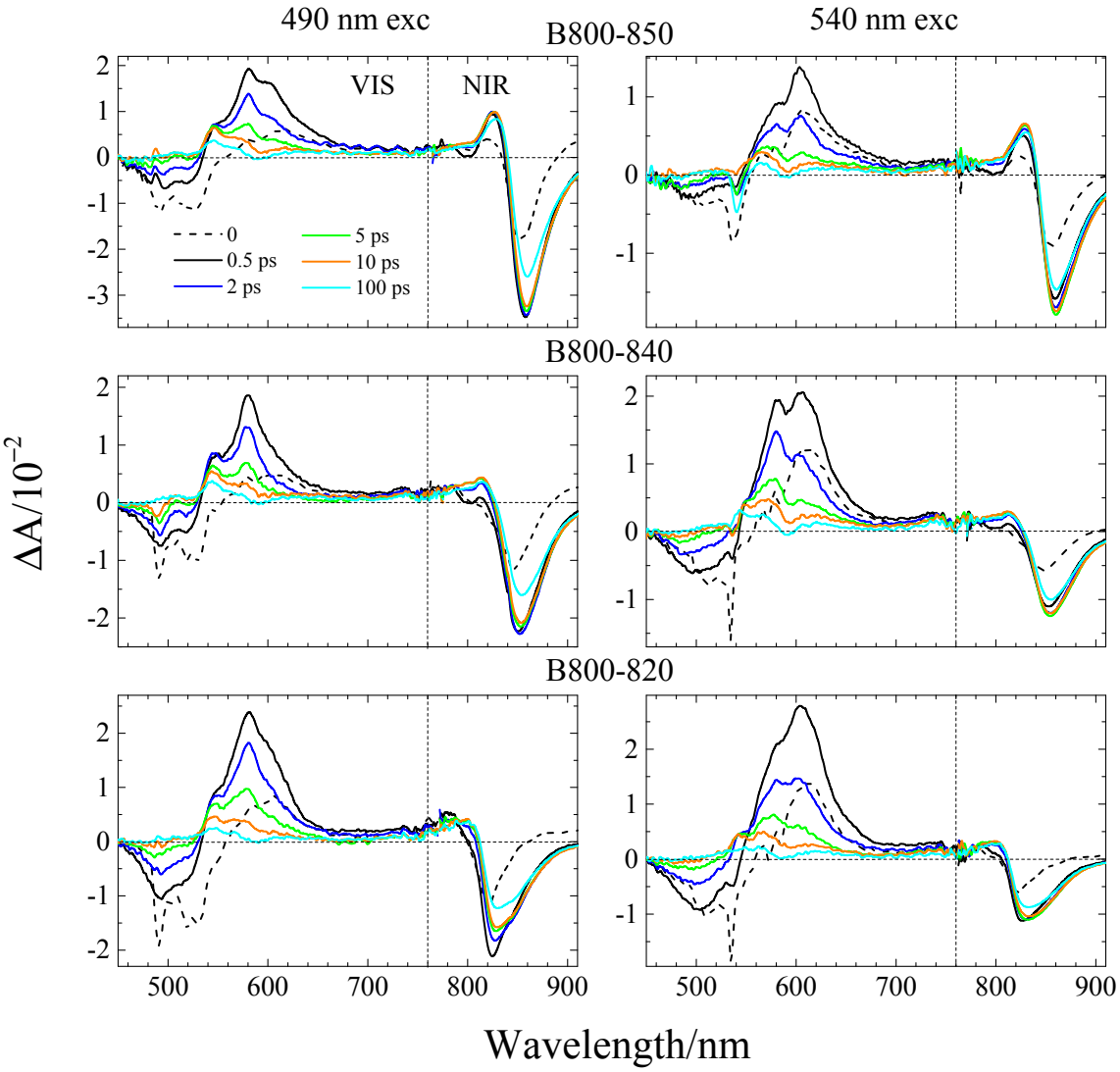


**Figure 6.** Transient absorption spectra of the B800-850 (top), B800-840 (middle) and B800-820 (bottom) LH2 complexes recorded at different time delays after excitation at the indicated wavelengths.

(compare the left and right column panels in Figure 6). If 490 nm excitation is used (left panels in Figure 6), the 581 nm band is largest. Based on room-temperature ultrafast spectra of rhodopin glucoside (N=11) dissolved in benzyl alcohol,[29] which, as mentioned above, is a solvent in which the absorption spectra of carotenoids bound to the LH2 complex are well-reproduced,[38] the 581 nm band can be assigned to an N=11 carotenoid, which in this case is rhodopin, because that carotenoid is present in large excess compared to the other N=11 chromophore, lycopene, found in the complexes (Table 1 and Figure 2). When 540 nm excitation is used (right panels in Figure 6), the 605 nm band is dominant. Based on the red-shift expected when the N value of an open-chain carotenoid is increased by one,[39,40] the 605 nm feature can be assigned to an N=12 carotenoid, which in the present case would be a combination of rhodovibrin and anhydrorhodovibrin, both of which are present in substantial amounts in these complexes (Table 1 and Figure 2). This assignment is further supported by considering the relative ESA peak intensities in the context of the carotenoid composition analysis done by HPLC and given in Table 1. Note that when 540 nm excitation is used (right hand column panels in Figure 6), the relative intensity of the 605 nm peak is significantly larger than the 581 nm peak for the B800-850 and B800-820 complexes, but not for the B800-840 complex where the two peaks are comparable in intensity. This is consistent with the carotenoid composition of the complexes which revealed that the total percentage of the N=12 carotenoid chromophores, rhodovibrin and anhydrorhodovibrin, is 31% for both the B800-850 and B800-820 complexes, but only 20% for the B800-840 complex.

In the TA spectral profiles taken in the visible region at 2 ps (blue traces in the panels labeled VIS in Figure 6), the preceding broad ESA signal (solid black traces in the

panels labeled VIS Figure 6) narrows slightly, and the ground state bleaching in the carotenoid region as well as the positive ESA features at 581 nm and 605 nm, decrease in intensity, but at this time delay the 605 nm feature is decreased more compared to the 581 nm feature. This is undoubtedly because the longer (N=12) carotenoids associated with the 605 nm ESA band have a shorter $S_1$ lifetime than the N=11 carotenoids associated with the 581 nm band, and hence the N=12 chromophores return to the ground state at a faster rate. However, only a very small amount of additional BChl *a* bleaching is built up in the NIR region, and this can be attributed to energy transfer from the 800 nm-absorbing BChl *a* whose band bleaching has disappeared at 2 ps. So, the decrease in the carotenoid ground state bleaching signal and in the intensities attributable to carotenoid $S_1 \rightarrow S_n$ ESA transitions are due solely to the direct decay of the carotenoid chromophores back to the ground state. Also, in the TA spectral profiles recorded in the visible region at 2 ps, a small positive signal appears at 543 nm with an even smaller one at 568 nm; e.g. See the 2 ps (blue) trace for the B800-840 LH2 complex (490 nm excitation, middle left panel of Figure 6). These signals persist well beyond 100 ps (light blue traces in Figure 6). Thus, they are very likely due to carotenoid triplet-triplet absorption. Carotenoid triplet states are readily formed in antenna complexes by triplet energy transfer from BChl *a*.[33,41-44] On the basis of triplet-triplet absorption spectra previously recorded in LH1 and LH2 complexes.[43,44] the signals at 543 nm and 568 nm can be assigned to rhodopin (N=11), and rhodovibrin plus anhydrorhodovibrin (N=12), respectively. These are the most abundant carotenoids in these LH2 complexes and therefore are expected to produce the strongest triplet absorption signals.

***Global Analysis of Transient Absorption Data***

Due to the large number of carotenoid molecules bound in these complexes and the spectral heterogeneity they exhibit, the TA datasets were globally fit using a procedure employing a multi-exponential function, $S(\lambda, t) = \sum_i IRF \oplus A_i(\lambda) exp(-t/\tau_i)$, where IRF is the instrument response function and $\oplus$ symbolizes convolution. $A_i(\lambda)$ is the pre-exponential amplitude factor associated with the kinetic component *i* having a lifetime $\tau_i$ from which the rate constants for the buildup and decay of the excited states of the chromophores in the LH2 complexes can be obtained from $k_i = 1/\tau_i$. This model, based on a sum of exponential terms, represents the dynamics of parallel, non-interacting kinetic components. The amplitude factors, $A_i(\lambda)$, resulting from fitting the data to such a model are termed Decay-Associated Difference Spectra (DADS).[45,46] Alternatively, the spectral and temporal datasets can be fit assuming a sequential process for the deactivation of the carotenoid excited states, in which case the resulting lineshapes are termed Evolution-Associated Decay Spectra (EADS).[46] Both the DADS and EADS models yield the same component lifetimes but different spectral lineshapes. Because the excited states of the pigments in the LH2 complexes from *Alc. vinosum* follow intricate energy transfer pathways involving five carotenoids representing three spectrally heterogeneous chromophores having N=11, 12 and 13 that cannot be excited by the pump laser independently, EADS lineshapes representing a sequential process would not be very informative. DADS profiles (Figure 7) show simply the wavelength dependence of the pre-exponential factors of the kinetic terms, so they are not biased by the application of any model associated with sequential or branching energy transfer pathways. DADS generally have positive amplitudes when there is a decay of an ESA or buildup of an

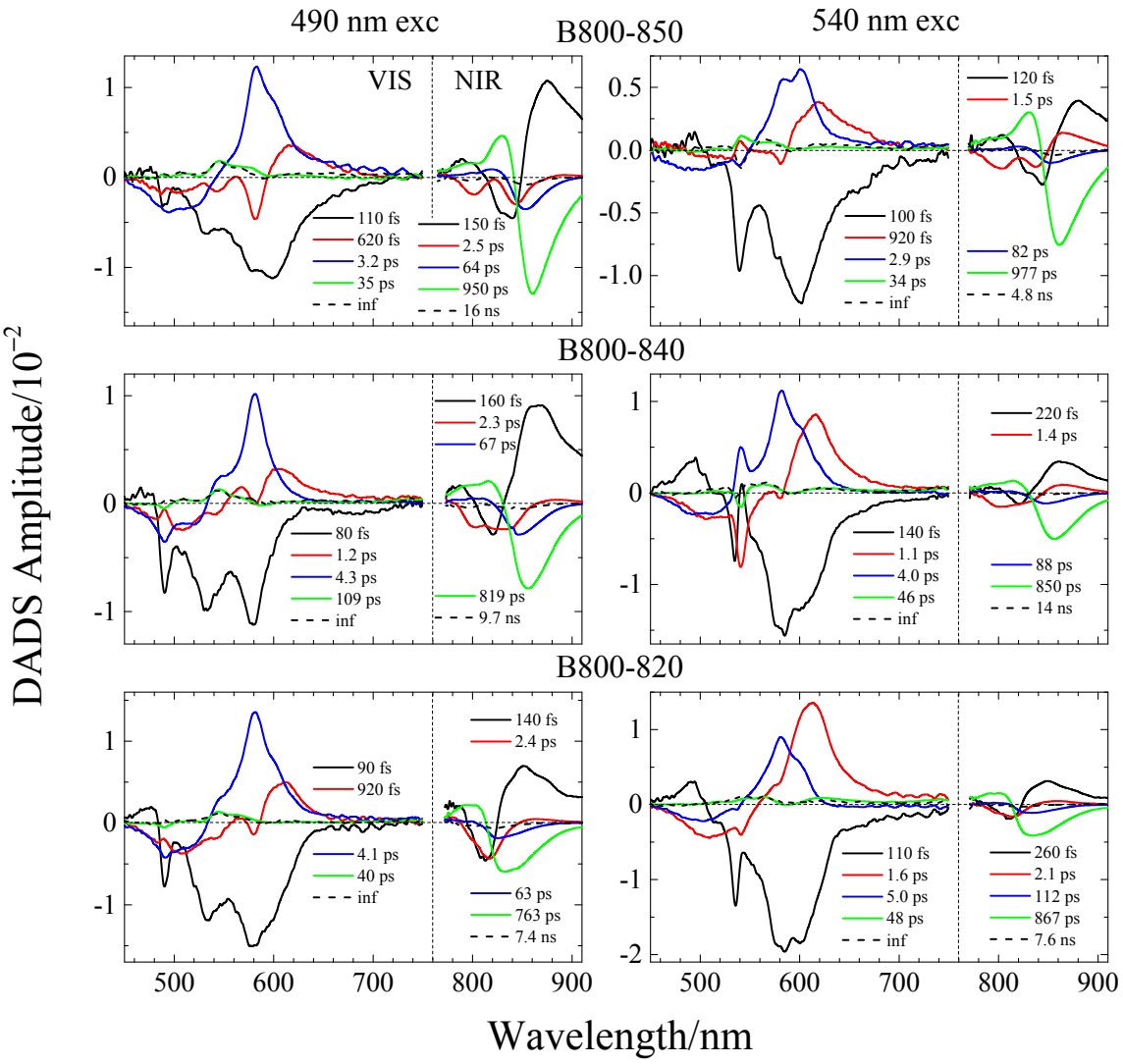


**Figure 7.** Decay associated difference spectra (DADS) of the B800-850 (top), B800-840 (middle) and B800-820 (bottom) LH2 complexes obtained from the global fits to the data shown in Figure 6.

absorption band bleaching, and negative amplitudes for a buildup of an ESA or the decay of a band bleaching. Because many readers may be more familiar with EADS lineshapes, these are given in Figure 8. Also, because the spectral and temporal data in the visible and NIR regions were recorded using different spectrometers, the global fitting analysis of these two datasets was done separately (Figures 7 and 8).

For all three types of LH2 complexes, five kinetic components were needed to achieve satisfactory global fits of the spectral and temporal datasets recorded in the visible and NIR ranges (Figures 7 and 8). The goodness of fits was evaluated based on a chi square ($\chi^2$) test and a minimization of their residual matrices. The experimental time-resolved build-up and decay profiles of the TA signals were also overlaid with the computed fits obtained at various individual wavelengths. Figure 9 demonstrates that there is good agreement between the experimental observations and the theoretical fits at various individual wavelengths which further attests to the validity of the kinetic analysis.

Global fitting of the datasets from all the LH2 complexes, regardless of excitation wavelength, revealed an initial DADS in the visible region (solid black traces in the panels labeled VIS in Figure 7) that is characterized by broad negative amplitude between ~500 nm and ~700 nm which occurs within the time range 80 fs and 140 fs, which is comparable to the time response of the laser spectrometer. Various negative features found in this first DADS correspond to the decay of a portion of the carotenoid ground state spectral bleaching, the decay of stimulated fluorescence and Raman bands, and the build-up of $S_1 \rightarrow S_n$ ESA transitions belonging to the carotenoids. Thus, this first DADS can be associated with the lifetime of the $S_2$ state of the carotenoids which decays either by internal conversion to the $S_1$ state or by direct energy transfer to BChl *a*.[47,48]

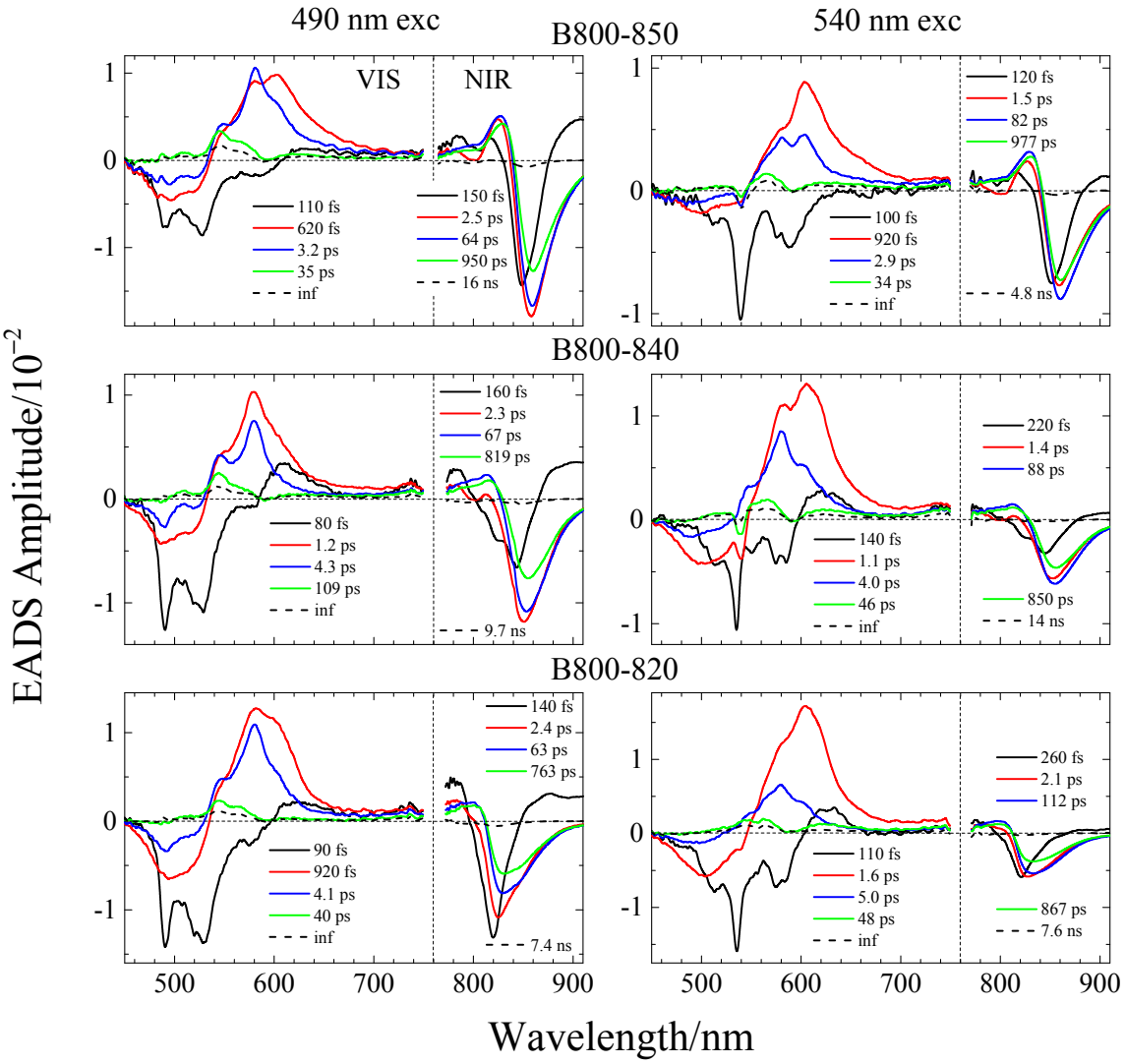


**Figure 8.** Evolution associated difference spectra (EADS) of the B800-850 (top), B800-840 (middle) and B800-820 (bottom) LH2 complexes obtained from the global fits to the data shown in Figure 6.

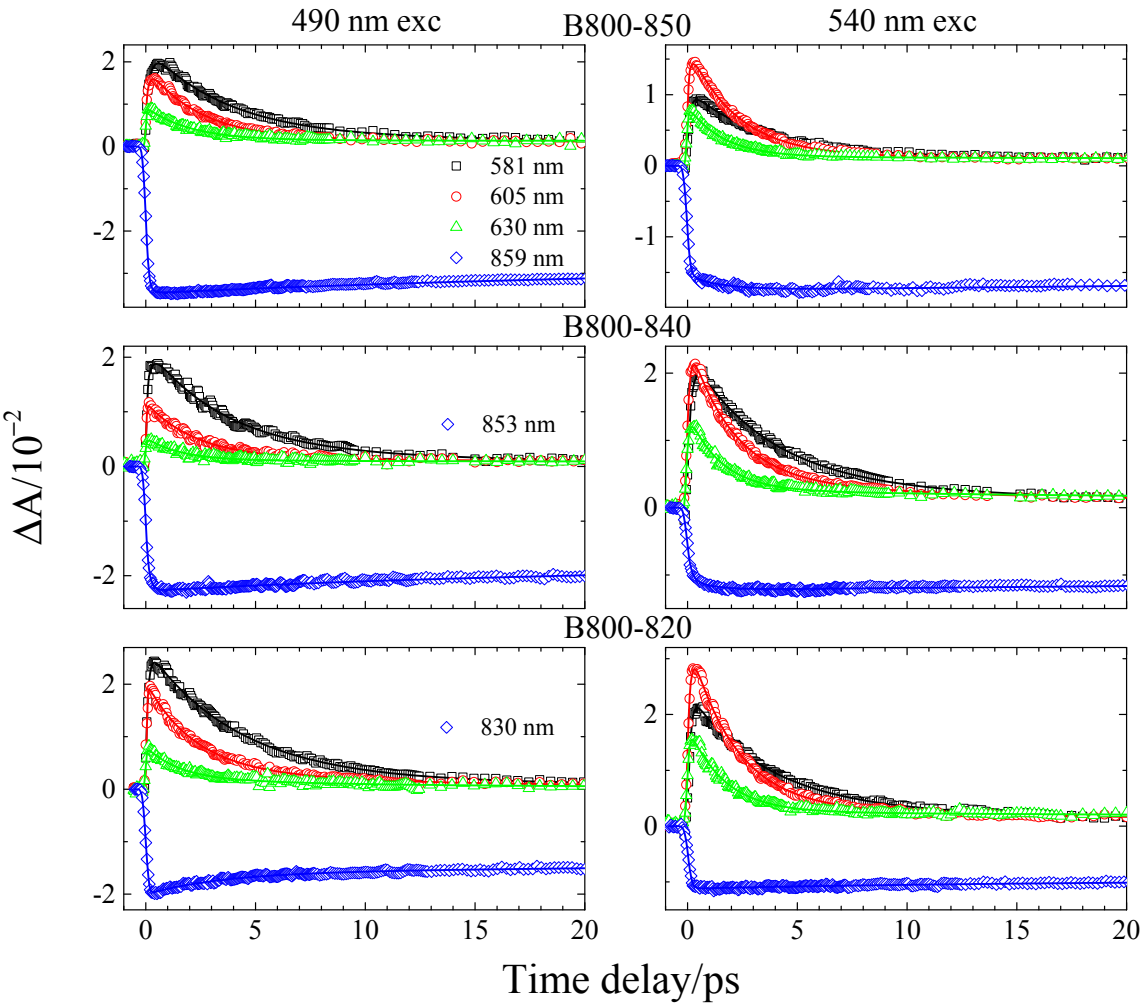


**Figure 9.** Kinetic traces (symbols) and fits (lines) of the B800-850 (top), B800-840 (middle) and B800-820 (bottom) TA obtained from single wavelength fitting of the TA datasets at the indicated wavelengths.

**Table 3.** Dynamics of the excited states of the pigments bound in the LH2 complexes from *Alc. vinosum* obtained from single wavelength fitting of the TA datasets as shown in Figure 9. $a_i$ where $i$=1–4, is the preexponential amplitude of the $i^{th}$ kinetic component; inf = infinite lifetime.

| LH2 complex | Exc λ/nm | Probe/nm | $\tau_1$/ ps | $a_1$ | $\tau_2$/ ps | $a_2$ | $\tau_3$/ ps | $a_3$ | $\tau_4$/ ps | $a_4$ |
|---|---|---|---|---|---|---|---|---|---|---|
| B800-850 | 490 | 581 | 0.20[a] | −0.410 | 3.7 | 0.531 | 26 | 0.043 | inf | 0.016 |
| | | 605 | 0.14 | −0.346 | 2.4 | 0.591 | 33 | 0.051 | inf | 0.012 |
| | | 630 | 0.10[a] | −0.067 | 2.0 | 0.789 | 151 | 0.081 | inf | 0.063 |
| | | 859 | 0.15[a] | 0.176 | 23 | −0.106 | 351 | −0.263 | 1443 | −0.455 |
| | 540 | 581 | 0.14[a] | −0.439 | 3.3 | 0.485 | 36 | 0.047 | inf | 0.029 |
| | | 605 | 0.14[a] | −0.279 | 2.2 | 0.664 | 48 | 0.033 | inf | 0.023 |
| | | 630 | 0.12[a] | −0.104 | 1.6 | 0.766 | 89 | 0.086 | inf | 0.043 |
| | | 859 | 0.12[a] | 0.198 | 1.5[a] | 0.090 | 139 | −0.109 | 1117 | −0.603 |
| B800-840 | 490 | 581 | 0.20[a] | −0.282 | 3.4 | 0.601 | 12 | 0.099 | inf | 0.018 |
| | | 605 | 0.10[a] | −0.031 | 2.3 | 0.849 | 28 | 0.067 | inf | 0.053 |
| | | 630 | 0.12[a] | −0.111 | 1.6 | 0.710 | 54 | 0.081 | inf | 0.098 |
| | | 853 | 0.15[a] | 0.338 | 14 | −0.075 | 201 | −0.213 | 1176 | −0.373 |
| | 540 | 581 | 0.17 | −0.432 | 3.4 | 0.449 | 11 | 0.100 | inf | 0.019 |
| | | 605 | 0.12[a] | −0.460 | 2.0 | 0.449 | 11 | 0.072 | inf | 0.018 |
| | | 630 | 0.10[a] | −0.522 | 1.5 | 0.394 | 26 | 0.051 | inf | 0.033 |
| | | 853 | 0.17[a] | 0.289 | 1.0[a] | 0.093 | 129 | −0.144 | 983 | −0.474 |
| B800-820 | 490 | 581 | 0.11[a] | −0.584 | 4.2 | 0.388 | 18 | 0.018 | inf | 0.010 |
| | | 605 | 0.10[a] | −0.034 | 2.1 | 0.730 | 7.2[a] | 0.206 | inf | 0.029 |
| | | 630 | 0.10[a] | −0.105 | 1.5 | 0.656 | 8.6[a] | 0.195 | inf | 0.044 |
| | | 830 | 0.05[a] | 0.020 | 3.5 | −0.203 | 152 | −0.265 | 1112 | −0.512 |
| | 540 | 581 | 0.12[a] | −0.518 | 3.1 | 0.356 | 9.5 | 0.109 | inf | 0.017 |
| | | 605 | 0.13 | −0.520 | 2.1 | 0.431 | 18 | 0.039 | inf | 0.010 |
| | | 630 | 0.12[a] | −0.187 | 1.6 | 0.701 | 54 | 0.068 | inf | 0.045 |
| | | 830 | 0.10[a] | 0.392 | 11 | −0.044 | 239 | −0.186 | 1156 | −0.378 |

[a]fixed parameter

This latter process is evidenced by the finding that in this same time domain, the initial DADS obtained from a fit to the datasets recorded in the NIR region (black traces in panels labeled NIR in Figure 7) show positive amplitude at ~860 nm, ~840 nm or ~820 nm depending on the LH2 complex, and negative amplitude at slightly shorter wavelengths. The positive feature represents the build-up of the bleaching of the BChl *a* $Q_Y$ band that results from ultrafast energy transfer from the $S_2$ state of the carotenoid. The negative amplitude part of this component in the NIR corresponds to the build-up of an $S_1 \rightarrow S_n$ ESA band of BChl *a*.

The second DADS obtained from the fits to the visible datasets (red traces in the panels labeled VIS in Figure 7) has a complex, multi-featured lineshape that includes a broad positive profile at long wavelengths, a zero crossing, and negative amplitude at short wavelengths that extends throughout the region corresponding to the ground state spectral bleaching. The lifetime of this second DADS falls within the range of 620 fs to 1.6 ps. The long wavelength positive part of this DADS most likely represents a combination of the decay of the $S_1$ state of the longer (N=12, 13) carotenoids either by internal conversion to the ground state or by energy transfer to BChl *a*, which as mentioned above, is clearly evident in the DADS components in the NIR range. The short wavelength part of the second DADS in the visible region shows a prominent downward peak at ~580 nm that clearly can be attributed to the build-up of the $S_1 \rightarrow S_n$ absorption band of the shorter (N=11) carotenoid, rhodopin.

The third DADS in the visible region (blue trace in the panels labeled VIS in Figure 7) shows very familiar characteristic strong ESA features associated with carotenoid $S_1 \rightarrow S_n$ transitions and has a lifetime ranging from 2.9 ps to 5.0 ps. Because

the TA spectra in Figure 6 indicate that no additional BChl *a* band bleaching occurs after 500 fs, the lifetime of the third DADS must be associated with the direct decay of the carotenoids back to the ground state by internal conversion. The shape of the strong positive visible band in this third DADS contains features that can be attributed to N=11 (rhodopin) and N=12 (rhodovibrin or anhydrorhodovibrin) carotenoid chromophores which are known from previous work[39,40] to have room temperature $S_1$ lifetimes of ~4.3 ps (N=11) and ~2.2 ps (N=12) which are within the experimental error of the lifetimes obtained from the present kinetic analysis.

The fourth and fifth DADS components in the visible region (green and black dashed traces in the panels labeled VIS in Figure 7) have lifetimes of between 34 ps and 109 ps for the fourth component, and infinitely long (on the time scale allowed by the spectrometer) for the fifth component. These two DADS have very similar, albeit very small, amplitude profiles, the most noticeable features of which are peaks at 543 nm and 568 nm, which as mentioned above, most likely arise from triplet-triplet absorption of a carotenoid. The two kinetic components suggest that there may be two avenues of carotenoid triplet state decay, possibly triplet-triplet annihilation due to close proximity of the carotenoid and BChl *a* chromophores[49] as well as the standard decay route of carotenoid triplet state radiationless intersystem crossing, but this remains to be verified.

In the NIR, the initial DADS decays in 120 fs to 260 fs and corresponds to the time constant for the arrival of excited state energy from the $S_2$ state of the carotenoids. The strong positive amplitude at ~850 nm, ~840 nm or ~820 nm, depending on the LH2 complex, indicates the onset of bleaching of the $Q_Y$ band of BChl *a* brought about by energy transfer from the carotenoids, and the negative band at shorter wavelength, most

noticeable at ~825 nm for the B800-850 complex (solid black trace in the top NIR panels in Figure 7) represents the buildup of an $S_1 \rightarrow S_n$ ESA transition of BChl *a*. These initial DADS decay into a second component (red traces in the panels labeled NIR in Figure 7) that has a lifetime of 1.4 ps to 2.5 ps and exhibits two negative peaks, one at ~800 nm and another at slightly longer wavelength. The negative feature at 800 nm in this second DADS represents the disappearance of the B800 $Q_Y$ band bleaching as this BChl *a* gives up its excited state energy to the 820 nm, 840 nm or 850 nm-absorbing BChl *a*, depending on the LH2 complex. The longer wavelength negative peak in this second DADS which represents the decay of a bleaching signal may be associated with exciton annihilation.[22,50-52] Evidence for this is seen in the kinetic traces monitored at the peak of the BChl *a* band bleaching in the NIR; *e.g.* see the kinetic trace for the B800-820 LH2 complex (blue diamond trace in the bottom left panel of Figure 9) where the downward bleaching signal is seen to partially recover in a few picoseconds. Singlet state annihilation would diminish the BChl *a* band bleaching in this time domain, whereas the normal internal conversion route of decay of the lowest excited singlet state of BChl *a* back to the ground state would occur on a much slower, nanosecond time scale which is also evident in Figure 9.

The second DADS in the NIR decays into a third DADS component (blue traces in the panels labeled NIR in Figure 7) that is red-shifted and has a lifetime ranging from 63 ps to 112 ps. The fact that this third DADS decays into a fourth DADS (green traces in the panels labeled NIR in Figure 7) that has negative amplitude even more red-shifted, suggests, as mentioned above, that this may be due to spectral equilibration of excitonic energy among the long wavelength absorbing BChls.[32] The fourth DADS obtained from

the fits to the datasets in the NIR region, in all cases, tracks precisely the inverse of the initial NIR DADS profile and therefore can be assigned to the decay of the lowest excited singlet state of the long wavelength-absorbing B850, B840 or B820 BChl *a* depending on the LH2 complex, by internal conversion to the ground state in a time of ~1 ns. Finally, the longest time DADS component obtained from global fitting the NIR datasets profiles for BChl *a* (black dashed traces in the panels labeled NIR in Figure 7) exhibits a very small DADS amplitude and most likely represents the decay of the lowest excited triplet state of BChl *a* as it is being quenched by a carotenoid. The 4.8 ns to 16 ns range of lifetimes found here for this component is well within that expected for an effective BChl *a* triplet lifetime in LH2 complexes which may involve not only BChl-to-carotenoid triplet energy transfer, but also potentially oxygen quenching and triplet-triplet annihilation.[41,49]

# Discussion

### *Spectral Heterogeneity*

The fact that at least four different carotenoid spectral traces positioned at different wavelengths and having different intensities were needed to achieve reasonable reconstructions of the absorption (1−T) spectra of the LH2 complexes, indicates that there exists substantial heterogeneity in the binding environment of the carotenoid molecules in the LH2 apoproteins. This is completely different from the much more homogeneous spectral forms associated with the carotenoid spectra in LH2 complexes from *Rb. sphaeroides* and *Rbl. acidophilus.*[29,53,54] Previous research on the origin of the splitting in the B800 absorption peak in some LH2 complexes from *Alc. vinosum*[23] may provide a clue to the source of the spectral heterogeneity in the carotenoid region. The investigation by these authors showed on the basis of CD and polarization-resolved single-molecule spectroscopic experiments that the LH2 pigment-protein complexes from *Alc. vinosum* contain a ring-like oligomer of 12 repeat units wherein the B800 BChl *a* molecules are dimerized. The researchers argued that heterogeneity in the 800 nm absorption band then arises due to variable interactions with different forms of the α and β apoproteins that alternate around the ring. Multiple forms of the α and β polypeptides were also revealed in a previous detailed characterization by HPLC and TOF/MS of the B800-820, B800-840 and B800-850 complexes from *Alc. vinosum.*[18] These studies demonstrated that all of LH2 pigment-protein complexes from this bacterium possess a heterogeneous polypeptide composition that differs depending on the type of complex. Because the absorption spectra of carotenoids are dependent on the polarity and polarizability of their surrounding environment, different amino acid sequences of the

polypeptides to which they are bound may lead to different spectral forms of the molecules. Assigning each of the four different carotenoid spectral forms required for reconstructing the experimental absorption (1−T) spectra as shown in Figure 5, to one of the five different carotenoid molecules bound in these complexes, can for the most part be accomplished by a consideration of the N values of the carotenoids and their composition in the protein as determined by HPLC. Thus, the longest wavelength-absorbing carotenoid component having a spectral origin between 550 nm and 553 nm (Table 2) is assigned to spirilloxanthin which has N=13. This is not only because the absorption spectrum of this long chromophore is expected to be more red-shifted than those of the other bound carotenoids, but also because the intensity of this spectral component that best reproduced the overall experimental 1−T spectra of the LH2 complexes (Figure 5) correlates well with the amount of spirilloxanthin revealed by the HPLC analysis (Table 1). Note that a very small amount of this component was used to generate the 1−T spectrum of the B800-850 complex (see the orange carotenoid spectral trace in the top left panel of Figure 5) consistent with only 6% spirilloxanthin being present in this complex. More intensity in this long-wavelength component was needed to reconstruct the 1−T spectrum of the B800-840 and B800-820 complexes (see the orange carotenoid trace in the middle and bottom left panels of Figure 5) which is in agreement with the additional spirilloxanthin found in this complex (Table 1). The dominant component having a spectral origin at 519 nm (B800-850) or 520 nm (B800-820 and B800-840) can be attributed to rhodopin (N=11) which is the most abundant carotenoid in all of the complexes (Table 1). The carotenoid component with a spectral origin at 534 nm (B800-840 and B800-850) or 536 nm (B800-820) can be assigned to rhodovibrin and

anhydrorhodovibrin which have identical spectra because both have N=12. Taken together they represent the second most abundant carotenoid chromophore in the complexes. The shortest wavelength-absorbing carotenoid that has a spectral origin at ~495 nm for all complexes is an anomaly. A spectral origin at that wavelength would be consistent with an N=9 carotenoid chromophore; e.g. neurosporene, but no such carotenoid exists in any of these complexes (Table 1). Therefore, this spectral form, which is unquestionably required to reconstruct the experimental 1−T spectra of the complexes (Figure 5), must result from either a major perturbation of the $S_0 \rightarrow S_2$ transition of one of the bound carotenoids due to strong, perhaps ionic, interactions with the protein structure, or to a twisting of the ends of one of the carotenoids in such a way that the longer molecule is able to take on the absorption spectral characteristics of a shorter (N=9) carotenoid chromophore. Because carotenoids having N≤10; *e.g.* neurosporene and spheroidene, in LH2 complexes exhibit carotenoid-to-BChl energy transfer efficiencies greater than 90%,[55,56] one might wonder why this is not the case here. Out-of-plane distortion of the polyene chain of long-chain carotenoids found in the B800-820 and B800-850 complexes has been reported from resonance Raman studies of native LH2 complexes from *Ch. vinosum* (now *Alc. vinosum*)[57] to be associated with low energy transfer efficiencies. Thus, a short, effective N value may be a necessary condition for achieving a high carotenoid-to-BChl energy transfer efficiency, but it is not sufficient. The type and magnitude of electronic coupling between the bound pigments also plays a crucial role.[58]

***Carotenoid-to-BChl Energy Transfer***

A consideration of the relative intensities of the carotenoid spectral lineshapes

needed to reconstruct the 1−T and fluorescence excitation spectra from the LH2 complexes (Figure 5, Table 2) reveals the individual carotenoid-to-BChl energy transfer efficiencies of each of the carotenoids bound in the complexes. The data show clearly that all of the carotenoids transfer singlet state energy to BChl *a* with efficiencies less than or equal to ~40% which is consistent with previous reports on LH2 complexes containing carotenoid chromophores having N≥11.[22,40,54,57] The low energy transfer efficiencies of these carotenoids can be attributed to a number of factors including a low energy $S_1$ state of the carotenoid relative to the $S_1$ energy of BChl *a*.[54] The effect of having the $S_1$ energies of these longer carotenoids lie near or below the $S_1$ state of BChl *a* would inhibit the rate of carotenoid-to-BChl excitation energy transfer by reducing the amount of spectral overlap between the carotenoid donor emission bands and the BChl *a* acceptor absorption features which would have the result of lowering the energy transfer efficiency.[54] Another factor to be considered is that the intrinsic $S_2$ lifetime of carotenoids gets shorter with increasing N.[39,59] Therefore, as a carotenoid chromophore gets longer, energy transfer from the $S_2$ state must compete with its shorter intrinsic $S_2$ lifetime. This results in less efficient carotenoid-to-BChl energy transfer despite the fact that energy transfer rates remain essentially unaffected by the conjugation length of the carotenoid.[60] It may also be the case that for longer carotenoids, the presence of one-photon forbidden "dark" states such as the $1^1B_u^-$ state of carotenoids[61-64] may be present in the vicinity of $S_1$ and $S_2$ and affecting the rate and efficiency of energy transfer.[65] The decrease in efficiency as the carotenoids become longer may also be caused by an alternative avenue of energy transfer being available. This may involve the so-called S* state which can transfer energy to BChl *a* and is also known to be a precursor for the formation of

carotenoid triplet states.[54,66] Very likely, a combination of these factors, as well as the nature of the electronic coupling between pigments, is responsible for the low carotenoid-to-BChl energy transfer efficiencies found here for the carotenoids bound in the LH2 complexes from *Alc. vinosum.*

It would be gratifying to be able to deconvolute the values of the kinetic components deduced from either the single wavelength or global fitting analyses and to obtain the rate constants for energy transfer to BChl *a* from the $S_1$ and $S_2$ (and perhaps other) excited states of the carotenoids. Unfortunately, the complexity in the ESA features due to spectral heterogeneity and overlap of the transient absorption bands precludes a detailed quantitative analysis. However, since two distinct $S_1 \rightarrow S_n$ transitions appear at 581 nm and 605 nm which can be attributed to rhodopin (N=11) and the combination of rhodovibrin and anhydrorhodovibrin (N=12), respectively, their lifetimes can be compared to the intrinsic lifetimes of these molecules measured in solution to see if they are at least qualitatively consistent with the measured energy transfer efficiencies. As shown above, when the laser excitation wavelength of 490 nm is changed to 540 nm, the longer wavelength ESA band belonging to rhodovibrin and anhydrorhodovibrin appearing at 605 nm becomes larger than the shorter wavelength ESA band of rhodopin which appears at 581 nm and is more prominent when 490 nm laser excitation is used (Figure 6). Thus, the $S_1$ lifetime, obtained from the time trace induced by 490 nm laser excitation and recorded at 581 nm and deduced from the fit to a sum of exponentials function, can be attributed to that of rhodopin which was found to range from 3.4 ps to 4.2 ps depending on the LH2 complex (Table 3). The intrinsic $S_1$ lifetime of rhodopin measured in solution at room temperature has been reported to be between 4.1 ps and 4.8

ps.[38,39] Because these two ranges of values overlap, there is a high statistical likelihood that the $S_1$ lifetimes in solution and in the LH2 complex are the same. The energy transfer efficiency from the $S_1$ state of a carotenoid can be determined using the equation

$$\phi_{ET} = \left(1 - \frac{\tau_{S_1}^{\mathrm{LH2}}}{\tau_{S_1}^{\mathrm{SOLN}}}\right) \times 100 \qquad (1)$$

where $\tau_{S_1}^{\mathrm{SOLN}}$ is the lifetime of the $S_1$ state of the carotenoid in solution, and $\tau_{S_1}^{\mathrm{LH2}}$ is that measured in the LH2 complexes. The similarity in the values of $\tau_{S_1}^{\mathrm{SOLN}}$ and $\tau_{S_1}^{\mathrm{LH2}}$ then suggests that very little of the $S_1$ excited state population is being transferred to BChl *a*. Similarly, the $S_1$ lifetime of rhodovibrin and anhydrorhodovibrin (N=12) can be obtained from the time trace of the ESA spectrum recorded at 630 nm which is a better wavelength than the peak wavelength of 605 nm from which to obtain the kinetics of these N=12 molecules. This is because 630 nm is more out of the range of the ESA signal from rhodopin that appears at 581 nm. A fit to a sum of exponentials function of the time trace recorded using 540 nm laser excitation and probed at 630 nm gives a value ranging from 1.5 ps to 1.6 ps depending on the LH2 complex (Table 3). The intrinsic $S_1$ lifetime of rhodovibrin measured in solution at room temperature has been reported to be in the range of 2.0 ps to 2.4 ps[39,40] which from Equation 1 also suggests that only a small percent of the excited $S_1$ state population of rhodovibrin and anhydrorhodovibrin is being transferred to BChl *a*. The primary route of carotenoid-to-BChl energy transfer must therefore be via the $S_2$ state of the carotenoids. This conclusion is consistent with the transient absorption spectral data shown in Figure 6 which clearly indicate that the bleaching of the BChl $Q_Y$ band is nearly complete after only a few hundred femtoseconds.

# Conclusions

*Allochromatium vinosum* produces a number of spectral forms of LH2 light-harvesting pigment-protein complexes depending on how the organism is grown. This chapter analyzed the carotenoid composition by HPLC and examined the steady state and ultrafast spectroscopic behavior of three of these spectral forms of LH2: B800-820, B800-840 and B800-850. The carotenoid composition of all of the LH2 complexes was found to consist of five carotenoids: lycopene, anhydrorhodovibrin, spirilloxanthin, rhodopin and rhodovibrin. Spectral reconstructions of the absorption and fluorescence excitation spectra based on the pigment composition revealed significant spectral heterogeneity that can be traced to substantial protein structural heterogeneity for *Alc. vinosum.* The data revealed ~40% carotenoid-to-bacteriochlorophyll energy transfer efficiencies for all of the bound carotenoids which, as evidenced by the data from ultrafast transient absorption spectroscopic experiments, originates almost entirely from the $S_2$ states of the carotenoids. These LH2 antenna proteins from *Alc. vinosum* possess significant structural and spectral heterogeneity which result in intricate, multi-chromophore pigmented, light-harvesting protein architectures very likely generated by the organism in order to adapt and survive under challenging environmental conditions.

## References


(1) Thornber, J. R.; Trosper, T. L.; Strouse, C. E. Bacteriochlorophyll *in vivo*: Relationships of Spectral Forms to Specific Membrane Components In *The Photosynthetic Bacteria*; Clayton, R. K., Sistrom, W. R., Eds.; Plenum Press: London, United Kingdom, **1978**, 133–160.

(2) Cogdell, R. J.; Thornber, J. P. *FEBS Lett.* **1980**, *122*, 1–8.

(3) Cogdell, R. J.; Zuber, H.; Thornber, J. P.; Drews, G.; Gingras, G.; Niederman, R. A.; Parson, W. W.; Feher, G. *Biochim. Biophys. Acta* **1985**, *806*, 185–6.

(4) Zuber, H.; Cogdell, R. J. Structure and Organization of Purple Bacterial Antenna Complexes In *Advances in Photosynthesis* Blankenship, R. E., Madigan, M. T., Bauer, C. E., Eds.; Kluwer Academic Publishers: Springer Netherlands, **1995**; Vol. 2, 315–48.

(5) McDermott, G.; Prince, S. M.; Freer, A. A.; Hawthornthwaite-Lawless, A. M.; Papiz, M. Z.; Cogdell, R. J.; Isaacs, N. W. *Nature* **1995**, *374*, 517–521.

(6) Hawthornthwaite, A. M.; Cogdell, R. J. *Chlorophylls* **1991**, 493–528.

(7) Cogdell, R. J.; Isaacs, N. W.; Howard, T. D.; McLuskey, K.; Fraser, N. J.; Prince, S. M. *J. Bacteriol.* **1999**, *181*, 3869–3879.

(8) Cogdell, R. J.; Howard, T. D.; Isaacs, N. W.; McLuskey, K.; Gardiner, A. T. *Photosynth. Res.* **2002**, *74*, 135–141.

(9) Prince, S. M.; Papiz, M. Z.; Freer, A. A.; McDermott, G.; Hawthornthwaite-Lawless, A. M.; Cogdell, R. J.; Isaacs, N. W. *J. Mol. Biol.* **1997**, *268*, 412–423.

(10) McLuskey, K.; Prince, S. M.; Cogdell, R. J.; Isaacs, N. W. *Biochemistry* **2001**, *40*, 8783–8789.

(11) Papiz, M. Z.; Prince, S. M.; Howard, T.; Cogdell, R. J.; Isaacs, N. W. *J. Mol. Biol.* **2003**, *326*, 1523–1538.

(12) Koepke, J.; Hu, X.; Schulten, K.; Michel, H. *Structure* **1996**, *4*, 581–597.

(13) Gall, A.; Gardiner, A. T.; Cogdell, R. J.; Robert, B. *FEBS Lett.* **2006**, *580*, 3841–4.

(14) Cogdell, R. J.; Gall, A.; Köhler, J. *Q. Rev. Biophys.* **2006**, *39*, 227–324.

(15) Wassink, E. C.; Katz, E.; Dorrestein, R. *Enzymologia* **1939**, *7*, 113–129.

(16) Garcia, A.; Vernon, L. P.; Mollenhauer, H. *Biochemistry* **1966**, *5*, 2399–2407.

(17) Hayashi, H.; Morita, S. *J. Biochem.* **1980**, *88*, 1251–1258.

(18) Carey, A.-M.; Hacking, K.; Picken, N.; Honkanen, S.; Kelly, S.; Niedzwiedzki, D. M.; Blankenship, R. E.; Shimizu, Y.; Wang-Otomo, Z.-Y.; Cogdell, R. J. *BBA-Bioenergetics* **2014**, *1837*, 1849–1860.

(19) Hayashi, H.; Nozawa, T.; Hatano, M.; Morita, S. *J. Biochem.* **1981**, *89*, 1853–1861.

(20) Cogdell, R. J.; Scheer, H. *Photochem. Photobiol.* **1985**, *42*, 669–78.

(21) Kereïche, S.; Bourinet, L.; Keegstra, W.; Arteni, A. A.; Verbavatz, J.-M.; Boekema, E. J.; Robert, B.; Gall, A. *FEBS Lett.* **2008**, *582*, 3650–3656.

(22) Niedzwiedzki, D. M.; Bina, D.; Picken, N.; Honkanen, S.; Blankenship, R. E.; Holten, D.; Cogdell, R. J. *BBA-Bioenergetics* **2012**, *1817*, 1576–1587.

(23) Löhner, A.; Carey, A.-M.; Hacking, K.; Picken, N.; Kelly, S.; Cogdell, R. J.; Köhler, J. *Photosynth. Res.* **2015**, *123*, 23–31.

(24) Cleary, L.; Chen, H.; Chuang, C.; Silbey, R. J.; Cao, J. *Proc. Natl. Acad. Sci. USA* **2013**, *110*, 8537–8542.

(25) Heinemeyer, E.-A.; Schmidt, K. *Arch. Microbiol.* **1983**, *134*, 217–221.

(26) Gardiner, A. T.; Takaichi, S.; Cogdell, R. J. *Biochem. Soc. Trans.* **1992**, *21*, 6S.

(27) Takaichi, S.; Gardiner, A. T.; Cogdell, R. J. *Res. Photosynth., Proc. Int. Congr. Photosynth., 9th* **1992**, *1*, 149–52.

(28) Gardiner, A. T.; Cogdell, R. J.; Takaichi, S. *Photosynth. Res.* **1993**, *38*, 159–167.

(29) Magdaong, N. M.; Lafountain, A. M.; Greco, J. A.; Gardiner, A. T.; Carey, A.-M.; Cogdell, R. J.; Gibson, G. N.; Birge, R. R.; Frank, H. A. *J. Phys. Chem. B* **2014**, *118*, 11172–11189.

(30) Weissgerber, T.; Zigann, R.; Bruce, D.; Chang, Y.-j.; Detter, J. C.; Han, C.; Hauser, L.; Jeffries, C. D.; Land, M.; Munk, C.et al. *Stand Genomic Sci* **2011**, *5*, 311–330.

(31) Zuber, H.; Brunisholz, R. A. In *The Chlorophylls*; Scheer, H., Ed.; CRC: Boca Raton, **1993**, 627.

(32) Kennis, J. T. M.; Streltsov, A. M.; Vulto, S. I. E.; Aartsma, T. J.; Nozawa, T.; Amesz, J. *J. Phys. Chem. B* **1997**, *101*, 7827–7834.

(33) Niedzwiedzki, D. M.; Kobayashi, M.; Blankenship, R. E. *Photosynth. Res.* **2011**, *107*, 177–186.

(34) Britton, G. Uv/Visible Spectroscopy In *Carotenoids Vol. 1B: Spectroscopy*; Britton, G., Liaaen-Jensen, S., Pfander, H., Eds.; Birkhäuser Verlag: Basel-Boston-Berlin, **1995**, 13–62.

(35) Schiedt, K.; Liaaen-Jensen, S. Isolation and Analysis In *Carotenoids Vol. 1A: Isolation and Analysis*; Birkhäuser Verlag: Basel- Boston-Berlin, **1995**; Vol. 1A: Isolation and Analysis.

(36) Ilagan, R. P.; Christensen, R. L.; Chapp, T. W.; Gibson, G. N.; Pascher, T.; Polivka, T.; Frank, H. A. *J. Phys. Chem. A* **2005**, *109*, 3120–3127.

(37) Fuciman, M.; Enriquez, M. M.; Polivka, T.; Dall'Osto, L.; Bassi, R.; Frank, H. A. *J. Phys. Chem. B* **2012**, *116*, 3834–3849.

(38) Macpherson, A. N.; Arellano, J. B.; Fraser, N. J.; Cogdell, R. J.; Gillbro, T. *Biophys. J.* **2001**, *80*, 923–930.

(39) Niedzwiedzki, D.; Koscielecki, J. F.; Cong, H.; Sullivan, J. O.; Gibson, G. N.; Birge, R. R.; Frank, H. A. *J. Phys. Chem. B* **2007**, *111*, 5984–98.

(40) Niedzwiedzki, D. M.; Fuciman, M.; Kobayashi, M.; Frank, H. A.; Blankenship, R. E. *Photosynth. Res.* **2011**, *110*, 49–60.

(41) Monger, T. G.; Cogdell, R. J.; Parson, W. W. *Biochim. Biophys. Acta* **1976**, *449*, 136–53.

(42) Farhoosh, R.; Chynwat, V.; Gebhard, R.; Lugtenburg, J.; Frank, H. A. *Photosynth. Res.* **1994**, *42*, 157–166.

(43) Feng, J.; Wang, Q.; Wu, Y.-S.; Ai, X.-C.; Zhang, X.-J.; Huang, Y.-G.; Zhang, X.-K.; Zhang, J.-P. *Photosynth. Res.* **2004**, *82*, 83–94.

(44) Kakitani, Y.; Akahane, J.; Ishii, H.; Sogabe, H.; Nagae, H.; Koyama, Y. *Biochemistry* **2007**, *46*, 2181–2197.

(45) Holzwarth, A. R. Data Analysis of Time-Resolved Measurements In *Biophysical Techniques in Photosynthesis*; Amesz, J., Hoff, A. J., Eds.; Kluwer Academiv Publishers: Dordrecht/Boston/London, **1996**; Vol. 3, 75–91.

(46) van Stokkum, I. H. M.; Larsen, D. S.; van Grondelle, R. *Biochim. Biophys. Acta* **2004**, *1657*, 82–104.

(47) Shreve, A. P.; Trautman, J. K.; Frank, H. A.; Owens, T. G.; Van Beek, J. B.; Albrecht, A. C. *J. Lumin.* **1992**, *53*, 179–86.

(48) Okamoto, H.; Ogura, M.; Nakabayashi, T.; Tasumi, M. *Chem. Phys.* **1998**, *236*, 309–318.

(49) Rondonuwu, F. S.; Taguchi, T.; Fujii, R.; Yokoyama, K.; Koyama, Y.; Watanabe, Y. *Chem. Phys. Lett.* **2004**, *384*, 364–371.

(50) Schubert, A.; Stenstam, A.; Beenken, W. J. D.; Herek, J. L.; Cogdell, R.; Pullerits, T.; Sundström, V. *Biophys. J.* **2004**, *86*, 2363–2373.

(51) Trautman, J. K.; Shreve, A. P.; Violette, C. A.; Frank, H. A.; Owens, T. G.; Albrecht, A. C. *Proc. Natl. Acad. Sci. USA* **1990**, *87*, 215–219.

(52) Kramer, H.; Amesz, J. *Photosynth. Res.* **1996**, *49*, 237–244.

(53) Law, C. J.; Roszak, A. W.; Southall, J.; Gardiner, A. T.; Isaacs, N. W.; Cogdell, R. J. *Mol. Membr. Biol.* **2004**, *21*, 183–191.

(54) Cong, H.; Niedzwiedzki, D.; Gibson, G. N.; LaFountain, A. M.; Kelsh, R. M.; Gardiner, A. T.; Cogdell, R. J.; Frank, H. A. *J. Phys. Chem. B* **2008**, *112*, 10689–10703.

(55) Angerhofer, A.; Bornhäuser, F.; Gall, A.; Cogdell, R. J. *Chem. Phys.* **1995**, *194*, 259–274.

(56) Frank, H. A.; Cogdell, R. J. *Photochem. Photobiol.* **1996**, *63*, 257–64.

(57) Noguchi, T.; Hayashi, H.; Tasumi, T. *Biochim. Biophys. Acta* **1990**, *1017*, 280–290.

(58) Krueger, B. P.; Scholes, G. D.; Fleming, G. R. *J. Phys. Chem. B* **1998**, *102*, 5378–5386.

(59) Kosumi, D.; Fujiwara, M.; Fujii, R.; Cogdell, R. J.; Hashimoto, H.; Yoshizawa, M. *J. Chem. Phys.* **2009**, *130*, 214506–214513.

(60) Akahane, J.; Rondonuwu, F. S.; Fiedor, L.; Watanabe, Y.; Koyama, Y. *Chem. Phys. Lett.* **2004**, *393*, 184–191.

(61) Cerullo, G.; Polli, D.; Lanzani, G.; De Silvestri, S.; Hashimoto, H.; Cogdell, R. J. *Science* **2002**, *298*, 2395–2398.

(62) Rondonuwu, F. S.; Yokoyama, K.; Fujii, R.; Koyama, Y.; Cogdell, R. J.; Watanabe, Y. *Chem. Phys. Lett.* **2004**, *390*, 314–322.

(63) Maiuri, M.; Polli, D.; Brida, D.; Lüer, L.; LaFountain, A. M.; Fuciman, M.; Cogdell, R. J.; Frank, H. A.; Cerullo, G. *Phys. Chem. Chem. Phys.* **2012**, *14*, 6312–6319.

(64) Ostroumov, E. E.; Mulvaney, R. M.; Cogdell, R. J.; Scholes, G. D. *Science* **2013**, *340*, 52–56.

(65) Koyama, Y.; Rondonuwu, F. S.; Fujii, R.; Watanabe, Y. *Biopolymers* **2004**, *74*, 2–18.

(66) Gradinaru, C. C.; Kennis, J. T. M.; Papagiannakis, E.; van Stokkum, I. H. M.; Cogdell, R. J.; Fleming, G. R.; Niederman, R. A.; van Grondelle, R. *Proc. Natl. Acad. Sci. USA* **2001**, *98*, 2364–2369.

# *Chapter VI*

# *Optical spectroscopic investigation of native and recombinant peridinin-chlorophyll a-protein complexes*

## Introduction

Light harvesting is carried out by several species of photosynthetic marine algae, including many dinoflagellates, using integral membrane antenna complexes and also a water-soluble pigment-protein complex known as the peridinin-chlorophyll (Chl) *a*-protein (PCP).[1-4] The minimal structural unit of PCP (Figure 1B) is comprised of two protein domains in each of which are one Chl *a* and four peridinins noncovalently bound. Peridinin is a carotenoid possessing a carbonyl group in conjugation with the linear polyene chain (Figure 1A), the presence of which gives rise to some unique photophysical properties. For example, the lifetime of the lowest lying excited state, $S_1$, of peridinin has been found to be shortened from ~160 ps when the molecule is dissolved in nonpolar solvents to ~10 ps when it is dissolved in polar solvents.[5-7] Carotenoids without carbonyl functional groups in conjugation with the polyene chain show essentially no effect of solvent on the $S_1$ lifetime. The effect has been attributed to the presence of an intramolecular charge transfer (ICT) state[5,8,9] in the excited state manifold of peridinin, which in conjunction with the $S_1$ and $S_2$ states, is involved in the transfer of excitation energy from peridinin to Chl *a*.[10-14]

This chapter will describe steady-state spectroscopic experiments carried out on three different PCP preparations: Main-form PCP (MFPCP), recombinant folded PCP

(RFPCP), and PCP from *Heterocapsa pygmaea* (formerly *Glenodinium sp.*) (HPPCP). MFPCP from *Amphidinium (A.) carterae* is known to form a trimeric quaternary structure as revealed by its 2.0 Å resolution crystal structure (Figure 1B) where each monomer contains two Chl *a* and eight peridinin molecules surrounded by a 32 kDa apoprotein[15] arranged in a pseudo two-fold symmetric configuration.[15,16] Differences in the primary sequence of the N- and C-terminal domains provides the interface by which trimerization of the protein subunits occurs.

RFPCP is a construct of the recombinant N-terminal domain of MFPCP reconstituted with 4:1 stoichiometric amounts of peridinin and Chl *a*.[17] RFPCP assembles into a monomeric quaternary form with two identical subunits. The sequence similarity of the proteins in the two subunits precludes it from forming the trimeric structure exhibited by MFPCP. The recombinant system that expresses RFPCP also provides the ability to carry out site-directed mutagenesis.[18,19] In combination with the 1.4 Å resolution crystal structure reported for RFPCP[18] (Figure 1B), this ability has been valuable in probing the effect that changing specific amino acids has on the spectral characteristics and energy transfer properties of the bound pigments.[18] RFPCP is also amenable to reconstitution with various Chls and therefore provides a system with which to systematically alter the energy levels of the energy acceptor molecules in order to elucidate the mechanism of energy transfer from the protein-bound peridinins.[20-26] It is also worthy of note that despite many attempts, there has been no success in reconstituting the recombinant apoprotein with any synthetically modified peridinins. Thus, although successful refolding of the apoprotein into a fully functioning RFPCP light-harvesting complex

similar to MFPCP can be carried out using many different Chls, the only carotenoid able to be incorporated is peridinin.

HPPCP has the same 4:1 peridinin-to-Chl *a* pigment stoichiometric ratio as MFPCP but the assembly of the minimum structural unit requires the dimerization of two ~15 kDa peptide units.[27,28] There are two main isoforms of the 15 kDa PCP monomers. These are denoted a and b,[29] which combine to form three possible complexes (a/a, a/b, b/b) that can be separated according to their difference in isoelectric points.[30] Each apoprotein binds one Chl *a* and four peridinins. The heterodimeric a/b HPPCP has been used for crystallographic studies and Figure 1B illustrates that HPPCP does not form a trimeric quaternary structure like MFPCP.[4,19]

In this chapter steady-state absorption and fluorescence spectroscopy were carried out at room and cryogenic temperatures on the MFPCP, RFPCP and HPPCP complexes. The objectives of the work are to examine whether any differences in the spectral properties of the peridinins and Chls arise from variations in the ability of the PCP complexes to form monomeric (RFPCP, HPPCP) or trimeric (MFPCP) quaternary structures from homodimeric (RFPCP) or heterodimeric (MFPCP, HPPCP) minimal units and to determine the individual peridinin-to-Chl *a* excitation energy transfer (EET) efficiencies. It is hoped that this information will lead to a better understanding of the relationship between the structure of PCP and the molecular factors controlling its function as a highly efficient light-harvesting pigment-protein complex in marine organisms.

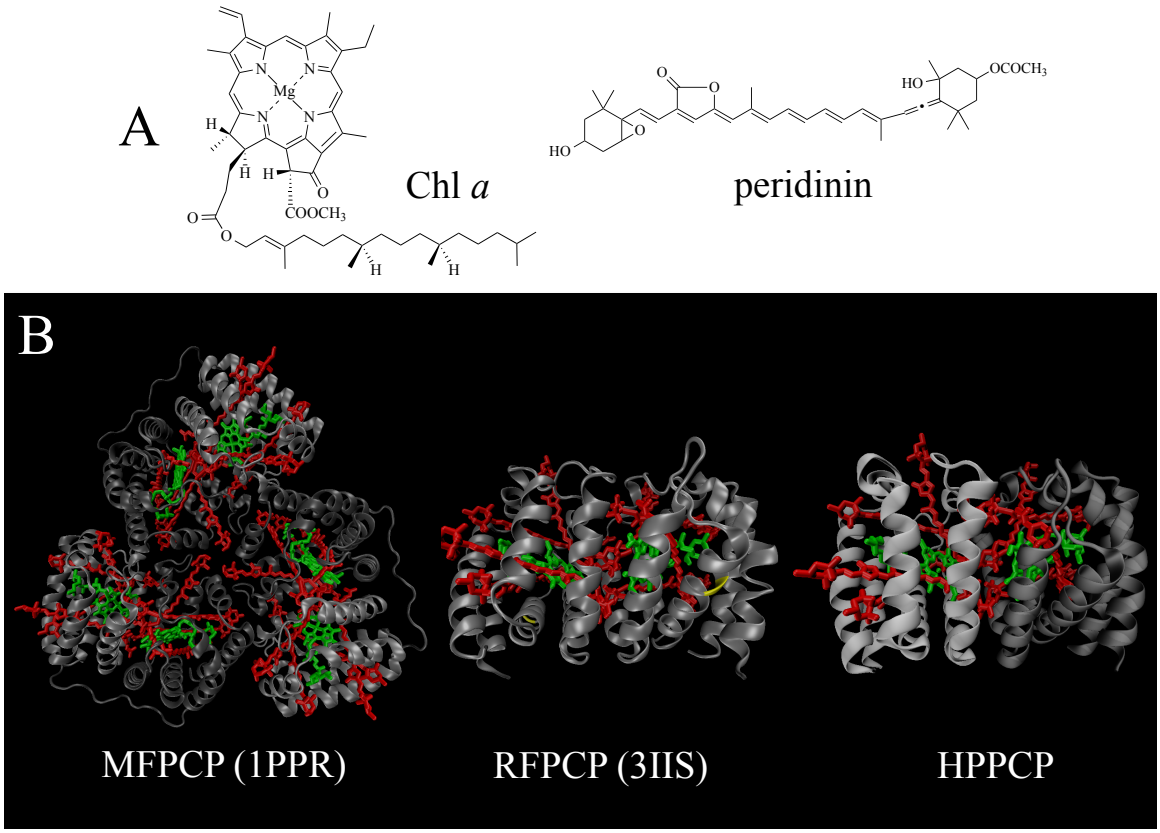


**Figure 1.** (A) Structures of the pigments in the PCP complexes. (B) Quaternary structures of the PCP complexes. Each minimal unit contains two Chl *a* (green) and four peridinins (red). MFPCP exists as a trimer whereas RFPCP and HPPCP are monomers. The structures were generated using Visual Molecular Dynamics (VMD) software[31] and the indicated PDB codes, except for HPPCP whose structure is given in Ref. 19.

## Materials and Methods

### *Sample preparation*

The PCP complexes used in this study were provided by Prof. Roger Hiller of Macquarie University, Australia and Prof. Eckhard Hofmann of Ruhr-University Bochum, Germany, and were obtained according to previously published protocols. MFPCP was extracted and purified from *A. carterae* as described by Sharples et al.[32] and dissolved in buffer containing 50 mM Tricine, 20 mM KCl, pH 7.5. RFPCP was obtained by expression of the N-terminal domain of the MFPCP apoprotein in *Escherichia (E.) coli* and reconstitution with the pigments according to Miller et al.[17] It was then dissolved in buffer containing 5 mM Tricine, 2 mM KCl, pH 7.6. HPPCP was prepared from *H. pygmaea*[19] and resuspended in a 50 mM sodium acetate buffer, pH 5.5 for the spectroscopic experiments.

### *Spectroscopic methods*

Steady-state absorption spectra were recorded using a Varian Cary 50 UV-Vis spectrometer. Steady-state fluorescence and fluorescence excitation spectra were recorded using a Jobin-Yvon Horiba Fluorolog-3 model FL3-22 fluorimeter equipped with a double emission and excitation monochromators having 1200/mm gratings, a Hamamatsu R928P photomultiplier tube (PMT) detector, and 450 W ozone-free Osram xenon arc lamp. The fluorescence spectra were corrected for the instrument response using a correction file generated by a reference photodiode. Unless otherwise noted the excitation and emission slit widths corresponded to a bandpass of 2 nm for the excitation and 6 nm for the emission monochromators. Samples used in the fluorescence

experiments were adjusted to have an optical density (OD) of ~0.01–0.02 in a 1 cm path length at the $\lambda_{max}$ of the Chl *a* $Q_Y$ band.

For the absorption and fluorescence experiments at cryogenic temperatures, the samples contained 60% (v/v) glycerol. Measurements at 77 K were carried out on samples placed in disposable plastic cuvettes (Plastibrand No. 759150) which were held in a custom-built holder that was lowered slowly into an optical immersion dewar cryostat containing liquid nitrogen. For experiments at 10 K, liquid helium was introduced via a transfer arm (Janis ST-LINE) into a cryostat (Janis Model STVP-100-1) containing the samples.

## Results and Discussion

The steady-state absorption spectra of the MFPCP, RFPCP and HPPCP complexes recorded at room and cryogenic temperatures are shown in Figure 2. The broad band between 400 nm and 600 nm corresponds to a composite lineshape formed from the absorption spectra of the different protein-bound peridinins, each of which have a different spectral position and intensity.[18,33-37] The peaks at ~435 and ~670 nm correspond to the Soret and $Q_Y$ transitions of Chl *a*, respectively. At room temperature, the absorption spectra of all three complexes are very similar, although the absorption spectrum of HPPCP (black traces in the top panel of Figure 2) shows a more pronounced shoulder on the red-edge of the carotenoid maximum absorption band compared to the spectra of MFPCP and RFPCP (red and blue traces in the top panel of Figure 2). The $Q_Y$ band of HPPCP is also red-shifted to 673 nm whereas MFPCP and RFPCP have their $Q_Y$ bands at 670 nm.

Upon lowering the temperature to 77 K (middle panel of Figure 2), the spectral features become more pronounced and a shift in intensity and position of some of the bands becomes apparent. Lowering the temperature to 10 K (bottom panel of Figure 2) sharpens these features further. For all PCPs, the carotenoid maximum absorption band red-shifts by ~7–8 nm in going from room to cryogenic temperatures (77 and 10 K). The Soret band also splits into two peaks suggestive of the two Chl *a* molecules in the minimal unit experiencing different protein environments. Also, upon lowering the temperature to 10K, the $Q_Y$ band narrows and blue-shifts by ~4 nm for MFPCP and RFPCP and 1 nm for HPPCP, and the intensity of the $Q_Y$ band of MFPCP and RFPCP doubles whereas that of HPPCP increases by a factor of three.

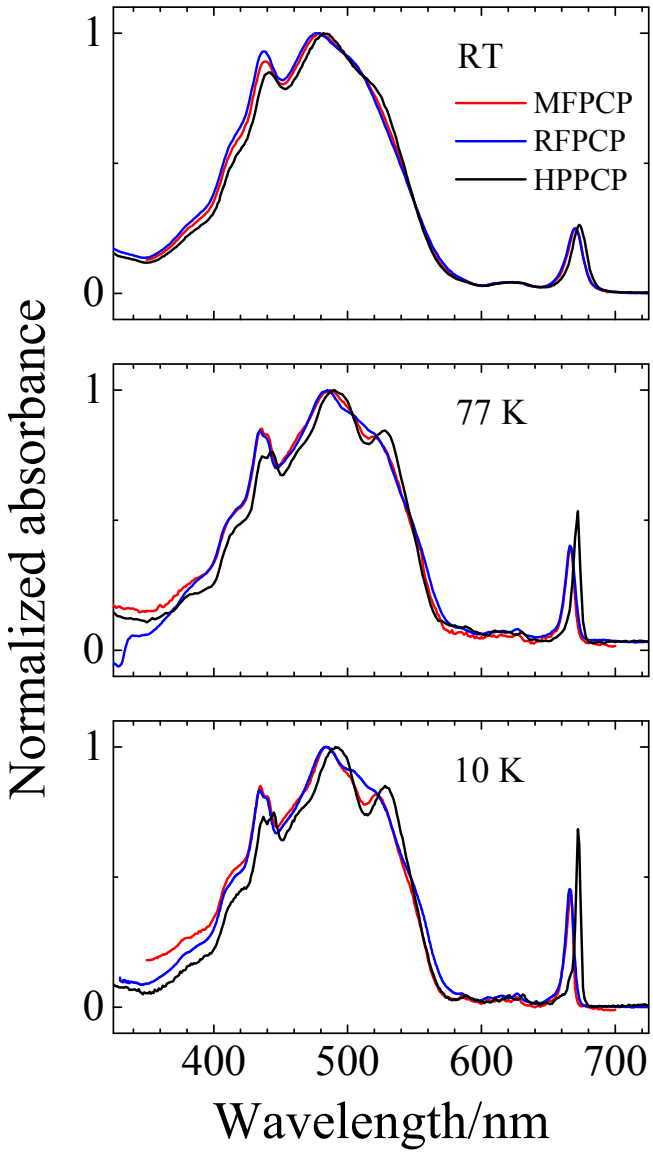


**Figure 2.** Absorption spectra of MFPCP (red traces), RFPCP (blue traces) and HPPCP (black traces) recorded at room and cryogenic temperatures. The spectra were normalized at their $\lambda_{max}$ values in the peridinin absorption region at ~480 nm.

In order to gain more information about the individual peridinins contributing to the overall absorption spectral lineshapes of the complexes, reconstruction of the 1−T spectra recorded at 10 K was performed for all three PCP complexes. The results are shown in Figure 3. The absorption spectra of purified peridinin and Chl *a* were recorded in 2-MTHF at 10 K and were summed to obtain the reconstructed spectra. The method for reconstruction followed that used previously by Ilagan et al.[35] for MFPCP and Schulte et al.[18] for RFPCP and the results served as guide for reconstructing the 1−T spectrum from HPPCP. For all PCPs, each individual peridinin spectrum was allowed to shift its spectral origin, and a different intensity for the most blue-shifted peridinin compared to the three longer wavelength absorbing peridinins was needed to achieve reasonable agreement with the experimental spectrum. The two Chl *a* spectra were permitted to have variable spectral origins and intensities. The intensity and wavelength parameters characterizing the spectral reconstructions are given in Table 1.

Satisfactory reconstruction of the 1−T spectral lineshape was obtained for MFPCP using five individual peridinin and two Chl *a* spectra (Figure 3 top panel). The five peridinin components can be assembled into two groups, one of which is made up of two blue-shifted peridinins with their spectral origins at 468 and 483 nm and a second group having three pairs of longer wavelength-absorbing peridinins having spectral origins at 521, 525 and 543 nm. This is consistent with the previous reconstruction of the 1−T spectrum of MFPCP which yielded peridinin components having spectral origins at 465, 485, 523, 528 and 545 nm.[35,37] In the previous work, the blue-shifted peridinins were assigned to peridinins 612/622 (Figure 4) and because of its orientation relative to Chl *a*, Per 612 has been suggested to transfer excited state energy to the other peridinins instead

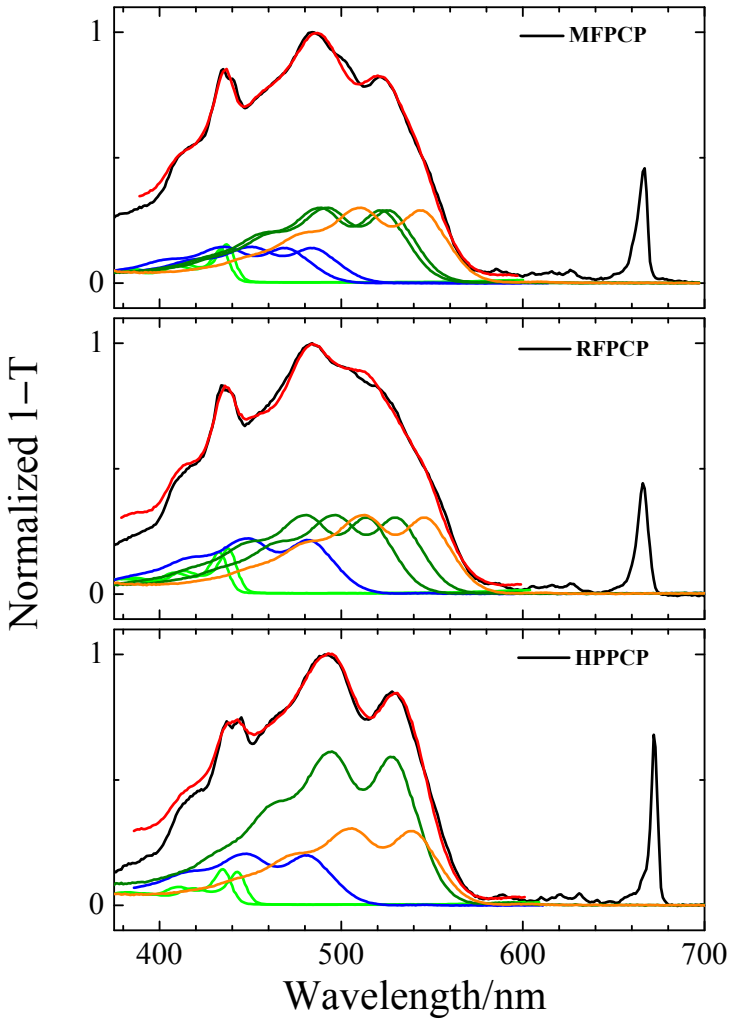


**Figure 3.** Reconstruction of the 10 K 1−T spectra (black traces) of MFPCP, RFPCP and HPPCP. Individual spectra of peridinin (blue, dark green and orange traces) and Chl *a* (light green traces) were taken in 2-MTHF at 10 K and summed to yield the reconstructed spectra (red traces).

***Table 1.*** Parameters from the spectral reconstruction shown in Figure 3.

| | Spectral origin/nm, Intensity | | |
|---|---|---|---|
| | MFPCP | RFPCP | HPPCP |
| Per 1 | 468/483, 0.14 | 481, 0.22 | 480, 0.20 |
| Per 2 | 521, 0.29 | 513, 0.30 | 527, 0.30 |
| Per 3 | 525, 0.29 | 529, 0.30 | 527, 0.30 |
| Per 4 | 543, 0.29 | 545, 0.30 | 538, 0.30 |

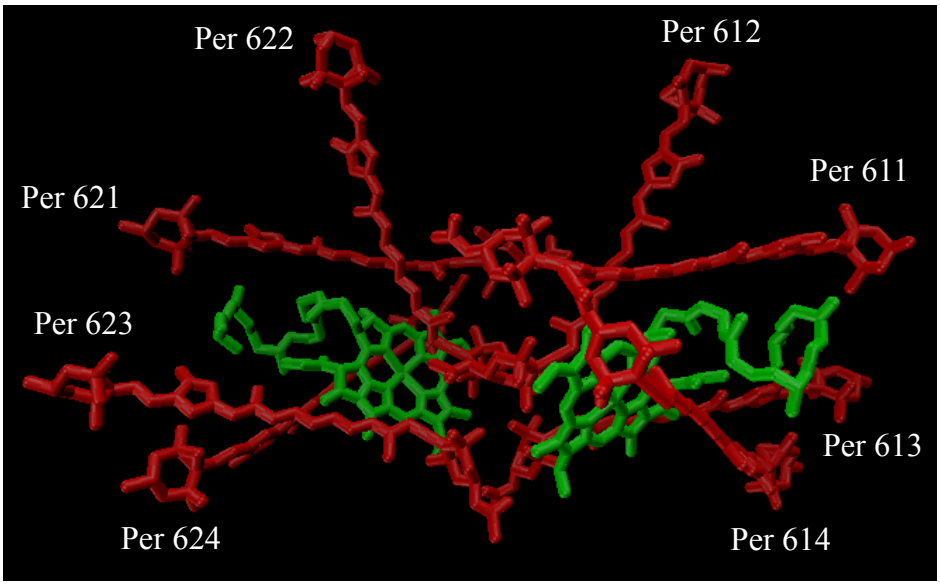


**Figure 4.** Structure and arrangement of the peridinins (red) and Chls (green) bound in a monomeric unit of MFPCP.

of directly to Chl *a*.[12,16,35,36,38] The Chl *a* spectra used in the reconstruction of the Soret region had absorption peaks at 434 and 437 nm which were also consistent with previous results of 434 and 439 nm.

The components obtained from the reconstruction of the 1–T spectrum from RFPCP (Figure 3, middle panel) had four pairs of peridinins with spectral origins at 481, 513, 529 and 545 nm and Chl *a* Soret bands at 433 and 438 nm, which are similar to previously published results[18] in which peridinin had spectral origins at 481, 515, 531, and 547 nm and Soret bands of Chl *a* at 433 and 438 nm. Because RFPCP is homodimeric, the Chl *a* molecules are purportedly in the same environment and should exhibit the same spectra. The present result (Figure 2, blue traces in the middle and bottom panels), consistent with previous investigations[18,22] however, shows a splitting of the Chl *a* Soret band which was explained based on structural modeling to be due to the vinyl functional group of Chl *a* having two conformations.[18] By combining site-directed mutagenesis and spectroscopic methods,[18] the red-most absorbing peridinin was assigned to Per 614 (Figure 4), which has been determined to have the strongest interaction with Chl *a*[12,20,38-43] and functions as the main Chl *a* triplet state quencher.[40-45]

The reconstruction of the 1–T spectrum from HPPCP (Figure 3, bottom panel) required four pairs of peridinins, with spectral origins at 480, 527 and 538 nm, two of which had the same spectral origin at 527 nm. The two blue-shifted peridinins in the monomeric HPPCP and RFPCP have the same spectral origin at 480 and 481 nm, respectively. In the trimeric MFPCP, the two blue-shifted peridinins have different spectral origins at 468 and 483 nm.

The EET efficiency from peridinin to Chl *a* in PCP has been reported to be higher than 85%.[11,18,27,35,36] An overlay of the 1−T spectra with the fluorescence excitation spectra, both recorded at 10 K, are shown in Figure 5. The figure shows remarkable similarity between the two spectral lineshapes for each complex. Thus, the finding that for all PCP complexes, the overall spectral intensities and lineshapes of the 1−T and fluorescence excitation spectra from the different complexes are almost indistinguishable, indicates that it makes no difference in terms of the peridinin-to-Chl *a* EET efficiency whether the protein assembles as monomers or trimers or from homodimers or heterodimers. The percent EET efficiency for each of the individual peridinins was not computed here as was done for the carotenoids in the LH2 complexes described in Chapters IV and V, because the similarity in the 1–T and fluorescence excitation intensities and lineshapes implies that all the peridinins are transferring energy to Chl *a* with nearly 100% efficiency.

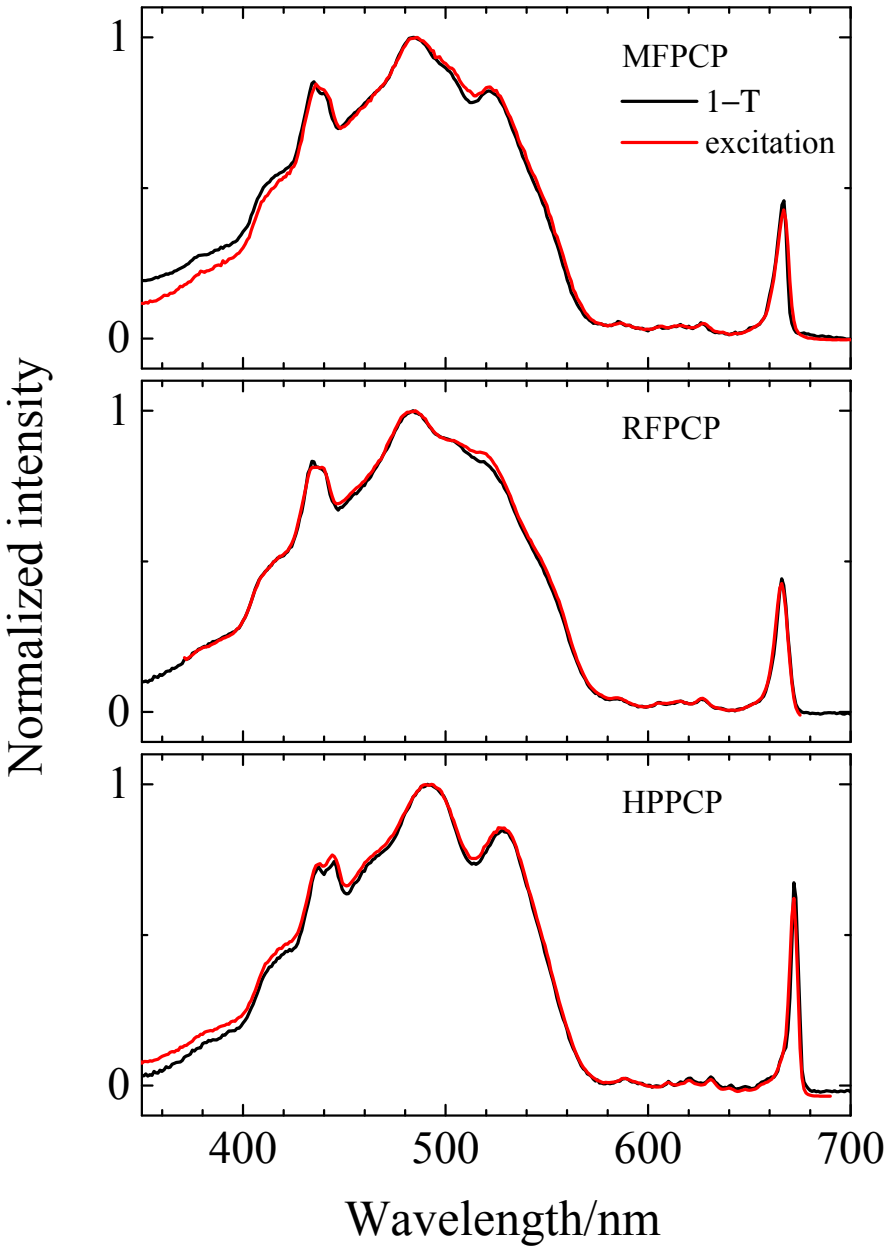


**Figure 5.** Overlay of 1−T (T, transmittance) and fluorescence excitation spectra of MFPCP, RFPCP and HPPCP recorded at 10 K. The spectra are normalized at the maximum of carotenoid absorption band.

## Conclusions

The objectives of this work were to explore whether the overall carotenoid-to-Chl EET efficiency depended on whether the PCP complex assembled as monomeric or trimeric quaternary structures or from homodimeric or heterodimeric subunits and to determine the individual peridinin-to-Chl *a* EET efficiencies by overlaying the spectral reconstructions of the 1−T and fluorescence excitation spectra, as was previously done for the LH2 complexes described in Chapters IV and V. The use of cryogenic temperatures for absorption and fluorescence spectroscopy provided a high resolution view of the spectral features of the bound peridinin and Chl *a* pigments in all three PCP complexes. It was confirmed by the spectral reconstructions of the 1−T spectra from the complexes (Figure 3) that the individual protein-bound peridinins exhibit distinct spectra that depend on the protein environment. However, it was found that there was no effect of protein structure on the EET efficiency. Moreover, the remarkable similarity between the 1–T and fluorescence excitation spectra (Figure 5) suggest that all of the individual peridinins are either transferring energy to Chl *a* with the same high (~100%) efficiency, or that the energy is rapidly shared between the closely associated peridinins prior to energy transfer to the acceptor Chl *a*. Ultrafast time-resolved spectroscopic studies will be required to distinguish between these energy transfer mechanisms.

# References


(1) Koka, P.; Song, P.-S. *Biochim. Biophys. Acta* **1977**, *495*, 220–231.

(2) Hiller, R. G.; Anderson, J. M.; Larkum, A. W. D. The Chlorophyll-Protein Complexes of Algae In *Chlorophylls*; Scheer, H., Ed.; CRC Press: Boca Raton, Florida, **1991**, 529–547.

(3) Macpherson, A. N.; Hiller, R. G. Light-Harvesting Systems in Chlorophyll *C*-Containing Algae In *Light-Harvesting Antennas in Photosynthesis*; Green, B. R., Parson, W. W., Eds.; Kluwer Academic Publishers: Dordrecht, The Netherlands, **2003**; Vol. 13, 323–352.

(4) Schulte, T.; Johanning, S.; Hofmann, E. *European Journal of Cell Biology* **2010**, *89*, 990–997.

(5) Bautista, J. A.; Connors, R. E.; Raju, B. B.; Hiller, R. G.; Sharples, F. P.; Gosztola, D.; Wasielewski, M. R.; Frank, H. A. *J. Phys. Chem. B* **1999**, *103*, 8751–8758.

(6) Zigmantas, D.; Hiller, R. G.; Yartsev, A.; Sundström, V.; Polivka, T. *J. Phys. Chem. B* **2003**, *107*, 5339–5348.

(7) Zigmantas, D.; Hiller, R. G.; Sharples, F. P.; Frank, H. A.; Sundström, V.; Polivka, T. *Phys. Chem. Chem. Phys.* **2004**, *6*, 3009–3016.

(8) Frank, H. A.; Bautista, J. A.; Josue, J.; Pendon, Z.; Hiller, R. G.; Sharples, F. P.; Gosztola, D.; Wasielewski, M. R. *J. Phys. Chem. B* **2000**, *104*, 4569–4577.

(9) Wagner, N. L.; Greco, J. A.; Enriquez, M. M.; Frank, H. A.; Birge, R. R. *Biophys. J.* **2013**, *104*, 1314–1325.

(10) Akimoto, S.; Takaichi, S.; Ogata, T.; Nishimura, Y.; Yamazaki, I.; Mimuro, M. *Chem. Phys. Lett.* **1996**, *260*, 147–152.

(11) Bautista, J. A.; Hiller, R. G.; Sharples, F. P.; Gosztola, D.; Wasielewski, M.; Frank, H. A. *J. Phys. Chem. A* **1999**, *103*, 2267–2273.

(12) Damjanovic, A.; Ritz, T.; Schulten, K. *Biophys. J.* **2000**, *79*, 1695–1705.

(13) Zigmantas, D.; Hiller, R. G.; Sundström, V.; Polivka, T. *Proc. Natl. Acad. Sci. USA* **2002**, *99*, 16760–16765.

(14) Krueger, B. P.; Lampoura, S. S.; van Stokkum, I. H. M.; Papagiannakis, E.; Salverda, J. M.; Gradinaru, C. C.; Rutkauskas, D.; Hiller, R. G.; van Grondelle, R. *Biophys. J.* **2001**, *80*, 2843–2855.

(15) Hofmann, E.; Wrench, P. M.; Sharples, F. P.; Hiller, R. G.; Welte, W.; Diederichs, K. *Science* **1996**, *272*, 1788–1791.

(16) Schulte, T.; Sharples, F. P.; Hiller, R. G.; E., H. *Biochemistry* **2009**, *48*, 4466–4475.

(17) Miller, D. J.; Catmull, J.; Puskeiler, R.; Tweedale, H.; Sharples, F. P.; Hiller, R. G. *Photosynth. Res.* **2005**, *86*, 229–240.

(18) Schulte, T.; Niedzwiedzki, D. M.; Birge, R. R.; Hiller, R. G.; Polívka, T.; Hofmann, E.; Frank, H. A. *Proc. Natl. Acad. Sci. USA* **2009**, *106*, 20764–20769.

(19) Schulte, T. Structural and Functional Investigations of the Soluble Light Harvesting Complex Peridinin-Chlorophyll *a*-Protein from Dinoflagellates *Doctoral Dissertation*, Ruhr-University Bochum, **2010**.

(20) Polívka, T.; Pascher, T.; Sundström, V.; Hiller, R. G. *Photosynth. Res.* **2005**, *86*, 217–227.

(21) Brotosudarmo, T. H. P.; Hofmann, E.; Hiller, R. G.; Wormke, S.; Mackowski, S.; Zumbusch, A.; Brauchle, C.; Scheer, H. *FEBS Lett.* **2006**, *580*, 5257–5262.

(22) Ilagan, R. P.; Chapp, T. W.; Hiller, R. G.; Sharples, F. P.; Polivka, T.; Frank, H. A. *Photosynth. Res.* **2006**, *90*, 5–15.

(23) Mackowski, S.; Wormke, S.; Brotosudarmo, T. H. P.; Jung, C.; Hiller, R. G.; Scheer, H.; Brauchle, C. *Biophys. J.* **2007**, *93*, 3249–3258.

(24) Polívka, T.; Pascher, T.; Hiller, R. G. *Biophys. J.* **2008**, *94*, 3198–3207.

(25) Wormke, S.; Mackowski, S.; Schaller, A.; Brotosudarmo, T. H. P.; Johanning, S.; Scheer, H.; Brauchle, C. *J. Fluor.* **2008**, *18*, 611–617.

(26) Di Valentin, M.; Agostini, G.; Salvadori, E.; Ceola, S.; Giacometti, G. M.; Hiller, R. G.; Carbonera, D. *BBA-Bioenergetics* **2009**, *1787*, 168–175.

(27) Song, P. S.; Koka, P.; Prézelin, B. B.; Haxo, F. T. *Biochemistry* **1976**, *15*, 4422–4427.

(28) Hiller, R. G.; Crossley, L. G.; Wrench, P. M.; Santucci, N.; Hofmann, E. *Molecular Genetics and Genomics* **2001**, *266*, 254–259.

(29) Prézelin, B. B.; Haxo, F. T. *Planta* **1976**, *128*, 133–141.

(30) Hofmann, E. Strukturanalyse Der Lichtsammler Peridinin-Chlorophyll a-Proteine (Pcps) Von Amphidinium Carterae Und Heterocapsa Pygmaea, **1999**.

(31) Humphrey, W.; Dalke, A.; Schulten, K. *J. Mol. Graphics Modell.* **1996**, *14*, 33–38.

(32) Sharples, F. P.; Wrench, P. M.; Ou, K.; Hiller, R. G. *Biochim. Biophys. Acta* **1996**, *1276*, 117–123.

(33) Iglesias-Prieto, R.; Govind, N. S.; Trench, R. K. *Proc. R. Soc. London, Ser. B* **1991**, *246*, 275–283.

(34) Kleima, F. J.; Wendling, M.; Hofmann, E.; Peterman, E. J. G.; van Grondelle, R.; van Amerongen, H. *Biochemistry* **2000**, *39*, 5184–5195.

(35) Ilagan, R. P.; Shima, S.; Melkozernov, A.; Lin, S.; Blankenship, R. E.; Sharples, F. P.; Hiller, R. G.; Birge, R. R.; Frank, H. A. *Biochemistry* **2004**, *43*, 1478–1487.

(36) Ilagan, R. P.; Koscielecki, J. F.; Hiller, R. G.; Sharples, F. P.; Gibson, G. N.; Birge, R. R.; Frank, H. A. *Biochemistry* **2006**, *45*, 14052–14063.

(37) Shima, S.; Ilagan, R. P.; Gillespie, N.; Sommer, B. J.; Hiller, R. G.; Sharples, F. P.; Frank, H. A.; Birge, R. R. *J. Phys. Chem. A* **2003**, *107*, 8052–8066.

(38) Carbonera, D.; Giacometti, G.; Segre, U.; Hofmann, E.; Hiller, R. G. *J. Phys. Chem. B* **1999**, *103*, 6349–6356.

(39) Van Stokkum, I. H. M.; Papagiannakis, E.; Vengris, M.; Salverda, J. M.; Polivka, T.; Zigmantas, D.; Larsen, D. S.; Lampoura, S. S.; Hiller, R. G.; van Grondelle, R. *Chem. Phys.* **2009**, *357*, 70–78.

(40) Alexandre, M. T. A.; Lührs, D. C.; van Stokkum, I. H. M.; Hiller, R.; Groot, M.-L.; Kennis, J. T. M.; van Grondelle, R. *Biophys. J.* **2007**, *93*, 1–11.

(41) Di Valentin, M.; Ceola, S.; Salvadori, E.; Agostini, G.; Carbonera, D. *BBA-Bioenergetics* **2008**, *1777*, 186–195.

(42) Di Valentin, M.; Ceola, S.; Salvadori, E.; Agostini, G.; Giacometti, G. M.; Carbonera, D. *BBA-Bioenergetics* **2008**, *1777*, 1355–1363.

(43) Niklas, J.; Schulte, T.; Prakash, S.; van Gastel, M.; Hofmann, E.; Lubitz, W. *J. Am. Chem. Soc.* **2007**, *129*, 15442–15443.

(44) Maxime, A.; van Grondelle, R. Time-Resolved FTIR Difference Spectroscopy Reveals the Structure and Dynamics of Carotenoid and Chlorophyll Triplets in Photosynthetic Light Havesting Complexes In *Infrared Spectroscopy- Life and Biomedical Sciences*; Theophile, T., Ed.; InTech, **2012**, 231–256.

(45) Carbonera, D.; Di Valentin, M.; Spezia, R.; Mezzetti, A. *Current Protein and Peptide Science* **2014**, *15*, 332–350.

# *Appendix A*

# *Processing Ultrafast Transient Absorption Data Using Surface XPlorer Pro v. 1.2.2.26 and ASUFit 3.0*

It is recommended to store each raw data to be processed in separate folders. Surface Xplorer and ASUFit are available in the Dell computer (Windows 7) in Frank Lab R215. A limited edition version of the Surface Xplorer software is installed on the laser spectrometer computer in Physics, but a USB key (available in the Frank Lab) is required to run the full version of Surface Xplorer.

A. Chirp and $t_0$ Correction

1. Open Surface Xplorer. Under the Dynamic Surface menu, click Open New 3D Data to open the file.

2. Under the Dynamic Surface menu, choose Subtract Scattered Light, a new window will open. Set the number of initial spectra to average. Click accept. Ideally, this will remove the laser pump signal.

3. Generate the file for chirp correction by determining the $t_0$ values over the entire spectral range. Start by positioning the cursor at the wavelength where a kinetic trace can be seen. Click on the Fit Kinetic menu, a new window will open. The parameters for fitting (number of exponentials, FWHM, etc.) can be set, then click on the Fit button. Check and repeat the fitting procedure until a satisfactory fit is obtained. When this is the case, click on the Save button and close the window. A file with the fitting parameters will automatically be generated in the folder where the raw data is stored. Repeat the fitting at ≤50 nm increment until no kinetic trace is seen. The trend for the $t_0$ values should be increasing with the wavelength.

4. Once the fittings are done, click on the Dynamic Surface menu and choose Chirp correction, then use the saved file.

5. After chirp correction, check to make sure there are no null surfaces. To remove null surface, use the 3D Surface Controls. The second icon contains the up and down control which will cut out the null surfaces.

6. Save file (.csv), the original file will be appended with a -ibg-chirp.

7. Open the saved file with Wordpad. Click Edit → Replace, which will open a new window. In the Find what column, place NaN and in the Replace with column, place 0.

This will remove any null surfaces that may have not been deleted in Step 5. Delete any comments after the numerical data at the end of the file. Save the file.

8. Open the file edited in Wordpad.

9. To correct t=0, perform a kinetic fit (As in Step 3) of the bands with the highest signal intensity. This will give the $t_0$ values that can be used for correction. The plot can also be checked visually for $t_0$ by inspecting the kinetic trace on the Kinetic Panel.

10. Once $t_0$ is determined, click on the Dynamic Surface menu and choose time zero correction. A new window should appear where a new t=0 can be entered. Save file (.csv), the original file will be appended with a -ibg-chirp-t0.

11. Open the saved file with Wordpad. Click Edit → Replace, which will open a new window. In the Find what column, put NaN and in the Replace with column, put 0. Delete any comments after the numerical data at the end of the file. Save the file.

12. The representative spectra at specific time delays are obtained by choosing the time in the Spectrum Panel Control. Click on the Spectra menu, then Save Spectrum. Repeat for all time traces needed. In the folder containing the data, a file will be saved appended with -ibg-chirp-t0 RepresentativeSpectra. This file may be imported directly in Origin for plotting.

B. Global fitting

For global fitting, a stand-alone version of ASUFit 3.0 provided by Darek Niedzwiedzki is used.

1. Open the ASUFit program, then open the file to be used for fitting.

2. Set the fitting parameters. An initial guess must be placed in the lifetimes and FWHM portions in order for the fitting to proceed. Perform the fitting procedure and repeat until a satisfactory agreement between the experimental data and fits is reached by checking the spectrum and kinetics, and their respective residuals.

3. The decay associated spectra (DAS) can be viewed in the Window menu→DAS, which will open a new window. In the new window menu, click File then Save. This will save as a .das file which can be imported to Origin.

4. The kinetic traces and fits at specific wavelengths can be obtained by setting the wavelength in the spectrum panel. Go to the File menu, click Save, then Save kinetics.

5. The data can be globally fit using either a sum of exponentials function, implying parallel non-interacting pathways of excited state deactivation, in which case DAS lineshapes are generated, or a sequential pathway of deactivation in which case evolution associated difference spectra (EADS) are produced.